NEW FRONTIERS IN NATURAL SCIENCE AND MATHEMATICS

Editor: Prof. Mehmet YILMAZ

DUVAR

NEW FRONTIERS IN NATURAL SCIENCE AND MATHEMATICS

EDITOR

Prof. Mehmet YILMAZ

New Frontiers in Natural Science and Mathematics
Editör: Prof. Mehmet YILMAZ

Genel Yayın Yönetmeni: Berkan Balpetek
Kapak ve Sayfa Tasarımı: Duvar Design
Yayın Tarihi: OCTOBER 2023
Yayıncı Sertifika No: 49837
ISBN: 978-625-6585-10-2

853 Sokak No:13 P.10 Kemeraltı-Konak/İzmir
Tel: 0 232 484 88 68

www.duvaryayinlari.com
duvarkitabevi@gmail.com

TABLE OF CONTENTS

Chapter 1

A Comparison of Bayesian and Frequentist Methods in Reliability Generalization Meta-Analysis: Coronavirus Anxiety Scale (CAS)

Esin AVCI[1], Elvan HAYAT[2]

[1]Doç.Dr.; Giresun Üniversitesi, Fen Edebiyat Fakültesi, İstatistik Bölümü, esin.avci@giresun.edu.tr ORCID No: 0000-0002-9173-0142
[2]Doç.Dr.; Aydın Adnan Menderes Üniversitesi, Aydın İktisat Fakültesi, Ekonometri Bölümü, elvan.hayat@adu.edu.tr, ORCID No: 0000-0001-8200-8046

INTRODUCTION

The Covid-19 disease, first reported in Wuhan, China, in December 2019, has rapidly spread in China and the rest of the world. With the declaration of a pandemic by the World Health Organization on March 11, 2020, the severity of the disease began to be understood. Until now over 611 million cases and over 6.52 million deaths have been reported worldwide (Worldometer, September 2022). Due to the increase in the number of cases and deaths and the rapid contagion of the disease, restrictions, and quarantines have been implemented in many countries to control the spread of the disease, and this has caused people to face very rapid changes in their daily life. In addition to these rapid changes, the mental health of individuals who had to cope with many emotions such as anxiety, worry, and stress was also affected.

The research carried out in previous epidemic periods such as SARS, Ebola, and MERS has shown that pandemic diseases and prevention measures are announced at a high rate by mass media, so that psychological effects such as anxiety and depression may occur in individuals (Lee et al, 2007; Liu et al., 2012; Wheaton et al., 2012). In research conducted during the past pandemics and epidemics, the various sources of stress have been identified, such as perceptions of the transparency of the information provided by the authorities, sudden changes and inability to plan for the future, concerns about his health of himself and his acquaintances, fear of being unemployed, and possible financial losses (Hawryluck et al., 2004; Kim et al., 2018; Huremović, 2019; Brooks et al., 2020). Also, it has been stated that serious worries about the fear of death due to quarantine, deterioration of social relations, as well as feelings of loneliness and anger may develop (Xiang et al., 2020).

During the Covid-19 pandemic, different scale development studies have been carried out to measure emotions such as fear and anxiety of people against the disease. (Lee, 2020; Ahorsu et al., 2020; Taylor et al., 2020; McElroy et al., 2020).

The Coronavirus Anxiety Scale (CAS), developed by Lee (2020), is one of the scales developed to identify cases of dysfunctional anxiety associated with Covid-19. In the CAS scale, which is created by using a Likert-type scale consisting of 5 items, the minimum possible score for each item is 0, the maximum score is 4, and the total score obtained by adding up each item score varies between 0 and 20 points. The higher the total score the means the anxiety associated with Covid-19 is so high. Studies using the CAS scale, which has been adapted to many languages and its use has spread rapidly, provided independent estimates of psychometric properties obtained with appropriate samples from various target populations.

An indicator of the stability of the measurement values obtained in repeated measurements with a measurement tool under the same conditions is reliability, which is one of the properties that the scale should have. In addition, reliability refers to the consistency of scores obtained by the same individuals participating in the same or equivalent tests. Although there are various reliability coefficient calculation methods in the literature that can be used in different situations, the Cronbach's alpha coefficient is the most commonly used reliability measure in interpreting internal consistency reliability. As with all coefficients, Cronbach's alpha coefficient differs from research to research, although it is calculated on the same scale as it is a sampling dependent coefficient (Graham and Unterschute, 2015; Sánchez-Meca et al., 2017).

Reliability coefficients, sample size, application conditions, application time, etc. depending on sample characteristics. Such differences in studies required the generalization of reliability.

A subset of meta-analysis known as reliability generalization (RG) studies synthesizes quantitative estimates of the reliability of scores obtained using a measurement tool from various samples (Vacha-Haase, 1998).

The frequentist meta-analysis for reliability generalization uses inverse variance weights to provide an overall estimate by combining information from independent studies. On the other hand, the Bayesian meta-analysis provides similar estimates to the frequentist approach if a common a priori is used, as well as "shrunken" local reliability estimates.

The purpose of this systematic review and meta-analysis is to estimate the mean reliability of the CAS scale using the Bayesian and frequentist reliability generalization (RG) meta-analyses and to compare the results from the two methods. In the second section, the search strategy and selection criteria, methodological quality assessment and statistical analysis are explained. Results are given in the third section. Finally, conclusions are given in the last section.

MATERIALS AND METHODS

This meta-analysis conducted the *Preferred Reporting Items for Systematic Reviews and Meta-Analyses* (PRISMA) guidelines, whose checklist was strictly followed.

Search strategy and selection criteria

This systematic review and meta-analysis have been conducted following the PRISMA guidelines. Two researchers independently searched Scopus and Web of Science databases using the terms "coronavirus anxiety scale" and

"coronavirus anxiety scale-CAS" from April 11 to May 30, 2022, for cross-sectional studies on the CAS.

Four inclusion criteria were applied: (1) to be an empirical study where the CAS, or a language adapted version of this scale during the COVID-19 outbreak; (2) to report Cronbach's alpha reliability score calculated with data; (3) to be written in English; (4) the full text was available. The flowchart presented in Figure 1 describes the literature search strategy and study selection process. The search process is shown in the flowchart (Fig. 1).

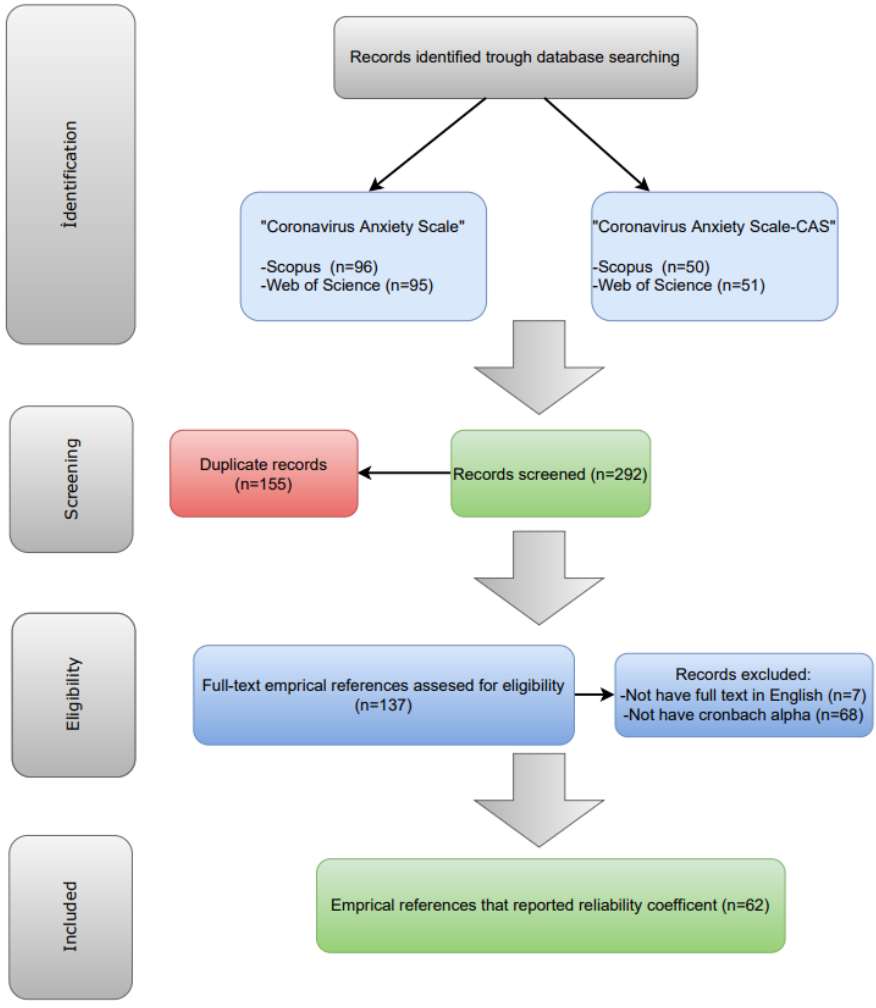

Figure 1. Flowchart of the study selection

Initially, 292 prospective records were found; however, after screening titles and abstracts, 155 duplicate records, 7 records not written in English, and 68 records with unreported Cronbach's alphas were eliminated because they did not match the inclusion criteria. After reading these 62 articles (40932 participants) in full, we included them in our meta-analysis (Figure 1).

Methodological quality assessment

After the studies is selected according to the meta-analysis inclusion criteria, the following sample and study characteristics have been recorded by the researchers: (i) the title of the article, (ii) the author(s) conducting the study, (iii) the year of the article, (iv) which scales were used and when they were applied to the participants (v) average age of the participants (vi) reliability coefficient, (vii) sample size/number of participants in the sample, (viii) participant characteristics, (ix) in which country it was conducted

The quality of the studies to be included in the meta-analysis have been scanned by two independent referees from the relevant databases and evaluated according to the following 6 criteria. The quality criteria have been determined as follows: (1) Has it been published in high-quality journals? (2) Was the sampling frame appropriately addressed to the target population? (3) Have the study subject and layout been explained in detail? (4) Was the sample size sufficient? (5) Was the response rate sufficient? (6) Were appropriate statistical methods used in data analysis? The score of each study was obtained by giving a score of 1 if these criteria were met, and 0 if they were not met. Any disagreements that arose between the reviewers were resolved through discussions.

Statistical analysis

Scales that are frequently used in health and social sciences must be reliable in order to have validity and practical use. Conceptually, reliability is defined as “the degree of accurate measures and hence giving consistent results” (Peter, 1979). The reliability of a scale can be estimated with many different reliability coefficients (Cronbach's alpha, McDonald's Omega, etc.). Cronbach's alpha coefficient, which reflects the general reliability structure best compared to other coefficients, is based on statistics and is calculated by considering all questions (Cronbach, 1951). Sijtsma (2009) reports that the number of citations to Cronbach's original article is more than 6500, surpassing even Watson and Crick's (1953) historical article on the discovery of the double helix structure of DNA. Literature reviews show that the Cronbach's alpha coefficient accounts

for more than two-thirds of the reported reliability estimates (Barry et al., 2014; Flake et al., 2017).

Cronbach's alpha coefficient always ranged between 0 and 1. In the evaluation; $0 \leq \alpha < 0.5$ is unreliable, $0.5 \leq \alpha < 0.6$ has low reliability, $0.6 \leq \alpha < 0.7$ is questionable, $0.7 \leq \alpha < 0.8$ is acceptable reliability, $0.8 \leq \alpha < 0.9$ is highly reliable, and $0.9 \leq \alpha < 1$ is highly reliable. (George and Mallery, 2003).

Reliability derived from a scientific study; it may not be obtained at a high level due to low number of participants, insufficient representation of the population, and random error. Therefore, combining the results of independent and comparable studies on the same subject provides stronger results. Meta-analysis, which is a statistical method, is widely used in synthesizing the results in a methodological way.

The frequentist meta-analysis can also be used to combine Cronbach's alpha values from multiple studies. This is often referred to as "reliability generalization meta-analysis" (Vacha-Haase, 1998). In the reliability generalization meta-analysis, the Cronbach alpha coefficient is defined as follows;

$$\alpha_i = \frac{J_i}{J_i - 1}\left[1 - \frac{\sum_{j=1}^{J_i} s_{ji}^2}{s_{i+}^2}\right] \tag{1}$$

where, s_{ji}^2 *i*.th study (*i=1,..., I*) *j*. item (*j=1,..., J*) total score variance and s_{i+}^2 shows the variance of the total test score of the study *i*.

Hakstian and Whalen (1976) showed that the T transformation of the Cronbach's alpha coefficient normally distributed, using the results of the sample theory developed by Feldt (1965) and Kristof (1963).

$$T_i = (1 - \alpha_i)^{1/3} \tag{2}$$

They defined the variance of the transformation as follows:

$$v_i = \frac{18\, J_i (N_i - 1)(1 - \alpha_i)^{2/3}}{(J_i - 1)(9N_i - 11)^2} \tag{3}$$

where N_i is the sample size of the study of *i.*

Another transformation applied to the Cronbach alpha coefficient was proposed by Bonett (2002):

$$T_i = ln(1 - \alpha_i) \quad (4)$$

The transformed Cronbach's alpha coefficients have a monotonically increasing function. With the "metafor" package in the R program, both raw Cronbach alpha values and meta-analysis of their transformations can be performed (Viechtbauer, 2010).

In the frequentist meta-analysis of Cronbach's alpha coefficients, the weighted mean value is obtained by weighting the Cronbach's alpha coefficients with the inverse of the variance. Here, the variance is determined only by within-study variance for the fixed-effects model, while for the random effects model is determined with the within-study and between-study variance (τ^2). The 95% confidence interval for the estimation of Cronbach's alpha coefficients is calculated by the method proposed by Hartung (1999).

Brannick and Zhang (2013) suggested the Bayesian approach instead of the frequentist meta-analysis approach of the Cronbach's alpha coefficient. Bayesian estimation is advantageous in dealing with outliers or small sample sizes, in the flexible inclusion of variables in the model, and in providing an intuitive probability interpretation of Bayesian credible intervals.

Nowadays, the Bayesian perspective has gained more importance due to the information theory that affects all branches of science. In the Bayesian approach, parameter estimates are obtained based on Bayes' theorem (Bolstad, 2007). Bayes' theorem is expressed proportionally as follows:

$$p(\theta|y) \propto p(y|\theta)p(\theta) \quad (5)$$

By using Bayes' theorem, the information obtained from previous studies about the parameter ($p(\theta)$ priors) is combined with the information obtained from the data ($p(y|\theta)$) to obtain up-to-date information about the parameter. Thus, parameter estimation contains more information.

In the Bayesian approach of meta-analysis of Cronbach's alpha coefficient, the real effect size in the ith study is a random variable. Hence, T_i is defined with the probability distribution.

As stated above since the *T* transformation of Cronbach's alpha coefficient of the ith study has a normal distribution, shown as follows.

$$T_i \sim N(\mu_i, v_i) \quad (6)$$

where μ_i, is the T-transformed value of the local Cronbach's alpha coefficient (which is denoted by α*)

$$\mu_i = (1 - \alpha_i^*)^{1/3} \tag{7}$$

Each μ_i is also modeled as a normal distribution.

$$\mu_i \sim N(\underline{\mu}, \tau^2) \tag{8}$$

where, τ^2 represents the random-effect variance component in the meta-analysis. $\underline{\mu}$ in Eqn [8] is related to the coefficient alpha of combined, $\underline{\alpha}$, by

$$\underline{\mu} = (1 - \underline{\alpha})^{1/3} \tag{9}$$

This means that $\underline{\mu}$ is a T-transformed value of the combined alpha parameter ($\underline{\alpha}$).

While determining the prior distributions for $\underline{\alpha}$ and τ; theoretical value range is taken into account. Since $\underline{\alpha}$, takes values between 0 and 1, a prior distribution for alpha is usually chosen as the Beta distribution:

$$\underline{\alpha} \sim Beta(a, b) \tag{10}$$

For the prior distribution τ, the standard half-Cauchy distribution is chosen:

$$\tau \sim Cauchy(0,1)_{I(0,\infty)} \tag{11}$$

Although Brannick and Zhang (2013) used the inverse gamma distribution for τ[1], some researchers, including Daniels (1999) and Gelman (2006), suggested that the estimation results to be obtained would be sensitive to the selected hyperparameters, so the inverse gamma distribution should not be used. Okada (2015) chose the standard half-Cauchy distribution based on the recommendations of Gelman (2006), Gelman and Hill (2007), and Polson and Scott (2012). Therefore, in this study, the half-Cauchy distribution was chosen as the prior distribution.

RESULTS

Identification and selection of articles

It was determined that there were 292 articles at the beginning in the search using keywords in Scopus and Web of Science databases. It was determined that 150 of them had duplicate records.Thus, the number of full-text articles evaluated for suitability was determined as 137. Afterwards, it was understood that 7 of the articles whose full texts were examined were not in English, and the Cronbach alpha value was not reported in 68 of them.

At the end of the process, it was determined that 62 articles reported the reliability coefficient and met the inclusion and disclusion criteria and were included in the meta-analysis. The selected studies have been read and classified by two researchers.

Characteristics of the studies

The 62 cross-sectional studies included 40932 participants. Of the 62 studies included in the analysis, 12 were conducted in Turkey, 7 in the USA, South Korea, and Iran 4 each, and in Brazil, Colombia, Peru, and Poland 3 each. 18% of the participants are healthcare workers, 15% are hospitalized or have cancer, etc. from people with a history of the disease. The mean age was reported in 53 of the 62 studies, with a mean age of approximately 37.

Statistical analysis results

The results of the frequentist and the Bayesian meta-analysis based on 62 studies that met the inclusion and exclusion criteria have been obtained as follows. Analyzes have conducted using the R program, respectively, “metafor” for frequentist meta-analysis and “BRugs” packages for Bayesian meta-analysis. The forest graphics obtained from both methods are given in Figure 2(a) and (b).

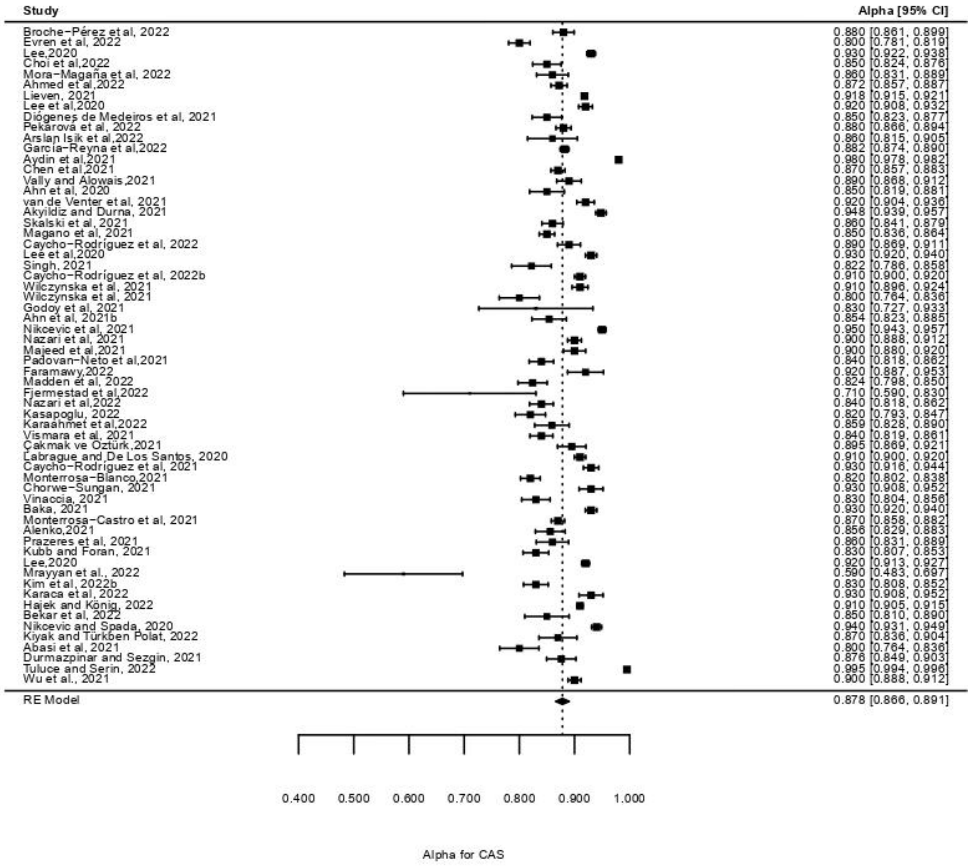
Study
Alpha [95% CI]
Broche−Pérez et al, 2022 0.880 [0.861, 0.899]
Evren et al, 2022 0.800 [0.781, 0.819]
Lee,2020 0.930 [0.922, 0.938]
Choi et al,2022 0.850 [0.824, 0.876]
Mora−Magaña et al, 2022 0.860 [0.831, 0.889]
Ahmed et al,2022 0.872 [0.857, 0.887]
Lieven, 2021 0.918 [0.915, 0.921]
Lee et al,2020 0.920 [0.908, 0.932]
Diógenes de Medeiros et al, 2021 0.850 [0.823, 0.877]
Pekárová et al, 2022 0.880 [0.866, 0.894]
Arslan Işık et al,2022 0.860 [0.815, 0.905]
García−Reyna et al,2022 0.882 [0.874, 0.890]
Aydin et al,2021 0.980 [0.978, 0.982]
Chen et al,2021 0.870 [0.857, 0.883]
Vally and Alowais,2021 0.890 [0.868, 0.912]
Ahn et al, 2020 0.850 [0.819, 0.881]
van de Venter et al, 2021 0.920 [0.904, 0.936]
Akyildiz and Durna, 2021 0.948 [0.939, 0.957]
Skalski et al, 2021 0.860 [0.841, 0.879]
Magano et al, 2021 0.850 [0.836, 0.864]
Caycho−Rodríguez et al, 2022 0.890 [0.869, 0.911]
Lee et al,2020 0.930 [0.920, 0.940]
Singh, 2021 0.822 [0.786, 0.858]
Caycho−Rodríguez et al, 2022b 0.910 [0.900, 0.920]
Wilczynska et al, 2021 0.910 [0.896, 0.924]
Wilczynska et al, 2021 0.800 [0.764, 0.836]
Godoy et al, 2021 0.830 [0.727, 0.933]
Ahn et al, 2021b 0.854 [0.823, 0.885]
Nikcevic et al, 2021 0.950 [0.943, 0.957]
Nazari et al, 2021 0.900 [0.888, 0.912]
Majeed et al,2021 0.900 [0.880, 0.920]
Padovan−Neto et al,2021 0.840 [0.818, 0.862]
Faramawy,2022 0.920 [0.887, 0.953]
Madden et al, 2022 0.824 [0.798, 0.850]
Fjermestad et al,2022 0.710 [0.590, 0.830]
Nazari et al,2022 0.840 [0.818, 0.862]
Kasapoglu, 2022 0.820 [0.793, 0.847]
Karaahmet et al,2022 0.859 [0.828, 0.890]
Vismara et al, 2021 0.840 [0.819, 0.861]
Çakmak ve Öztürk,2021 0.895 [0.869, 0.921]
Labrague and De Los Santos, 2020 0.910 [0.900, 0.920]
Caycho−Rodríguez et al, 2021 0.930 [0.916, 0.944]
Monterrosa−Blanco,2021 0.820 [0.802, 0.838]
Chorwe−Sungani, 2021 0.930 [0.908, 0.952]
Vinaccia, 2021 0.830 [0.804, 0.856]
Baka, 2021 0.930 [0.920, 0.940]
Monterrosa−Castro et al, 2021 0.870 [0.858, 0.882]
Alenko,2021 0.856 [0.829, 0.883]
Prazeres et al, 2021 0.860 [0.831, 0.889]
Kubb and Foran, 2021 0.830 [0.807, 0.853]
Lee,2020 0.920 [0.913, 0.927]
Mrayyan et al., 2022 0.590 [0.483, 0.697]
Kim et al, 2022b 0.830 [0.808, 0.852]
Karaca et al, 2022 0.930 [0.908, 0.952]
Hajek and König, 2022 0.910 [0.905, 0.915]
Bekar et al, 2022 0.850 [0.810, 0.890]
Nikcevic and Spada, 2020 0.940 [0.931, 0.949]
Kiyak and Türkben Polat, 2022 0.870 [0.836, 0.904]
Abasi et al, 2021 0.800 [0.764, 0.836]
Durmazpinar and Sezgin, 2021 0.876 [0.849, 0.903]
Tuluce and Serin, 2022 0.995 [0.994, 0.996]
Wu et al., 2021 0.900 [0.888, 0.912]
RE Model 0.878 [0.866, 0.891]
0.400
0.500
0.600
0.700
0.800
0.900
1.000
Alpha for CAS

(a)

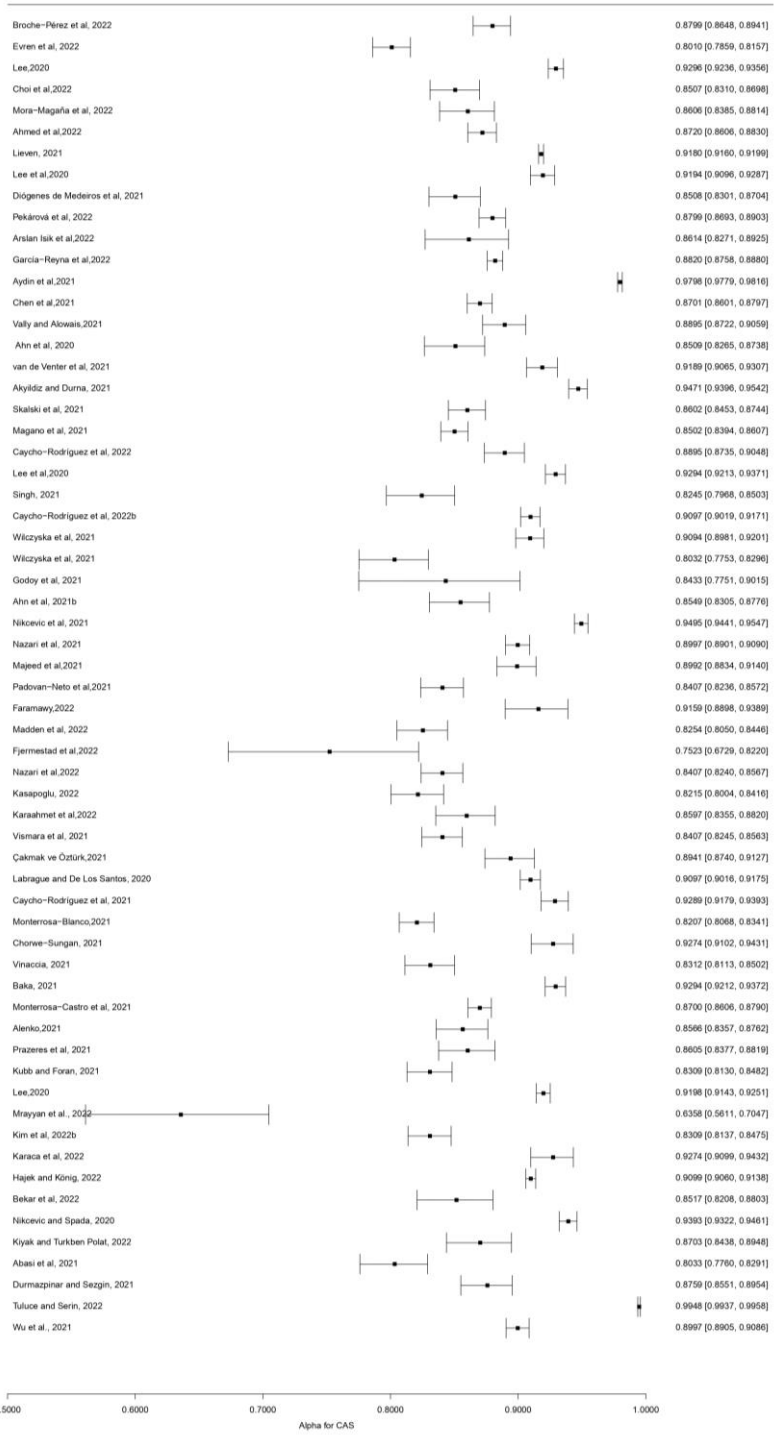
Broche−Pérez et al, 2022 0.8799 [0.8648, 0.8941]
Evren et al, 2022 0.8010 [0.7859, 0.8157]
Lee,2020 0.9296 [0.9236, 0.9356]
Choi et al,2022 0.8507 [0.8310, 0.8698]
Mora−Magaña et al, 2022 0.8606 [0.8385, 0.8814]
Ahmed et al,2022 0.8720 [0.8606, 0.8830]
Lieven, 2021 0.9180 [0.9160, 0.9199]
Lee et al,2020 0.9194 [0.9096, 0.9287]
Diógenes de Medeiros et al, 2021 0.8508 [0.8301, 0.8704]
Pekárová et al, 2022 0.8799 [0.8693, 0.8903]
Arslan Isik et al,2022 0.8614 [0.8271, 0.8925]
García−Reyna et al,2022 0.8820 [0.8758, 0.8880]
Aydin et al,2021 0.9798 [0.9779, 0.9816]
Chen et al,2021 0.8701 [0.8601, 0.8797]
Vally and Alowais,2021 0.8895 [0.8722, 0.9059]
Ahn et al, 2020 0.8509 [0.8265, 0.8738]
van de Venter et al, 2021 0.9189 [0.9065, 0.9307]
Akyildiz and Durna, 2021 0.9471 [0.9396, 0.9542]
Skalski et al, 2021 0.8602 [0.8453, 0.8744]
Magano et al, 2021 0.8502 [0.8394, 0.8607]
Caycho−Rodriguez et al, 2022 0.8895 [0.8735, 0.9048]
Lee et al,2020 0.9294 [0.9213, 0.9371]
Singh, 2021 0.8245 [0.7968, 0.8503]
Caycho−Rodríguez et al, 2022b 0.9097 [0.9019, 0.9171]
Wilczyska et al, 2021 0.9094 [0.8981, 0.9201]
Wilczyska et al, 2021 0.8032 [0.7753, 0.8296]
Godoy et al, 2021 0.8433 [0.7751, 0.9015]
Ahn et al, 2021b 0.8549 [0.8305, 0.8776]
Nikcevic et al, 2021 0.9495 [0.9441, 0.9547]
Nazari et al, 2021 0.8997 [0.8901, 0.9090]
Majeed et al,2021 0.8992 [0.8834, 0.9140]
Padovan−Neto et al,2021 0.8407 [0.8236, 0.8572]
Faramawy,2022 0.9159 [0.8898, 0.9389]
Madden et al, 2022 0.8254 [0.8050, 0.8446]
Fjermestad et al,2022 0.7523 [0.6729, 0.8220]
Nazari et al,2022 0.8407 [0.8240, 0.8567]
Kasapoglu, 2022 0.8215 [0.8004, 0.8416]
Karaahmet et al,2022 0.8597 [0.8355, 0.8820]
Vismara et al, 2021 0.8407 [0.8245, 0.8563]
Çakmak ve Öztürk,2021 0.8941 [0.8740, 0.9127]
Labrague and De Los Santos, 2020 0.9097 [0.9016, 0.9175]
Caycho−Rodriguez et al, 2021 0.9289 [0.9179, 0.9393]
Monterrosa−Blanco,2021 0.8207 [0.8068, 0.8341]
Chorwe−Sungan, 2021 0.9274 [0.9102, 0.9431]
Vinaccia, 2021 0.8312 [0.8113, 0.8502]
Baka, 2021 0.9294 [0.9212, 0.9372]
Monterrosa−Castro et al, 2021 0.8700 [0.8606, 0.8790]
Alenko,2021 0.8566 [0.8357, 0.8762]
Prazeres et al, 2021 0.8605 [0.8377, 0.8819]
Kubb and Foran, 2021 0.8309 [0.8130, 0.8482]
Lee,2020 0.9198 [0.9143, 0.9251]
Mrayyan et al., 2022 0.6358 [0.5611, 0.7047]
Kim et al, 2022b 0.8309 [0.8137, 0.8475]
Karaca et al, 2022 0.9274 [0.9099, 0.9432]
Hajek and König, 2022 0.9099 [0.9060, 0.9138]
Bekar et al, 2022 0.8517 [0.8208, 0.8803]
Nikcevic and Spada, 2020 0.9393 [0.9322, 0.9461]
Kiyak and Turkben Polat, 2022 0.8703 [0.8438, 0.8948]
Abasi et al, 2021 0.8033 [0.7760, 0.8291]
Durmazpinar and Sezgin, 2021 0.8759 [0.8551, 0.8954]
Tuluce and Serin, 2022 0.9948 [0.9937, 0.9958]
Wu et al., 2021 0.8997 [0.8905, 0.9086]
0.5000
0.6000
0.7000
0.8000
0.9000
1.0000
Alpha for CAS

(b)

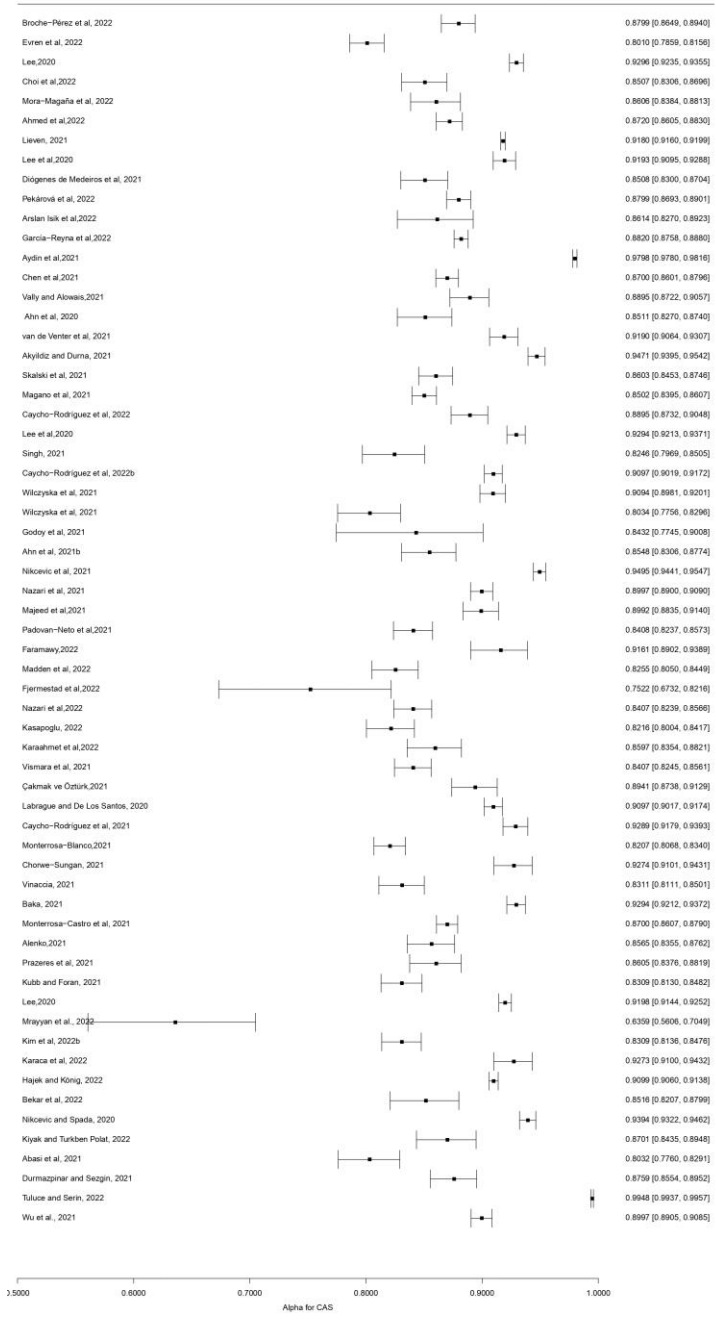

(c)

Figure 2: Forest graphs: (a) the frequentist meta-analysis; (b) the Bayesian meta-analysis of non-informative a prior; and (c) the Bayesian meta-analysis of informative a prior.

The forest graphics obtained from both methods are given in Figure 2. Figure 2 (a) represents the frequentist method forest plot, while (b) and (c) represent the Bayesian method forest plots of non-informative and informative prior, respectively. The forest plots of the Bayesian method for both priors display a relatively narrower credible interval than the frequentist confidence interval.

The Beta distribution was determined as prior distribution for the Bayesian meta-analysis of Cronbach's alpha coefficient. Beta (1,1) distribution was used for the non-informative prior, and the informative prior was obtained from the percentile values of the 4286 studies in the literature which is a comprehensive review of the studies with Cronbach's alpha coefficient reported by Peterson (1994). The 25th, 50th, 51st, and 86th percentiles were obtained as 0.7, 0.79, 0.8, and 0.9, respectively. The parameters of the Beta distribution were obtained from the R program as a=8.73 and b=2.52. Parameter estimates were revealed from the posterior distribution using the Gibbs sampling algorithm. In order to reduce possible bias, the first 5000 of the 500000 iterations are removed as the Burn period. The trace and Kernel density plots of the estimation of the Cronbach's alpha coefficient for both priors are given in Figure 3 (a) and (b).

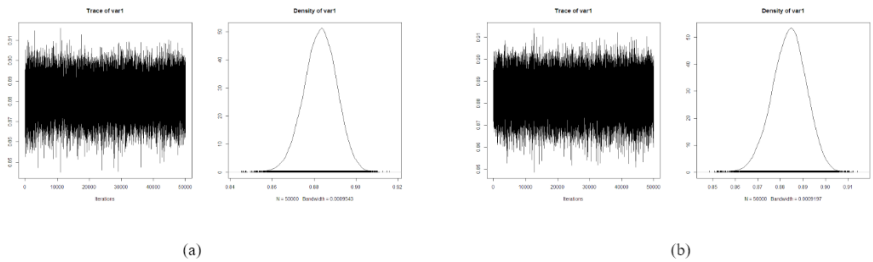

Figure 3: Trace and Kernel density plots; (a) non-informative a prior, (b) informative a prior

When the convergence graphs in Figure 3 are examined; The high and frequent oscillations of the trace graphs indicate rapid convergence, while the bell-shaped and single-peaked appearance of the Kernel density graphs indicates convergence to the posterior distributions.

The results of the frequentist and Bayesian meta-analysis of Cronbach's alpha coefficient are summarized in Table 1. When comparing the two approaches; Although Hakstian and Whalen's (1976) T-transformation was made to Cronbach's alpha coefficient, all tables and figures were converted to

the relevant coefficient to facilitate interpretation, and combined means and confidence /credible intervals were obtained.

Table 1: Cronbach's alpha estimate of CAS and 95% confidence/credible intervals

Method	Estimation of Cronbach Alpha	Lower Limit	Upper Limit	MSE
Frequentist	0.878	0.866	0.891	0.232
Bayes (Beta(1,1))	0.874	0.856	0.891	0.004
Bayes (Beta(8.73,2.52))	0.876	0.858	0.892	0.004

From Table 1, the combined means and confidence/credible limits of Cronbach's alpha coefficient were between 0.878 and 0.866 and 0.891 for the frequentist method, respectively; it ranged from 0.874 and 0.856 to 0.891 for Bayesian non-informative prior, 0.876 and 0.858 to 0.892 for non-informative a prior. In the comparison of the two approaches, the mean squares of error (MSE) are considered. The approach with the smallest MSE gives more accurate prediction values. Based on the mean squared error, it was determined that the Bayesian approach obtained a more precise Cronbach's alpha estimation of the combined means than the frequentist approach.

CONCLUSIONS

The new COVID-19 pandemic that caused great panic and repression around the world, has caused anxiety and depression by increasing feelings of worry and fear in people. Many scales development process has been conducted during the pandemic to investigate these psychological problems. The current Reliability Generalization (RG) meta-analysis of the CAS scale, which is one of the most frequently used scales, estimates the mean reliability of the CAS scale using the frequentist and Bayesian method.

In RG studies, both the Bayesian method and the frequentist method calculate overall mean estimates and confidence/credible intervals for each primary study considered in the meta-analysis. Calculation of confidence intervals is important because the population parameter shows uncertainty due to sampling error. Confidence intervals also estimate the limits of the value of the population parameter as well as the point estimate from the data.

In both the Bayesian and frequentist methods, a general mean and the confidence/credible interval of this mean are calculated. If the overall mean and related estimates are obtained from studies compiled from the same population, a fixed-effects or joint-effects model is used. The predictive value and confidence/credible interval obtained from this model indicate the magnitude of

uncertainty about the population parameter. While in the random effects model estimates overall mean from studies compiled from different populations, is used. The predictive value and confidence/credible interval obtained from this model represents the sampling error as well as the magnitude of the uncertainty about the population parameter.

The Bayesian approach to the reliability generalization allows calculation of an overall mean and estimation interval consistent with results from the frequentist method. In addition, the Bayesian approach allows to obtain individual study estimates corrected for sampling error of each study. Thus, it allows the development of hypothesis tests to identify studies that are included in the meta-analysis and differ from the general one, and to determine the shape of the reliability distribution of Cronbach's alpha. On the other hand, the Bayesian approach, unlike the frequentist method, gives stronger predictions by making use of not only the information obtained from the data but also the information from previous studies (a prior information).

Random effects models have been used in this study, in which CAS reliability generalization has been conducted by frequentist and Bayesian methods. Non-informative (Beta (1,1)) and informative a prior Beta (8.73, 2.52) distribution, which is obtained by utilizing previous studies, have been used for the Bayesian reliability generalization, the standard half-Cauchy (0.1) prior distribution have been used for the variance.

Rather than addressing narrow or wide confidence/credible intervals for each study's meta-analytical estimate, both for the frequentist method and for the two different prior distributions of the Bayesian method, the mean squared error has been calculated and compared. The MSE values obtained from two different prior distributions of the Bayesian method were calculated close to each other and were found to be considerably smaller than the MSE value calculated from the frequentist method.

Brannick and Zhang (2013) used the Gamma distribution as prior distribution for variance and found the frequentist method and Bayesian method estimates to be the same. Whereas, when standard half-Cauchy distribution is used for variance in our study, although the reliability intervals of the general estimates obtained for Cronbach alpha are wider, it is also seen from the mean square error that narrower intervals are obtained in the estimation of individual studies.

The generalized Cronbach alpha value obtained using both frequentist and Bayesian two-prior distributions was calculated over 0.80 (frequentist method 0.878; Bayesian method Beta (1.1)) and Beta (8.73, 2.52) 0.876. Thus, it has

been determined that the CAS scale is quite reliable in measuring anxiety related to coronavirus.

As a result, it is thought that this study contributes to the literature by examining the generalization of the reliability of the CAS scale developed to measure anxiety due to COVID-19 with both frequentist and Bayesian meta-analysis methods and comparing the results.

REFERENCES

Abasi, I., Sohrabzadeh Fard, A., Farzin, A., Lee, S., Masjedi Arani, A., & Poursharifi, H. (2021). Psychometric properties of Coronavirus Anxiety Scale in Iranian population. Iranian Journal of Psychiatry and Behavioral Sciences, 15(4). doi:10.5812/ijpbs.112707

Abdelrehem Faramawy, M. A. E., & Abd El Kader, A. I. (2021). COVID-19 anxiety and organizational commitment among front-line nurses: Perceived role of nurse managers' caring behavior. Nursing Practice Today. doi:10.18502/npt.v9i1.7328

Ahmed, O., Faisal, R. A., Sharker, T., Lee, S. A., & Jobe, M. C. (2022). Adaptation of the Bangla version of the COVID-19 anxiety scale. International Journal of Mental Health and Addiction, 20(1), 284–295. doi:10.1007/s11469-020-00357-2

Ahn, J., Lee, J., Hong, Y., Park, J., & Chung, S. (2021). Stress and anxiety to Viral Epidemics-6 for medical students: Psychometric properties of the anxiety measure for the COVID-19 pandemic. Frontiers in Psychiatry, 12, 705805. doi:10.3389/fpsyt.2021.705805

Ahn, M. H., Lee, J., Suh, S., Lee, S., Kim, H. J., Shin, Y.-W., & Chung, S. (2020). Application of the Stress and anxiety to Viral Epidemics-6 (SAVE-6) and Coronavirus Anxiety Scale (CAS) to measure anxiety in cancer patient in response to COVID-19. Frontiers in Psychology, 11, 604441. doi:10.3389/fpsyg.2020.604441

Ahorsu, D. K., Lin, C.-Y., Imani, V., Saffari, M., Griffiths, M. D., and Pakpour, A. H. (2020). The Fear of COVID-19 Scale: Development and Initial Validation. In International Journal of Mental Health and Addiction (Vol. 20, Issue 3, pp. 1537–1545). Springer Science and Business Media LLC. https://doi.org/10.1007/s11469-020-00270-8.

Akyildiz, D., & Durna, S. (2021). Determining the research status and coronavirus anxiety scores of academics during the flexible working arrangements initiated after the COVID-19 pandemic. Journal of Taibah University Medical Sciences, 16(3), 336–343. doi:10.1016/j.jtumed.2021.01.005

Alenko, A., Agenagnew, L., Beressa, G., Tesfaye, Y., Woldesenbet, Y. M., & Girma, S. (2021). COVID-19-related anxiety and its association with dietary diversity score among health care professionals in Ethiopia: A web-based survey. Journal of Multidisciplinary Healthcare, 14, 987–996. doi:10.2147/JMDH.S305164

Al-Rawashdeh, S., Mrayyan, M. T., Abu Khait, A., & Rababa, M. (2022). Differences in cyberchondria, internet addiction, anxiety sensitivity,

health anxiety, and Coronavirus anxiety among students: A web-based comparative survey. Electronic Journal of General Medicine, 19(3), em371. doi:10.29333/ejgm/11876

Aydın, A., Kulakaç, N., & Aydın Sayılan, A. (2021). The effect of COVID-19 anxiety levels of healthcare professionals on the quality of working life and related factors. International Journal of Clinical Practice, 75(12), e14889. doi:10.1111/ijcp.14889

Baka, Ł. (2021). Coronavirus anxiety and exhaustion among Polish front-line healthcare workers - the mediation effect of insomnia. International Journal of Occupational Medicine and Environmental Health, 34(2), 263–273. doi:10.13075/ijomeh.1896.01745

Barry, A. E., Chaney, B., Piazza-Gardner, A. K., & Chavarria, E. A. (2013). Validity and Reliability Reporting Practices in the Field of Health Education and Behavior. In Health Education & Behavior (Vol. 41, Issue 1, pp. 12–18). SAGE Publications. https://doi.org/10.1177/1090198113483139

Bekar, P., Erkul, M., & Efe, E. (2022). Investigation of coronavirus anxiety and caregiving burden among the parents of children with cancer during the COVID-19 outbreak: A descriptive and cross-sectional study. European Journal of Cancer Care, 31(4), e13600. doi:10.1111/ecc.13600

Bolstad WM. (2007). Introduction to Bayesian Statistics, Wiley-Interscience, UK.

Bonett, D. G. (2002). Sample Size Requirements for Testing and Estimating Coefficient Alpha. In Journal of Educational and Behavioral Statistics (Vol. 27, Issue 4, pp. 335–340). American Educational Research Association (AERA). https://doi.org/10.3102/10769986027004335

Brannick, M. T., and Zhang, N. (2013). Bayesian meta-analysis of coefficient alpha. In Research Synthesis Methods (Vol. 4, Issue 2, pp. 198–207). Wiley. https://doi.org/10.1002/jrsm.1075

Broche-Pérez, Y., Fernández-Castillo, E., Fernández-Fleites, Z., Jiménez-Puig, E., Vizcaíno-Escobar, A., Ferrer-Lozano, D., … Martín-González, R. (2022). Adaptation of the Cuban version of the Coronavirus Anxiety Scale. Death Studies, 46(3), 603–607. doi:10.1080/07481187.2020.1855610

Brooks, S. K., Webster, R. K., Smith, L. E., Woodland, L., Wessely, S., Greenberg, N., & Rubin, G. J. (2020). The psychological impact of quarantine and how to reduce it: rapid review of the evidence. In The Lancet (Vol. 395, Issue 10227, pp. 912–920). Elsevier BV. https://doi.org/10.1016/s0140-6736(20)30460-8

Çakmak, G., & Öztürk, Z. A. (2021). Being both a parent and a healthcare worker in the pandemic: Who could be exhausted more? Healthcare (Basel, Switzerland), 9(5), 564. doi:10.3390/healthcare9050564

Caycho-Rodríguez, T., Vilca, L. W., Carbajal-León, C., White, M., Vivanco-Vidal, A., Saroli-Araníbar, D., … Moreta-Herrera, R. (2022). Coronavirus Anxiety Scale: New psychometric evidence for the Spanish version based on CFA and IRT models in a Peruvian sample. Death Studies, 46(5), 1090–1099. doi:10.1080/07481187.2020.1865480

Caycho-Rodríguez, T., Vilca, L. W., Peña-Calero, B. N., Barboza-Palomino, M., White, M., & Reyes-Bossio, M. (2022). Measurement of coronaphobia in older adults: Validation of the Spanish version of the Coronavirus Anxiety Scale. Revista Espanola de Geriatria y Gerontologia, 57(1), 20–27. doi:10.1016/j.regg.2021.09.001

Caycho-Rodríguez, T., Vilca, L. W., Plante, T. G., Vivanco-Vidal, A., Saroli-Araníbar, D., Carbajal-León, C., … White, M. (2022). Strength of religious faith in Peruvian adolescents and adults: Psychometric evidence from the original and short versions of the Santa Clara Strength of Religious Faith Questionnaire in Spanish. Pastoral Psychology, 71(3), 399–418. doi:10.1007/s11089-021-00972-3

Chen, J. H., Tong, K. K., Su, X., Yu, E. W.-Y., & Wu, A. M. S. (2021). Measuring COVID-19 related anxiety and obsession: Validation of the Coronavirus Anxiety Scale and the Obsession with COVID-19 Scale in a probability Chinese sample. Journal of Affective Disorders, 295, 1131–1137. doi:10.1016/j.jad.2021.08.104

Choi, E., Lee, J., & Lee, S. A. (2022). Validation of the Korean version of the obsession with COVID-19 scale and the Coronavirus anxiety scale. Death Studies, 46(3), 608–614. doi:10.1080/07481187.2020.1833383

Chorwe-Sungani, G. (2021). Assessing COVID-19-related anxiety and functional impairment amongst nurses in Malawi. African Journal of Primary Health Care & Family Medicine, 13(1), e1–e6. doi:10.4102/phcfm.v13i1.2823

Cronbach LJ. (1951). Coefficient Alpha and the Internal Structure of Tests. Psychometrika.

Daniels, M. J. (1999). A prior for the variance in hierarchical models. In Canadian Journal of Statistics (Vol. 27, Issue 3, pp. 567–578). Wiley. https://doi.org/10.2307/3316112

Diógenes de Medeiros, E., Gregório Nascimento da Silva, P., Mota Reis, L., P Monteiro, R., Lins de Holanda Coelho, G., Lohana Cardoso Guimarães, C., & C Bezerra de Medeiros, P. (2022). Psychometric properties of the

Coronavirus Anxiety Scale (CAS) in Brazil. Death Studies, 46(10), 2424–2434. doi:10.1080/07481187.2021.1961175

Evren, C., Evren, B., Dalbudak, E., Topcu, M., & Kutlu, N. (2022). Measuring anxiety related to COVID-19: A Turkish validation study of the Coronavirus Anxiety Scale. Death Studies, 46(5), 1052–1058. doi:10.1080/07481187.2020.1774969

Feldt, L. S. (1965). The approximate sampling distribution of Kuder-Richardson reliability coefficient twenty. In Psychometrika (Vol. 30, Issue 3, pp. 357–370). Springer Science and Business Media LLC. https://doi.org/10.1007/bf02289499

Fjermestad, K. W., Orm, S., Silverman, W. K., & Cogo-Moreira, H. (2022). Short report: COVID-19-related anxiety is associated with mental health problems among adults with rare disorders. Research in Developmental Disabilities, 123(104181), 104181. doi:10.1016/j.ridd.2022.104181

Flake, J. K., Pek, J., and Hehman, E. (2017). Construct Validation in Social and Personality Research. In Social Psychological and Personality Science (Vol. 8, Issue 4, pp. 370–378). SAGE Publications. https://doi.org/10.1177/1948550617693063

García-Reyna, B., Castillo-García, G. D., Barbosa-Camacho, F. J., Cervantes-Cardona, G. A., Cervantes-Pérez, E., Esparza-Estrada, I., … Cervantes-Guevara, G. (2022). Anxiety and COVID-19: Coronavirus Anxiety Scale scores in medical and non-medical personnel in urban hospitals in Guadalajara. A cross-sectional survey study. Death Studies, 46(3), 581–589. doi:10.1080/07481187.2021.1936297

Gelman, A. (2006). Prior distributions for variance parameters in hierarchical models (comment on article by Browne and Draper). In Bayesian Analysis (Vol. 1, Issue 3). Institute of Mathematical Statistics. https://doi.org/10.1214/06-ba117a

Godoy, L. D., Falcoski, R., Incrocci, R. M., Versuti, F. M., & Padovan-Neto, F. E. (2021). The psychological impact of the COVID-19 pandemic in remote learning in higher education. Education Sciences, 11(9), 473. doi:10.3390/educsci11090473

Graham, J. M., & Unterschute, M. S. (2014). A Reliability Generalization Meta-Analysis of Self-Report Measures of Adult Attachment. In Journal of Personality Assessment (Vol. 97, Issue 1, pp. 31–41). Informa UK Limited. https://doi.org/10.1080/00223891.2014.927768

Hajek, A., & König, H.-H. (2023). Prevalence and correlates of coronavirus anxiety in Germany: Results of a nationally representative survey. Death Studies, 47(3), 287–295. doi:10.1080/07481187.2022.2059722

Hakstian, A. R., & Whalen, T. E. (1976). A k-sample significance test for independent alpha coefficients. In Psychometrika (Vol. 41, Issue 2, pp. 219–231). Springer Science and Business Media LLC. https://doi.org/10.1007/bf02291840

Hartung, J. (1999). An Alternative Method for Meta-Analysis. In Biometrical Journal (Vol. 41, Issue 8, pp. 901–916). Wiley. https://doi.org/10.1002/(sici)1521-4036(199912)41:8<901::aid-bimj901>3.0.co;2-w

Hawryluck, L., Gold, W. L., Robinson, S., Pogorski, S., Galea, S., & Styra, R. (2004). SARS Control and Psychological Effects of Quarantine, Toronto, Canada. In Emerging Infectious Diseases (Vol. 10, Issue 7, pp. 1206–1212). Centers for Disease Control and Prevention (CDC). https://doi.org/10.3201/eid1007.030703

Huremović, D. (Ed.). (2019). Psychiatry of Pandemics. Springer International Publishing. https://doi.org/10.1007/978-3-030-15346-5

Işik, N. A., Çelik, G. K., & Ayran, G. (2022). Turkish validity and reliability of coronavirus anxiety scale. Current Psychology (New Brunswick, N.J.), 41(8), 5612–5620. doi:10.1007/s12144-021-02552-3

Karaahmet, E., Angın, Ü., Yılmaz, O., Deniz, D., & Konuk, N. (2022). Assessment of psychometric characteristics of the Coronavirus Anxiety Scale in patients with preexisting psychiatric disorders. Death Studies, 46(3), 569–573. doi:10.1080/07481187.2021.1876184

Karaca, P. P., Koyucu, R. G., & Aksu, S. Ç. (2022). The relatıonshıp between pregnant women's anxıety levels about coronavırus and prenatal attachment. Archives of Psychiatric Nursing, 36, 78–84. doi:10.1016/j.apnu.2021.12.001

Kasapoğlu, F. (2022). The relationship among spirituality, self-efficacy, COVID-19 anxiety, and hopelessness during the COVID-19 process in Turkey: A path analysis. Journal of Religion and Health, 61(1), 767–785. doi:10.1007/s10943-021-01472-7

Kim H-C, Yoo S-Y, Lee B-H, Lee SH, Shin H-S. (2018). Psychiatric findings in suspected and confirmed Middle East respiratory syndrome patients quarantined in hospital: a retrospective chart analysis. Psychiatry Investig. 15(4):355–60. https://doi. org/10.30773/pi.2017.10.25.1

Kim, H., Kim, H., Lee, H. J., Cho, E., Koh, S.-J., Ahmed, O., & Chung, S. (2022). The validation study of the Stress and anxiety to Viral Epidemics-6 scale among patients with cancer in the COVID-19 pandemic. Frontiers in Psychiatry, 13, 811083. doi:10.3389/fpsyt.2022.811083

Kiyak, S., & Türkben Polat, H. (2022). The relationship between death anxiety and COVID-19 fear and anxiety in women with breast cancer. Omega, 302228221086056. doi:10.1177/00302228221086056

Kristof, W. (1963). The statistical theory of stepped-up reliability coefficients when a test has been divided into several equivalent parts. In Psychometrika (Vol. 28, Issue 3, pp. 221–238). Springer Science and Business Media LLC. https://doi.org/10.1007/bf02289571

Kubb, C., & Foran, H. M. (2020). Measuring COVID-19 related anxiety in parents: Psychometric comparison of four different inventories. JMIR Mental Health, 7(12), e24507. doi:10.2196/24507

Labrague, L. J., & De Los Santos, J. A. A. (2021). Prevalence and predictors of coronaphobia among frontline hospital and public health nurses. Public Health Nursing (Boston, Mass.), 38(3), 382–389. doi:10.1111/phn.12841

Lee, A. M., Wong, J. G., McAlonan, G. M., Cheung, V., Cheung, C., Sham, P. C., Chu, C.-M., Wong, P.-C., Tsang, K. W., & Chua, S. E. (2007). Stress and Psychological Distress among SARS Survivors 1 Year after the Outbreak. In The Canadian Journal of Psychiatry (Vol. 52, Issue 4, pp. 233–240). SAGE Publications. https://doi.org/10.1177/070674370705200405

Lee, S. A. (2020). Coronavirus Anxiety Scale: A brief mental health screener for COVID-19 related anxiety. In Death Studies (Vol. 44, Issue 7, pp. 393–401). Informa UK Limited. https://doi.org/10.1080/07481187.2020.1748481

Lee, S. A. (2020). Coronavirus Anxiety Scale: A brief mental health screener for COVID-19 related anxiety. Death Studies, 44(7), 393–401. doi:10.1080/07481187.2020.1748481

Lee, S. A. (2020). Replication analysis of the Coronavirus anxiety scale. Düşünen Adam Psikiyatri ve Nörolojik Bilimler Dergisi. doi:10.14744/dajpns.2020.00079

Lee, S. A., Jobe, M. C., Mathis, A. A., & Gibbons, J. A. (2020). [Review of Incremental validity of coronaphobia: Coronavirus anxiety explains depression, generalized anxiety, and death anxiety]. Journal of anxiety disorders, 74(102268), 102268. doi:10.1016/j.janxdis.2020.102268

Lee, S. A., Mathis, A. A., Jobe, M. C., & Pappalardo, E. A. (2020). Clinically significant fear and anxiety of COVID-19: A psychometric examination of the Coronavirus Anxiety Scale. Psychiatry Research, 290(113112), 113112. doi:10.1016/j.psychres.2020.113112

Lieven, T. (2021). Global validation of the Coronavirus Anxiety Scale (CAS). Current Psychology (New Brunswick, N.J.), 1–11. doi:10.1007/s12144-021-02583-w

Liu, X., Kakade, M., Fuller, C. J., Fan, B., Fang, Y., Kong, J., Guan, Z., & Wu, P. (2012). Depression after exposure to stressful events: lessons learned from the severe acute respiratory syndrome epidemic. In Comprehensive Psychiatry (Vol. 53, Issue 1, pp. 15–23). Elsevier BV. https://doi.org/10.1016/j.comppsych.2011.02.003

Madden, M., Kneavel, M. E., & Bowman, T. G. (2022). Lessons learned and potential long-term effects on athletic trainers and clinical practice after a global pandemic. Journal of Athletic Training, 57(11–12), 1111–1121. doi:10.4085/1062-6050-0541.21

Magano, J., Vidal, D. G., Sousa, H. F. P. E., Dinis, M. A. P., & Leite, Â. (2021). Validation and psychometric properties of the Portuguese version of the Coronavirus Anxiety Scale (CAS) and fear of COVID-19 Scale (FCV-19S) and associations with travel, tourism and hospitality. International Journal of Environmental Research and Public Health, 18(2), 427. doi:10.3390/ijerph18020427

Majeed, S., Schwaiger, E. M., Nazim, A., & Samuel, I. S. (2021). The psychological impact of COVID-19 among Pakistani adults in Lahore. Frontiers in Public Health, 9. doi:10.3389/fpubh.2021.578366

McElroy, E., Patalay, P., Moltrecht, B., Shevlin, M., Shum, A., Creswell, C., & Waite, P. (2020). Demographic and health factors associated with pandemic anxiety in the context of COVID-19. In British Journal of Health Psychology (Vol. 25, Issue 4, pp. 934–944). Wiley. https://doi.org/10.1111/bjhp.12470

Monterrosa-Blanco, A., Monterrosa-Castro, Á., & González-Sequeda, A. (2021). Online assessment of the perception of loneliness and associated factors in Colombian climacteric women during the COVID-19 pandemic: A cross-sectional study. Health Promotion Perspectives, 11(2), 230–239. doi:10.34172/hpp.2021.28

Monterrosa-Castro, Á., Monterrosa-Blanco, A., & González-Sequeda, A. (2021). Perceived loneliness and severe sleep disorders in adult women during the covid-19 quarantine: A cross-sectional study in Colombia. Journal of Primary Care & Community Health, 12, 21501327211025170. doi:10.1177/21501327211025170

Mora-Magaña, I., Lee, S. A., Maldonado-Castellanos, I., Jiménez-Gutierrez, C., Mendez-Venegas, J., Maya-Del-Moral, A., … Jobe, M. C. (2022). Coronaphobia among healthcare professionals in Mexico: A

psychometric analysis. Death Studies, 46(2), 280–289. doi:10.1080/07481187.2020.1808762

Nazari, N., Hernández, R. M., Ocaña-Fernandez, Y., & Griffiths, M. D. (2022). Psychometric validation of the Persian self-Compassion Scale Youth version. Mindfulness, 13(2), 385–397. doi:10.1007/s12671-021-01801-7

Nazari, N., Zekiy, A. O., Feng, L.-S., & Griffiths, M. D. (2022). Psychometric validation of the Persian version of the COVID-19-Related Psychological Distress Scale and association with COVID-19 Fear, COVID-19 anxiety, optimism, and lack of resilience. International Journal of Mental Health and Addiction, 20(5), 2665–2680. doi:10.1007/s11469-021-00540-z

Nikčević, A. V., & Spada, M. M. (2020). The COVID-19 anxiety syndrome scale: Development and psychometric properties. Psychiatry Research, 292(113322), 113322. doi:10.1016/j.psychres.2020.113322

Nikčević, A. V., Marino, C., Kolubinski, D. C., Leach, D., & Spada, M. M. (2021). Modelling the contribution of the Big Five personality traits, health anxiety, and COVID-19 psychological distress to generalised anxiety and depressive symptoms during the COVID-19 pandemic. Journal of Affective Disorders, 279, 578–584. doi:10.1016/j.jad.2020.10.053

Okada, K. (2015). Bayesian meta-analysis of Cronbach's coefficient alpha to evaluate informative hypotheses. In Research Synthesis Methods (Vol. 6, Issue 4, pp. 333–346). Wiley. https://doi.org/10.1002/jrsm.1155

Padovan-Neto, F. E., Lee, S. A., Guimarães, R. P., Godoy, L. D., Costa, H. B., Zerbini, F. L. S., & Fukusima, S. S. (2023). Brazilian adaptation of the Coronavirus Anxiety Scale: A psychometric investigation of a measure of coronaphobia. Omega, 86(3), 769–787. doi:10.1177/0030222821991325

Parla Meva, D., & Güzide, S. (2021). Characteristics and Coronavirus anxiety levels of endodontic patients during the covid-19 pandemic. Clinical and Experimental Health Sciences. doi:10.33808/clinexphealthsci.938847

Pekárová, V., Rajčániová, E., & Tomšik, R. (2023). Slovak adaptation of the Coronavirus Anxiety Scale. Death Studies, 47(2), 172–182. doi:10.1080/07481187.2022.2039812

Peter JP. Reliability: A review of psychometric basics and recent marketing practices. Journal of Marketing Research. 1979; 16 (1): 6-17. DOI:10.2307/3150868

Peterson, R. A. (1994). A Meta-Analysis of Cronbach's Coefficient Alpha. In Journal of Consumer Research (Vol. 21, Issue 2, p. 381). Oxford University Press (OUP). https://doi.org/10.1086/209405

Polson, N. G., & Scott, J. G. (2012). On the Half-Cauchy Prior for a Global Scale Parameter. In Bayesian Analysis (Vol. 7, Issue 4). Institute of Mathematical Statistics. https://doi.org/10.1214/12-ba730

Prazeres, F., Passos, L., Simões, J. A., Simões, P., Martins, C., & Teixeira, A. (2020). COVID-19-related fear and anxiety: Spiritual-religious coping in healthcare workers in Portugal. International Journal of Environmental Research and Public Health, 18(1), 220. doi:10.3390/ijerph18010220

Sánchez-Meca, J., Rubio-Aparicio, M., Núñez-Núñez, R. M., López-Pina, J., Marín-Martínez, F., & López-López, J. A. (2017). A Reliability Generalization Meta-Analysis of the Padua Inventory of Obsessions and Compulsions. In The Spanish Journal of Psychology (Vol. 20). Cambridge University Press (CUP). https://doi.org/10.1017/sjp.2017.65

Sijtsma, K. (2008). On the Use, the Misuse, and the Very Limited Usefulness of Cronbach's Alpha. In Psychometrika (Vol. 74, Issue 1, pp. 107–120). Springer Science and Business Media LLC. https://doi.org/10.1007/s11336-008-9101-0

Singh, K.D. (2021). Coronavirus anxiety scale: A validation study in an Indian population. Medical Journal of Dr. D.Y. Patil Vidyapeeth, 14, 303 - 307.

Skalski, S., Uram, P., Dobrakowski, P., & Kwiatkowska, A. (2021). The link between ego-resiliency, social support, SARS-CoV-2 anxiety and trauma effects. Polish adaptation of the Coronavirus Anxiety Scale. Personality and Individual Differences, 171(110540), 110540. doi:10.1016/j.paid.2020.110540

Taylor, S., Landry, C. A., Paluszek, M. M., Fergus, T. A., McKay, D., & Asmundson, G. J. G. (2020). Development and initial validation of the COVID Stress Scales. In Journal of Anxiety Disorders (Vol. 72, p. 102232). Elsevier BV. https://doi.org/10.1016/j.janxdis.2020.102232

Tülüce, D., & Kaplan Serin, E. (2022). The death anxiety experienced by cardiac patients in the covid-19 pandemic and its affecting factors. Omega, 302228221093461. doi:10.1177/00302228221093461

Vacha-Haase, T. (1998). Reliability Generalization: Exploring Variance in Measurement Error Affecting Score Reliability Across Studies. In Educational and Psychological Measurement (Vol. 58, Issue 1, pp. 6–20). SAGE Publications. https://doi.org/10.1177/0013164498058001002

Vally, Z., & Alowais, A. (2021). Measuring anxiety related to COVID-19: Factor analysis and psychometric properties of the Arabic Coronavirus Anxiety Scale. PloS One, 16(11), e0260355. doi:10.1371/journal.pone.0260355

van de Venter, R., Williams, R., Stindt, C., & Ten Ham-Baloyi, W. (2021). Coronavirus-related anxiety and fear among South African diagnostic radiographers working in the clinical setting during the pandemic. Journal of Medical Imaging and Radiation Sciences, 52(4), 586–594. doi:10.1016/j.jmir.2021.09.016

Viechtbauer, W. (2010). Conducting Meta-Analyses inRwith themetaforPackage. In Journal of Statistical Software (Vol. 36, Issue 3). Foundation for Open Access Statistic. https://doi.org/10.18637/jss.v036.i03

Vinaccia, S., Bahamón, M. J., Trejos-Herrera, A. M., Lee, S. A., Quiceno, J. M., Gómez, C. A., … Pelaez, E. C. (2022). Validating the Coronavirus Anxiety Scale in a Colombian sample. Death Studies, 46(10), 2366–2375. doi:10.1080/07481187.2021.1944401

Vismara, M., Vitella, D., Biolcati, R., Ambrosini, F., Pirola, V., Dell'Osso, B., & Truzoli, R. (2021). The impact of COVID-19 pandemic on searching for health-related information and Cyberchondria on the general population in Italy. Frontiers in Psychiatry, 12, 754870. doi:10.3389/fpsyt.2021.754870

Watson, J. D., & Crick, F. H. C. (1953). Molecular Structure of Nucleic Acids: A Structure for Deoxyribose Nucleic Acid. In Nature (Vol. 171, Issue 4356, pp. 737–738). Springer Science and Business Media LLC. https://doi.org/10.1038/171737a0

Wilczyńska, D., Li, J., Yang, Y., Fan, H., Liu, T., & Lipowski, M. (2021). Fear of COVID-19 changes the motivation for physical activity participation: Polish-Chinese comparisons. Health Psychology Report, 9(2), 138–148. doi:10.5114/hpr.2021.105007

Worldometers, 2022. https://www.worldometers.info/coronavirus/, Access to date: September, 16, 2022.

Wu, X., Nazari, N., & Griffiths, M. D. (2021). Using fear and anxiety related to COVID-19 to predict cyberchondria: Cross-sectional survey study. Journal of Medical Internet Research, 23(6), e26285. doi:10.2196/26285

Xiang, Y.-T., Yang, Y., Li, W., Zhang, L., Zhang, Q., Cheung, T., & Ng, C. H. (2020). Timely mental health care for the 2019 novel coronavirus outbreak is urgently needed. In The Lancet Psychiatry (Vol. 7, Issue 3, pp. 228–229). Elsevier BV. https://doi.org/10.1016/s2215-0366(20)30046-8

Chapter 2

Recent Developments of Furocoumarin Derivatives (2020-2023)

Gönül YILDIZ[1] , Rahmi KASIMOĞULLARI[2]

[1] Responsible Author, Research Assistant, Faculty of Arts and Sciences/Department of Chemistry, Kütahya Dumlupınar University, Kütahya, Turkey, e-mail: gonul.yildiz@dpu.edu.tr, ORCID No: 0000-0002-1886-5964

[2] Professor Dr., Faculty of Arts and Sciences/Department of Chemistry, Kütahya Dumlupınar University, Kütahya, Turkey, e-mail: rahmi.kasimogullari@dpu.edu.tr, ORCID No: 0000-0001-6391-7121

ABSTRACT

Furocoumarins, also known as psoralens, are important compounds due to their various biological and pharmacological properties. Here are some of the key aspects of their importance:

Medical Applications: Furocoumarins have been used in medicine for the treatment of certain skin conditions, such as psoriasis and vitiligo. They are used in phototherapy, often in combination with ultraviolet (UV) light, in a treatment known as PUVA (Psoralen plus UV-A) therapy.

Photosensitivity: Furocoumarins can cause photosensitivity in humans and animals. When these compounds come into contact with the skin and are exposed to UV light, they can induce a phototoxic reaction, resulting in skin inflammation and damage. This reaction is known as phytophotodermatitis and can occur after contact with certain plants containing furocoumarins.

Phytochemicals: Furocoumarins are often found in various plants, particularly in the *Apiaceae* (Formerly Umbelliferae) family. They serve as secondary metabolites that can help protect plants from UV radiation and predators. Additionally, they are involved in the photoregulation of plant growth and development.

Chemotherapy: Furocoumarins have been studied for their potential anticancer properties. Some furocoumarins have shown cytotoxic effects on cancer cells and are being researched for their role in cancer chemotherapy.

Antibacterial Properties: Some furocoumarins have demonstrated antibacterial activity and are being explored for their potential in developing new antibiotics.

Anti-inflammatory Effects: Certain furocoumarins have anti-inflammatory properties and may be useful in the treatment of inflammatory conditions.

Phototoxicity Research: Furocoumarins have been extensively studied for their phototoxic properties, which can cause skin reactions when exposed to UV light. This research has led to a better understanding of the mechanisms behind phototoxicity and the development of safety guidelines for their use in medicine and cosmetics.

Cosmetics and Perfumes: Some furocoumarins are used in the fragrance industry due to their pleasant odor. However, their use in cosmetics and perfumes is regulated to ensure that phototoxicity risks are minimized.

Keywords: Coumarin, Furan, Furocoumarin, Psoralen, Biological Activity.

1. INTRODUCTION

Coumarins, which chemically belong to the subgroup of lactones, are defined as 1,2-benzopyrone or *o*-hydroxycinnamic acid-8-lactone. Natural coumarins can be divided into six basic groups: simple coumarins, bicoumarins, pyrano coumarins (linear type and angular type), furocoumarins, phenyl coumarins, and dihydrofurano coumarins (Lonˇcari´c, 2020).

Furans are heterocyclic aromatic compounds that are formed as products or intermediates in heat-dependent reactions (Anese, 2013). Furthermore, furans are heterocyclic organic compounds formed in various heated foods through the thermal decomposition of natural food components (Mogol, 2016).

Furan and coumarin compounds are widely available in biologically active natural products and different synthetic materials. They are also very important compounds in organic synthesis and medicinal chemistry. The fusion of a coumarin ring with a furan ring gives rise to a unique and valuable class of heterocyclic compounds called furocoumarins. Combining the coumarin and furan groups in a single polycyclic frame provides furocoumarins with a highly aromatic structure, and biologically active, even unprecedented, pharmaceutical properties (Chen, 2023).

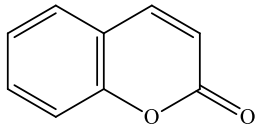

2*H*-chromen-2-one
(Coumarin)

furan

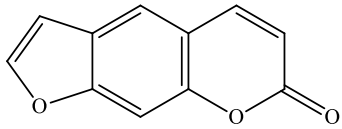

7*H*-furo[3,2-*g*]chromen-7-one
(Furanocoumarin)

By fusing the furan ring into various shapes, several different isomers of the furocoumarin can be produced. The main compounds of the most common isomers are psoralen and angelicin **(Figure 1).** Derivatives of these two compounds are called linear and angular furocoumarins, respectively, because they exhibit linear or angular chemical structures (Zou, 2023).

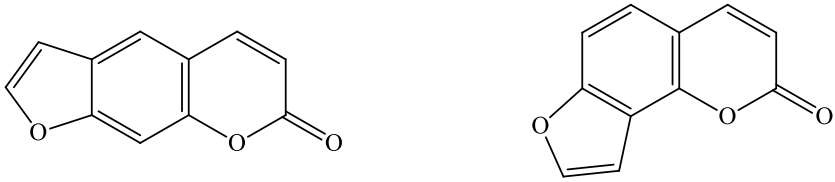

Psoralen Angelicin

Fig. 1. Two furocoumarin isomers

Psoralens are a subgroup of furocoumarins and are known for their phototoxic properties. They can be found in a variety of plants, such as celery, parsley, and figs. When exposed to UV light, psoralens can become activated and bind to DNA, leading to the formation of DNA adducts. This can result in skin reactions and increased sensitivity to UV radiation, a condition known as phototoxicity. Psoralens have been used in phototherapy for treating certain skin conditions like psoriasis (Bonamonte, 2010).

Angelicins are another subgroup of furocoumarins and are also known for their phototoxic effects. They can be found in plants like parsnips and dill. Like psoralens, angelicins can react with DNA upon exposure to UV light, leading to DNA damage and skin reactions (Mahendra, 2020).

Furocoumarin compounds have a wide range of biological and pharmaceutical properties, cytotoxic, including insecticidal, photosensitizing, antifungal, and antibacterial activities. This property makes them one of the most widely available of biologically active natural products. Today, they are of great interest in medical applications and are increasingly being studied. Although some synthetic methods for furocoumarins have been known for a long time, significant efforts have been made in the last few years to develop new methods for the efficient preparation of this class of compounds (Cadierno, 2015).

2. SOME FUROCOUMARIN DERIVATIVES

Theoretically, the c, f, g, or h bonds of the coumarin part can be combined with the 2,3-, 3,2- or 3,4-positions of the furan ring, severally, to form many linear structures or angular isomer derivatives of furocoumarins (Singh, 2022).

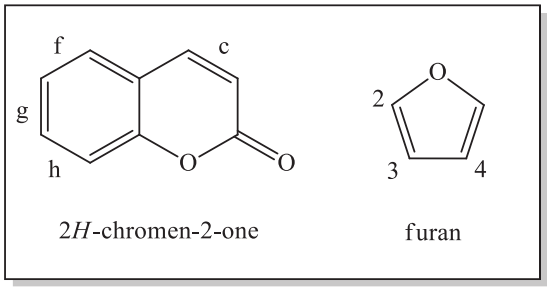

2*H*-chromen-2-one furan

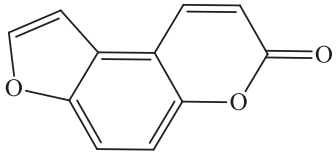

7*H*-furo[3,2-*f*]chromen-7-one

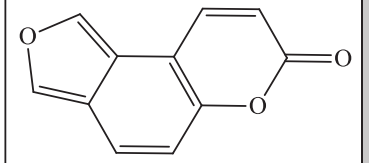

7*H*-furo[3,4-*f*]chromen-7-one

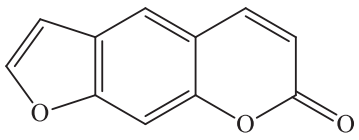
7*H*-furo[3,2-*g*]chromen-7-one

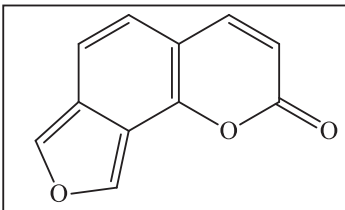
2*H*-furo[3,4-*h*]chromen-2-one

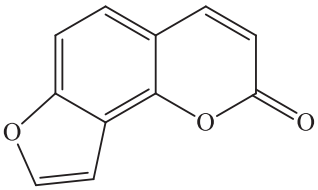
2*H*-furo[2,3-*h*]chromen-2-one

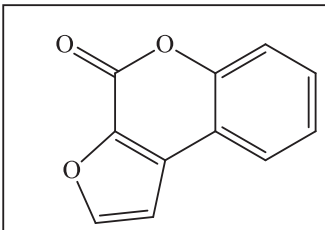
4*H*-furo[2,3-*c*]chromen-4-one

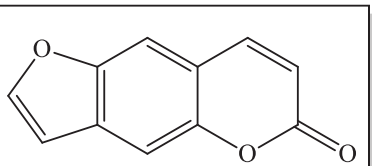
6*H*-furo[2,3-*g*]chromen-6-one

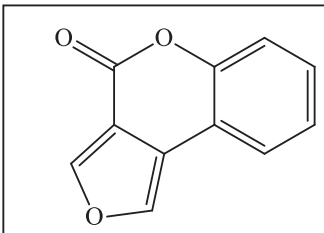
4*H*-furo[3,4-*c*]chromen-4-one

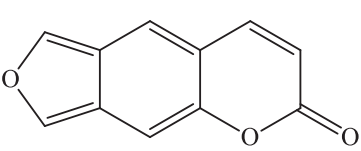
2*H*-furo[3,4-*g*]chromen-2-one

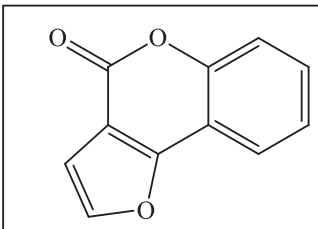
4*H*-furo[3,2-*c*]chromen-4-one

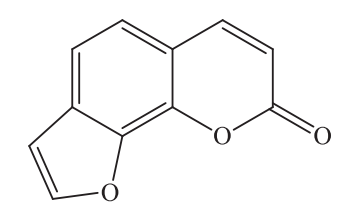
8*H*-furo[3,2-*h*]chromen-8-one

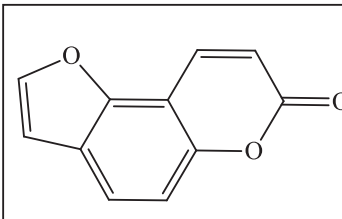
7*H*-furo[2,3-*f*]chromen-7-one

It's important to note that the synthesis and study of furocoumarin derivatives are ongoing, and researchers continue to explore their potential pharmacological properties, including anticancer, antibacterial, and anti-inflammatory activities. The structural modifications to furocoumarins aim to enhance their efficacy and reduce potential side effects. These derivatives play a role in pharmaceutical research and drug development as scientists seek new compounds with therapeutic potential.

3. RECENT ADVANCES in FUROCOUMARINS SYNTHESIS

Elinson *et al.* (2022) synthesized substituted unsymmetric spirobarbituric 2,3-dihydro-4*H*-furo[2,3-*c*]chromen-4-ones compounds with 72–83% efficiency as a result of the rapid and effective cascade selective electrocatalytic approach of the 4-hydroxy-2-oxo-2*H*-chromen-6-ylium compound with benzylidenebarbiturates. Based on the screened molecular docking data, it was concluded that all synthesized compounds are important for various medical applications, like pain control, breast cancer treatment, and treatment of hypertension, obesity, epilepsy, diabetes, and cardiovascular disease (Elinson, 2022).

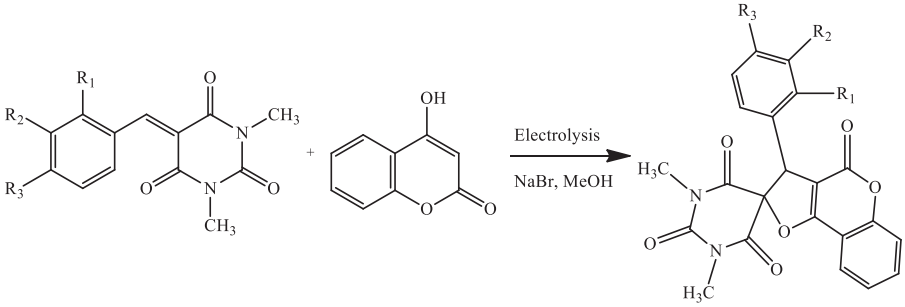

R_1: H, Me, Br
R_2: H, NO_2
R_3: H, OMe, Cl, Br, NO_2, CO_2Me

Pelipko *et al.* (2022) synthesized new 4-oxo-4*H*-furo[3,2-*c*]pyran-3-carboxylates derivatives in a short time and with high efficiency based on 3-bromo-3-nitroacrylates compounds (Pelipko, 2022).

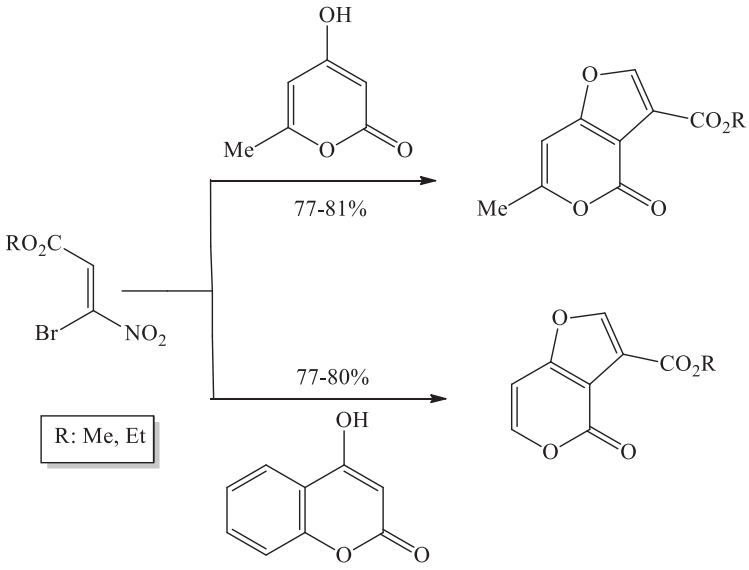

Lei *et al* (2023) synthesized 28 new furo[3,2-*c*]coumarin derivative compounds as a result of the reaction of 4-hydroxycoumarin derivatives and 4-ethynyl-4-methyl-1,3-dioxolan-2-one derivative compounds. When determining the method, the reaction conditions were optimized by testing varied Cu salts, solvents, and bases. Using $Cu(ClO_4)_2 \cdot 6H_2O$ as salt, DCM as a solvent, and DIPEA as a base, compound 3-(hydroxymethyl)-2-methylene-3-phenyl-2*H*-furo[3,2-*c*]chromen-4(3*H*)-one was synthesized with %98 efficiency (Lei, 2023).

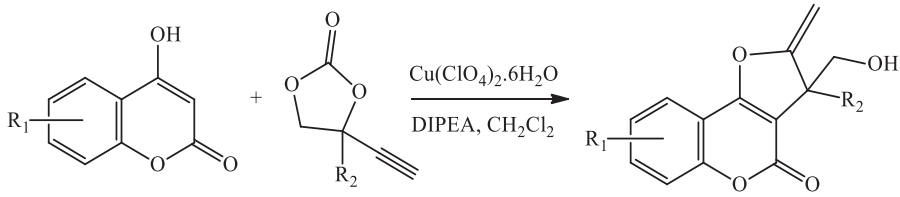

R_1: 6-Me, 6-OMe, 6-Br, 6-Cl, 7-Me, 7-OMe, 7-Br, 7-F, 8-Me, 8-'Bu, 5,8-diMe
R_2: 4-MeC_6H_4, 4-$MeOC_6H_4$, 4-ClC_6H_4, 4-$CF_3C_6H_4$, 3-MeC_6H_4, 3-$MeOC_6H_4$, 3-ClC_6H_4, 3-BrC_6H_4, 3-$CF_3C_6H_4$, 2-$MeOC_6H_4$, 2-FC_6H_4, 2-Py, 2-Furyl, 2-Thienyl, Me, Cyclohexyl

4.INVESTIGATION of THE PHARMACEUTICAL and BIOLOGICAL ACTIVITIES of FUROCOUMARIN DERIVATIVES

According to Xie *et al*. eleven 5-Schiff base-substituted furocoumarin derivatives were prepared and tested *in vitro* for the promotion of melanin production in B16 cells and antibacterial properties against three types of

bacteria. The findings showed this when compared with 8-MOP (positive control, activation rate 136%), a significant increase of more than 1.7 times in the amount of melanin was observed with compound (*Z*)-5-(4-hydroxystyryl)-7*H*-furo[3,2-*g*]chromen-7-one (237%). Equally impressive, compound 7-oxo-7*H*-furo[3,2-*g*]chromene-5-carbaldehyde not only showed greater activity against *C. albicans* than the positive control (Amphotericin B) but also had wide-spectrum antibacterial activity against *E. coli* and *S. aureus* (Xie, 2020).

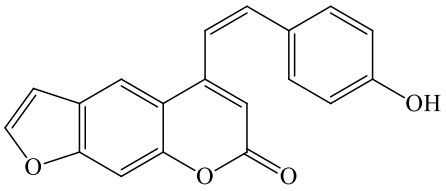

(*Z*)-5-(4-hydroxystyryl)-7*H*-furo[3,2-*g*]chromen-7-one

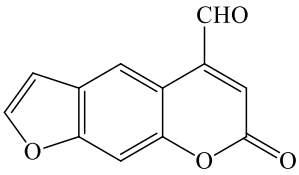

7-oxo-7*H*-furo[3,2-*g*]chromene-5-carbaldehyde

Wu *et al.* (2021) documented that among the total 2-aryl furocoumins they synthesized, the compound 5-methyl-2-(thiophen-2-yl)-7*H*-furo[3,2-*g*]chromen-7-one exhibited potent photo-activated insecticidal activity against fourth instar larvae of *Aedes aegypti (A. aegypti)*. The insecticidal activity tests showed that the compound concentrations in *A. aegypti larvae* effective for insecticidal activity were 53.96, 64.99, and 78.27 mg/L, after 48 h of treatment. Under UVA radiation, 2-thiophenylfurocoumarin can cause the midgut cells to release high levels of reactive oxygen species (ROS), which then inhibit antioxidant enzymes, resulting in apoptosis of the midgut tissue and ultimately the death of *A. aegypti larvae* (Wu, 2021).

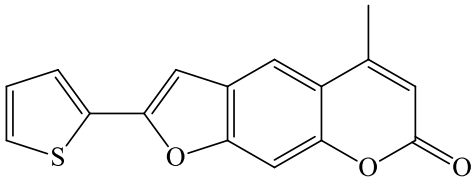

5-methyl-2-(thiophen-2-yl)-7*H*-furo[3,2-*g*]chromen-7-one

In 2023, Dong *et al.* Forty-five new psoralen derivatives containing sulfonohydrazide or acyl thioureas were prepared and then examined for their in vitro antifungal activity against 7 plant pathogens. The findings showed that these prepared psoralens exhibited safe and elevated bactericidal activity. In particular, the EC_{50} values of compounds furo[3,2-*g*]chromen derivative against *Bc* were 9.09 μg/ml and 12.49 μg/ml showing their excellent bactericidal activity.

According to the molecular docking results, it was supported that these two compounds could be effectively inserted into the active site of the *Bc*PK enzyme. Additionally, some psoralen derivatives containing sulfonylhydrazides or acylthioureas could lead to the development of new highly effective fungicides (Dong, 2023).

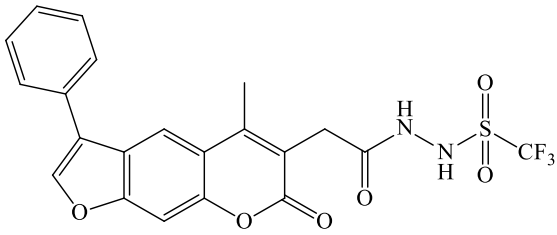

1,1,1-trifluoro-*N*'-(2-(5-methyl-7-oxo-3-phenyl-7*H*-furo[3,2-*g*]chromen-6-yl)acetyl)methanesulfonohydrazide

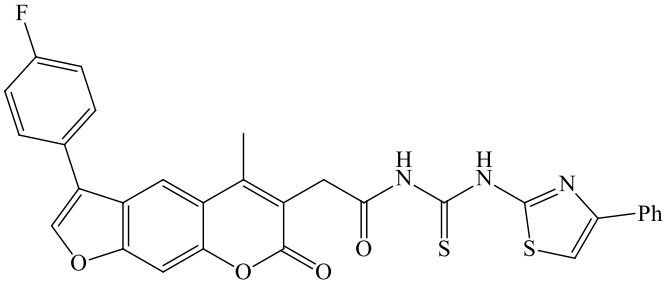

2-(3-(4-fluorophenyl)-5-methyl-7-oxo-7*H*-furo[3,2-*g*]chromen-6-yl)-*N*-((4-phenylthiazol-2-yl)carbamothioyl)acetamide

CONCLUSIONS

In conclusion, furocoumarins are a group of compounds with unique chemical structures and diverse biological activities. They are best known for their role in photosensitivity reactions and their use in PUVA therapy for certain skin conditions. However, caution should be exercised when handling or consuming furocoumarin-containing substances due to their potential for toxicity and phototoxicity. Always consult with healthcare professionals when considering the use of furocoumarins for medicinal purposes.

In this study, the synthesis methods of furocoumarins in recent years, their biological activities, and usage areas in recent years were examined. It is thought to be useful for researchers who want to study furocoumarin and its derivatives.

REFERENCES

Anese, M., & Suman, M. (2013). Mitigation strategies of furan and 5-hydroxymethylfurfural in food. *Food Research International*, *51*(1), 257-264.

Bonamonte, D., Foti, C., Lionetti, N., Rigano, L., & Angelini, G. (2010). Photoallergic contact dermatitis to 8-methoxypsoralen in Ficus carica. *Contact dermatitis*, *62*(6), 343-348.

Cadierno, V. (2015). Metal-catalyzed routes for the synthesis of furocoumarins and coumestans. In *Green Synthetic Approaches for Biologically Relevant Heterocycles* (pp. 77-100).

Chen, C., Tang, Z. B., & Liu, Z. (2023). Recent advances in the synthesis and applications of furocoumarin derivatives. *Chinese Chemical Letters*, 108396.

Dong, J., Li, K., Hong, Z., Chen, L., Tang, L., Han, L., ... & Fan, Z. (2023). Design, synthesis and fungicidal evaluation of novel psoralen derivatives containing sulfonohydrazide or acylthiourea moiety. *Molecular Diversity*,*27*(2), 571-588.

Elinson, M. N., Vereshchagin, A. N., Ryzhkova, Y. E., Karpenko, K. A., Ryzhkov, F. V., & Egorov, M. P. (2022). Electrocatalytic Cascade Selective Approach to 3-Aryl-2'*H*,3 *H*,4*H*-Spiro{Furo[2,3-*c*]chromene-2,5'-Pyrimidine}-2',4,4',6'(1'*H*,3'*H*)tetraones and Its Automatic Screening Docking Studies. *Polycyclic Aromatic Compounds*, 1-15.

Lei, R., Lan, W., Li, M., Qin, Z., & Fu, B. (2023). Cu(II)-mediated annulation of 4-hydroxycoumarins with propargyl carbonates: Facile access to furo[3,2-*c*]coumarin scaffold. *Tetrahedron Letters*, *128*, 154697.

Lončarić, M., Gašo-Sokač, D., Jokić, S., & Molnar, M. (2020). Recent advances in the synthesis of coumarin derivatives from different starting materials. *Biomolecules*, *10*(1), 151.

Mahendra, C. K., Tan, L. T. H., Lee, W. L., Yap, W. H., Pusparajah, P., Low, L. E., ... & Goh, B. H. (2020). Angelicin-A Furocoumarin compound with vast biological potential. *Frontiers in Pharmacology*, *11*, 366.

Mogol, B. A., & Gökmen, V. (2016). Thermal process contaminants: Acrylamide, chloropropanols and furan. *Current Opinion in Food Science*, *7*, 86-92.

Pelipko, V. V., Baichurin, R. I., Lyssenko, K. A., Dotsenko, V. V., & Makarenko, S. V. (2022). A convenient synthesis of furo[3,2-*c*]pyran-3-carboxylates from 3-bromo-3-nitroacrylates. *Mendeleev Communications*, *32*(4), 454-456.

Singh, N., Rajotiya, K., Lamba, N., Singh, H. L., Ameta, K. L., & Singh, S. (2022). Versatile Approach for the Synthesis of Furo-coumarin Derivatives. *Current Organic Chemistry*, *26*(3), 324-341.

Wu, J., Wang, L., Zhang, Y., Zhang, S., Ahmad, S., & Luo, Y. (2021). Synthesis and photoactivated toxicity of 2-thiophenylfurocoumarin induce midgut damage and apoptosis in aedes aegypti larvae. *Journal of Agricultural and Food Chemistry*, *69*(3), 1091-1106.

Xie, H., Niu, C., Chao, Z., Mamat, N., & Akber Aisa, H. (2020). Synthesis and activity of new schiff bases of furocoumarin. *Heterocyclic Communications*, *26*(1), 176-184.

Zou, Y., Teng, Y., Li, J., & Yan, Y. (2023). Recent advances in the biosynthesis of coumarin and its derivatives. *Green Chemical Engineering*.

Chapter 3

Aminopyrimidines: Recent Synthesis Methods and Biological Activities

Gönül YILDIZ[1] , Rahmi KASIMOĞULLARI[2]

[1] Responsible Author, Research Assistant, Faculty of Arts and Sciences/Department of Chemistry, Kütahya Dumlupınar University, Kütahya, Turkey, e-mail: gonul.yildiz@dpu.edu.tr, ORCID No: 0000-0002-1886-5964

[2] Professor Dr., Faculty of Arts and Sciences/Department of Chemistry, Kütahya Dumlupınar University, Kütahya, Turkey, e-mail: rahmi.kasimogullari@dpu.edu.tr, ORCID No: 0000-0001-6391-7121

ABSTRACT

Aminopyrimidine and its derivatives are heterocyclic compounds of great biological and pharmacological importance (Ali, 2009). In recent years, many aminopyrimidine derivative compounds with biological activity such as antimicrobial, anticancer, antioxidant, antitumor, antiallergic, antiviral, herbicide, etc. have been synthesized and brought to the literature. Due to the importance of pyrimidines, especially in the pharmaceutical sector, new and current studies are still needed (Dwivedi, 2009).

In this study, the general properties of aminopyrimidines, some synthesis methods, and some biological activities were examined.

Keywords: Aminopyrimidine, Pyrimidines, Biological Activity, Anticancer

1. INTRODUCTION

Aminopyrimidines are a heterocyclic compound containing a pyrimidine ring with an amino group (-NH_2) attached. Pyrimidine is a heterocyclic aromatic compound consisting of two nitrogen atoms and four carbon atoms in a six-membered ring. The aminopyrimidine nucleus is present in the structure of some natural substances Thiamine (vitamin B1) and other products and seafood Alkaloid meridian with anti-cancer, anti-malarial, and anti-inflammatory effects Antituberculous activity **(Fig. 1**) (Filho, 2021).

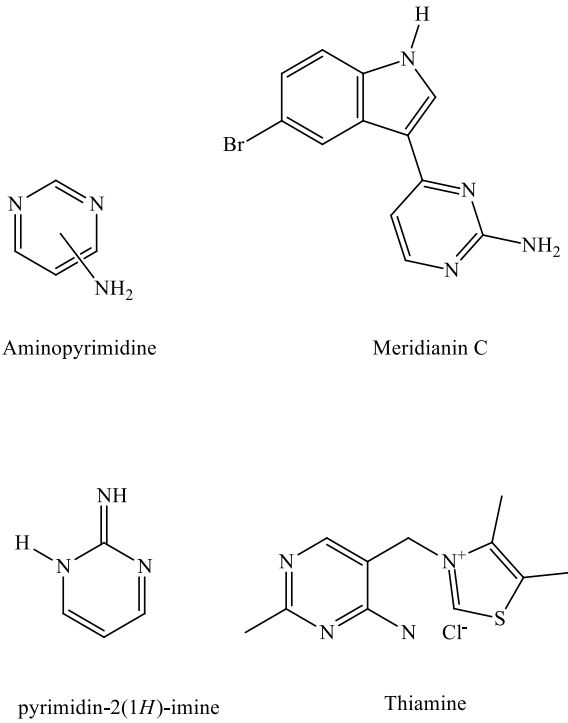

Aminopyrimidine Meridianin C

pyrimidin-2(1*H*)-imine Thiamine

Fig. 1. The structure of aminopyrimidine in natural products.

2. SYNTHESIS of AMINOPYRIMIDINES

2-aminopyrimidine derivatives were synthesized by Bayramoğlu and his team using guanidine hydrochloride and *β*-diketone derivatives by ultrasound-assisted method in the basic environment. In the literature, these compounds were synthesized with high efficiency in as little as 30 minutes with the Ultrasound-assisted method, while these compounds were synthesized in 5 hours with the traditional method (Bayramoğlu, 2020).

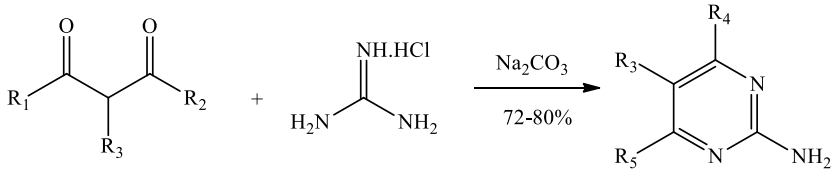

R_1: CH_3, OC_2H_5
R_2: CH_3, OC_2H_5
R_3: H, C_2H_5, C_4H_9
R_4: CH_3, OH
R_5: CH_3, OH

As a result of the condensation reaction of *β*-enaminonitrile and aromatic nitriles by Zhu *et al*., substitute 4-aminopyrimidines were synthesized with high efficiency. In this method, the reaction temperature was controlled using lithium hexamethyldisilazide (LiHMDS) catalyst and it was reported to be a very practical and economical method (Zhu, 2019).

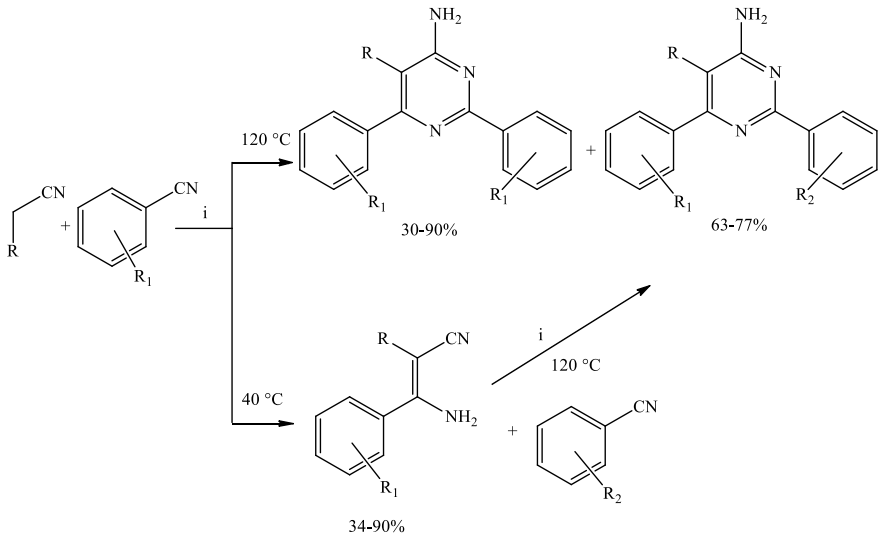

i: LiHMDS, DME, 24 h
R: alkyl, aryl
R_1: H, 2-Br, 4-Br, 4-Cl, 4-I, 2-Me, 4-Me, 4-OMe, 4-*t*-Bu, etc.
R_2: H, 3-Me, 4-Br, 4-I, etc.

Saikia and his team synthesized 3,4-dihydropyrimidione derivatives based on acetophenone, aromatic aldehydes, and urea components. In a single-pot container, the multi-component cyclization reaction method is adopted, and the reaction conditions are simple to reflect the advantages of the method. The

reaction is catalyzed by [TSPi][CF_3CO_2]$_2$ and 2-amino-4,6-diarylpyrimidines are synthesized by condensation-aromatization method using phenylhydrazine under solvent-free grinding method in 15-25 minutes (Saikia, 2019).

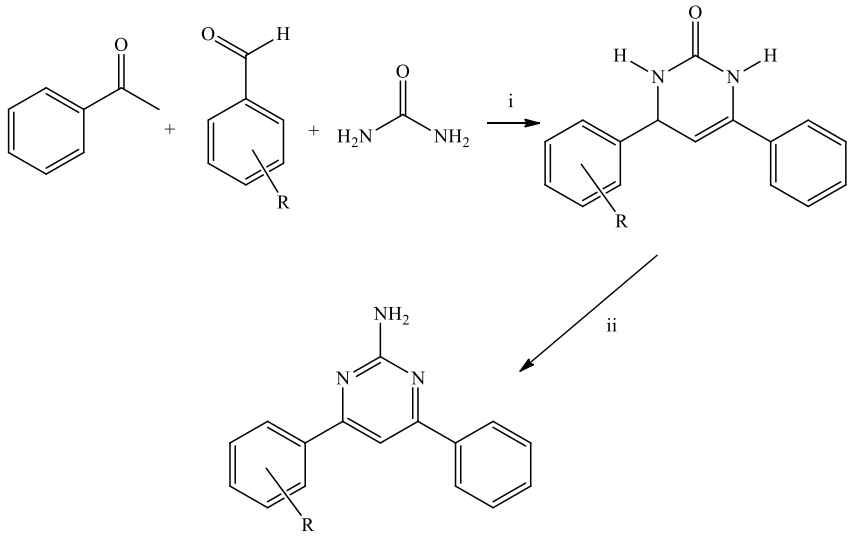

i: 2.5 mol % [TSPi][CF_3CO_2]$_2$, neat, griding, r.t.
ii: phenylhydrazine hydrochloride, neat, griding, r.t., 15-25 min., 80-90%
R: H, 4-Cl, 2-OH, 4-OH, 4-Me, 4-OMe, 4-NO_2, 2,4-dichloro, 3,4,5-trimethoxy

3. BIOLOGICAL ACTIVITY of AMINOPYRIMIDINES

Recent literature studies have revealed the application of aminopyrimidines as anti-leukemic (Pitchaimani, 2016), anti-tumor (Guo, 2020), anti-angiogenic (Miltz, 2017), DNA-interactive (Miyan, 2017), pro-apoptotic (Font, 2011), and anti-tubulin (Devambatla, 2017), drugs and their remarkable anticancer effects by inhibiting different cell types (Lindgren, 2014).

Tufail and his team synthesized aminopyrimidine derivatives and screened these compounds for anticancer and *rh*DHFR inhibitory activity. MTT assay was used for the in vitro anticancer test. Doxorubicin was used as the reference drug. The Cl-binding compound was the most active of the others against hDHFR with an IC_{50} of 180 nM, but was less active compared to the standard drug methotrexate (IC_{50}: 48 nM) (Tufail 2021).

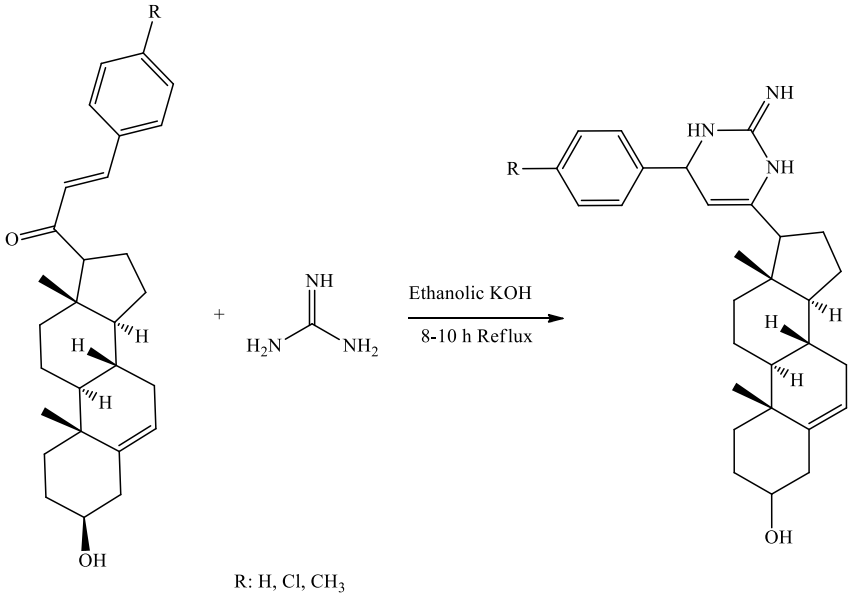

Synthesizing *N*-(4-(benzyloxy)phenyl)-3-phenylisoxazole[5,4-*d*]pyrimidine-4-amine derivatives, Gaikwad and his group evaluated these compounds using an NCI-60 cell line panel. Examination with single-dose NCI-60 cell lines and a five-dose study showed that the 3-Fluoro-bound compound HCT-50 (Colon Cancer)-0.0221 μM, MDA-MB-435 (Melanoma) has promising growth inhibitory effects on various cancer cell lines. To understand the mechanism of action In 10-hour phase-contrast microscopic evaluation, DAPI, acridine orange/ethidium bromide (AO/EB) staining, and additional V-FITC tests showed that elevation in intracellular ROS led to changes in mitochondrial membrane potential, which in turn induced apoptosis in BT-474 cancer cells. It has also been revealed that there may be a plausible mechanism of action for the 3-fluoro-bound compound. MTT (3-(4,5-dimethylthiazol-2-yl)-2,5-diphenyltetrazolium bromide) testing against triple-negative breast cancer cell line BT-474 showed that the 10-hour IC_{50} (μM) value (i.e., the concentration required for the inhibition of 50% of cancer cell growth) was 0.64 ± 0.07 μM (Gaikwad, 2021).

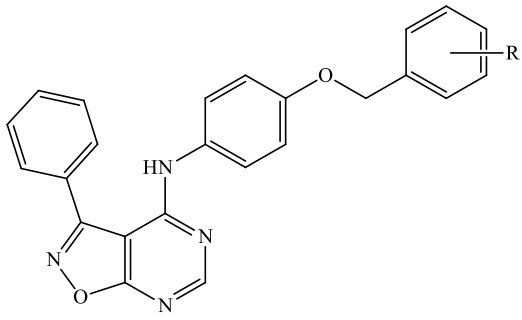

R: H, 3-chloro, 4-chloro, 3-methoxy, 4-methyl, 4-bromo, 3-fluoro, 4-fluoro, 2,4-dichloro

Giridhar *et al.* developed the 4,6-diaryl-2-aminopyrimidines series as antiplatelet agents and used them *in vitro* evaluated. According to the results obtained; the compound 2-(2-amino-6-(2,4-dichlorophenyl)pyrimidin-4-yl)-5-methoxyphenol (% inhibition of platelet aggregation: 77.47) was found to be twice as potent as aspirin and was predicted to be useful for the development of new antiplatelet compounds (Giridhar, 2012).

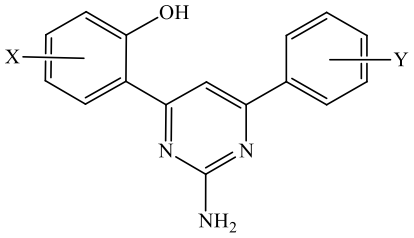

X: 4-OCH_3, 5-OCH_3
Y: H, 3-OCH_3, 4-OCH_3, 2-Cl, 3-Cl, 4-Cl, 3-CH_3, 4-CH_3, 4-NO_2, 2,4-dichloro

CONCLUSION

The inclusion of an amino group in the structure of pyrimidine leads to aminopyrimidines, which exhibit unique properties and find applications in a variety of fields, including pharmaceuticals, agrochemicals, and materials science. The presence of the amino group makes aminopyrimidines more reactive and versatile than pyrimidine itself.

In the pharmaceutical industry, aminopyrimidines have been researched and used as active ingredients in drugs that target a wide range of diseases. For example, some aminopyrimidines have shown promise as kinase inhibitors, which are substances that can interfere with the activity of enzymes called kinases

involved in cellular signaling pathways. Kinase inhibitors are important in the development of targeted therapies for cancer and other diseases.

Aminopyrimidines can also be used in materials science, especially in the synthesis of dyes and pigments. These compounds often have vibrant colors and can be incorporated into coatings, inks, and other materials for their visual appeal.

Numerous research teams have so far collaborated to create a large array of aminopyrimidine derivatives that evaluate their effectiveness in a variety of biological contexts. Given the broad spectrum of biological activities exhibited by aminopyrimidine derivatives, they have potential synthesizing flows and testable research in the context of numerous diseases.

This review discusses the chemical properties of aminopyrimidine compounds, recent methods of synthesis, and the biological activity of aminopyrimidines. It provides valuable information for researchers who are beginning to work on this topic and want a comprehensive understanding of its functional characteristics.

REFERENCES

Ali, T. E. S. (2009). Synthesis of some novel pyrazolo [3,4-*b*]pyridine and pyrazolo [3,4-*d*]pyrimidine derivatives bearing 5,6-diphenyl-1,2,4-triazine moiety as potential antimicrobial agents. *European Journal of Medicinal Chemistry*, *44*(11), 4385-4392.

Bayramoğlu, D., Kurtay, G., & Güllü, M. (2020). Ultrasound-assisted rapid synthesis of 2-aminopyrimidine and barbituric acid derivatives. *Synthetic Communications*, *50*(5), 649-658.

Devambatla, R. K. V., Li, W., Zaware, N., Choudhary, S., Hamel, E., Mooberry, S. L., & Gangjee, A. (2017). Design, synthesis, and structure–activity relationships of pyrimido [4,5-*b*]indole-4-amines as microtubule depolymerizing agents that are effective against multidrug resistant cells. *Bioorganic & medicinal chemistry letters*, *27*(15), 3423-3430.

Dwivedi, P. K., Tripathi, K., & Mishra, M. (2009). The Aminopyrimidines-II. *Asian Journal of Research in Chemistry*, *2*(4), 365-368.

Font, M., González, Á., Palop, J. A., & Sanmartín, C. (2011). New insights into the structural requirements for pro-apoptotic agents based on 2,4-diaminoquinazoline, 2,4-diaminopyrido[2,3-*d*]pyrimidine and 2,4-diaminopyrimidine derivatives. *European journal of medicinal chemistry*, *46*(9), 3887-3899.

Gaikwad, N. B., Bansod, S., Mara, A., Garise, R., Srinivas, N., Godugu, C., & Yaddanapudi, V. M. (2021). Design, synthesis, and biological evaluation of *N*-(4-substituted)-3-phenylisoxazolo [5,4–*d*]pyrimidin-4-amine derivatives as apoptosis-inducing cytotoxic agents. *Bioorganic & Medicinal Chemistry Letters*, *49*, 128294.

Giridhar, R., Tamboli, R. S., Ramajayam, R., Prajapati, D. G., & Yadav, M. R. (2012). Assessment of antiplatelet activity of 2-aminopyrimidines. *European Journal of Medicinal Chemistry*, *50*, 428-432.

Guo, W., Xing, Y., Zhang, Q., Xie, J., Huang, D., Gu, H., ... & Chen, Y. (2020). Synthesis and biological evaluation of B-cell lymphoma 6 inhibitors of *N*-phenyl-4-pyrimidinamine derivatives bearing potent activities against tumor growth. *Journal of Medicinal Chemistry*, *63*(2), 676-695.

Lindgren, E. B., de Brito, M. A., Vasconcelos, T. R., de Moraes, M. O., Montenegro, R. C., Yoneda, J. D., & Leal, K. Z. (2014). Synthesis and anticancer activity of (*E*)-2-benzothiazole hydrazones. *European Journal of Medicinal Chemistry*, *86*, 12-16.

Miltz, W., Velcicky, J., Dawson, J., Littlewood-Evans, A., Ludwig, M. G., Seuwen, K., ... & Loetscher, P. (2017). Design and synthesis of potent and orally active GPR4 antagonists with modulatory effects on nociception,

inflammation, and angiogenesis. *Bioorganic & Medicinal Chemistry*, *25*(16), 4512-4525.

Miyan, L., Ahmad, A., Alam, M. F., & Younus, H. (2017). Synthesis, single-crystal, DNA interaction, spectrophotometric and spectroscopic characterization of the hydrogen-bonded charge transfer complex of 2-aminopyrimidine with π-acceptor chloranilic acid at different temperature in acetonitrile. *Journal of Photochemistry and Photobiology B: Biology*, *174*, 195-208.

Pitchaimani, J., Raja, M. R. C., Sujatha, S., Mahapatra, S. K., Moon, D., Anthony, S. P., & Madhu, V. (2016). Arene ruthenium (ii) complexes with chalcone, aminoantipyrine and aminopyrimidine based ligands: synthesis, structure and preliminary evaluation of anti-leukemia activity. *RSC Advances, 6*(93), 90982-90992.

Saikia, S., & Borah, R. (2019). One-Pot Sequential Synthesis of 2-Amino-4, 6-Diaryl Pyrimidines Involving SO_3H-Functionalized Piperazinium-Based Dicationic Ionic Liquids as Homogeneous Catalysts. *ChemistrySelect*, *4*(30), 8751-8756.

Tufail, M. B., Javed, M. A., Ikram, M., Mahnashi, M. H., Alyami, B. A., Alqahtani, Y. S., ... & Rashid, U. (2021). Synthesis, pharmacological evaluation and Molecular modelling studies of pregnenolone derivatives as inhibitors of human dihydrofolate reductase. *Steroids*, *168*, 108801.

Venturini Filho, E., Pinheiro, E. M., Pinheiro, S., & Greco, S. J. (2021). Aminopyrimidines: Recent synthetic procedures and anticancer activities. *Tetrahedron*, *92*, 132256.

Zhu, Y., Li, Y., Xiang, S., Fan, W., Jin, J., & Huang, D. (2019). Utilization of nitriles as the nitrogen source: practical and economical construction of 4-aminopyrimidine and *β*-enaminonitrile skeletons. *Organic Chemistry Frontiers*, *6*(17), 3071-3077.

Chapter 4

Classical Chemometric Method For Simultaneous Determination Of Alzheimer's Drugs

Güzide PEKCAN[1]

[1] *Doç.Dr., Department of Chemistry, Faculty of Science & Art, Süleyman Demirel University, guzideertokus@sdu.edu.tr, ORCID No: 0000-0001-9230-5634.*

Abstract

For the Alzheimer's medications in pharmaceutical tablets, in this work, precise, sensitive, and accurate spectrophotometric-chemometric methods were created. Donepezil and rivastigmine are the two Alzheimer's medications under review. Classical Least Squares-CLS is the chemometric technique that is employed. For the chemometric analysis of donepezil and rivastigmine in synthetic mixes and pharmaceutical tablets, CLS was successfully used. Binary mixes of donepezil and rivastigmine in 10 distinct combinations were created at random in 0.1 M HCl as part of a concentration set. The suggested method's accuracy and precision were confirmed by examining synthetic mixes containing the tested medicines. High recoveries and low standard deviations were discovered as a result of the determination. To estimate concentrations with CLS, a chemometric software employed values for absorbance and concentration.

Keywords: CLS, chemometry, Rivastigmine, Donepezil.

Introduction

Dementia is most commonly caused by Alzheimer's disease (Salem et al., 2010). A neurodegenerative disorder called Alzheimer's disease is characterized by a gradual loss of memory followed by total dementia (Katakam et al., 2013). In this investigation, the spectrophotometric and chemometric concentrations of the Alzheimer's medications donepezil and rivastigmine were determined. Chemically speaking, donepezil is 2,3-dihydro-5,6-dimethoxy-2-[[1-(phenylmethyl)-4-piperidinyl]methly].Hydrochloride of -1H-inden-1-one (Jagadeeswaran et al., 2011). It is an inhibitor of acetyl cholinesterase (Rajput et al., 2015). The primary cholinesterase in the brain is inhibited by the piperidine-based reversible inhibitor donepezil (Bhateria et al., 2015). (S)-3-[(1-dimethylamino)ethyl]-N-methylphenly-carbamate hydrogen tartrate is the chemical name for rivastigmine. It is an acetylcholinesterase carbamate inhibitor used to treat persons with Alzheimer's disease (Amini et al. 2010). It exhibits strong cortical and hippocampal region selectivity (Iranifam et al., 2017).

It is challenging to do simultaneous quantitative analysis of pharmaceuticals using the traditional spectrophotometric approach because to overlapping spectra (Khoshayand et al., 2008). This is why one of the multivariate calibration methods was used in this investigation as the classical least squares.

Material and Methods

Chemometry and UV/VIS spectrophotometry techniques were employed in this work to identify the drugs utilized on the outside of medications. Chemometric software was used to calculate the collected data. The amount of drugs in medicines was calculated using UV-Vis spectra, the spectrum values obtained using the UV-1700 PHARMASPEC SHIMADZU spectrophotometer fitted with a computer-controlled 1 cm-long cell.

In this work, spectrophotometric measurements were made on the spectra of donepezil, rivastigmine and synthetic mixes that were initially generated one at a time, and subsequently in various ratios. As a last step, measurements were taken to establish the hue of the medicinal ingredients. The gathered information was assessed using several chemometric techniques. The calibration (resetting operation) of the UV spectrophotometer instrument was carried out in the first step. First, the calibration procedure was carried out against the air with both cells empty. After that, the identical procedure was carried out by inserting a blind sample that had been made using the same solvent as us into both light routes. The blind are always prepared in this way for all readings. The blind solvent was preferred in order to reduce interference effects when making the decision. The

coated portion of the commercial tablet was produced by peeling it off, drugs were identified, and absorbance measurements were taken in the final phase.

Results and Discussion

Rivastigmine and donepezil both fall within the category of very absorbent drugs. The absorbance-wavelength (nm) curves are displayed in Figure 1. The wavelengths of donepezil and rivastigmine's spectra are between 200 and 400 nm. Figure 1. shows absorption spectra for Donepezil and rivastigmine hydrochloride mixtures in 0.1 M HCl.

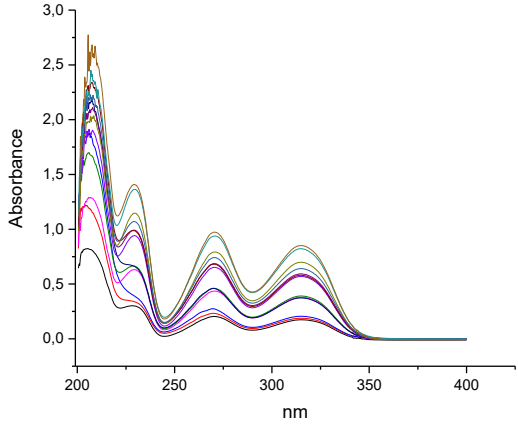

Figure 1. The spectrum of donepezil and rivastigmine mixtures.

This study's goal is to use chemometry to create a less expensive, quicker, and more accurate analytical approach. This method avoids time and effort loss caused by the trial and error method and enables the analysis of active components without pre-separation. For many simultaneous detections of very linear components, the CLS technique and absorption spectra can be employed singly or in combination. For the purpose of validating the calibrations for drug synthetic mixes, some statistical parameters were provided.

Table 1. displays the retrieved and relative standard deviation (BSS) values computed for each chemometric technique. Values for precision and accuracy have been examined. Cross-validation was used to compare the concentrations against the additional values in order to eliminate any potential errors.

Table 1. Results calculated by CLS calibration of drug active ingredients in artificially prepared mixture

Mix number	Donepezil Recovery %	Rivastigmine Recovery %
1	98.6	96.8
2	95.2	97.5
3	89.9	99.2
4	95.6	98.6
5	96.2	97.5
6	97.8	96.2
7	97.2	96.3
8	95.6	97.5
9	98.3	98.6
10	98.1	98.3
11	98.3	97.3
12	96.2	96.3
13	97	96.7
14	95.2	98.3
15	97.9	98.9
Mean(χ)	96.47	97.60
Relative Standard Deviation(RSD)	2.26	1.03

One of the chemometric approaches, the classical least squares method, was utilized in this work to calculate the results of spectrophotometric studies of color compounds used in medications. UV spectrum of the coloring chemicals donepezil and rivastigmine. Values for absorbance were taken. The chemometric approach was statistically validated for donepezil and rivastigmine. The recovery values are large enough and the relative standard deviation values are small enough when fake mixtures are investigated using the results. This research serves as a preliminary investigation of the colorants found in medications. The following method combines different chemometric techniques with the standard least squares method to analyze medication tablets and biological samples like urine.

REFERENCES

Amini, H., Ahmadiani, A., High-performance liquid chromatographic determination of rivastigmine in human plasma for application in pharmacokinetic studies, *Iranian Journal Of Pharmaceutical Research,* **2010,** 9(2), 115-121.

Bhateria, M., Ramakrishna, R., Pakala, D.B., Bhatta, R.S., Development of an LC–MS/MS method for simultaneous determination of memantine and donepezil in rat plasma and its application to pharmacokinetic study, *Journal Of Chromatography B,* **2015,** 1001, 131-139.

Iranifam, M., Hendekhale, N.R., CuO nanoparticles-catalyzed hydrogen peroxide-sodium hydrogen carbonate chemiluminescence system used for quenchometric determination of atorvastatin, rivastigmine and topiramate, *Sensors And Actuators B: Chemical,* **2017,** 243, 532-541.

Jagadeeswaran, M., Gopal, N., Gandhimathi, M., Rajavel, R., Ganesh, M., Sivakumar, T., A validated HPTLC method for the estimation of donepezil HCl in bulk and its tablet dosage form, *Eurasian Journal Of Analytical Chemistry,* **2011,** 6(1), 40-45.

Katakam, P., Kalakuntla, R.R., Adiki, S.K., Development and validation of a liquid chromatography mass spectrometry method for the determination of donepezil in human plasma, *Journal Of Pharmacy Reserarch,* **2013,** 7, 720-726.

Khoshayand, M.R., Abdollahi, H., Shariatpanahi, M., Saadatfard, A., Mohammadi. A., Simultaneous Spectrophotometric Determination of Paracetamol, Ibuprofen and Caffeine in Pharmaceuticals by Chemometric Methods, *Spectrochimica Acta Part A*, **2008**, 70(3), 491-499.

Rajput, M., Jain, V.K., Hamid, H., Aggarwal, M., Khandal, R.K., Quantitative determination of platinum and palladium in donepezil hydrochloride using inductively coupled plasma-optical emission spectroscopy, *International Journal Of Pharmacy And Pharmaceutical Sciences,* **2015,** 7(2),323-329.

Salem, M.Y., El-Kosasy, A.M., El-Bardicy, M.G., Abd El-Rahman, M.K., Spectrophotometric and spectrodensitometric methods for the determination of rivastigmine hydrogen tartrate in presence of its degradation product, *Drug Testing and Analysis,* **2010**, 2, 225-233.

Chapter 5

On Boundedness of Caputo-Fabrizio Integral Operator on Lebesgue-Bochner Space with Δ-Integral

Lütfi AKIN[1]

[1] *Doç. Dr.;Mardin Artuklu Üniversitesi İktisadi ve İdari Bilimler Fakültesi İşletme Bölümü.*
lutfiakin@artuklu.edu.tr ORCID No: 0000-0002-5653-9393

INTRODUCTION

Integral inequalities and differential equations of arbitrary $n > 0$ $(n \in \mathbb{R})$ used for modeling a variety of physical concepts that arise in many fields of science. Applications of mathematical methods of this type appear in scientific fields such as statistical mechanics, quantum mechanics, biosciences, optics, economics models, etc. The cited references in [1–15] can be consulted. The prominence of the development of the mathematical field called fractional analysis has led to the emergence of various ways of defining fractional derivatives and fractional integrals. The cited references in [16-19] can be consulted.

Moreover, three new classifications of fractional operators have recently been introduced [20].

MATHEMATICAL BACKGROUND

The theory of time scales is a mathematical concept first introduced by Stefan Hilger. On this basis, many authors examined dynamic integral inequalities and integral operators on time scales. The findings obtained as a result of these studies attracted great attention. Because it has become an important field of study not only in mathematics but also in positive sciences such as engineering, mechanics, physics, optics, economics, etc. If readers want to obtain more information, they can look at the bibliography [22-28, 31]. $\mathbb{T}$ (time scale calculus) is an arbitrary non-empty closed subset of $\mathbb{R}$ (real numbers). The $(0,\infty)_{\mathbb{T}}$ is denoted by $(0,\infty) \cap \mathbb{T}$.

Now let's give definitions about time scales that will help us prove our result.

Definition 1 [23] The functions $p, q: \mathbb{T} \to \mathbb{T}$ are defined by $p(t) = inf\{s \in \mathbb{T}: s > t\}$, $q(t) = sup\{s \in \mathbb{T}: s > t\}$ for $t \in \mathbb{T}$.

i. $p(t)$ is forward jump operator,
ii. $q(t)$ is backward jump operator.
iii. if $p(t) > t$, then t is right-scattered,
iv. if $p(t) = t$, then t is called right-dense.
v. if $q(t) < t$, then t is left-scattered,
vi. if $q(t) = t$, then t is called left-dense.

Definition 2 [23] Suppose that two functions $\mu, \vartheta: \mathbb{T} \to \mathbb{R}^+$,and $\mu(t) = p(t) - t$, $\vartheta(t) = t - q(t)$. μ(t) and $\vartheta(t)$ are called graininess functions.

If time scale calculus ($\mathbb{T}$) has a left-scattered maximum n, then $\mathbb{T}^k = \mathbb{T} - \{n\}$. Otherwise $\mathbb{T}^k = \mathbb{T}$. In [22-24], $\mathbb{T}^{\mathrm{k}}$ is defined as follows

$$\mathbb{T}^k = \begin{cases} \mathbb{T} \setminus (q\ sup\ \mathbb{T}, sup\ \mathbb{T}], & if \quad sup\ \mathbb{T} < \infty \\ \mathbb{T}, & if \quad sup\ \mathbb{T} = \infty, \end{cases}$$

and

$$\mathbb{T}_k = \begin{cases} \mathbb{T} \setminus [inf\ \mathbb{T}, p(inf\ \mathbb{T})], & |inf\ \mathbb{T}| < \infty \\ \mathbb{T}, & inf\ \mathbb{T} = -\infty. \end{cases}$$

Assume that $h: \mathbb{T} \to \mathbb{R}$ is a function, and s right-dense.

If h is Δ −differentiable at point s ($s \in \mathbb{T}^k (t \neq min\mathbb{T})$), then h is continuous at point s.

If h is left continuous at point s, and s is right-scattered, then h is Δ −differentiable at point s,

$$h^{\Delta}(s) = \frac{h^p(s) - h(s)}{\mu(s)}.$$

If h is Δ −differentiable at point s and $\lim\limits_{t \to s} \frac{h(s)-h(t)}{s-t}$, then

$$h^{\Delta}(s) = \lim_{t \to s} \frac{h(s) - h(t)}{s - t}.$$

If h is Δ −differentiable at point s, then $h^p(s) = h(s) + \mu(s)h^{\Delta}(s)$.

Remark 3 [22] If $\mathbb{T} = \mathbb{R}$, then $h^{\Delta}(s) = h'(s)$, and if $\mathbb{T} = \mathbb{Z}$, then $h^{\Delta}(s)$ reduces to $\Delta h(s)$.

Definition 4 [24] If $H: \mathbb{T} \to \mathbb{R}$ is defined a Cauchy antiderivative (delta) of $h: \mathbb{T} \to \mathbb{R}$, then $H^{\Delta} = h(s)$ holds for all $s \in \mathbb{T}$, and we define the delta (Hilger) integral of h by

$$\int_t^s h(\tau)\Delta\tau = H(s) - H(t),$$

for all $s, t \in \mathbb{T}$.

Now, we will give the definition of the Bochner integral over. According to our approach, the extended measure does not play any role. On the other hand, it is important that $(X, \varphi, \mathbb{R})$ can be used to define of Lebesgue integrable space real-valued mappings on X according to the extension of φ to a fully additive measure on X (see [29]). We will denote this space by $L^1(X, \varphi)$.

Definition 5 [30] A function $g: X \to E$ is called Bochner integrable if there exist functions $g_n \in S(E)$ such that

i. $\sum_{n=1}^{\infty} \|g_n\|_1 < \infty$,

ii. $g(x) = \sum_{n=1}^{\infty} g_n(x)$ at those points $x \in X$

where $\sum_{n=1}^{\infty} \|g_n(x)\| < \infty$.

If conditions (i) and (ii) are satisfied we will write

$$g \simeq g_1 + g_2 + \cdots \text{ or } g \simeq \sum_{n=1}^{\infty} g_n.$$

The space of all Bochner integrable functions will be denoted by $L^1(X, \varphi, E)$.

Main Result

Now let's give the following lemmas to prove our main result.

Lemma 6 Let v be the integrable weight function in the sense of Bochner-Lebesgue, h, u, v integrable functions in the sense of delta (Hilger). If $0 < p \leq q < \infty$, then

$$\left(\int_{\mathbb{R}^n} h(x)^q v(x) \Delta x \right)^{1/q} \leq C \left(\int_{\mathbb{R}^n} u(x)^p v(x)^{p/q} \Delta x \right)^{1/p},$$

$$\|h\|_{L^q(\mathbb{R}^n)} \leq C \|u\|_{L^p(\mathbb{R}^n)}.$$

Lemma 7 Suppose that h, v integrable functions in the sense of delta (Hilger), and $0 \leq \propto \leq 1$, $a \in (-\infty, t)$. If $0 < p \leq q < \infty$, then there exist a constant C independent of h such that

$$\left(\int_{\mathbb{R}^n} \left| \mathfrak{D}_t^{(\propto)} h(x) v(x) \right|^q \Delta x \right)^{1/q} \leq C \left(\int_{\mathbb{R}^n} |h(x) v(x)|^p \Delta x \right)^{1/p}.$$

Theorem 8 Let $L^p(X, \varphi, \mathbb{R}^n)$ be Lebesgue space (Lebesgue-Bochner space for $p = 1$) and $X \subset \mathbb{R}^n$ with $0 < p \leq q < \infty$. If $h: \Omega \to X$ is strongly φ −measurable (finite) and Bochner-Lebesgue integrable function, then

$$\left\| \mathfrak{D}_t^{(\propto)} h \right\|_{L^q(\mathbb{R}^n)} \leq C \|h\|_{L^p(\mathbb{R}^n)}$$

where $0 \leq \propto \leq 1$, $a \in (-\infty, t)$ and $M(\propto)$ is a normalization function such that $M(0) = M(1) = 1$.

Proof Suppose that $0 \leq \propto \leq 1$, $a \in (-\infty, t)$ and $0 < p \leq q < \infty$.

$$\left\| \mathfrak{D}_t^{(\propto)} h \right\|_{L^q(\mathbb{R}^n)} = \left(\int_{\mathbb{R}^n} \left(\frac{M(\propto)}{1-\propto} \int_a^t h'(\varphi) e^{-\frac{\propto}{1-\propto}(t-\varphi)} \Delta\varphi \right)^q \Delta x \right)^{1/q}$$

$$\leq \frac{M(\propto)}{1-\propto} h(\varphi) \left(\int_{\mathbb{R}^n} \left(\int_a^t e^{-\frac{\propto}{1-\propto}(t-\varphi)} \Delta\varphi \right)^q \Delta x \right)^{1/q}$$

$$\leq Ch(\varphi) \leq C \left(\int_{\mathbb{R}^n} \left(\int_a^t h'(\varphi)\Delta\varphi \right)^p \Delta x \right)^{1/p} = C\|h\|_{L^p(\mathbb{R}^n)}.$$

From Lemma 6 and Lemma 7,

$$\left\| \mathfrak{D}_t^{(\propto)} h \right\|_{L^q(\mathbb{R}^n)} \leq C\|h'\|_{L^p(\mathbb{R}^n)}.$$

Remark 9 If $p = q = 1$ and $\mathbb{T} = \mathbb{R}$ $\left(h^{\Delta}(t) = h'(t)\right)$, then Caputo-Fabrizio the bounded in Lebesgue-Bochner space is obtained.

Remark 10 If μ is finite, then

$$L^{\infty}(\varphi; X) \subset L^q(\varphi; X) \subset L^p(\varphi; X) \subset L^1(\varphi; X),$$

whenever $1 \leq p < q \leq \infty$.

Conclusion

Many important studies have been carried out on the Caputo-Fabrizio operator in the mathematical literature. For example, some mathematicians have studied the fractional case, its limitation, etc. Some mathematicians have even made studies stating that the fractional state of Caputo-Fabrizio operator is not possible. A short proof of boundedness of fractional Caputo-Fabrizio integral operator was made on time scales by means of the delta (Δ) (Hilger) integral with Lebesgue-Bochner spaces. The boundedness of fractional Caputo-Fabrizio operator can be proven through nabla (∇) integral and diamond alpha $(\diamond_{\propto})$ integral with Lebesgue-Bochner spaces.

REFERENCES

Soontharanon, J., Chasreechai, S., Sitthiwirattham, T. (2019). A Coupled System of Fractional Difference Equations with Nonlocal Fractional Sum Boundary Conditions on the Discrete Half-Line. Mathematics, 7, 256.

Podlubny, I. (1999). *Fractional differential equations: An introduction to fractional derivatives, fractional differential equations, to methods of their solution and some of their applications.* In Mathematics in Science and Engineering; Elsevier: New York, NY, USA, 1999; Volume 198.

Dalir, M., Bashour, M. (2010). Applications of fractional calculus. Appl. Math. Sci. 4, 1021–1032.

Muhammad Altaf, K., Atangana, A. (2019). Dynamics of Ebola Disease in the Framework of Different Fractional Derivatives. Entropy, 21, 303.

Mainardi, F. (2018). A note on the equivalence of fractional relaxation equations to differential equations with varying coefficients. Mathematics, 6, 8.

Owolabi, K.M., Abdon, A.(2018). Chaotic behaviour in system of noninteger-order ordinary differential equations.Chaos Solitons Fractals, 115, 362–370.

Mahmudov, N.I., Bawaneh, S., Al-Khateeb, A.(2019). On a Coupled System of Fractional Differential Equations with Four Point Integral Boundary Conditions. Mathematics, 7, 279.

Owolabi, K.M., Abdon, A.(2018). Numerical simulations of chaotic and complex spatiotemporal patterns in fractional reaction–diffusion systems. Comput. Appl. Math., 37, 2166–2189.

Owolabi, K.M., Abdon, A.(2018). Modelling and formation of spatiotemporal patterns of fractional predation system in subdiffusion and superdiffusion scenarios. Eur. Phys. J. Plus, 133, 43.

Rangaig, N.A., Convicto, V.C. (2018). On fractional modelling of dye removal using fractional derivative with non-singular kernel. J. King Saud-Univ.-Sci.

Rangaig, N.A., Pido, A.A.G.(2019). Finite Difference Approximation Method for Two-Dimensional Space-Time Fractional Diffusion Equation Using Nonsingular Fractional Derivative. Prog. Fract. Differ. Appl., in press.

Baitiche, Z., Guerbati, K., Benchohra, M., Zhou, Y.(2019). Boundary Value Problems for Hybrid Caputo Fractional Differential Equations. Mathematics, 7, 282.

Abro, K.A., Memon, A.A., Memon, A.A. (2018). Functionality of circuit via modern fractional differentiations. Analog. Integr. Circuits Signal Process.

Arqub, O.A., Al-Smadi, M.(2018). Atangana–Baleanu fractional approach to the solutions of Bagley-Torvik and Painlevé equations in Hilbert space. Chaos Solitons Fractals, 117, 161–167.

Qureshi, S., Yusuf, A.(2019). Modeling chickenpox disease with fractional derivatives: From caputo to

atangana-baleanu. Chaos Solitons Fractals, 122, 111–118.

Li, C., Zeng, F. (2015). *Numerical Methods for Fractional Calculus*; Chapman and Hall/CRC: New York, NY, USA.

Ahmad, S.N., Ali, F., Saqib, M., Khan, I., Jan, S.A.A., Alshomrani, A.S., Alghamdi, M.S. (2017). Comparison and analysis of the Atangana–Baleanu and Caputo–Fabrizio fractional derivatives for generalized Casson fluid model with heat generation and chemical reaction. Results Phys., 7, 789–800.

Atangana, A., Baleanu, D.(2017). Caputo-Fabrizio derivative applied to groundwater flow within confined aquifer. J. Eng. Mech., 143.

Diethelm, K., Ford, N.J. (2002). Analysis of fractional differential equations. J. Math. Anal. Appl., 265, 229–248.

Hilfer, R., Luchko, Y.(2019). Desiderata for Fractional Derivatives and Integrals. Mathematics, 7, 149.

Hilger, S. (1988). Ein Maßkettenkalkül mit Anwendung auf Zentrmsmannigfaltingkeiten, Ph.D. Thesis,

Univarsi. Würzburg.

Agarwal, R.P., O'Regan, D., Saker, S.H. (2016). *Hardy Type Inequalities on Time Scales*, Springer,

Switzerland.

Bohner, M., Agarwal, R.P. (1999). Basic calculus on time scales and some of its applications, Resultate der Mathematic. 35, 3-22.

Bohner, M., Peterson, A. (2001). *Dynamic equations on time scales, An introduction with applications*.

Birkhauser, Boston.

Akın, L. (2021). On innovations of n-dimensional integral-type inequality on time scales. Adv. Differ. Equ. 148 (2021).

Akın, L. (2021). A New Approach for the Fractional Integral Operator in Time Scales with Variable

Exponent Lebesgue Spaces. Fractal Fract. 5(7), 1-13.

Akın, L. (2020). On some results of weighted Hölder type inequality on time scales, Middle East Journal of Science. 6(1), 15-22.

Tan, J., Liu, Z. G. (2015). Some Boundedness of Homogeneous Fractional Integrals on Variable Exponent Function Spaces [J]. Acta Mathematica Sinica, Chinese Series, 58(2): 309-320.

P. Mikusi´nski, Measures, http://mikusinski.cos.ucf.edu/measures.pdf.

Mikusi´nski, P., Weiss, E. (2014). The Bochner Integral. arXiv:1403.5209 [math.FA]

(or arXiv:1403.5209v1 [math.FA] for this version).

Akın, L. (2020). On the Fractional Maximal Delta Integral Type Inequalities on Time Scales, Fractal Fract. 4(2), 1-10.

Chapter 6

A Research on the Reflections of Fractional Integral-Type Inequalities on Time Scale

Lütfi AKIN[1]

[1] *Doç. Dr.;Mardin Artuklu Üniversitesi İktisadi ve İdari Bilimler Fakültesi İşletme Bölümü.*
lutfiakin@artuklu.edu.tr ORCID No: 0000-0002-5653-9393

INTRODUCTION

Hardy's inequality has many applications in harmonic analysis and in different spaces, such as variable exponent Lebesgue spaces, Grand Lebesgue spaces, Morrey spaces, Sobolev spaces, etc. Hardy-type integral inequalities is essential in fluids dynamics, harmonic analysis, and time scale calculus. At the same time, the fractional position of this integral is one of the essential focal points of applied mathematics. We find it useful to start with the historical background of Hardy's inequality. I believe it will be more descriptive for the reader.

The following inequality was proved by G.H. Hardy [2]. If (b_n) is a sequence, then

$$\sum_{m=1}^{\infty}\left(\frac{b_1+b_2+b_3+\cdots+b_m}{m}\right)^c < \left(\frac{c}{c-1}\right)^c \sum_{m=1}^{\infty} b_m^c,$$

where $c > 1$, $c \in \mathbb{R}$.

The following inequality was proved by G.H. Hardy [3]. If g^c is integrable, then

$$\int_0^{\infty}\left(\frac{1}{s}\int_0^{s} g(\tau)d\tau\right)^c ds \le \left(\frac{c}{c-1}\right)^c \int_0^{\infty} g^c(s)ds, \quad \text{for } c > 1, g \geq 0. \tag{1}$$

holds.

In [4], inequality (1) has been generalized by G.H. Hardy. If g integrable on $(0,\infty)$, then

$$\int_0^{\infty}\left(\frac{1}{t^n}\int_t^{\infty} g(\tau)d\tau\right)^c dt \le \left(\frac{c}{1-n}\right)^c \int_0^{\infty} \frac{1}{t^{n-c}} g^c(t)dt, \quad n < 1, \tag{2}$$

holds.

$$\int_0^{\infty}\left(\frac{1}{t^n}\int_0^{t} g(\tau)dr\right)^c dt \le \left(\frac{c}{n-1}\right)^c \int_0^{\infty} \frac{1}{t^{n-c}} g^c(t)dt, \quad n > 1, \tag{3}$$

where $c > 1$, $g(t) > 0$.

In [5], G.H. Hardy demonstrated inequalities (2) and (3).

If (b_n) is a sequence, then we have

$$\sum_{n=1}^{\infty}\frac{1}{n^k}\left(\sum_{m=n}^{\infty} b_m\right)^c \le M\sum_{n=1}^{\infty}\frac{1}{n^{k-c}} b_n^c, \quad k < 1,$$

$$\sum_{n=1}^{\infty}\frac{1}{n^k}\left(\sum_{m=1}^{n} b_m\right)^c \le M\sum_{n=1}^{\infty}\frac{1}{n^{k-c}} b_n^c, \quad k > 1,$$

where $c > 1$, and $M > 0$. For more detailed see [6-9]. Now let's give our basic theorems, which will form the backbone of our work.

Theorem A: *[10] Let* $\mathbb{T}$ *be a time scalecalculus and* $b \in (0,\infty)_{\mathbb{T}}$, $p,q>0$, $\frac{p}{q} \geq 2$, *and* $\delta>1$. *Moreover suppose that* $f(\tau)\geq 0$, *and* $\int_b^\infty x^{\frac{p}{q}-\delta} g^{\frac{p}{q}}(x)\Delta x$. *If* $\Lambda(x)$ *operator is defined as follows,*

$$\Lambda(x)=\int_a^x f(\tau)\Delta\tau, \qquad for\ any\quad x \in [b,\infty)_{\mathbb{T}}, \tag{4}$$

then we have

$$\int_b^\infty \frac{1}{x^\delta}(\Lambda^\sigma(x))^{p/q}\Delta x \leq \frac{2^{\frac{p}{q}-2}pm^\delta}{q(\delta-1)}\left\{\int_a^\infty x^{\frac{p}{q}-\delta} f^{\frac{p}{q}}(x)\Delta x\right\}^{\frac{p}{q}} \times \left\{\int_b^\infty x^{-\gamma}\Lambda^\sigma(x)\Lambda^{\frac{p}{q}}\Delta x\right\}^{1-\frac{q}{p}} + \frac{2^{\frac{p}{q}-2}pm^\delta}{q(\delta-1)}\int_b^\infty x^{1-\delta}\left(\mu^{\frac{p}{q}}-1\right) f^{\frac{p}{q}}(x)\Delta x.$$

Theorem B: *[10] Let* $\mathbb{T}$ *be a time scale calculus and* $b \in (0,\infty)_{\mathbb{T}}$, $p,q>0$, $\frac{p}{q}\geq 2$, $\delta>1$. *Moreover suppose that*$f(\tau)\geq 0$, *and*$\int_a^\infty x^{\frac{p}{q}-\delta} f^{\frac{p}{q}}(x)\Delta x$. *If* $\Lambda(x)$ *operator is defined as in (4), then we have*

$$\int_b^\infty \frac{1}{x^\delta}(\Lambda^\sigma(x))^{p/q}\Delta x \leq \left(\frac{2^{\frac{p}{q}-1}m^\delta}{(\delta-1)}\right)^{\frac{p}{q}}\int_b^\infty x^{\frac{p}{q}-\delta} f^{\frac{p}{q}}(x)\Delta x.$$

Let H_β and $\widetilde{H}_\beta$ be the fractional Hardy operator and its adjoint on $(0,\infty)$,

$$H_\beta f(t)=\frac{1}{t^{1-\beta}}\int_0^t f(s)ds, \qquad \widetilde{H}_\beta f(t)=\int_t^\infty \frac{1}{t^{1-\beta}}f(s)ds,$$

where $0\leq\alpha<1$ (see [11]). When $\beta=0$, we denote H_0 as H and $\widetilde{H}_0$ as $\widetilde{H}$. In [2, 5], Hardy established the following integral inequalities,

$$\int_0^\infty |Hf(x)|^p dx \leq (p')^p\int_0^\infty |f(x)|^p dx, \quad p>1,$$

$$\int_0^\infty \left|\widetilde{H}f(x)\right|^p dx \leq p^p\int_0^\infty |f(x)|^p dx, \qquad p>1,$$

where $1/p+1/p'=1$. The above Hardy inequalities have many applications in analysis (for details see [12-14]). This study aims to extend A-B Theorems to n-variable integral inequalities in time scale calculation and present their different reflections.

MATHEMATICAL BACKGROUND

Time scale has been the field of study of many scientists for nearly half a century. These works were generally on inequalities and integrals. This inequalities and integrals have shed light on the solution of many problems encountered in various fields of science. For example, economics, optics, physics and of course mathematics, for details [1, 15, 16, 17, 18-23]. $\mathbb{T}$ (time scale calculus) is an arbitrary non-empty closed subset of $\mathbb{R}$. We will consider this equality $(0,\infty)_{\mathbb{T}} = (0,\infty) \cap \mathbb{T}$.

Definition 2.1 [16] The functions $\delta, \varepsilon: \mathbb{T} \to \mathbb{T}$ defined by $\delta(t) = \inf\{s \in \mathbb{T}: s > t\}$, $\varepsilon(t) = \sup\{s \in \mathbb{T}: s > t\}$, for $t \in \mathbb{T}$. $\delta(t)$ is the forward operator and $\varepsilon(t)$ is the backward operator.

If $\delta(t) > t$, then t is right-scattered.

If $\delta(t) = t$, then t is called right-dense.

If $\varepsilon(t) < t$, then t is left-scattered.

If $\varepsilon(t) = t$, then t is called left-dense.

Definition 2.2 [22] Let functions $\mu, \vartheta: \mathbb{T} \to \mathbb{R}^+$ such that $\mu(t) = \delta(t) - t$, $\vartheta(t) = t - \varepsilon(t)$ are called graininess functions.

If $\mathbb{T}$ (time scale calculus) has a left-scattered maximum m, then $\mathbb{T}^k = \mathbb{T} - \{m\}$. Or $\mathbb{T}^k = \mathbb{T}$.

$$\mathbb{T}^k = \begin{cases} \mathbb{T} \setminus (\varepsilon \sup \mathbb{T}, \sup \mathbb{T}], & \text{if} \quad \sup \mathbb{T} < \infty, \\ \mathbb{T}, & \text{if} \quad \sup \mathbb{T} = \infty. \end{cases}$$

At the same time

$$\mathbb{T}_k = \begin{cases} \mathbb{T} \setminus [\inf \mathbb{T}, \delta(\mathbb{T})], & |\inf \mathbb{T}| < \infty, \\ \mathbb{T}, & \inf \mathbb{T} = -\infty. \end{cases}$$

Also suppose that $h: \mathbb{T} \to \mathbb{R}$ is a function, and $t \in \mathbb{T}^k (t \neq min\mathbb{T})$.

If h is $\Delta -$ differentiable at point t, then h is continuous at point t.

If h is left continuous at point t and t is right-scattered, then h is $\Delta -$ differentiable at point t,

$$h^{\Delta}(t) = \frac{h^{\delta}(t) - h(t)}{\mu(t)}$$

Let t is right-dense. If h is $\Delta -$ differentiable at point t and $\lim_{s \to t} \frac{h(t)-h(s)}{t-s}$, then

$$h^{\Delta}(t) = \lim_{s \to t} \frac{h(t) - h(s)}{t - s}.$$

If h is $\Delta -$ differentiable at point t, then $h^{\delta}(t) = h(t) + \mu(t) h^{\Delta}(t)$. If $\mathbb{T}$ is real numbers, then $h^{\Delta}(t) = h'(t)$. If $\mathbb{T}$ is integers, then $h^{\Delta}(t)$ reduces to $\Delta h(t)$. The $C_{rd}(\mathbb{T})$ is all rd-continuous functions.

Let $h, h^{\delta}: \mathbb{T} \to \mathbb{R}$ by $h^{\delta}(t) = h(\delta(t))$ for all $t \in \mathbb{T}$, i.e., $h^{\delta} = h \circ \delta$, and let $h, h^{\varepsilon}: \mathbb{T} \to \mathbb{R}$ by $h^{\varepsilon}(t) = h(\varepsilon(t))$ for all $t \in \mathbb{T}$, i.e., $h^{\varepsilon} = h \circ \varepsilon$.

Definition 2.3 [16] The $h^{\Delta}(t)$ delta derivative is defined as follows. A neighborhood V of t for every $\varepsilon > 0$ and $s, t \in V$ such that

$$\left|h(\delta(t)) - \mathrm{h(s)} - h^{\Delta}(t)(\delta(t) - s)\right| \leq |\delta(t) - s|.$$

Suppose that $H: \mathbb{T} \to \mathbb{R}$ is defined Δ −antiderivative of $h: \mathbb{T} \to \mathbb{R}$, then $H^{\Delta} = h(t)$ holds for all $t \in \mathbb{T}$, and we define Cauchy Δ −integral of h by

$$\int_{s}^{t} h(\tau)\Delta\tau = H(t) - H(s),$$

for $s, t \in \mathbb{T}$. If $a, b \in \mathbb{T}$ and $u, v \in C_{rd}(\mathbb{T})$, then

$$\int_{a}^{b} u(x)v^{\Delta}(x)\Delta x = [u(x)v(x)]_{a}^{b} - \int_{a}^{b} v^{\sigma}(x)u^{\Delta}(x)\Delta x. \tag{5}$$

Suppose that $f, g : \mathbb{R} \to \mathbb{R}$ is Δ −differentiable, then $f \circ g: \mathbb{R} \to \mathbb{R}$ is Δ − differentiable, and

$$(f \circ g)^{\Delta}(x) = \left\{\int_{0}^{1} f'(g(x) + h\mu(x)g^{\Delta}(x))\, dh\right\} g^{\Delta}(x). \tag{6}$$

If f, g satisfy the conditions of [16], then $f \circ g: \mathbb{T} \to \mathbb{R}$ is Δ − differentiable (Hilger), and $d \in [x, \sigma(x)]$ such that

$$(f \circ g)^{\Delta}(x) = f'\big(g(d)\big)g^{\Delta}(x). \tag{7}$$

If $g, h: \mathbb{T} \to \mathbb{R}$ functions, $a, b \in \mathbb{T}$, $p > 1$, and $1/p + 1/q = 1$, then

$$\int_{a}^{b} g(x)h(x)dx \leq \left(\int_{a}^{b} (g(x))^{p} dx\right)^{\frac{1}{p}} \left(\int_{a}^{b} (h(x))^{q} dx\right)^{\frac{1}{q}}. \tag{8}$$

Let (Φ, N, μ_{Δ}), and let (Ψ, M, η_{Δ}) be measure spaces (see [17]). If $\Lambda: \Phi \times \Psi \to \mathbb{R}$ is a $\mu_{\Delta} \times \eta_{\Delta}$ −integrable function, then $\varphi_1(x_2) = \int_{\Phi} \Lambda(x_1, x_2)\Delta x_1$ exists for any $x_1 \in \Psi$ and $\varphi_2(x_1) = \int_{\Psi} \Lambda(x_1, x_2)\Delta x_2$ exists for $x_2 \in \Phi$, and

$$\int_{\Phi} \Delta x_1 \int_{\Psi} \Lambda(x_1, x_2)\Delta t_2$$

$$= \int_{\Psi} \Delta x_2 \int_{\Phi} \Lambda(x_1, x_2)\Delta x_1. \tag{9}$$

We suppose that there exists $m_i > 0$ with

$$\frac{m_i \tau_i}{\sigma_i(\tau_i)} \geq 1, \tag{10}$$

$$\text{for } \tau_i \geq b_i,\ i \in \{1, \dots, n\}.$$

$$\Lambda_m^{\sigma_1,\dots,\sigma_j}(x_1, \dots, x_n) \doteq \Lambda_m^{\sigma_1,\dots,\sigma_j} \doteq \Lambda_m\left(\sigma_1(x_1), \dots, \sigma_j(x_j), x_{j+1}, \dots, x_n\right),$$

$$\text{for } m, j \in \{1, \dots, n\}.$$

$$\int_{b_1}^{\infty} \dots \int_{b_n}^{\infty} g(x_1, \dots, x_n)\Delta x_1, \dots, \Delta x_n \doteq \int_{\prod_{i=1}^{n} b_i}^{\infty} g(x_1, \dots, x_n) \prod_{i=1}^{n} \Delta x_i.$$

We will use the following inequalities to prove our results.

$$a^{\gamma} + b^{\gamma} \leq (a+b)^{\gamma} \leq 2^{\gamma-1}(a^{\gamma} + b^{\gamma}) \text{ for } a, b \geq 0, \gamma \geq 1 \tag{11}$$

$$2^{\gamma-1}(a^{\gamma} + b^{\gamma}) \leq (a+b)^{\gamma} \leq a^{\gamma} + b^{\gamma} \text{ for } a, b \geq 0, 0 \leq \gamma \leq 1. \tag{12}$$

Main Result

We will use the mathematical induction method to reach our research results.

Theorem 3.1 *Assume that $\mathbb{T}_i$ is a time scale calculus and $i \in \{1, \dots, n\}$, $b_i \in (0, \infty) \cap \mathbb{T}_i$, $\delta_i > 1$. Moreover suppose that $f: [b_1, \infty)_{\mathbb{T}_1} \times \dots \times [b_n, \infty)_{\mathbb{T}_n} \to \mathbb{R}^+$ is a non-negative function such that the Hilger integrals*

$$\int_{\prod_{i=1}^{n} b_i}^{\infty} \prod_{i=1}^{n} (b_i)^{\beta-1} \prod_{i=1}^{n} (x_i)^{\frac{p}{q}-\delta_i} f^{\frac{p}{q}}(x_1, \dots, x_n)\Delta x_i$$

for any $(x_1, \dots, x_n) \in [b_1, \infty)_{\mathbb{T}_1} \times \dots \times [b_n, \infty)_{\mathbb{T}_n}$ exist. Let define

$$\widetilde{H}_{\beta,m}(x_1, \dots, x_n) = \int_{\prod_{j=1}^{m} b_j}^{\infty} \prod_{j=1}^{m} (b_j)^{\beta-1} f(\tau_1, \dots, \tau_n) \prod_{j=1}^{m} \Delta\tau_j, \tag{13}$$

then for $p, q > 0$, $m \in \{1, \dots, n\}$, and $p/q \geq 2$

$$\int_{\prod_{i=1}^{n} b_i}^{\infty} \left(\widetilde{H}_{\beta,n}^{\sigma_1 \dots \sigma_n}\right)^{\frac{p}{q}} \prod_{i=1}^{n} x_i^{-\delta_i} \Delta x_i$$

$$\leq \sum_{s=1}^{n} \prod_{j=s+1}^{n} d_j \widetilde{d_s} \int_{\prod_{j=s+1}^{n} b_j}^{\infty} \prod_{j=s+1}^{n} x_j^{1-\delta_j} \left(\mu_j(x_j)\right)^{\frac{p}{q}-1} \int_{\prod_{i=1}^{s-1} b_i} \prod_{i=1}^{s-1} x_i^{-\delta_i}$$

$$\times \left\{ \int_{b_s}^{\infty} \left(\widetilde{H}_{\beta,s-1}^{\sigma_1 \dots \sigma_{s-1}}\right)^{\frac{p}{q}} x_s^{\frac{p}{q}-\delta_s} \Delta x_s \right\}^{\frac{q}{p}} \times \left\{ \left(\widetilde{H}_{\beta,s}^{\sigma_1 \dots \sigma_s}\right) \left(\widetilde{H}_{\beta,s}^{\sigma_1 \dots \sigma_{s-1}}\right)^{\frac{p}{q}} \Delta x_s \right\}^{1-\frac{q}{p}} \prod_{i=1}^{s-1} \Delta x_i \prod_{j=s+1}^{n} \Delta x_j$$

$$+\prod_{i=1}^{n}\widetilde{d_i}\int\limits_{\prod_{i=1}^{n}b_i}^{\infty}\prod_{i=1}^{n}{x_i}^{1-\delta_i}(\mu_i(x_i))^{\frac{p}{q}-1}f^{\frac{p}{q}}(x_1,\dots,x_n)\prod_{i=1}^{n}\Delta x_i \tag{14}$$

holds, where $\widetilde{d_s}=d_s\frac{p}{q}$, $d_s=\frac{2^{\frac{p}{q}-2}{m_s}^{\delta_s}}{\delta_{s-1}}$.

Proof. Theorem A is true for $n=1$ and $\beta=1$. Let's assume that the statement for $1\le n\le m$ is true. We have to prove that the statement for $n=m+1$ is true. Therefore

$$\int\limits_{\prod_{i=1}^{m+1}b_i}^{\infty}\left(\widetilde{H}_{\beta,m+1}^{\sigma_1\dots\sigma_{m+1}}\right)^{\frac{p}{q}}\prod_{i=1}^{m+1}{x_i}^{-\delta_i}\,\Delta x_i. \tag{15}$$

Denote

$$\int\limits_{b_{m+1}}^{\infty}\left(\widetilde{H}_{\beta,m+1}^{\sigma_1\dots\sigma_{m+1}}\right)^{\frac{p}{q}}{x_{m+1}}^{-\delta_{m+1}}\Delta x_{m+1}=J_{m+1}.$$

If we apply (5) with $\frac{\partial}{\Delta x_{m+1}}v(x_{m+1})={x_{m+1}}^{-\delta_{m+1}}$ and $u^{\sigma_{m+1}}(x_{m+1})=\left(\widetilde{H}_{\beta,m+1}^{\sigma_1\dots\sigma_{m+1}}\right)^{\frac{p}{q}}$ by keeping fix $(x_1,\dots,x_m)\in[b_1,\infty)_{\mathbb{T}_1}\times\dots\times[b_m,\infty)_{\mathbb{T}_m}$, then we obtain

$$J_{m+1}=\left[\frac{\left(\widetilde{H}_{\beta,m+1}^{\sigma_1\dots\sigma_{m+1}}\right)^{\frac{p}{q}}}{v(x_{m+1})^{-1}}\right]\mathrm{I}_{b_{m+1}}^{\infty}\int\limits_{b_{m+1}}^{\infty}-v(x_{m+1})\frac{\partial}{\Delta x_{m+1}}\left(\widetilde{H}_{\beta,m+1}^{\sigma_1\dots\sigma_{m+1}}\right)^{\frac{p}{q}}\Delta x_{m+1}, \tag{16}$$

where,

$$v(x_{m+1})=-\int\limits_{x_{m+1}}^{\infty}\tau_{m+1}^{-\delta_{m+1}}\Delta\,\tau_{m+1}. \tag{17}$$

If we use (6) and $\sigma_{m+1}(\tau_{m+1})\ge\tau_{m+1}$ to get

$$\frac{\partial}{\Delta\tau_{m+1}}\left(-\tau_{m+1}^{1-\delta_{m+1}}\right)=(\delta_{m+1}-1)\int_0^1[g_{m+1}\sigma_{m+1}(\tau_{m+1})+(1-g_{m+1})\tau_{m+1}]^{-\delta_{m+1}}dg_{m+1}$$

$$\ge\frac{(\delta_{m+1}-1)}{\sigma_{m+1}^{\delta_{m+1}}(\tau_{m+1})} \tag{18}$$

(10) together with (19) gives

$$\frac{\partial}{\Delta\tau_{m+1}}\left(-\tau_{m+1}^{1-\delta_{m+1}}\right)\ge\frac{(\delta_{m+1}-1)}{m_{m+1}^{\delta_{m+1}}\tau_{m+1}^{\delta_{m+1}}}.$$

Therefore

$$\int\limits_{x_{m+1}}^{\infty}-\tau_{m+1}^{-\delta_{m+1}}\Delta\,\tau_{m+1}\ge\int\limits_{x_{m+1}}^{\infty}-\frac{m_{m+1}^{\delta_{m+1}}}{\delta_{m+1}-1}\frac{\partial}{\Delta\tau_{m+1}}\left(-\tau_{m+1}^{1-\delta_{m+1}}\right)\Delta\,\tau_{m+1}$$

$$=-\frac{m_{m+1}^{\delta_{m+1}}}{\delta_{m+1}-1}\left(x_{m+1}^{1-\delta_{m+1}}\right) \tag{19}$$

(17) together with (19) gives

$$-v(x_{m+1}) = \int_{x_{m+1}}^{\infty} \tau_{m+1}^{-\delta_{m+1}} \Delta\tau_{m+1}$$

$$\leq \frac{m_{m+1}^{\delta_{m+1}}}{\delta_{m+1}-1}\left(x_{m+1}^{1-\delta_{m+1}}\right). \tag{20}$$

From (13), (16), (17), (20), we have

$$J_{m+1}$$

$$= \frac{m_{m+1}^{\delta_{m+1}}}{\delta_{m+1}-1} \int_{b_{m+1}}^{\infty} x_{m+1}^{1-\delta_{m+1}} \frac{\partial}{\Delta x_{m+1}}\left(\widetilde{H}_{\beta,m+1}^{\sigma_1\ldots\sigma_m}\right)^{\frac{p}{q}} \Delta x_{m+1}. \tag{21}$$

If we apply (6), then we have

$$\frac{\partial}{\Delta x_{m+1}}\left(\widetilde{H}_{\beta,m+1}^{\sigma_1\ldots\sigma_m}\right)^{\frac{p}{q}} = \frac{p}{q}\frac{\partial}{\Delta x_{m+1}}\widetilde{H}_{\beta,m+1}^{\sigma_1\ldots\sigma_m}$$

$$\times \int_0^1 \Big[\widetilde{H}_{\beta,m+1}$$

$$+ g_{m+1}\mu_{m+1}(x_{m+1})\frac{\partial}{\Delta x_{m+1}}\widetilde{H}_{\beta,m+1}^{\sigma_1\ldots\sigma_m}\Big]^{\frac{p}{q}-1} dg_{m+1}. \tag{22}$$

If we apply (11) to (22), then we have

$$\frac{\partial}{\Delta x_{m+1}}\widetilde{H}_{\beta,m+1}^{\sigma_1\ldots\sigma_m} \leq \frac{p2^{\frac{p}{q}-2}}{q}\left(\widetilde{H}_{\beta,m+1}^{\sigma_1\ldots\sigma_m}\right)^{\frac{p}{q}-1}\frac{\partial}{\Delta x_{m+1}}\left(\widetilde{H}_{\beta,m+1}^{\sigma_1\ldots\sigma_m}\right)$$

$$+\frac{p2^{\frac{p}{q}-2}}{q}\left(\mu_{m+1}(x_{m+1})\right)^{\frac{p}{q}-1}\left(\frac{\partial}{\Delta x_{m+1}}\widetilde{H}_{\beta,m+1}^{\sigma_1\ldots\sigma_m}\right)^{\frac{p}{q}}. \tag{23}$$

Substitute (23) into (21), then we obtain

$$J_{m+1} \leq \frac{p2^{\frac{p}{q}-2}m_{m+1}^{\delta_{m+1}}}{q(\delta_{m+1}-1)} \int_{b_{m+1}}^{\infty} x_{m+1}^{1-\delta_{m+1}}\left(\widetilde{H}_{\beta,m+1}^{\sigma_1\ldots\sigma_m}\right)^{\frac{p}{q}-1}\frac{\partial}{\Delta x_{m+1}}\widetilde{H}_{\beta,m+1}^{\sigma_1\ldots\sigma_m}\Delta x_{m+1}$$

$$+\frac{p2^{\frac{p}{q}-2}m_{m+1}^{\delta_{m+1}}}{q(\delta_{m+1}-1)} \int_{b_{m+1}}^{\infty} x_{m+1}^{1-\delta_{m+1}}\left(\mu_{m+1}(x_{m+1})\right)^{\frac{p}{q}-1}\left(\frac{\partial}{\Delta x_{m+1}}\widetilde{H}_{\beta,m+1}^{\sigma_1\ldots\sigma_m}\right)^{\frac{p}{q}}\Delta x_{m+1}. \tag{24}$$

Since

$$\frac{\partial}{\Delta x_{m+1}}\widetilde{H}_{\beta,m+1}^{\sigma_1\ldots\sigma_m} = \widetilde{H}_{\beta,m}^{\sigma_1\ldots\sigma_m}$$

$$\geq 0. \tag{25}$$

If we use (25) in (24), then we obtain

$$J_{m+1} \leq \frac{p2^{\frac{p}{q}-2}m_{m+1}^{\delta_{m+1}}}{q(\delta_{m+1}-1)} \int_{b_{m+1}}^{\infty} x_{m+1}^{1-\delta_{m+1}}\left(\widetilde{H}_{\beta,m+1}^{\sigma_1\ldots\sigma_m}\right)^{\frac{p}{q}-1}\widetilde{H}_{\beta,m}^{\sigma_1\ldots\sigma_m}\Delta x_{m+1}$$

$$+\frac{p2^{\frac{p}{q}-2}m_{m+1}^{\delta_{m+1}}}{q(\delta_{m+1}-1)} \int_{b_{m+1}}^{\infty} x_{m+1}^{1-\delta_{m+1}}\left(\mu_{m+1}(x_{m+1})\right)^{\frac{p}{q}-1}\left(\widetilde{H}_{\beta,m}^{\sigma_1\ldots\sigma_m}\right)^{\frac{p}{q}}\Delta x_{m+1}. \tag{26}$$

Substitute (26) in (15), then we obtain

$$\int_{\prod_{i=1}^{m+1}b_i}^{\infty}\left(\widetilde{H}_{\beta,m+1}^{\sigma_1\ldots\sigma_{m+1}}\right)^{\frac{p}{q}}\prod_{i=1}^{m+1}x_i^{-\delta_i}\Delta x_i$$

$$\leq \int_{\prod_{i=1}^{m} b_i}^{\infty} \frac{p2^{\frac{p}{q}-2} m_{m+1}^{\delta_{m+1}}}{q(\delta_{m+1}-1)} \int_{b_{m+1}}^{\infty} x_{m+1}^{1-\delta_{m+1}} \left(\widetilde{H}_{\beta,m+1}^{\sigma_1 \dots \sigma_m}\right)^{\frac{p}{q}-1} \widetilde{H}_{\beta,m}^{\sigma_1 \dots \sigma_m} \prod_{i=1}^{m} x_i^{-\delta_i} \Delta x_{m+1} \Delta x_i$$

$$+ \int_{\prod_{i=1}^{m} b_i}^{\infty} \frac{p2^{\frac{p}{q}-2} m_{m+1}^{\delta_{m+1}}}{q(\delta_{m+1}-1)}$$

$$\times \int_{b_{m+1}}^{\infty} x_{m+1}^{1-\delta_{m+1}} \left(\mu_{m+1}(x_{m+1})\right)^{\frac{p}{q}-1} \left(\widetilde{H}_{\beta,m}^{\sigma_1 \dots \sigma_m}\right)^{\frac{p}{q}} \prod_{i=1}^{m} x_i^{-\delta_i} \Delta x_{m+1} \Delta x_i . \tag{27}$$

If we replace the integrals of (27) m-times by using (9), then

$$= \frac{p2^{\frac{p}{q}-2} m_{m+1}^{\delta_{m+1}}}{q(\delta_{m+1}-1)} \int_{b_{m+1}}^{\infty} x_{m+1}^{1-\delta_{m+1}} \int_{\prod_{i=1}^{m+1} b_i}^{\infty} \left(\widetilde{H}_{\beta,m+1}^{\sigma_1 \dots \sigma_m}\right)^{\frac{p}{q}-1} \widetilde{H}_{\beta,m}^{\sigma_1 \dots \sigma_m} \prod_{i=1}^{m} x_i^{-\delta_i} \Delta x_i \Delta x_{m+1}$$

$$+ \frac{p2^{\frac{p}{q}-2} m_{m+1}^{\delta_{m+1}}}{q(\delta_{m+1}-1)} \left(\mu_{m+1}(x_{m+1})\right)^{\frac{p}{q}-1} \int_{b_{m+1}}^{\infty} x_{m+1}^{1-\delta_{m+1}}$$

$$\times \int_{\prod_{i=1}^{m+1} b_i}^{\infty} \left(\widetilde{H}_{\beta,m}^{\sigma_1 \dots \sigma_m}\right)^{\frac{p}{q}} \prod_{i=1}^{m} x_i^{-\delta_i} \Delta x_i \Delta x_{m+1} . \tag{28}$$

If we use the induction method with $\widetilde{H}_{\beta,m}^{\sigma_1 \dots \sigma_m}$ in (28) for $x_{m+1} \in \mathbb{T}_{m+1}$ and apply (9) m-times, then we obtain

$$= \frac{p2^{\frac{p}{q}-2} m_{m+1}^{\delta_{m+1}}}{q(\delta_{m+1}-1)} \int_{b_{m+1}}^{\infty} x_{m+1}^{1-\delta_{m+1}} \int_{\prod_{i=1}^{m+1} b_i}^{\infty} \left(\widetilde{H}_{\beta,m+1}^{\sigma_1 \dots \sigma_m}\right)^{\frac{p}{q}-1} \widetilde{H}_{\beta,m}^{\sigma_1 \dots \sigma_m} \prod_{i=1}^{m} x_i^{-\delta_i} \Delta x_i \Delta x_{m+1}$$

$$+ \frac{p2^{\frac{p}{q}-2} m_{m+1}^{\delta_{m+1}}}{q(\delta_{m+1}-1)} \left(\mu_{m+1}(x_{m+1})\right)^{\frac{p}{q}-1} \int_{b_{m+1}}^{\infty} x_{m+1}^{1-\delta_{m+1}}$$

$$\times \sum_{s=1}^{m} \prod_{j=s+1}^{m} d_j \widetilde{d_s} \int_{\prod_{j=s+1}^{m} b_j}^{\infty} \prod_{j=s+1}^{m} x_j^{\delta_j - 1} \left(\mu_j(x_j)\right)^{\frac{p}{q}-1}$$

$$\times \int_{\prod_{i=1}^{s-1} b_i}^{\infty} \prod_{i=1}^{s-1} x_i^{-\delta_i} \left(\int_{b_s}^{\infty} x_s^{\frac{p}{q}-\delta_s} \left(\widetilde{H}_{\beta,s-1}^{\sigma_1 \dots \sigma_{s-1}}\right)^{\frac{p}{q}} \Delta x_s \right)^{\frac{q}{p}}$$

$$\times \left\{ \left(\widetilde{H}_{\beta,s}^{\sigma_1 \dots \sigma_s}\right) \left(\widetilde{H}_{\beta,s}^{\sigma_1 \dots \sigma_{s-1}}\right)^{\frac{p}{q}} \Delta x_s \right\}^{1-\frac{q}{p}} \prod_{i=1}^{s-1} \Delta x_i \prod_{j=s+1}^{m} \Delta x_j$$

$$+ \prod_{i=1}^{m} \widetilde{d}_i \int_{\prod_{i=1}^{m} b_i}^{\infty} \prod_{i=1}^{m} x_i^{1-\delta_i} \left(\mu_i(x_i)\right)^{\frac{p}{q}-1} f^{\frac{p}{q}}(x_1, \dots, x_m) \prod_{i=1}^{m} \Delta x_i .$$

Hence, we obtain

$$\int_{\prod_{i=1}^{m+1} b_i}^{\infty} \left(\widetilde{H}_{\beta,n}^{\sigma_1\dots\sigma_n}\right)^{\frac{p}{q}} \prod_{i=1}^{m+1} x_i^{-\delta_i}\,\Delta x_i$$

$$\leq \sum_{s=1}^{m+1} \prod_{j=s+1}^{m+1} d_j \widetilde{d_s} \int_{\prod_{j=s+1}^{m+1} b_j}^{\infty} \prod_{j=s+1}^{m+1} x_j^{1-\delta_j} \left(\mu_j(x_j)\right)^{\frac{p}{q}-1} \int_{\prod_{i=1}^{s-1} b_i}^{\infty} \prod_{i=1}^{s-1} x_i^{-\delta_i}$$

$$\times \left(\int_{b_s}^{\infty} x_s^{\frac{p}{q}-\delta_s} \left(\widetilde{H}_{\beta,s-1}^{\sigma_1\dots\sigma_{s-1}}\right)^{\frac{p}{q}} \Delta x_s \right)^{\frac{q}{p}} \left\{ \left(\widetilde{H}_{\beta,s}^{\sigma_1\dots\sigma_s}\right) \left(\widetilde{H}_{\beta,s}^{\sigma_1\dots\sigma_{s-1}}\right)^{\frac{p}{q}} \Delta x_s \right\}^{1-\frac{q}{p}} \prod_{i=1}^{s-1} \Delta x_i \prod_{j=s+1}^{m+1} \Delta x_j$$

$$+ \prod_{i=1}^{m+1} \widetilde{d_i} \int_{\prod_{i=1}^{m+1} b_i}^{\infty} \prod_{i=1}^{m+1} x_i^{1-\delta_i} \left(\mu_i(x_i)\right)^{\frac{p}{q}-1} f^{\frac{p}{q}}(x_1, \dots, x_{m+1}) \prod_{i=1}^{m+1} \Delta x_i.$$

Hereby, we reach the desired result for all $n \in \mathbb{N}$. □

Theorem 3.2 *Assume that $\mathbb{T}_i$ is a time scale calculus and $i \in \{1, \dots, n\}$, $b_i \in (0, \infty) \cap \mathbb{T}_i$, $\delta_i > 1$. Moreover suppose that $f: [b_1, \infty)_{\mathbb{T}_1} \times \dots \times [b_n, \infty)_{\mathbb{T}_n} \to \mathbb{R}^+$ is a non-negative function such that the Hilger integrals*

$$\int_{\prod_{i=1}^{n} b_i}^{\infty} \prod_{i=1}^{n} (b_i)^{\beta-1} \prod_{i=1}^{n} (x_i)^{\frac{p}{q}-\delta_i} f^{\frac{p}{q}}(x_1, \dots, x_n) \prod_{i=1}^{n} \Delta x_i$$

for any $(x_1, \dots, x_n) \in [b_1, \infty)_{\mathbb{T}_1} \times \dots \times [b_n, \infty)_{\mathbb{T}_n}$ exist. Let define

$$\widetilde{H}_{\beta,m}(x_1, \dots, x_n) = \int_{\prod_{j=1}^{m} b_j}^{\infty} \prod_{j=1}^{m} (b_j)^{\beta-1} f(\tau_1, \dots, \tau_n) \prod_{j=1}^{m} \Delta\tau_j, \quad m \in \{1, \dots, n\},$$

then for $p, q > 0$, and $p/q \geq 2$

$$\int_{\prod_{i=1}^{n} b_i}^{\infty} \left(\widetilde{H}_{\beta,n}^{\sigma_1\dots\sigma_n}\right)^{\frac{p}{q}} \prod_{i=1}^{n} x_i^{-\delta_i} \prod_{i=1}^{n} \Delta x_i \leq \left(\frac{p}{q}\right)^{\frac{np}{q}} \prod_{i=1}^{n} \left(\frac{2^{\frac{p}{q}-1} m_i^{\delta_i}}{\delta_i - 1} \right)^{\frac{p}{q}}$$

$$\times \int_{\prod_{i=1}^{n} b_i}^{\infty} \prod_{i=1}^{n} (b_i)^{\beta-1} \prod_{i=1}^{n} (x_i)^{\frac{p}{q}-\delta_i} f^{\frac{p}{q}}(x_1, \dots, x_n) \prod_{i=1}^{n} \Delta x_i, \tag{29}$$

holds.

Proof. Theorem B is true for $n = 1$ and $\beta = 1$. Let's assume that the statement for $1 \leq n \leq m$ is true. We have to prove that the statement for $n = m + 1$ is true.

If we apply (6), yields

$$\frac{\partial}{\Delta x_{m+1}} \widetilde{H}_{\beta,m+1}^{\sigma_1\dots\sigma_m} = \left(\frac{p}{q}\right) \frac{\partial}{\Delta x_{m+1}} \widetilde{H}_{\beta,m+1}^{\sigma_1\dots\sigma_m}$$

$$\times \int_0^1 \left[g_{m+1} \widetilde{H}_{\beta,m+1}^{\sigma_1\dots\sigma_{m+1}} + \widetilde{H}_{\beta,m+1}^{\sigma_1\dots\sigma_m} (1 - g_{m+1}) \right]^{\frac{p-q}{q}} dg_{m+1}. \tag{30}$$

If we use (11), then we have

$$\leq \left(\frac{p}{q}\right)2^{\frac{p}{q}-2}\left(\widetilde{H}_{\beta,m+1}^{\sigma_1\dots\sigma_{m+1}}\right)^{\frac{p-q}{q}}\frac{\partial}{\Delta x_{m+1}}\widetilde{H}_{\beta,m+1}^{\sigma_1\dots\sigma_m}+\left(\frac{p}{q}\right)2^{\frac{p}{q}-2}\left(\widetilde{H}_{\beta,m+1}^{\sigma_1\dots\sigma_m}\right)^{\frac{p-q}{q}}\frac{\partial}{\Delta x_{m+1}}\widetilde{H}_{\beta,m+1}^{\sigma_1\dots\sigma_m},$$

use $\sigma_{m+1}(x_{m+1}) \geq x_{m+1}$

$$=\left(\frac{p}{q}\right)2^{\frac{p}{q}-2}\left(\widetilde{H}_{\beta,m+1}^{\sigma_1\dots\sigma_{m+1}}\right)^{\frac{p-q}{q}}\frac{\partial}{\Delta x_{m+1}}\widetilde{H}_{\beta,m+1}^{\sigma_1\dots\sigma_m}+\left(\frac{p}{q}\right)2^{\frac{p}{q}-2}\left(\widetilde{H}_{\beta,m+1}^{\sigma_1\dots\sigma_{m+1}}\right)^{\frac{p-q}{q}}\frac{\partial}{\Delta x_{m+1}}\widetilde{H}_{\beta,m+1}^{\sigma_1\dots\sigma_m}$$

$$=\left(\frac{p}{q}\right)2^{\frac{p}{q}-1}\left(\widetilde{H}_{\beta,m+1}^{\sigma_1\dots\sigma_{m+1}}\right)^{\frac{p-q}{q}}\frac{\partial}{\Delta x_{m+1}}\widetilde{H}_{\beta,m+1}^{\sigma_1\dots\sigma_m}. \tag{31}$$

Since

$$\frac{\partial}{\Delta x_{m+1}}\widetilde{H}_{\beta,m+1}^{\sigma_1\dots\sigma_m}=\widetilde{H}_{\beta,m}^{\sigma_1\dots\sigma_m}$$

$$\geq 0. \tag{32}$$

Use (32) in (31) and substitute in (21) to get

$$J_{m+1}\leq\frac{p2^{\frac{p}{q}-1}m_{m+1}^{\delta_{m+1}}}{q(\delta_{m+1}-1)}\int_{b_{m+1}}^{\infty}x_{m+1}^{\delta_{m+1}}\left(\widetilde{H}_{\beta,m+1}^{\sigma_1\dots\sigma_{m+1}}\right)^{\frac{p-q}{q}}\widetilde{H}_{\beta,m}^{\sigma_1\dots\sigma_m}\Delta x_{m+1}. \tag{33}$$

If we apply Hölder's inequality, then we obtain

$$J_{m+1}\leq\frac{p2^{\frac{p}{q}-1}m_{m+1}^{\delta_{m+1}}}{q(\delta_{m+1}-1)}\left[\int_{b_{m+1}}^{\infty}\left[\frac{\left(x_{m+1}^{\delta_{m+1}}\right)^{\frac{p-q}{q}}}{\left(x_{m+1}^{\delta_{m+1}}\right)^{-1}}\widetilde{H}_{\beta,m}^{\sigma_1\dots\sigma_m}\right]^{\frac{p}{q}}\Delta x_{m+1}\right]^{\frac{q}{p}}\times\left(J_{m+1}\right)^{\frac{p-q}{q}}.$$

After simplification, we get

$$J_{m+1}\leq\left(\frac{p2^{\frac{p}{q}-1}m_{m+1}^{\delta_{m+1}}}{q(\delta_{m+1}-1)}\right)^{\frac{p}{q}}\int_{b_{m+1}}^{\infty}x_{m+1}^{\frac{p}{q}-\delta_{m+1}}\left(\widetilde{H}_{\beta,m}^{\sigma_1\dots\sigma_m}\right)^{\frac{p}{q}}\Delta x_{m+1}. \tag{34}$$

Substitute (35) into (16)

$$\int_{\prod_{i=1}^{m+1}b_i}^{\infty}\left(\widetilde{H}_{\beta,m+1}^{\sigma_1\dots\sigma_{m+1}}\right)^{\frac{p}{q}}\prod_{i=1}^{m+1}x_i^{-\delta_i}\prod_{i=1}^{m+1}\Delta x_i$$

$$\leq\int_{\prod_{i=1}^{m}b_i}^{\infty}\left(\frac{p2^{\frac{p}{q}-1}m_{m+1}^{\delta_{m+1}}}{q(\delta_{m+1}-1)}\right)^{\frac{p}{q}}\prod_{i=1}^{m}x_i^{-\delta_i}\int_{b_{m+1}}^{\infty}x_{m+1}^{\frac{p}{q}-\delta_{m+1}}\left(\widetilde{H}_{\beta,m}^{\sigma_1\dots\sigma_m}\right)^{\frac{p}{q}}\Delta x_{m+1}. \tag{35}$$

If we replace the integrals of (35) m-times by using (9), then

$$\int_{\prod_{i=1}^{m+1}b_i}^{\infty}\left(\widetilde{H}_{\beta,m+1}^{\sigma_1\dots\sigma_{m+1}}\right)^{\frac{p}{q}}\prod_{i=1}^{m+1}x_i^{-\delta_i}\prod_{i=1}^{m+1}\Delta x_i=\left(\frac{p2^{\frac{p}{q}-1}m_{m+1}^{\delta_{m+1}}}{q(\delta_{m+1}-1)}\right)^{\frac{p}{q}}$$

$$\times\int_{b_{m+1}}^{\infty}x_{m+1}^{\frac{p}{q}-\delta_{m+1}}\left[\int_{\prod_{i=1}^{m}b_i}^{\infty}\left(\widetilde{H}_{\beta,m}^{\sigma_1\dots\sigma_m}\right)^{\frac{p}{q}}\prod_{i=1}^{m}x_i^{-\delta_i}\prod_{i=1}^{m}\Delta x_i\right]\Delta x_{m+1}.$$

If we use the induction method with $\widetilde{H}_{\beta,m}^{\sigma_1\dots\sigma_m}$ in (36) for $x_{m+1}\in\mathbb{T}_{m+1}$ and apply (9) m-times, then we obtain

$$\int\limits_{\prod_{i=1}^{m+1} b_i}^{\infty} \left(\widetilde{H}_{\beta,m+1}^{\sigma_1 \dots \sigma_{m+1}}\right)^{\frac{p}{q}} \prod_{i=1}^{m+1} x_i^{-\delta_i} \prod_{i=1}^{m+1} \Delta x_i$$

$$\leq \left(\frac{p}{q}\right)^{\frac{(m+1)p}{q}} \prod_{i=1}^{m+1} \left(\frac{2^{\frac{p-q}{q}} m_i^{\delta_i}}{\delta_i - 1}\right)^{\frac{p}{q}} \int\limits_{\prod_{i=1}^{m+1} b_i}^{\infty} \prod_{i=1}^{m+1} (x_i)^{\frac{p}{q}-\delta_i} f^{\frac{p}{q}}(x_1, \dots, x_{m+1}) \prod_{i=1}^{m} \Delta x_i.$$

Herewith, we reach the desired result for all $n \in \mathbb{N}$. □

Corollary 3.3 *Our results below are obtained from Theorem 3.2*

(1) If $\mathbb{T}_1 = \cdots = \mathbb{T}_n = \mathbb{R}$, $\frac{p}{q} > 1$, $\beta = 1$, *and* $\delta_i < 1$, *then (29) becomes the following Wirtinger type inequality*

$$\int\limits_{\prod_{i=1}^{n} b_i}^{\infty} (K(x_1, \dots, x_n))^{\frac{p}{q}} \prod_{i=1}^{n} x_i^{-\delta_i} \prod_{i=1}^{n} dx_i$$

$$\leq \prod_{i=1}^{n} \left(\frac{\frac{p}{q} 2^{\frac{p}{q}-1}}{1-\delta_i}\right)^{\frac{p}{q}} \int\limits_{\prod_{i=1}^{n} b_i}^{\infty} \prod_{i=1}^{n} (x_i)^{\frac{p}{q}-\delta_i} \left(\frac{\partial^n}{\partial x_1 \dots \partial x_n} K^{\frac{p}{q}}(x_1, \dots, x_n)\right) \prod_{i=1}^{n} dx_i,$$

where $K(x_1, \dots, x_n) = \int_{\prod_{i=1}^{n} b_i}^{x_i} K(\tau_1, \dots, \tau_n) \prod_{i=1}^{n} d\tau_i$.

(2) When $\delta_1 = \cdots = \delta_n > 1$, *and* $\beta = 1$, *we obtain the following inequality for n-variables*

$$\int\limits_{\prod_{i=1}^{n} b_i}^{\infty} \prod_{i=1}^{n} x_i^{-1} \left(\int\limits_{\prod_{i=1}^{n} b_i}^{x_i} f(\tau_1, \dots, \tau_n) \prod_{i=1}^{n} d\tau_i\right)^{\frac{p}{q}} \prod_{i=1}^{n} dx_i \leq \left(\frac{\frac{p}{q} 2^{\frac{p}{q}-1}}{\frac{p}{q}-1}\right)^{\frac{p}{q}} f^{\frac{p}{q}}(x_1, \dots, x_n) \prod_{i=1}^{n} dx_i.$$

Suppose that $\mathbb{T}_1 = \cdots = \mathbb{T}_n = \mathbb{N}$, $\frac{p}{q} > 1$, $\beta = 1$, *and* $b_i, \delta_i > 1$ *for* $i \in \{1, \dots, n\}$, *further suppose that* $\sum_{y_1=1}^{\infty} \dots \sum_{y_n=1}^{\infty} f^{\frac{p}{q}}(y_1, \dots, y_n)$ *is convergent. Then (29) becomes the following inequality*

$$\sum_{y_1=1}^{\infty} \dots \sum_{y_n=1}^{\infty} \frac{1}{y_1^{\delta_1} \dots y_n^{\delta_n}} \left(\sum_{m_1=1}^{y_1} \dots \sum_{m_n=1}^{y_n} f(m_1, \dots, m_n)\right)^{\frac{p}{q}}$$

$$\leq \prod_{i=1}^{n} \left(\frac{\frac{p}{q} 2^{\frac{p}{q}-1}}{\delta_i - 1}\right)^{\frac{p}{q}} \sum_{y_1=1}^{\infty} \dots \sum_{y_n=1}^{\infty} \prod_{i=1}^{n} y_i^{\frac{p}{q}-\delta_i} f^{\frac{p}{q}}(y_1, \dots, y_n)$$

Conclusion

In this study, we focused on fractional integral-type inequalities, generalizing and improving the results presented in previous studies. To be more specific, we have created some generalizations of fractional Hardy-type inequalities on time

scale. In this context, we have reached new situations of the fractional Hardy inequality. These new inequalities will guide us by al-lowing us to think about working in different spaces. In other words, it will lead to the expansion of our field of work. When we look at it from the rea-der's perspective, it can be seen that it is a pioneering work. I believe that it will lead to new approaches and studies.

REFERENCES

Hilger, S. (1990). Analysis on measure chains-a unified approach to continuous and discrete calculus, Results Maths. 18(1-2) 18–56.

Hardy, G.H. (1920). Note on a theorem of Hilbert, Math. Z. 6(3–4), 314–317

Hardy, G.H.(1925). Notes on some points in the integral calculus, LX. An inequality between integrals, Mess. Math. 54,150–156.

Hardy, G.H., Littlewood, J.E. (1927). Elementary theorems concerning power series with positive coefficients and moment constants of positive functions, J. Reine Angew. Math. 157, 141–158.

Hardy, G.H. (1928). Notes on some points in the integral calculus, LXIV. Mess. Math. 57, 12–16.

Ahmad, W., Khan, K.A., Nosheen, A., Sultan, M.A. (2019). Copson, Leindler type inequalities for function of several variables on time scales, Punjab Univ. J. of Math. 51(8),157–168.

Ashraf, M.S., Khan, K.A., Nosheen, A. (2019). Hardy-Copson type inequalities on time scales for the functions of n independent variables, Int. J. Anal. Appl. 17(2), 244–259.

Baric, J., Bibi, R., Bohner, M., Nosheen, A., Pecaric, J. (2015). Jensen inequalities and their applications on time scales, Element, Zagreb, Croatia

Nosheen, A., Nawaz, A., Khan, K.A., Awan, K.M. (in press) Multivariate Hardy and Littlewood inequalities on time scales, Arap Journal of Mathematical Science.

Saker, S.H., O'Regan, D. (2016) Hardy and Littlewood Inequalities on time scales, Bull. Malays. Math. Sci. Soc. 39(2) 527–543.

Li, W., Liu, D., Liu, J. (2019). Weighted inequalities for fractional Hardy operators and commutators, Journal of Inequalities and Applications 2019:158, 1-14.

Bradley, J. (1978). Hardy inequalities with mixed norms. Can. Math. Bull. 21(4), 405-408.

Kufner, A., Persson, L.E. (2003). Weighted Inequalities of Hardy Type. World Scientific, Singapore.

Opic, B., Kufner, A. (1990). Hardy-Type Inequalities. Pitman Research Notes in Mathematics Series, Longman Scientific and Technical, Harlow, Essex.

Akın, L. (2020). On some results of weighted Hölder type inequality on time scales. Middle East Journal of Science 6(1), 15-22.

Akın L.(2021). On innovations of n-dimensional integral-type inequality on time scales. Adv. Differ. Equ. 2021:148.

Bohner, M., Nosheen, A., Pecaric, J., Younas, A. (2014). Some dynamic Hardy type inequalities on time scales, J. Math. Inequal. 8(1), 185–199.

Agarwal, R.P., Bohner, M., O'Regan, D., Saker, S.H. (2011). Some Wirtinger-type inequalities on time scales and their applications, Pacific J. Math. 252, 1–26 (2011)

Akın, L. (2020). On the Fractional Maximal Delta Integral Type Inequalities on Time Scales. Fractal Fract. 4, 26, 1-10.

Bohner, M., Petereson, A. (2001). Dynamic Equations on Time Scales. An Introduction with Applications, Birkhauser, Boston.

Akın L. (2021). A New Approach for the Fractional Integral Operator in Time Scales with Variable Exponent Lebesgue Spaces. Fractal Fract. 5(7), 1-13.

Bohner, M., Georgiev, S.G. (2016). Sequences and Series of Functions. In: Multivariable Dynamic Calculus on Time Scales, Springer Int. Publ. Switzerland.

Akın L. (2023). On generalized weighted dynamic inequalities for diamond-$\propto$ integral on time scales calculus. Indian J Pure Appl Math. https://doi.org/10.1007/s13226-023-00366-6.

Chapter 7

Astrochemistry

Nihal ERCAN[1]

[1] Prof.Dr., Boğaziçi University Department of Physics
Head of High Energy Astrophysics Group
ORCHID ID: https://orcid.org/0000-0003-0639-7048, ercan@boun.edu.tr

ABSTRACT

In this review, I will give a brief review of astrochemistry which is a research field that includes chemistry and astronomy together under one umbrella. Its aim is to achieve the main goal of the composition of gas and dust particles and understanding the chemical processes occurring in stars and planets and also measure the chemical composition of stars and galaxies.

Key words: Astrochemistry, stellar abundances

INTRODUCTION

Astrochemistry is an interesting study area since it includes together astronomy and chemistry. Astrochemistry is the interdisciplinary science that aims to understand the chemical processes that determine the composition of gas and interstellar dust particles the chemical processes that occur in interstellar gas that regulate the formation of stars and planets.[1] Those particles are the raw material from which planets are formed, but how do we determine the chemical composition of objects that are extremely far away from us through spectroscopy or detailed analysis of the emission or absorption of the spectrum of stars planets, and interstellar medium? The analysis allows us to identify their chemical composition and its surface temperature.

Each chemical element has a characteristic emission spectrum that can be identified. In the case of the interstellar medium, the emission spectrum in the far infrared is used. The analysis of the absorption spectrum of the vacuum light, allows us to infer data on the amounts of material in interstellar clouds. [3] In the case of the atmospheres of the planets of the solar system, they are investigated using the refraction spectrum of sunlight on the planet and the infrared emission spectrum of the planet. In the case of the stellar atmospheres, it is investigated using visible and ultraviolet wavelengths [2]. Astrochemistry is of great importance, since it can understand the formation of complex molecules such as amino acids and have implications for understanding the formation of life on our planet and in the universe.

A molecular signature has been discovered in interstellar space that contains over 200 distinct substances. Although the fundamental issues in Astrochemistry involve questions such as when, where, why, and how all other issues are subservient to all these three points. The actual conditions, including parameters such as temperatures, and densities are communicated to us using the term "operational." What stages do they go through? Is there a limit to the intricacy of the chemical processes? Alexander Dalgarno referred to this subject as "astrochemistry" in 2008, saying that it is the study of the creation, annihilation, and molecule stimulations in astronomical settings, as well as their impact on the structure, dynamics, and development of celestial objects [1].

This concept encompasses not just the chemical elements of the subject, and also acknowledges that molecules are good diagnostic indicators of the physical conditions and processes occurring in the areas where they dwell. Furthermore, by acting as essential coolants, they actively contribute to the physical condition of the gas being produced. [4] Dense molecular clouds are significant in astronomy because they serve as the incubators for new generations of stars and

planets, many of which will even contain life. From the standpoint of pure chemistry, interstellar space offers a one-of-a-kind environment in which molecule behavior may be investigated under extraordinary situations.

Another point is that are there perhaps interstellar molecules that might then be incorporated into new planetary systems and afterward form the fundamental ingredients for life in space? This project focuses on how multidisciplinary elements of this area intertwine on both sides of the exchange. Without a solid foundation of information in molecular spectroscopy, and chemical processes, space chemistry would not inspire new developments in chemistry. The combination of astronomy and chemistry through which one of these areas aids the other, strengthening and enhancing one another. The area is rapidly expanding its range of disciplines, including many disciplines outside of chemistry and physics that are starting to play a significant role.

In addition, there are differences between astrophysics and astrochemistry. It is quite well-known astrophysics revolves around the physical laws of nature. [4] It concerns stars and other big celestial bodies, how they are forming, what their properties are, and how they interact with other celestial bodies. In contrast, astrochemistry is the chemical interactions that occur in space. So, there are the celestial bodies in space but within them what are the difficult chemicals and the different chemical interactions? That is what is covered under astrochemistry. It concerns, how these chemical interacts, and how the chemicals interact in the environment without gravity. That is very different from when we are studying molecules in our terrestrial environments, where we have space, different densities, and completely different conditions.

The major key distinction is astrophysics will always involve chemical species you would have lighter atoms like hydrogen, helium, and maybe carbon monoxide, but it will never go beyond that. [5] It would also have maybe really heavy metals but that is about it. Whereas, in astrochemistry, we actually start seeing species which we are used to in our chemistry courses. Actually, even beyond that, there are some species that were not known to be present on Earth but were first seen in astrochemical environments. Then, it can be realized that we could actually form these species. That is just because the conditions are just so different, the chemistry that can happen there is vastly different.

Additionally, when considering life in space, astrochemistry becomes really important and the discoveries in this area can be done thanks to lots of telescopes built for observation. [6] Many of the molecules we find are the organic building blocks of life on Earth. We want to know why we are finding them out in space. So, astronomers have built powerful radio telescopes capable of detecting fainter and weaker signals, and chemists have built state-of-the-art laboratories that

recreate the incredible temperatures and densities in which molecules seem to form in space. They study how molecules grow and transform on the surfaces of tiny dust grains and even in the near-vacuum found in molecular clouds. [8] Chemists are sharing this large catalog of molecular spectra, those fingerprints of molecules, with astronomers to help them identify mysterious molecules found in space. This astrochemistry collaboration may one day uncover the cosmic origins of the complex molecules that make life possible. [9]

Within astrochemistry, there are three main types of scientific activities. The first is the identification of species. [7] So, the first thing that is involved is how we know this chemistry happening in space because we have been able to identify various species using various techniques. The second one is the construction and appliances of chemical models and the last consideration is experimental and theoretical efforts which may happen. These points will be considered throughout the project.

1. OBSERVATIONAL PROPERTIES of ASTROCHEMISTRY

The history of astrochemistry is based on the shared history of the two disciplines as an extension of astronomy and chemistry. Advanced observational and experimental spectroscopy has enabled the detection of a growing number of chemicals within solar systems and the surrounding interstellar medium. As a result of advances in spectroscopy and other technologies, the number of compounds found has increased, expanding the extent and scope of the chemical space available for astrochemical research.

Athanasius Kircher (1646), Jan Marek Marci (1648), Robert Boyle (1664), and Francesco Maria Grimaldi (1665) all observed solar spectra before Newton's work in 1666, which confirmed the spectrum character of light and led to the invention of the first spectroscope. The investigations of William Hyde Wollaston, who created a spectrometer to observe the spectral lines present inside solar light, were the first to employ spectroscopy as an astronomy tool in 1802. Through Joseph Von Fraunhofer's research, these spectral lines were later quantified.

Following the publication of Charles Wheatstone's 1835 observation that different metals emit different emission spectra, spectroscopy was first used to discern between them. Léon Foucault expanded on this observation in 1849, demonstrating that the same substance produces identical absorption and emission lines at different temperatures. Anders Jonas Angström separately proposed an identical assertion in his 1853 work Optiska Undersökningar, in which he posited that luminous gases release light beams at the same frequencies as light that they may absorb.

With Johann Balmer's discovery that the spectral lines shown by hydrogen samples followed a simple empirical connection that became known as the Balmer Series, this spectroscopic data began to take on theoretical significance. This series was designed to characterize the spectral lines found for Hydrogen. It is a specific example of the more general Rydberg Formula developed by Johannes Rydberg in 1888. Rydberg's work improved this formula by permitting the calculation of spectral lines for a variety of chemical elements.

With the introduction of quantum mechanics, the theoretical significance of these spectroscopic observations was substantially increased, as the theory allowed these results to be compared to a priori computed atomic and molecule emission spectra.

Astrochemistry

In the 1930s, radio astronomy was created. There was no strong evidence for the definitive identification of an interplanetary molecule until 1937. The only atomic chemical compound known to exist in interstellar space till now was McKellar et al. found and assigned spectroscopic lines in an unexplained radio observation in interstellar space to CH and CN molecules in 1940, validating these findings. [1] A limited number of additional molecules were identified in interstellar space after thirty years, the most notable of which being the OH. It was found in 1963 and is useful as an interplanetary oxygen source. The H2CO (Formaldehyde), which was found in 1969, was the other. It is interesting to note that it was the first organic, polyatomic molecule to be discovered in interstellar space. Some regard the finding of interstellar formaldehyde as compelling evidence for abiogenetic theories of life. Other molecules of biological importance, such as water or carbon monoxide, also played a role in this hypothesis. Theories that claim that the basic chemical components of life come from alien origins, in particular.

This has sparked a quest for interstellar chemicals that are either directly physiologically important or have biologically relevant characteristics such as Chirality. Interstellar glycine, discovered in 2009, may be used as an example of direct biological importance, while propylene oxide, discovered in 2016, can be used as an example of Chirality, alongside more fundamental astrochemical study.

Observational Properties in General

While researching in the field of astrochemistry, several methods are used to determine the chemical properties of space and the gas that may fill the interstellar medium. For this reason, light, radiation, etc. observed and analyzed. In a broader

way, we can say that the Milky Way Galaxy is filled with enormous islands of gas. These great clouds glow from the radiation of super-bright stars shining nearby. Astronomers discover the nature of these clouds by studying the colors of light their glowing gas emits. When we spread open the light, each element or molecule in the gas reveals a unique "barcode" of colored lines. We do not analyze these barcodes as colored lines, however. We plot the strength and width of the lines as a light graph we call a "spectrum." These colors come from excited electrons. A nearby star energizes an atom of gas, making its electrons jump into higher orbits. When it relaxes again, the electrons take a quantum leap back down to their normal orbits, spritzing out the excess energy as packets of colored light we call "photons." Some gas clouds are dark and cold, no stars energize them. No electrons are jumping orbits here to make photons for us to see. So, how can we learn what dark clouds are made of? Not, all photons are visible to us. Visible light is just a tiny sliver of a vast spectrum of many more colors. Beyond the "red" end of the visible spectrum is the radio spectrum.

Radio is a kind of light traveling as a wave too long for our eyes to detect. Clouds that appear dark to our eyes are actually shining in radio light. We build immense radio telescopes to gather these feeble radio waves from these dark islands in space. We graph the wave strength of the radio "colors" (what we call "frequencies") to make a radio spectrum. With radio spectroscopy, we have discovered dozens of complex molecules in these dark clouds and throughout space. Recall, that these complex molecules don't emit photons by excited electrons jumping between "orbits." Instead, these cold molecules radiate weak radio waves whenever they change their rotation speeds. Each molecule can spin at only a few specific speeds, with no speeds in between. So each speed change results in a specific spectrum spritz or gulp of radio light, and every molecule reveals its own unique spectrum each time it changes its speed. Therefore, even when there are lots of molecules in a vast cloud, we can tell what kind they are by examining the radio spectrum coming from the cloud. Different methods and telescopes are used in astrochemistry research.

Spectroscopy

The most crucial experimental technique in astrochemistry is spectroscopy, in which light is absorbed and emitted by molecules and atoms in different settings to detect their locations. Astronomers are able to deduce the amount of certain elements, their chemical structure, and their temperature based on astronomical observations and laboratory experiments. The color that molecules, ions, and atoms emit (which you can't see) has a distinctive spectrum; this means that it can be detected with certain wavelengths of light. Despite these measures having

limits, radiation (ranging from radio waves to infrared to visible and ultraviolet light) can only identify specific species based on the molecule's chemical characteristics. As an example of radiation types radio, infrared, visible, ultraviolet, etc. can be given. Formaldehyde, the first organic molecule found in the interstellar medium, was the first interstellar compound discovered.

Because of the capability of radio astronomy, over 100 interstellar elements have been discovered, notably radicals and ions. Aldehydes, ketones, and alcohols are also identified. CO is among the most common chemicals in the universe, it is one of the simplest to identify using radio waves. That is because Co has a high electric dipole moment). CO is so often found in interstellar space that it is utilized for the purpose of mapping out specific chemical areas. One of the most interesting radio observations of humanity is the assertion of interstellar glycine, the simplest amino acid, which has been met with significant criticism. Apparently, comparatively small compounds, like amino acids, may remain undetected by radio. Rotational spectroscopy is an effective means of detection, as well.

Furthermore, techniques that make use of the dipole are oblivious to particles that lack a dipole. In addition, the vast majority of molecules in the universe are comprised of H2, and this molecule does not have a dipole moment. Radio telescopes do not see it, therefore it is invisible to them. A further disadvantage of gas chromatography is that it can't identify species that are not in the gas phase. The vast majority of molecules inside thick molecular clouds are frozen, remaining solid. Hydrogen is the only non-frozen element. Instead, different wavelengths of light are used to identify hydrogen and other compounds. Hydrogen is readily identified by its absorption and emission of light in the ultraviolet and visible regions (the hydrogen line). The most important point here is that most organic molecules will absorb and emit infrared light, making IR-based technology an excellent choice for detecting methane on Mars. The 3-meter Infrared Telescope Facility, at Mauna Kea in Hawaii, included this telescope. Investigators from NASA's IR telescope SOFIA and space telescope Spitzer utilize airborne IR telescopes for all of their scientific studies, investigations, and operations. Methane has just been detected in the atmosphere of Mars, which is somewhat linked to the current discovery of methane in the atmosphere of Saturn. It was reported in June 2012 by Christopher Oze and his colleagues that measurements of the hydrogen-to-methane ratio on Mars may assist in assessing the possibility of life on Mars. The scientists at the University of Canterbury in New Zealand are focused on innovation. A recent study indicates that the existence of life on Earth is tied to a certain ratio of hydrogen and carbon dioxide. reduced concentrations of H2 and CH4 indicate that the ratio is smaller than

roughly 40. Several researchers in the last several years have revealed new techniques to find hydrogen and methane in alien atmospheres.

The existence of polyaromatic hydrocarbons, or PACs, in the interplanetary medium, was previously discovered using infrared astronomy. These carbon-ring compounds are the most prevalent carbon component in the universe. Comet and asteroidal dust have the highest amount of carbon in them of any other carbon-containing molecular type (cosmic dust). The isotopes of carbon, nitrogen, and oxygen, as well as the amino acids, nucleobases, and many other chemicals found in meteorites, have deuterium and carbon-isotope levels that are very uncommon on Earth, making clear that these objects originate beyond our planet. In heated circumstellar settings, PAHs are believed to develop (around dying, carbon-rich red giant stars).

Astrochemistry is used to the investigation of both solid objects in the interstellar medium and molecular clouds to make up their solids, along with other carbon-rich solids. As visible light cannot travel through tiny interstellar particles, IR radiation may, and this process results in a different set of absorptions for grains of different compositions. Due to the aforementioned, there are certain practical limits to detection by IR or radio astronomy, for example, N2 is hard to detect with either method.

When ice exists in such high concentrations, it may surround the particles and form protective ice layers, allowing certain low-temperature chemistry to proceed. The initial chemistry of these ices is dictated by the composition of hydrogen. Hydrogen atoms are found inside water (H2O), methane (CH4), and ammonia (NH3). These atoms may combine with all the oxygen supply, carbon, and nitrogen atoms to produce reduced species like water (H2O), methane (CH4), and ammonia (NH3). Hydrogen, if molecular, will prevent heavier atoms from reacting, thus CO, CO2, CN, etc. may be produced. The complicated radiation-driven chemistry that is caused by exposure to UV radiation and cosmic rays is created in these mixed-molecular ices. Amino acids may be generated in lab studies for the photochemistry of simple interstellar ice. Other studies have concluded that the similarities between ice found in space and that found on comets indicate that there is a link between interstellar and cometary chemistry. It is consistent with the findings of the analysis of the organic from the comet samples returned by the Stardust project, which shows a significant role of solar nebula chemistry at elevated temperatures, and moreover assisted by the mineral analysis, which indicates the unexpected participation of solar nebula chemistry at elevated temperatures in comet formation.

ALMA Telescope: **Molecular 'Fingerprints' in Space:**

The greatest minds said that people never be able to form a molecule in space, because space is too empty, space is too harsh, it's just going to break apart molecules, it's going to break apart bonds. Now, we find molecules routinely. A lot of people have probably seen all the great pictures from the Hubble Space Telescope. What they do is they look at a particular color, a yellow, a green, and a blue, and then they combine all the colors together to make a picture. Well at ALMA, a better version can be done. What is done is to actually see shades of yellow, and actually see shades of red, and it is this shading that tells what the universe is made out of in molecules. It is studied in the laboratory of the University of Virginia, and the researchers actually put molecules in a large bottle or a large cell. Then, they excite the molecules and actually measure the colors that come off of those molecules. After that, they take those colors and directly compare it to the data that they get from space, to see if those molecules are actually present in space. So, the little bumps and wiggles represent the shades of color. Then, researchers know exactly what this molecule is because they put that in our laboratory cell, so they know what molecule they are looking at, and they are able to identify that molecule by all these little bumps and wiggles.

Figure 1: *The AEC ALMA prototype antenna.*
(Credits: Evaluation of the ALMA Prototype Antennas - Scientific Figure on ResearchGate) [10]

They then took ALMA and pointed it in the direction of Orion and they are able to take some data there. When they put the laboratory data right on top of the data from ALMA, it is an exact match. That is exactly how they know that this molecule is sitting in the Orion cloud over 1,000 lightyears away. It is basically the sensitivity of ALMA that allows them to do that. It is so sensitive, it can actually see the traces of these molecules in these clouds that are over 1000 lightyears away. How common, then, is the chemistry on the Earth found in the galaxy? There is always some idea that the organic chemistry, the molecules that contain carbon, nitrogen, and oxygen, that the Earth had to be very, very special in order to drive this organic chemistry to form big molecules, big organic molecules, like RNA, DNA, proteins, amino-acids. Not so much. The universe is doing this naturally. It forms ü these molecules naturally in these very harsh environments in space. And this is what researchers are able to find out with these observations that they did with ALMA. The research group has averaged at least one new molecule detection per year for the last decade, so there's a huge amount of space to explore. They could investigate chemistry going on in regions across the entire galaxy.

ALMA in Action

The Atacama millimeter/submillimeter array, or ALMA, is a single telescope made up of 66 individual antennas that work together in unison. By harnessing these extremely precise dish antennas, ALMA is able to study the birth of stars and planets, helping us better understand the life cycle of solar systems, including our own. Each antenna is able to quickly switch from point to point in the sky. This ability is essential to allow astronomers to calibrate the telescope and measure atmospheric moisture, ensuring ALMA is able to perform exquisitely.

It is situated in one of Earth's highest and driest deserts the most complex astronomical observatory ever is taking shape known as Alma. It is a vast array of radio telescopes so advanced, it has taken the world's top scientists and engineers to design and build it. Alma will appear in two hidden regions of space with unprecedented sharpness and sensitivity. Even now, with less than a third of its telescopes up and running Alma is the most powerful Observatory of its kind. It is ready to begin probing the invisible universe, all ordinary matter in the universe gives off light some of it is in colors, and our eyes can see. The rest from short-wavelength gamma rays to long-wavelength radio waves require special instruments to detect.

ALMA, the Atacama Large Millimeter/submillimeter Array, studies a barely explored part of the spectrum opening up a new window into the universe. ALMA telescope is an effort, that no one has ever attempted before. It is using scientists

engineers and technical staff all around the world to build a telescope that will change the landscape of astronomy literally. Scientists in North America Europe and East Asia have worked toward this moment for decades. They redefined technological possibilities in every area that has been pushing the limits of technology. The antennas, the correlator that processes the data, and the receiver are all of these pushed past previous boundaries. Furthermore, in many dimensions, these revolutionary designs and technologies must function flawlessly in one of the most extreme environments on earth.

The ALMA site in Chile is higher than any other major ground-based observatory. Putting Alma above most of the water vapor that would otherwise disrupt the millimeter-wavelength light, monster trucks called transporters move the Alma antennas into position on the Mars-like landscape. Alma's radio telescopes work together to make images of space that get better and better as more of them join the array. The telescope has already delivered tantalizing views of space, two galaxies collide their stars and gas intermingling the Hubble telescope sees bursts of star formation erupting where great clouds of gas and dust crash into one another but areas that look dark to existing telescopes are ablaze with light as seen by Alma. Therefore, there are patches of dark regions that contain very dense gas and dust within which the next generation of stars may already be forming. So, ALMA is a brand new window into the universe.

2. THEORETICAL ASPECTS of ASTROCHEMISTRY RESULTS

There is a large or diverse range of environments within the space. When chemistry is considered, four key parts are really concerned. There are dense clouds so, the key reason why chemistry within space was not thought of for a long time was because it is always thought of space as the vacuum. In addition, it is thought of as being empty, and maybe there are some stars there is some hydrogen, and there is some helium but that's about it. They are really far apart. That is actually true, a large part of the universe is vast empty space and really low densities. However, sometimes what can happen is a few molecules can start to come together and they end up forming these really dense clouds. It can be said that dense clouds but that is totally in the context of space how dense they are. There are these dense clouds that come together then, slowly and steadily they can actually even form the proto-stellar environments where the star is starting to form essentially. Then, these materials, because of the gravity, they will start revolving. A figure showing dense clouds, protostars, planetary disks, and planetary systems is shown below, these terms will be explained later in this part.

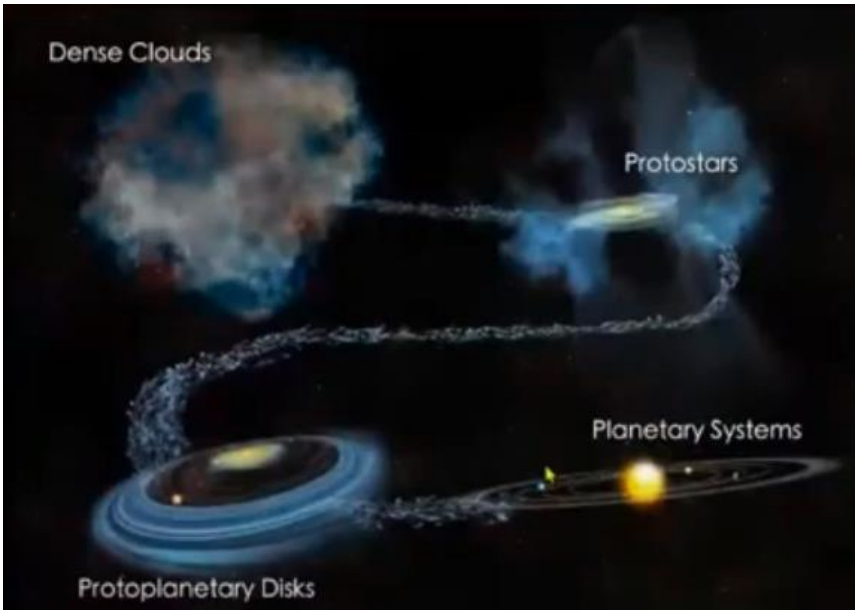

Figure 2: *Evolution of dense clouds, protostars, planetary disk and planetary systems*
(Credits: Bill Saxton (NRAO)) [14]

There might be outflows and then, there is the protoplanetary disk where the planets are starting to form. Finally, the final thing would be a primary system like our solar system. In our solar system, there is the sun and different planets. Through all these environments, there are various environments in terms of temperature and very different densities of molecules as well. There are three key species that are the dust crane, the ice, and the gas. Molecules are dispersed in the universe and they can be found everywhere in space. The regions where molecules can be found are evolved stars, planetary nebulae, molecular clouds, comets, galaxies, protoplanetary disks, stellar and exo-planetary atmospheres, solar photosphere, etc. At the atmosphere, sea level conditions are: T_{kin} is equal to about 300 Kelvins and n is about $3x10^9$ cm^3. By considering this, some of the basic conditions of the space are given below:

Diffuse clouds: T_{kin}~100 K, n~100 cm^{-3}
Dense clouds: T_{kin}~10-100 K, n~10^4-10^8 cm^{-3}
Hot cores: T_{kin}~100-1000 K, n~10^6-10^8 cm^{-3}
Disk midplane: T_{kin}~10-1000 K, n~10^8-10^{13} cm^{-3}

So, the interstellar clouds are where stars are born, and astrochemistry investigates the development and the presence of molecules (abundances). Lots of areas of science are involved in the astrochemistry.

Dense Clouds

Dense clouds are these molecular clouds where the molecules have come together in a slightly denser environment. Within these environments, there are also some dust grains which are basically silicate. Additionally, there are rich dust grains as well. The formation of that is not known quite well yet. There is also ice chemistry because the pressures in space are so that there is not really a liquid phase. So, ice is observed there which would sublime directly off into the gas phase. Depending on the temperature conditions there is either ice or gas. Within these dense clouds, there can be other stars around it. There is the environment of different UV photons, and different cosmic rays coming in. The process is that the rays can penetrate into dense clouds. Within the outer region, they end up ionizing atoms and they can break apart molecules. This changes as it goes deeper inside the cloud but in the outer regions there are high ionization rates and higher dissociated molecules so within these clouds, there have been more than 200 species detected. This even includes really complex chemical compounds like fluorine and benzonitrile which was the first aromatic compound to be detected in interstellar space. As mentioned before, astrochemistry helps chemistry on earth in terms that some of the long carbon chain molecules, like 11 carbon chain long molecules.

So, these were first detected in space in these dense clouds and then they were thought as is it possible to actually have them, to form them then, they were formed or not. That is really because of the availability of space. Since there was high in environments where there is high carbon presence but low hydrogen what is end up being is that there are really long carbon chains compared to the terrestrial environments, the large amount of hydrogen and water exists. That is why almost everything is hydrogenated. In this environment, ice formation and heavy deuterium fractionation occur. Compared to the earth, the hydrogen freedom ratio is very high on Earth but in these dense clouds, the deuterium fraction is higher. In dense interstellar clouds, the main part is molecular ion H_3^+. Its formation reaction is:

$$H_2^+ + \frac{1}{2}H_2 \rightarrow H_3^+ \quad (1)$$

This was first recognized in 1971 by the scientists Martin, Meeks, and McDaniel. $H_3^+$is detected in space by astronomical spectroscopy and this was collaborated with laboratory studies.

Protostars

In the protostar stellar environments, there are radicals. In these environments, the temperatures actually increase a little bit in the dense clouds. There might be really low temperatures in their inner regions. The outer regions would have slightly higher temperatures because of the cosmic ray. However, in the proto-stellar, there is a slightly higher temperature,s and the radicals and other gas species can actually now move a little bit freely on the ice surfaces.

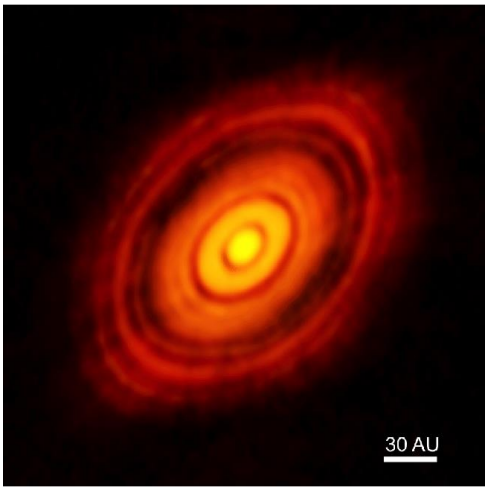

Figure 3: *ALMA image of HL Tau, a protostar with an embedded disk that shows signs of planet formation. The region inside the first gap is optically thick (T > 200 K). (Credits: This image is based on Figure 2 of Partnership et al.)* [17]

They are not stuck because of the low temperature, there is low kinetic energy so, the molecules now in the higher temperature regions are not as stuck. They can actually move around a little bit and they can then recombine to form even complex molecules. Also, some of the UV photons and X-rays can also trigger some further chemistry in these environments which are studied by many groups. The dust temperatures in these regions actually become high enough that the ice can sublimate, and then go into the gas phase. This gas phase chemistry is also enriched.

Warm Gas:

Some bright stars like our Sun release and re-absorb massive amounts of heat in interstellar space. This process is accomplished by dissociative shocks and

non-dissociative shocks. In addition, this process can be achieved by strong ultraviolet and X-ray radiation. So, for this release of heat to happen, atoms and molecules both accumulate onto grains. Then, these grains get involved in processes on their surfaces. In turn, these processed grains become to gas phase where a gas phase reaction is carried out. Throughout these reactions, endothermic, where heat is needed reaction to start, and exothermic, where heat is released, reactions of H_2 occur.

Protoplanetary Disks

These are the discs that have the initial chemical abundances for the planet formations. There are actually the dust strains that start to coagulate a little bit more. There is a huge range of densities and temperatures in these regions and actual severity. This is the most rich chemical environment in terms of the chemistry that there is the most chemistry in these regions because the densities are high enough and the molecules have actually come together a lot more.

There is a range of temperatures which are really high temperatures like 1000+ Kelvins the disk and less than 10 Kelvins. It can be said that it is the opposite way compared to the dense clouds since a star starts to be formed. Inner regions, actually are at higher temperatures and there is still chemistry that takes place in these environments. There are research groups who actually study chemistry at 1000+ Kelvin temperatures. Whereas in the outer regions, there are still really low temperatures less than 10 Kelvins. In addition, the densities in this region can vary quite a bit so, in the inner middle midplane. Thus, now 3D structure must be thought. because it is sub 3d of course so in the inner middle plane you would have densities of 10 part 13 molecules per centimeter cube whereas as you start to move around the outer layers the density reduces to 10 000 molecules per centimeter cube okay and within this protoplanetary disc there's a very interesting things thing which comes into picture so now you start to form these snow lines okay and these snow lines are formed because of this range of temperature

There is a gradient of temperature starting from 10 Kelvins all the way up to 1000 Kelvins. Depending on this gradient of temperature, different species can freeze out at different temperatures. As an example, the CO can only freeze until 25 Kelvins whereas water can freeze up to 150 Kelvins. This means that all CO would be trapped in regions that are up to 25 K. Afterwards, they will start to dissolve as the temperature increases. Then until 150 K, there can be most of your water in the ice phase. The moment when the temperature is higher than 150 K, the water also starts to come off,

therefore there is a huge gradient. Thus the amount of ice chemistry and the ice versus gas chemistry becomes really interesting because there are different amounts of the different photons the far UV photons the X-ray photons can penetrate into. Finally, there is a huge variety of chemistry that can happen and the type of chemistry, and the type of molecules involved change as we move inside the disk.

Interstellar Medium (ISM)

The interstellar medium is any material that is found between the stars, so it does not matter what it is. We consider it any material and it is broken down into two components. There is the gas the interstellar gas, which is 99% of the interstellar material and there is interstellar dust, which is slightly larger particles, which make up the remaining 1% of interstellar material. It can be said that this is an extremely low-density material. So, as we can see from the figure below, there is a picture of a nebula where the gases that have been ionized are and are being excited to glow can be seen.

Figure 4: *Picture of a nebula*
(Credits: Search for Signatures of Extra-Terrestrial Neutrinos with a Multipole Analysis of the AMANDA-II Sky-Map) [18]

That's part of the material between the stars and that's a very small part that actually is visible. However, the material that is seen is actually very low density in general terms about one atom for every cubic centimeter (1 atom/cm^3). For comparison, the Earth's atmosphere has 10 to the 19th atoms in every cubic

centimeter (10^{19} atoms/cm^3) so, lots of atoms exist on Earth and very few are scattered around the universe, of course, because there are lots of cubic centimeters in space it still ends up being a lot of material. However, this is extremely low density and better vacuums than that can be created on Earth.

From now on, two components of the interstellar medium can be considered separately. First of all, is interstellar gas. The gas between the clouds can be seen in a number of ways. One of the ways that we can see these is in ionized hydrogen or what is called H II regions. These are only visible near hot stars.

Figure 5: *Picture of an Orion nebula*
(Star Formation in the Orion Nebula I: Stellar Content - Scientific Figure on ResearchGate.) [19]

In the figure above, there is an example of it which is called as Orion Nebula. In the Orion Nebula, at the center, there is an area where a few hot stars are located. So, it is a few hot stars located down at the center, and those stars are giving off ionizing ultraviolet radiation (UV light). It excites atoms that are left over around it and causes them to glow. It would not be just hydrogen but hydrogen is prominent because as it can be seen, most of the material in the universe is made up of hydrogen. So, this is an example where we can actually see the gas, where it is excited to glow and we can see it glowing but it is only a small portion of the interstellar gas. There is a lot more material out there that would be invisible to us. The only time ionized hydrogen regions can be seen is

when there is a bright star giving off lots of ultraviolet light near it, a star like our Sun would not give off enough ultraviolet light to ionize a cloud like this.

Planetary Systems

Astrochemistry does not just end with the disks. It carries on in binary systems because there are planetary atmospheres. One of the most interesting ones is Titan which is the moon of Saturn. Titan has interesting chemistry; it has methane and cyanides in its environment. Thus, a lot of chemical reactions occur. Additionally, there are various exoplanets based on the type of planets like Superox which have environments very similar to Earth and own their own core and lava. Besides, there are many Neptune's which have atmospheres that are more hydrogen and helium based like the Neptune planet in our system. Jordan planets are another type of planet which are more like Saturn and Jupiter. Among the exoplanets, different chemical species are observed like carbon monoxide, water, trace of methane, ammonia, etc. There are different galaxies outside of the Milky Way galaxy and exoplanets are outside our solar system and Milky Way galaxy. Therefore, exoplanetary research is so a novel and interesting field that it is awarded a Nobel prize. The exoplanetary research is very difficult to study because of their distance. However, these planets show very interesting chemistry, and various reactions, and events are observed.

Dust-Ice-Gas Interplay

In the early ice formation, there is a silicate crust dust grain surface which is mainly water, carbon dioxide, and ammonia and carbon monoxide is also can be observed. In the early ice formation, the temperature is very low. While the temperature increases, small molecules begin to be formed. Some chemistry is observed. Methanol is formed and there is a carbon monoxide freeze-out. In cold UV processing, UV photons hit the ice on the dust grains and form even bigger molecules like formal aldehyde and other molecules. Then these molecules can also dissolve off. A representation of the Dust-Ice-Gas interplay is shown in the figure below:

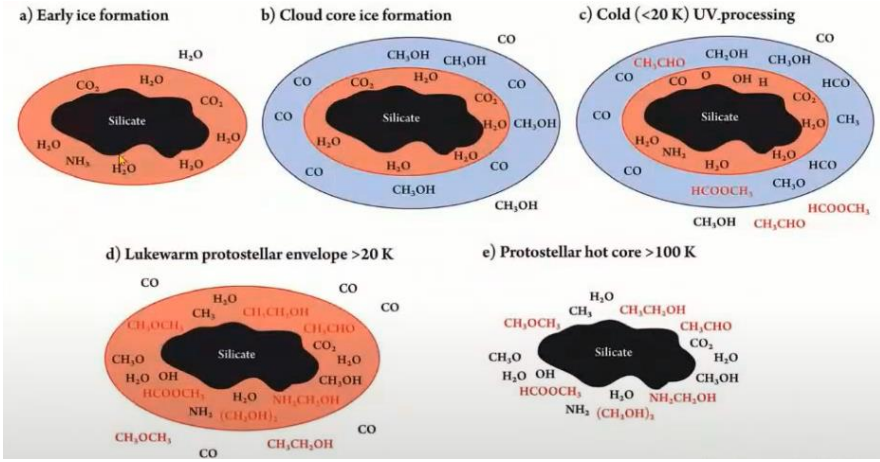

Figure 6: *Dust-Ice-Gas Interplay*
(Credits: E.F. van Dishoeck, 2014, Faraday Discussion) [9]

If the temperature increases higher slightly, a lot of chemistry happens in these temperatures. Increasing temperature causes be form of really big molecules in terms of interstellar chemistry. Then, in the proto-stellar hot core phase, the temperatures are higher than 100 Kelvin. Because the dust is very hot, all these species cannot remain frozen out and different types of species are coming out. The species go to the gas phase. Therefore, the proto-stellar hot core has really rich gas-based chemistry. Within ice phase chemistry, different people study different aspects like electron chemistry, ice composition, and ice chemical evolution because of different types of energies such as UV photons or cosmic rays hitting the ice phase. Within the ices, there is a large research field that explores the mobility within these ices. Because when these molecules are stuck in the ice, they are not just completely stuck always. They can sometimes move around like the case of the radicals. Additionally, as the temperature increases and the molecules start to come out, the ice and gas interplay.

Ice Phase Chemistry

In the ice phase chemistry temperatures are really low less than 150 Kelvin because 150 Kelvin is the temperature at which water was frozen out. However, a lot of the chemistry is generally really low temperatures such as 5 to 10 Kelvin. There are two major mechanisms for the reactions that take place in the ice phase conditions. One of the mechanisms is the elevated mechanism. The surface actually sometimes can help catalyze your reactions. For instance, a hot atom or a molecule that comes from the gas phase on the surface has enough energy. Thus, it can move around for a while and meet the other species which

is frozen out and form a new product. After forming new species, the molecule goes out into the gas space.

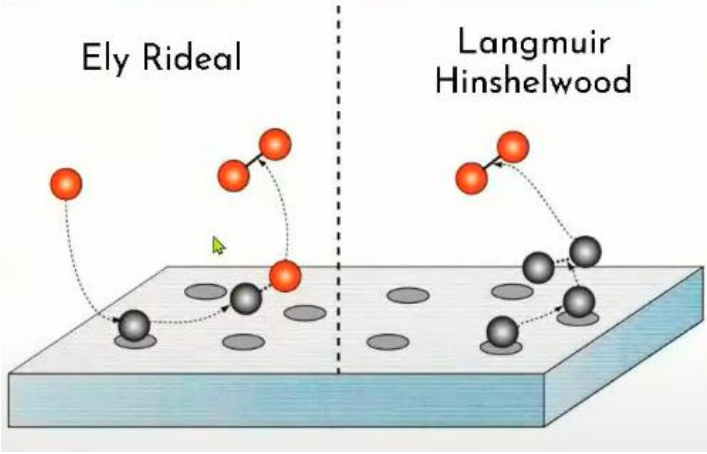

Figure 7: *Mechanism of Ice Phase Chemistry (Credits: Fundamentals on Adsorption, Membrane Filtration, and Advanced Oxidation Processes for Water Treatment*) [20]

The other mechanism is the Langmuir-Hinshelwood model. In the model unlike the other, both the species are already on the surface. If the molecules have enough energy, they can move around for a while, and the molecules can come close to each other. Then, the molecules can react with the excess energy because the only chemical reactions that occur are exothermic reactions. Then the molecules go into the gas phase with the excess energy. In conclusion, in both cases, the formed product will always dissolve off the surface and go into the gas phase. Additionally, there are also a lot of UV photons that hit the ice surfaces and make different reactions**.**

Gas Phase Kinetics for Astrochemistry

Gas phase chemistry can have a large range of physical conditions and the rate constants over the wide range of temperatures should be known in order to predict the different molecules and how much they are present in these conditions. It is important to know which reactions can occur at which speed. There are two main types of gas phase reactions. One of the reaction types is the iron molecule reaction. In iron molecule reactions, one of the molecules is iron and another is a neutral species. The molecules have rates like 10^{-9} molecules per cm^3 per second and they come together and react. Another type of reaction is a neutral-neutral reaction. In this type of reaction, the species are uncharged species and have rates of 10^{-11} to 10^{-9} molecules per cm^3 per

second. There are advantages of iron molecule reactions. Since ions have electrostatic force, they can attract the other molecules and can create dipoles. Ion-molecule reactions as shown in the equation below occur:

$$X^+ + YZ \rightarrow XY^+ + Z \qquad (2)$$
$$10^{-9} - 10^{-8}\ cm^3/s$$

Also, iron molecule reaction rates are slightly higher than neutron-neutral reactions. Because of the Arrhenius law, it was thought that there could not be any chemistry in space for a long time. Arrhenius's law states that the rate of reaction is directly dependent on the temperature which means that higher temperatures give higher the rate of the reaction. Thus, at really low temperatures in space, it was thought under the Arrhenius law that the reactions would be too slow to proceed. There would be slow reactions. It would not be enough to explain the reason for the chemical reactions that are happening in space. However, now it is known that the neutral-neutral reactions show non-Arrhenius behavior which means both reaction types can either become fast as the temperature proceeds. The reason is mainly due to the changed potential surface. The barrier is not needed to reactions occur.

The two reactants come close and become stable. The molecules give an intermediate and form the product. In Non-Arrhenius behavior, molecules come together either forming an intermediate or forming a complex. Although in these reactions there is a transition state, it is a submerged barrier which means the energy level of the barrier is less than the reactant energy. Thus, the reactants essentially have enough energy to cross over and from the product. As a result, this is the reason that the reactions with a completely negative temperature occur. Either the reactions become faster when the temperature decreases, or they follow the Arrhenius law at higher temperatures but below the threshold point, reactions start to show positive temperature dependence. To conclude, because the research area is a new field, there is a minor number of experiments and data available for low temperatures. It is very challenging in terms of experiments because extremely low temperatures like 10 Kelvin should be reached.

3. RESULTS

There should be various ways to define what astrochemistry is. One way is to describe it like this, astrochemistry is the study of abundances, how much they exist of chemical elements, in those cases primarily atomic and molecular form. In addition, elements and molecules in the universe interact with radiation since

they emit or absorb electromagnetic signals. That is why scientists are able to observe them. Also, chemistry is a discipline that overlaps between astronomy and chemistry.

The origin of matter in our universe is the main consideration of astrochemistry, basically the chemistry of the stars. It focuses on what's going on in outer space that makes the existence of our elements possible. The way stars tend to work is that they actually have a lot of energy processes going on. The most important of them would be fusion, which is the addition of two nuclei to form an element that is higher in atomic numbers. Fusion is a very energetic process and it allows the star to produce a lot of energy that prevents it from collapsing in on itself. The Sun in our galaxy is able to commune functioning because it has enough hydrogen to fuse into helium where the outward force of the fusion prevents it from collapsing inward on itself and that's due to the tremendous gravity that it has. The fusion in the Sun and in most stars only occurs at the core because that's the only place where the temperature is high enough. It has to be at least over 5,000,000 °C which is relatively high. The surface of a star is cooler compared to the core, so fusion only really happens in the core. In the core of the Sun, the temperature is about 15,000,000 °C whereas on the surface of the Sun, the temperature is only about 5,500 °C, so there's a really big difference there.

At this point, the question of where stars come from should be considered. They essentially form from big clouds of hydrogen and dust and these are generally called nebulas. This cloud condenses due to gravity and eventually, the mass becomes so great in this condensation of the nebula and the temperature is at least 15,000,000 °C where nuclear fusion can occur at the core of our Sun. This is essentially when a star is born, so those clouds of gas and dust are kind of the breeding places of the stars. When it comes to the law of conservation of mass, we can say that the law of conservation of mass which states that the mass of the reactants and the mass of the products must equal each other in a chemical reaction does not apply to nuclear fusion just because there's the inherent definition nuclear fusion is the formation of a product that has by definition a higher mass. Therefore, that law doesn't work for nuclear reactions because a lot of the matter in the reactants actually becomes straight energy and just radiates out into space. The radiation, formed through nuclear fusion, is actually really important for stars to avoid collapse. They point in the opposite direction of the gravitational force. If there's not enough of this energy to keep the star continually working, the gravity is gonna take over and the star is going to collapse on itself, and at some point in the star's lifetime that's exactly what happens. The star continues to convert hydrogen to helium until there is not enough hydrogen to

feel the process. At that point, there is a momentary collapse and this generates higher temperatures at this stage helium is now able to fuse with other heliums and with other hydrogens to form larger atoms. It allows the star to get like beryllium, carbon, nitrogen, and oxygen which allows us to classify the star as a red giant.

As for a red giant stars are going to fuse heavier nuclei and form even heavier elements because the temperature is just continuing to rise, so the star is going to have elements like calcium, potassium, and sulfur. As the temperature continues to rise into 1,000,000,000 °C which is very high, the energy from the reactions starts to keep from collapsing because at that stage the star is getting higher energy and radiation and more reactions. The next stage of the life cycle of the star is the collapsing of the star to get enough energy where it can start to fuse heavier elements together. The energy from this reaction can form elements as high as magnesium from the fusion of nitrogen and boron. At some point, a very stable nucleus is going to be formed. The star is going to get higher elements in other words more elements whose atomic numbers are relatively high. This process continues till the Iron-56. This is an isotope of Iron that is actually so stable that there isn't enough energy to use for the fusion of the Iron-56 even when the temperature is over 1,000,000,000 °C and the stars are red giants. Once this happens, stars don't have enough energy to fuel the reactants. The inward gravity is going to overtake the outward force from the fusion and the gravity essentially wins at this point. Even if the star collapses even more, there is no possible way for it to fuse anything and Iron-56. This scenario forms a supernova. Since gravity wins out, the star collapses in on its own gravity and at this point, there is an explosion that is so astronomically huge that all elements beyond iron-56 can be produced. Due to the nuclear reactions that take place in the cores of stars, all the other elements than Hydrogen can be formed in the same way.

The elements form in stars, but it is also important to think about how they go from stars to being part of planets. Following a supernova, the core of the dead star can form two different things. In the first case, it's going to become really dense and condensed into itself to form a neutron star with a lot of magnetic waves around it with a small ring shape. In another case, it can form a black hole. In either way, what is left of the original star is extremely dense. When it comes to what happens to the rest of it, the formation of the nebula at the very beginning of the discussion should be considered. The rest of the original star forms another nebula, a cloud of hydrogen, dust, and all kinds of elements. This nebula is going to have all of the elements that were actually fused within the star before, so all of the elements that we know today or all the elements that we know to exist are going to be in this nebula, and the formation of the planets is essentially what

kind of happens out of this nebula and even some stars. When we have packets of the nebula started collapsing due to gravity, they form second-generation stars. For example, our Sun is a second-generation star largely because it has a solar system.

The solar system is a star with planets orbiting it and the planets are formed because of the condensation of the elements that are in the nebula as well. For example, our Earth is basically just a condensed form of what was in the nebula following a huge supernova of another star. Our Sun is said to be another one of those children of the supernova, so essentially we, all, descend from stars.

From Figure 8, if we examine the elements that can be fused within the cores of stars, the elements in blue squares in the periodic table figure above show the elements that can be formed within the star during its lifetime. Before the supernova, all the elements up to Iron-56 can be formed as we may recall from the earlier discussion. Once it reaches at Iron-56 isotope, however, there is no possible way for the star to continue fusing unless it forms a supernova. When it collapses and when gravity wins, all the other elements can be got from the supernova, in other words, all these elements can be formed through a supernova. Hydrogen and Helium are the elements that take part in the essential fusion that goes on within the star during the earlier part of its lifetime before it becomes a red giant.

We are really going through a Golden Age of astrochemistry at the moment because we have powerful telescopes available including the Herschel Space Observatory but also the IRAM 30-meter telescope in Granada. We are discovering new molecules and one major discovery over the last few years has been the discovery of negative ions in space, i.e., not molecules that are neutral but actually have a negative charge on them. They were predicted in the 1980s, but it took almost 30 years to discover them. Another very exciting discovery is dead of organic molecules and water in the inner regions of disks in which young stars are forming. It was from the Spitzer Space Telescope mission and this actually came a bit as a surprise. Why nobody was expecting to see these molecules is the capabilities of that particular instrument, but it turned out on very good analysis that these molecules were actually present. The analysis actually demonstrated that simple organic molecules could be the building blocks of life and they are really present in the zones of the disks around young stars and in which Astro-chemists actually think that the terrestrial planets may be forming. It really provides us with sort of a view of how our own young solar system could have been and where it got its organic material.

I would like to thank Aysun Çeçe, one of my undergraduate students, for helping me in preparing this review article.

REFERENCES

[1] Dalgarno, A.. (2000). Astrochemistry: Historical Perspective and Future Challenges. Proceedings of The International Astronomical Union. 197. 10.1017/S0074180900164630.

[2] Millar, T. (2015). Astrochemistry. Plasma Sources Science and Technology. 24. 10.1088/0963-0252/24/4/043001.

[3] Yamamoto, Satoshi. (2017). Introduction to Astrochemistry. 10.1007/978-4-431-54171-4.

[4] Brown, Wendy. (2014). Astrochemistry. Physical chemistry chemical physics: PCCP. 16. 10.1039/c4cp90004a.

[5] Smith, Ian & Cockell, Charles & Leach, Sydney. (2013). Astrochemistry and Astrobiology. 10.1007/978-3-642-31730-9.

[6] Shaw, Andrew. (2006). Astrochemistry: from astronomy to astrobiology.

[7] Ishak, B., 2019. Introduction to astrochemistry: chemical evolution from interstellar clouds to star and planet formation, Contemporary Physics. Ogle, R., Carpenter, A., 2014

[8] Shaw, Andrew. (2006). Astrochemistry: From astronomy to astrobiology. Astrochemistry: From Astronomy to Astrobiology by Andrew M. Shaw. Wiley, 2006. ISBN: 978-0-470-09137-1.

[9] Ehrenfreund, Pascale & Sephton, Mark. (2006). Carbon molecules in space: From astrochemistry to astrobiology. Faraday discussions. 133. 277-88; discussion 347. 10.1039/B517676J.

[10] Evaluation of the ALMA Prototype Antennas - Scientific Figure on ResearchGate. Available from: https://www.researchgate.net/figure/The-AEC-ALMA-prototype-antenna_fig1_1789859 [accessed 27 Jun 2021]

[11] Baudry, A.. (2009). The ALMA radio telescope. 002. 10.22323/1.065.0002.

[12] Webber, John. (2013). The ALMA telescope. IEEE MTT-S International Microwave Symposium digest. IEEE MTT-S International Microwave Symposium. 1-3. 10.1109/MWSYM.2013.6697433.

[13] Shen, Tzu-Chiang & Soto, Ruben & Ovando, Nicolás & Vélez, Gastón & Fuica, Soledad & Schemrl, Anton & Robles, Andres & Ibsen, Jorge & Filippi, Giorgio & Pietriga, Emmanuel. (2014). Exploring Remote Operation for ALMA Observatory. 10.1117/12.2054860.

[14] Wootten, Alwyn. (2002). Atacama large millimeter array (ALMA). Proc. SPIE. 4837. 10.1117/12.456705.

[15] Brown, Robert & Wild, Wolfgang & Cunningham, Charles. (2002). ALMA - The Atacama large millimeter array. Advances in Space Research. 34. 555-559. 10.1016/j.asr.2003.03.028.

[16] Rigopoulou, D. & Pearson, C. & Ellison, Brian & Wiedner, M. & Okada, V. & Tan, Burak & García-Bernete, Ismael & Gerin, M. & Yassin, Ghassan & Caux, Emmanuel & Molinari, S. & Goicoechea, J. & Savini, Giorgio & Hunt, Leslie & Lis, D. & Goldsmith, Paul & Aalto, S. & Magdis, G. & Kramer, Carsten. (2021). The far-infrared spectroscopic surveyor (FIRSS). Experimental Astronomy. 10.1007/s10686-021-09716-w.

[17] almaobservatory.org. Next Generation Very Large Array Memo No. 6, Science Working Group 1: The Cradle of Life - Scientific Figure on ResearchGate. Available from: https://www.researchgate.net/figure/ALMA-image-of-HL-Tau-a-protostar-with-an-embedded-disk-that-shows-signs-of-planet_fig7_283117652 [accessed 2 Jun 2021]

[18] Search for Signatures of Extra-Terrestrial Neutrinos with a Multipole Analysis of the AMANDA-II Sky-Map 2007-07-03 - 2007-07-11 - Scientific Figure on ResearchGate. Available from: https://www.researchgate.net/figure/Picture-of-a-part-of-the-crab-nebula-a-supernova-remnant_fig68_27423568 [accessed 9 May 2021])

[19] (Star Formation in the Orion Nebula I: Stellar Content - Scientific Figure on ResearchGate. Available from: https://www.researchgate.net/figure/Drapers-1882-photographic-image-of-the-Orion-Nebula-North-is-up-and-East-is-to-the_fig3_23625261 [accessed 1 Jun 2021]

[20] : Fundamentals on Adsorption, Membrane Filtration, and Advanced Oxidation Processes for Water Treatment - Scientific Figure on ResearchGate. Available from: https://www.researchgate.net/figure/Top-model-Langmuir-Hinshelwood-Mechanism-two-molecules-adsorb-onto-the-surface-and_fig7_265385173 [accessed 2 May 2021])

Chapter 8

Analysis of Secondary School Science Textbooks in terms of Material Availability and Teachers' Opinions on the Use of Materials

Ezgi ÖNDER[1], Nuran EKİCİ[2*]

[1]Trakya University, Institute of Science, Department of Science Education, Edirne /TURKEY
[2]Trakya University, Faculty of Education, Department of Science Education, Edirne/TURKEY
**(nuranekici@yahoo.com) Email of the corresponding author*

Abstract

This study aimed to examine the accessibility levels of the tools, equipment and materials used in the experimental activities in the secondary school science textbooks that were decided to be taught in the 2020-2021 academic year, and the teachers' views on the use of materials in terms of various variables. This study is a mixed method research. The quantitative data of the research were collected through an online questionnaire to determine the views of science teachers on the use of materials. The qualitative data of the study were collected with a form created by the researcher to determine the accessibility levels of the tools, materials and materials used in the Secondary School Science Textbooks. The data obtained from the research showed that most of the activities can be done with simple materials or alternative tools. The results of this research showed that male teachers were compared to female teachers, experienced teachers compared to unexperienced teachers, and higher education school graduate teachers compared to the teachers who graduated from the faculty of arts and sciences. It is recommended that teachers should be supported in this regard by including teaching materials as much as possible during the lessons.

Keywords: Basic materials, experimental activity, science textbook

INTRODUCTION

Education enables individuals to make sense of the events they encounter in daily life by using their mental activities and prior knowledge by approaching them with a critical and questioning approach [1], [2]. In the age of technology and information, in which we are constantly changing and developing, it is possible for countries and societies to adapt to changing living conditions with the importance they give to education [3]. Science shows an ongoing development since the existence of human beings by raising the welfare levels of countries and living standards of individuals through experiences and accumulations [4]. Technological innovations that emerged as result of developments in science are the product of manpower and it is inevitable that countries that do not have a qualified workforce will life under the yoke of other countries in technology and science [5]. With the changes in science, technology and scientific knowledge over time, societies and countries are moved one step further [6]. Along with the reform movements, other disciplines, especially science classes. All lessons have moved away from the traditional teaching approach and focused on an approach where knowledge is structured in the mind rather than acquisition, and the importance given to science lessons has been emphasized once again [7]. In this direction the vision of the Science Education Curriculum is to "raise all students as scientifically literate individuals" [8]. The activities carried out systematically in schools within the framework of certain goals and plans are called teaching. Textbooks, which serve as a resource for individuals to reach these goals in line with their goals, are among the most frequently used materials in the education process [9]. Textbooks, which are the source of this process, play an important role in science courses [10]. It is a prerequisite that the course books are prepared in a qualified and purposeful way, in order carrying out education in a quality way. In this way, students are provided with meaningful learning by structuring scientific knowledge in their minds. Science, which emerges as result of phenomena and situations in daily life, allows individuals to understand both themselves and their social and physiological environment, to approach the problems they encounter with a critical approach and to offer solutions [11]. At the same time, students who take science lessons gain scientific reasoning skills such as asking questions, working in groups with their peers, and accessing information using scientific inquiry protocols [12], [13]. Scientific process skills are defined as skills that encourage the formation of knowledge and enable students to learn the world of science and technology in a systematic way [14]. Scientific process skills, which should not be left in primary care after they are acquired, develop as they are used [15]. The only way to acquire these skills is through inquiry-based teaching. Science learned by

questioning plays a key role in individuals' access to scientific knowledge by developing their reasoning skills and attitudes, by doing and living [16]. With the increase in the effectiveness of science teaching towards the end of the 19th century, it was understood that students should learn science by doing and living [17]. School laboratories are environments where inquiry-based teaching is carried out most effectively and scientific knowledge is produced [18]. Laboratory environments that allow students to work individually or in groups by prioritizing mental activities help them to integrate abstract concepts into their cognitive structures and to learn meaningfully [19]. Since applied activities aim to develop high-level thinking skills, the inclusion of laboratory practices in the curriculum lays the groundwork for raising individuals who can think critically and scientifically [20]. As a result of supporting laboratory environments where knowledge is produced and meaningful learning is provided with various tools and equipment, students' education quality and academic success will increase [21], [22]. In addition to the positive effects of laboratories and applied activities supported by various tools and equipment, the use of these environments supported by efficient and simple tools is of greater importance [23]. After graduating from education faculties, teachers are not trained to work with tools and equipment that are almost never used in the schools they work in, and they may have to include easily accessible materials in the teaching process [24]. In this context, necessary in-service training should be given to teachers to integrate teaching materials into the curriculum, to develop laboratory environments and to actively use tools and materials [25]. Science lessons enriched with various tools and materials support the development of students' scientific process skills through concrete experiences. However, some equipment-assisted experimental activities require expensive and high-end equipment. At this point, the economic conditions of the schools should be considered, and all kinds of support should be provided by the relevant institutions. Haury & Rillero [26] emphasized that many of the tools, materials and materials used in the activities in the textbooks can be easily obtained by teachers and students from daily life. Educators have great responsibilities in the efficient use of laboratory environments and integrating simple tools and equipment into the teaching process. At this point, teachers and prospective teachers who continue their undergraduate education should be subjected to in-service training programs on how to include scientific activities enriched with various tools and materials into their lessons [27].

MATERIALS AND METHOD

This research is a mixed method research in which qualitative and quantitative research methods are used together to determine the accessibility levels of tools,

materials and materials used in experimental activities in secondary school science textbooks and science teachers' views on this subject. Mixed method is a research method in which qualitative and quantitative research data are used together [28]. Science teachers' views on the use of teaching materials were determined through a five-point Likert-type questionnaire developed by Karamustafaoglu [29]. For this part of the research the survey model, which is one of the quantitative research methods, was adopted. With the screening model applied on large groups, the beliefs, attitudes, views, and tendencies of the examined group are defined numerically and the relationships between previous situations are explained [30], [31]. The examination of secondary school science textbooks was done by document analysis, one of the qualitative research methods. The document review method includes the analysis of written materials for the cases intended to be investigated in cases where the persons related to the research subject cannot be reached directly [32], [33].

Sampling of the Study

The sample of the quantitative research consists of 44 science teachers working in public secondary schools in Edirne city center in the 2020-2021 academic year. Appropriate sampling method was used to determine the sample.

The science textbooks of twenty different publishers were proposed by the Ministry of National Education Board of Education and Discipline for the 5^{th}, 6^{th}, 7^{th}, and 8^{th} grade levels to be taught in the 2020-2021 academic year [34]. The sample of the qualitative research consists of the 5^{th}, 6^{th}, 7^{th}, and 8^{th} Grade Science textbooks selected by stratified sampling, one of the random sampling methods among the recommended books [35]-[38].

I.RESULTS

Quantitative Findings

In this part of the research, the use of teaching materials in the lessons of science teachers was examined in terms of various variables and the findings were included.

According to the results of the Kruskal-Wallis H Test performed in Table 1. a statistically significant difference was found between the socio-economic status of the schools where the science teachers work and their use of tools, materials, and teaching materials (X^2=37,07; p<0,05). The data obtained has shown that with the increase in the socio-economic status of the school, the teachers' use of tools, materials and teaching materials was more positive.

According to the Mann-Whitney U Test results in Table 2. a statistically significant difference was found between the gender of science teachers and their

use of tools, materials, and teaching materials (U=,500; p<0,05). This difference was in favor of male teachers ($S.O_F$ = 16,52) compared to female teachers ($S.O_M$ = 38,46). The data obtained has shown that male teachers' use of tools, materials and materials in the lesson were more positive than female teachers.

Table 1. The Results of the Kruskal-Wallis H Test Conducted to Determine the Difference Between the Socio-Economic Levels of the Schools Where the Teachers Work in Terms of Science Teachers' Use of Tools, Materials, and Instructional Materials.

Survey	Type of School Served	N	S.O	sd	X^2	P
Survey on using teaching materials	Low Socio-Economic Level	12	6,54	2	37,07	,000
	Intermediate Socio-Economic Level	16	20,84			
	High Socio-Economic Level	16	36,13			
	Total	44				

Table 2. The Results of Mann-Whitney U Test Conducted to Determine the Difference Between the Gender of the Teachers in Terms of Science Teachers' Use of Tools, Materials, and Instructional Materials.

Survey	Gender	N	S.O	S.T	U	Z	P
Survey on using teaching materials	Female	32	16,52	528,50	,500	-5,07	,000
	Male	12	38,46	461,50			
	Total	44					

According to the Kruskal-Wallis H Test results in Table 3., a statistically significant difference was found between the type of faculty from which science teachers graduated and the teachers' use of tools, materials, and teaching materials (X^2=31,12; p<0,05). The data obtained the use of tools, equipment and materials by the teachers who graduated from the school of education was more positive than the teachers who graduated from the faculty of education and faculty of arts and sciences. It has been determined that the level of use of tools, materials

and materials was the lowest among the teachers who graduated from the faculty of education.

Table 3. The Results of the Kruskal-Wallis H Test Which Was Conducted to Determine the Effect of the Faculty of Tools, Materials and Teaching Materials.

Survey	**Type of Faculty Graduated**	**N**	**S.O**	**sd**	**X^2**	**P**
Survey on using teaching materials	Faculty of Education	26	13,69	2	31,12	,000
	Faculty of Arts and Sciences	15	33,87			
	High School of Education	3	42,00			
	Total	44				

According to the Kruskal-Wallis H Test results in Table 4., a statistically significant difference was found between the seniority years of the science teachers and the teachers' use of tools, materials, and teaching materials (X^2=36,90; p<0,05). The data obtained has shown that with the increase in years of seniority, teachers' use of tools materials and teaching materials was more positive.

B. Qualitative Findings

In this part of the research, the accessibility levels of the tools, materials and materials used in the experimental activities in the secondary school science textbooks were examined and the findings were included.

Table 4. The Results of the Kruskal-Wallis H Test Conducted to Determine the Effects of Science Teachers' Years of Seniority on Their Use of Tools, Materials, and Instructional Materials.

Survey	Seniority Year	N	S.O	Sd	X^2	P
Survey on using teaching materials	**0-10 Year**	9	5,22	2	36,90	,000
	11-20 Year	15	16,87			
	21-30 Year	20	34,50			
	Total	44				

According to Table 5., the activities examined according to the levels based on units mainly *(Level 1)* consisted of activities that could be done with easily accessible tools, equipment, and materials in daily life *(Level 2)*, and partially easy to access and alternative tools, equipment, and materials.

Table 5. Experimental Activities Examined by Levels Based on Units.

Units	5th and 6th Grades	7th Grade	8th Grade
Unit 1	S1 and S2	S1 and S2	S1 and S2
Unit 2	S1 and S2	S3	S1 and S2
Unit 3	S1 and S2	S1 and S2	S1 and S2
Unit 4	S1 and S2	S1 and S3	S1 and S3
Unit 5	S1 and S2	S1 and S2	S3
Unit 6	S1 and S2	S1 and S2	S1 and S2
Unit 7	S1 and S2	S1 and S2	S1 and S2

According to Table 6., Science-Engineering activities which were examined according to the levels based on units mainly *(Level 1)* consisted of activities that could be done with easily accessible tools, equipment, and materials in daily life *(Level 2)*, and partially easy to access and alternative tools, equipment, and materials.

Table 6. Science-Engineering Activities Examined by Levels Based on Units.

Units	**5th, 6th, and 7th Grades**	**8th Grade**
Unit 1	S1 and S2	*Tools, Equipment and Materials List Not Given.*
Unit 2	S1 and S2	
Unit 3	S1 and S2	
Unit 4	S1 and S2	
Unit 5	S1 and S2	
Unit 6	S1 and S2	
Unit 7	S1 and S2	

According to Table 7., experimental activities examined by levels based on learning areas were mainly *(Level 1)* consisted of activities that could be done with easily accessible tools, equipment, and materials in daily life *(Level 2)*, and partially easy to access and alternative tools, equipment, and materials. It has been concluded that the activities that could be done with tools, equipment and materials that are difficult to access and require high-level equipment were only included in the field of material and nature learning with low rates.

Table 7. Experimental Activities Examined by Levels Based on Learning Areas.

Learning Areas	**5th Grades**	**6th Grade**	**7th Grade**	**8th Grade**
Earth and Universe	-	-	-	S2
Creatures and Life	S1	S1	S1	S2
Physical Events	S2	S2	S2	S2
Matter and Nature	S3	S2	S1 and S3	S1 and S3

According to Table 8., Science-Engineering activities which were examined according to the levels based on learning areas mainly *(Level 1)* consisted of activities that could be done with easily accessible tools, equipment, and materials in daily life *(Level 2)*, and partially easy to access and alternative tools, equipment, and materials.

Table 8. Science-Engineering Activities Examined by Levels Based on Learning Areas.

Learning Areas	**5thGrades**	**6th Grade**	**7th Grade**	**8th Grade**
Earth and Universe	S2	S2	S2	*Tools, Equipment and Materials List Not Given.*
Creatures and Life	-	S2	-	
Physical Events	S2	S2	S1 and S2	
Matter and Nature	-	S1	S1	

According to Table 9., the experimental activities examined based on grade levels mainly included activities that could be done at the 5th, 7th, and 8th grade levels (Level 2) with tools, equipment and materials that were partially accessible and had alternatives. The 6th grade level mainly consisted of activities that could be done with easily accessible tools, equipment, and materials in daily life (Level 1).

Table 9. Experimental Activities Examined by Level Based on Class Levels.

Grade Level	**Level 1 (%)**	**Level 2 (%)**	**Level 3 (%)**
5th	%34	%37	%29
6th	%41	%38	%21
7th	%37	%39	%24
8th	%33	%40	%27

According to Table 10., the science-engineering applications activities, which were examined according to the levels based on grade levels, mainly included activities that could be done with tools, equipment and materials that were partially easy to access and had alternatives (Level 2) at the 5th, 6th, and 7th grade levels.

Table 10. Science-Engineering Activities Examined by Level Based on Class Levels.

Grade Level	**Level 1 (%)**	**Level 2 (%)**	**Level 3 (%)**
5th	%20	%80	%0
6th	%46	%51	%3
7th	%46	%54	%0
8th	*Tools, Equipment and Materials List Not Given.*		

II. DISCUSSION

In the literature, no study has been found in which the socio-economic status of the schools and the teachers' use of tools, equipment and materials are examined comparatively. Therefore, the results related to the related variable were discussed in relation to the literature on teachers' use of materials in science education. In their study, Yapici and Leblebiciler [39] examined the opinions of teachers about the renewed primary education program and found that the lack of laboratories, libraries and technological materials was against the village schools compared to the city schools. Similarly, Gurdal [40] stated that the frequency of use of tools and equipment increases according to the level of development of the schools. Unlike these results, Isman [41] in her study, in which she examined teachers' use of educational technologies in terms of various variables, concluded that there was no statistical difference between teachers' use of educational technologies and where they work. Simple teaching materials are designed with materials that can be easily obtained from daily life, regardless of socio-economic level, even if environmental opportunities are limited [42]. Tulving [43] emphasized that while designing instructional materials, designs could be made with cheap and economical materials as much as possible. In a study like this explanation made in India, the inadequacy of teaching tools and materials shows that teachers working in village schools design teaching materials with local materials [44]. In another study, Ozturk [45] carried out the activities in the 7th grade unit "The Meeting of Force and Motion and Energy" with basic materials. The result of the research showed that the students better comprehend the activities done with simple materials. In a similar study, Celik [46] concluded that teaching with simple experiments improves students' thinking skills in a positive way. However, the findings obtained from this study show the situation of developing and using simple teaching materials that they can easily access in daily life, although teachers working in schools with low socio-economic level attach importance to the use of materials in their lessons. In a study like these results, Karamustafaoglu [29] found that some of the teachers showed a positive attitude towards developing simple teaching materials despite the limited opportunities of the school they work in, while some of them did not try at all. It was stated that many of the activities in the curriculum can be easily done without the need for simple and inexpensive tools and equipment [47] and that the results of this study can also be used with students. In the study a significant difference was found between the socio-economic levels of the schools where the teachers work in terms of the use of tools, materials, and teaching materials by science teachers. It has been determined that this difference is in favor of schools with high socio-economic level. From this point of view, it is possible to say that the increase in the socio-economic status of schools positively affects teachers' use of tools, equipment, and materials. It is thought that

teachers working in schools with low socio-economic level compared to other schools, have difficulty in obtaining the materials they need and do not take sufficient responsibility. In the literature, it is seen that different results have been obtained in studies examining the variables of gender, seniority and the type of faculty graduated. Akpinar and Turan [48] aimed to determine the needs, usability, and suitability levels of the teaching materials of primary schools' science and technology teachers in a study supporting the research results. As a result of this research, it has been determined that male teachers use teaching materials more than female teachers, teachers with professional seniority use more teaching materials than newly graduated teachers, and teachers who are graduated from Teachers' School and Education High School use more teaching materials than teachers who are graduated from Education Faculty. The results obtained support the results of this study. Many studies conducted on pre-service teachers who take the instructional technologies and material development course given in faculties of education in our country show that the course contributes to the development of the pre-service teachers' skills in developing and using various teaching materials [49], [50]. Similarly in developed countries, "Multi-media Lehren und Lernen Method" and lessons for the teaching and use of instructional technologies are included in the curriculum [51]. However, according to the results of this study, the low frequency of using materials by the teachers who graduated from the Faculty of Education makes us think that the use of materials is a matter of preference. Teachers' use of tools, equipment and materials depends on the usefulness of the tool used and their willingness to do so [52]. Erdemir, Bakirci and Eyduran [53], in the study they conducted to determine the views of pre-service teachers on the skills of preparing technological materials for instructional purposes, it was concluded that female pre-service teachers had a positive attitude towards choosing, preparing, and evaluating materials compared to male pre-service teachers. In a similar study, Galpin and Sanders [54] emphasized that women developed a more positive attitude towards the use of technology-supported teaching materials than men. In the study by Karamustafaoglu, Cakir and Topuz [55] in which they examined primary school science and classroom teachers' attitudes towards the use of materials and technology, no statistically significant difference was found between female and male teachers. When the years of seniority are examined, teachers with 0-10 years of professional seniority do not make a significant difference with other teachers, but the data obtained from the scale shows that teachers with a seniority of 21-30 years have a positive attitude towards the use of material technology. While the results obtained regarding the seniority year variable are like the results of this study, the results obtained regarding the gender variable do not coincide with the results of this study. Unlike these results, Koseoglu [56], in his study in which he examined the competencies of biology teachers

regarding the use of tools; According to the teachers who graduated from education institute and education associate degree, it was concluded that the teachers who graduated from the Faculty of Education and Science, and the teachers with 0-10 years and 11-20 years of seniority compared to the teachers with 21 years and more seniority, have higher tool-equipment proficiency scores. Similarly, Yapici and Leblebiciler [39] examined teachers' use of technology-supported teaching materials in terms of seniority and found that newly graduated teachers had a positive attitude compared to experienced teachers. In another study in the related literature, Koseoglu and Soran [57] aimed to examine the attitudes of biology teachers towards the use of tools. The results obtained showed that there was no statistically significant difference between the variables of gender, seniority and graduated faculty and the level of teachers' use of tools and equipment. In a similar study, Karamustafaoglu [29] examined the views of science and technology teachers on the use of teaching materials in their classes. According to the results of the study, there is no statistically significant difference between male and female teachers and teachers with professional seniority of 1-10 years, 11-20 years. It was concluded that there is a statistically significant difference in favor of the teachers who graduated from the Faculty of Education compared to the teachers who graduated from the Faculty of Education and the Faculty of Arts and Sciences. In another study, Sahin [58] determined the views of 1029 teachers on the function and frequency of use of instructional technology and materials. According to the results obtained, it was concluded that there was no significant difference between the variables of gender and seniority and the frequency of teachers' material use. Like these results, Taiwo [59] did not find a statistically significant difference between the genders of teachers and their attitudes towards the use of technological materials in a study conducted on 150 secondary school teachers. When the literature was examined, no study was found to determine the accessibility levels of the tools and materials used in the activities in the Secondary School Science Textbooks. The findings obtained from this study were compared with the studies examining the applicability of the activities in the science textbooks. In the literature, there are various studies that show that the activities cannot be carried out due to various negativities such as lack of equipment in schools, crowded classrooms, inadequate course times and physical conditions [60]-[62]. Kurtulus and Cavdar [63] examined the applicability of the activities within the scope of teacher and student views in a study they conducted within the scope of primary school science and technology lesson. The results show that due to the lack of equipment and materials, the activities were passed only by explaining them before they could be performed. However, the results of this study show that the activities can be done with simple and alternative materials. In a similar study, Bulus-Kirikkaya [64] determined that there is not enough time for activities due to

the large number of classrooms and the long duration of applied activities. Teachers are the cornerstone of education. For a qualified learning-teaching process to take place, it is thought that teachers should have a rich content knowledge, ability to develop materials and use time effectively, and renewed methods and techniques [65]. Unlike these statements, Ayvaci & Er-Nas [66] determined that the time required for the lesson and experimental activities was limited in the study they aimed to determine the applicability of science and technology guidebooks within the scope of teachers' opinions. Unlike the results of the study, most of the teachers in this study benefit from guidebooks. Unlike the results of the study, most of the teachers in this study benefit from guidebooks. Bakar, Keles and Kocakoglu [67] evaluated the 6th grade science and technology book sets within the scope of teachers' opinions, and it was concluded that the time allocated to science activities in the sets was insufficient. In their study on primary school teachers, Dindar and Yangin [68] aimed to determine teachers' views on the structure and objectives of the 2004 science and technology curriculum. The results of the research indicated that the teachers had negative views on the aims and structure of the renewed program, they had deficiencies in equipment and materials, and the school administration should allocate a budget and provide teaching materials. Similarly, Bozdogan and Yalcin [69] aimed to determine the realization of the science curriculum in their study on teachers and students. The results of the research show that the curriculum is not followed adequately due to the inadequacy of the course hours, the unconsciousness of the students towards the applied activities, the lack of tools and equipment or the technically defective tools. Sunar [70] states that teachers have sufficient economic freedom to procure easily tools and equipment and they can easily design these teaching tools both individually and together with their students. The results of the study also support this statement. Most of the activities have the quality to be carried out by means of easy materials that are easily accessible or alternatives in daily life. In a study supporting these results, Yucel and Karamustafaoglu [71] examined the 5th and 6th Grade Science Textbooks within the scope of teacher opinions and concluded that the tools and equipment used in laboratory activities are easily accessible materials. In a study like the results of this, Aydogdu & Akilli [72] emphasized that science activities can be carried out with easy materials as an alternative in experimental activities at primary education level. Science activities with simple materials play an important role in the development of students' scientific process skills, technical skills, and science lesson perceptions [73]. In a study like these results Anilan, Berber and Suder [74] aimed to determine the situation of pre-service teachers performing activities using simple materials. The results of the research showed that pre-service teachers could easily perform the activities in and out of school environments with easily and inexpensive materials, and at the same time easy materials provided equal experience for all

students. In his study on students, Taskoyan [75] examined the reflections of activities based on inquiry learning strategy on students' academic achievement, attitudes towards science lesson and inquiry learning skills. Based on the results obtained, it has been suggested that teachers should be supported to conduct science lessons in laboratory environments, to have sufficient tools and equipment, and to provide easy materials that students can easily access in daily life. Ayvaci and Devecioglu [76] examined the applicability of the activities in the 10th Grade Physics Textbook within the scope of teachers' opinions, and most of the teachers stated that the content, design, and applicability of the textbook were insufficient. Some of them stated that the activities and the materials used were quite easy. Karamustafaoglu and Ustun [77], investigated the pre-school teacher candidates' ability to apply science and nature activities. The results of the research showed that pre-service teachers had negative attitudes towards applied activities. In a similar study, Kallery and Psillos [78], aimed to determine the perceptions of Greek pre-school teachers towards science concepts and applied activities. The results of the study showed that the teachers had various misconceptions, negatively affecting the realization of the activities.

CONCLUSION

As a result, it is possible to say that the results of the accessibility levels of the tools, equipment and materials used in the experimental and science-engineering activities examined within the scope of secondary school science textbooks show parallelism. Most of the activities in the 5^{th}, 6^{th}, 7^{th}, and 8^{th} Grade Science Textbooks consist of activities that can be done with tools, equipment and materials that are easily accessible in daily life, and activities that can be done with tools, materials and materials that are partially easy. It has been determined that the activities that can be done with tools, equipment are distributed at low rates in the textbooks.

ACKNOWLEDGMENT

This study is a part of Ezgi Onder's master thesis.

ETHICS STATEMENT

Approval was obtained from Trakya University Social and Human Sciences Research Ethics Committee with the document dated 02.12.2020 and numbered 2020.08.08 to carry out this study.

REFERENCES

B. Aybek, A. Cetin and F. Basarır, "Analyzing the science and technology textbook in line with critical thinking standards," *Journal of Education and Training Research*, vol. 3(1), pp. 313-325, 2014.

B. Costu, S. Unal and A. Ayas, "The use of events in daily life in science teaching," *Ahi Evran University Journal of Kirsehir Education Faculty (KEFAD)*, vol. 8(1), pp. 197-207, 2007.

M. Demirbas and H. M. Pektas, "The level of realization of the basic concepts related to the environmental problem of primary school students," *Necatibey Education Faculty Electronic Journal of Science and Mathematics Education (EFMED)*, vol. 3(2), pp. 195-211, 2009.

B. Demirci, "Contemporary science education and educators," *H.U. Journal of the Faculty of Education*, vol.9, pp. 155-160, 1993.

H. Bayram, U. H. Patli and H. Savci, "Learning circle model in science teaching," *Marmara University Ataturk Faculty of Education Journal of Educational Sciences*, vol. 10(10), pp. 31-40, 1998.

A. Tekbiyik and A. R. Akdeniz, "Teachers' views on accepting and applying the primary school science and technology curriculum," *Necatibey Education Faculty Electronic Journal of Science and Mathematics Education*, vol. 2(2), pp. 23-37, 2008.

F. Onen-Ozturk, "The effect of science fiction movies on pre-service science teachers' views on science-technology-society," *Bartin University Journal of Education Faculty*, vol. 6(2), pp. 715-736, 2017.

MEB, *Science lesson curriculum (primary and secondary school 3, 4, 5, 6, 7 and 8th grades).* Ankara: MEB,2018. http://mufredat.meb.gov.tr/ProgramDetay.aspx?PID=325

A. Kilic and S. Seven, *The place of the textbook in teaching*. Ankara, PEGEM Publishing, 2007.

K. Penney, S. P. Norris, L. M. Phillips and G. Clark, "The anatomy of junior high school science textbooks: An analysis of textual characteristics and a comparison to media reports of science," *Canadian Journal of Science, Mathematics and Technology Education*, vol. 3(4), pp. 415-436, 2003.

B. Ceger and C. Aydogdu, "Examining the fifth-grade science book in terms of laboratory safety, achievements and scientific process skills," *Eskisehir Osmangazi University Turkish World Application and Research Center (ESTUDAM) Education Journal*, vol. 2(2), pp. 12-34, 2017.

C. Aydogdu and F. Sener, "Research on the importance of laboratory use technique and safety in science education and the benefits of the CLP regulation," *Eskisehir Osmangazi University Turkish World Application and Research Center (ESTUDAM) Education Journal*, vol. 1(1), pp. 39-54, 2016.

N. Valanides, M. Papageorgiou and P. Rigas, *Science and science teaching*, M. S. Khine (Ed.), *Critical analysis of science textbooks evaluating instructional effectiveness* pp. 259-286. Springer Publishing, 2013.

P. Turiman, J. Omar, A. M. Daud and K. Osman, "Fostering the 21st century skills through scientific literacy and science process skills" *Procedia - Social and Behavioral Sciences*, vol. 59, pp. 110-116, 2012.

G. Bagci-Kilic, "Third international mathematics and science research (TIMSS): Science teaching, scientific research and the nature of science," *Elementary-Online*, vol. 2(1), pp. 42-51, 2003.

W. Harlen, "Inquiry-based learning in science and mathematics," *Review of Science, Mathematics and Ict Education*, vol. 7(2), pp. 9-33, 2013.

N. Lerner, "Laboratory lessons for writing and science," *Massachusetts Institute of Technology*, vol. 24(3), pp. 191-222, 2007.

J. F. Donnelly, "The place of the laboratory in secondary science teaching" *International Journal of Science Education*, vol. *20*(5), pp. 585-596, 1998.

E. Ceylan, S. Guzel Yuce, and Y Koc, "Science teaching laboratory practices course in the way of teaching: A case study," *Journal of Ataturk University Kazim Karabekir Education Faculty*, vol. 39, pp. 22-47, 2019.

C. Zimmerman, "The development of scientific thinking skills in elementary and middle school," *Developmental Review*, vol. 27(2), pp. 172-223, 2007.

A. Hofstein, and P. M. Kind, *Learning in and from science laboratories,* In B. J. Fraser, K. G. Tobin and C. J. McRobbie (Eds.), *Second International Handbook of Science Education* (pp.189-207). Springer Dordrecht, 2012.

P. Koseoglu and H. Soran, "Biology teachers' opinions on equipment use proficiency," *Journal of Hacettepe University Faculty of Education*, vol. 27(27), pp. 189-195, 2004.

F. Onen and A. Comek, "Science experiments with simple equipment from the perspective of pre-service teachers" *Western Anatolian Journal of Educational Sciences (BAED)*, vol. 1(3), pp. 45-71, 2011.

A. Musar, *Equipment for science education constraints and opportunities (English)*, Washington, D. C. USA: World Bank Group, 1993.

M. Barak and S. Waks, "An Israel study of longitudinal in-service training of mathematics, science and technology teachers," *Journal of Education for Teaching*, vol. 23(2), pp. 179-190, 1997.

D. L. Haury and P. Rillero, *Perspectives of hands-on science teaching,* Columbus, Ohio, USA, ERIC Clearinghouse for Science, Mathematics and Environmental Education, 1994.

S-M. Yu, L. J. Bethel and J. Lowell "The influence of hands-on science process skills training on preservice elementary teachers' anxiety and concerns about teaching science activities in Taiwan, Republic of China," Annual Meeting of the National Association for Research in Science Teaching, The University of Texas, Austin, USA,1991- April, paper ED332870 p.1-26.

J. W. Creswell, *Research design: Qualitative, quantitative, and mixed methods approaches,* 3rd ed*.,* V. Knight Ed., Thousand Oaks, California USA: Sage Publishing, 2009.

O. Karamustafaoglu, "Science and technology teachers' level of use of teaching materials: The example of Amasya province," *Journal of Ataturk University Bayburt Faculty of Education*, vol. 1(1), pp. 90-101, 2006.

T. Kalafat and R. Y. Kincal, "Examining the relationship between university students' body satisfaction levels and social skill levels," *Dokuz Eylul University Buca Education Faculty Journal*, vol. 23, pp. 41-47, 2008.

G. Sezgin-Selcuk, *Research Methods in Education,* H. Ozmen & O. Karamustafaoglu (Eds.), Ankara, Turkey: Pegem A. Publishing, 2019.

M. Cansiz-Aktas, *Research Methods in Education,* H. Ozmen and O. Karamustafaoglu (Eds.), Ankara Turkey: Pegem A Publishing, 2019.

A. Yildirim and H. Simsek, *Qualitative research methods in the social sciences,* 11th ed., Ankara, Turkey: Seckin Publishing, 2016.

MEB Journal of Notifications (December-Add 2019). https://tebligler.meb.gov.tr/index.php/tuem-sayilar/viewcategory/87-2019

C. Cigdem, G. Minoglu-Balcık and O. Karaca, *Secondary School, and Imam Hatip Secondary School Science 6th Grade Textbook*, Ankara, Turkey: Sevgi Publishing, 2019.

A. Seyrek, S. Turker, T. Bozkaya and Z Ucuncu, *Secondary School and, Imam Hatip Secondary School Science 7th Grade Textbook,* Ankara, Turkey: Tutku Publishing, 2019.

E. Unver, M. V. Yancı and Z. Arslan, *Secondary School and Imam Hatip Secondary School Science 5th Grade Textbook*, Ankara, Turkey: SDR Dikey Publishing, 2019.

M. V. Yanci, *Secondary School and Imam Hatip Secondary School Science 8th Grade Textbook,* Ankara, Turkey: SDR Dikey Publishing, 2019.

M. Yapici and N. H. Leblebiciler, "Opinions of teachers about the new curriculum," *Elementary Education Online,* vol. 6(3), pp. 480-490, 2007.

A. Gurdal, "The use of laboratories and tools in primary school science education," *Marmara University Ataturk Faculty of Education Journal of Educational Sciences*, vol. 3(3), pp. 145-155, 1991.

A. Isman, "The competencies of teachers in Sakarya province in the direction of educational technologies," *The Turkish Online Journal of Educational Technology – TOJET*, vol. 1(1), pp. 7291, 2002.

G. Uzal, A. Erdem, F. Onen and A. Gurdal, "Teachers' views on science experiments with simple tools and evaluation of in-service training," *Necatibey Education Faculty Electronic Journal of Science and Mathematics Education*, vol. 4(1), pp. 64-84, 2010.

E. Tulving, "The effects of presentation and recall of material in free-recall learning," *Journal of Verbal Learning and Verbal Behavior*, vol. 6(2), pp. 175-184, 1967.

R. Mohan, *Innovative Science Teaching,* 4th ed. Delhi, India: PHI Learning Private Limited, 2019.

G. Ozturk, "The effect of students' experiments with simple materials on their learning of the concept of force-energy and their attitudes towards science," Master thesis, Marmara University Institute of Educational Sciences, Istanbul, Turkey, 2007.

M. Celik, "Evaluation of the effect of simple experiments on learning in biology education with learning diaries," Master thesis, Hacettepe University Institute of Educational Sciences, Ankara, Turkey, 2023.

H-J. Jodl and B. Eckert, "Low-cost, high-tech experiments for educational physics," Physics Education, vol. 33(4), pp. 226-235, 1998.

B. Akpinar and M. Turan, "The use of materials in science education in primary schools," Paper presentation, V. National Science and Mathematics Education Congress, Middle East Technical University, Ankara, 2002 September, p. 219–225.

N. Bektas, A. Nalcaci and H. Ercoskun, "Opinions of prospective classroom teachers on the achievements of the "instructional technologies and material development/design" course." *Theoretical Educational Science*, vol. 2(2), pp. 19-31, 2009.

E. Bozpolat and A. Arslan, "Opinions of pre-service teachers on instructional technologies and material design course," *E-International Journal of Educational Research*, vol. 9(3), pp.60-84, 2018.

C. Baytekin, *Learning Teaching Techniques and Material Development,* 3rd ed. Ankara, Turkey: Anı Publishing, 2011.

H. I. Yalin, *Instructional technologies and material development* 30th ed., Ankara, Turkey: Nobel Publishing, 2020.

N. Erdemir, H. Bakirci and E. Eyduran, "Determination of teacher candidates' self-confidence in using technology in education" *Turkish Journal of Science Education,* vol. 6(3), pp. 99-113, 2009.

V. C. Galpin, and I. D. Sanders, "Perceptions of computer science at a South African University," *Computers and Education*, vol. 49(4), pp. 1330-1356, 2007.

O. Karamustafaoglu, R. Cakır and F. G. Topuz. "Examination of teachers' attitudes towards the use of materials and technology in their lessons in science teaching" Paper presentation, X. National Science and Mathematics Education Congress, Nigde University, Nigde, 2012 June, p. 609-610.

P. Koseoglu, "Teacher competencies in terms of use of tools and materials in biology lesson," PhD. thesis. Hacettepe University, Institute of Natural and Applied Sciences, Ankara, Turkey, 2004.

P. Koseoglu and H. Soran, "Attitudes of biology teachers towards the use of tools," *Journal of Hacettepe University Faculty of Education*, vol. 30, pp. 159-165, 2006.

M. Sahin, "Analysis of teachers' views on the function of teaching materials in the learning-teaching process," *Kastamonu University Kastamonu Journal of Education*, vol. 23(3), pp. 995-1012, 2014.

S. Taiwo, "Teachers' perception of the role of media in classroom teaching in secondary schools," *The Turkish Online Journal of Educational Technology – TOJET*, vol. 8(1), pp. 75-83, 2009.

M. Basaran, "Evaluation of information literacy of primary school teacher candidates," *Gazi University Journal of Gazi Education Faculty*, vol. 25(3), pp. 163-177, 2005.

Z. Bayram, "Examining the difficulties faced by pre-service teachers while designing guided inquiry-based science activities," *Hacettepe University Faculty of Education Journal*, vol. 30(2), pp. 15-29, 2015.

R. Sogukpınar and K. Gundogdu, "Student and teacher views on science course and laboratory practices: A case study," *IBAD Journal of Social Sciences*, vol. 8, pp. 275-295, 2020.

N. Kurtulus and O. Cavdar, "Teacher and student thoughts on the activities in the science and technology curriculum," *Necatibey Education Faculty Electronic Journal of Science and Mathematics Education (EFMED)*, vol. 5(1), pp. 1-23, 2011.

E. Bulus-Kirikkaya, "Opinions of science teachers in primary schools about science and technology program," *Turkish Journal of Science Education*, vol. 6(1), pp. 133-148, 2009.

H. Karacengel, F. Ceylan, K. Gedik and H. Ipek-Akbulut, "Determining the views of science teacher candidates about teaching materials and their use," Paper presentation, International Science, Mathematics, Entrepreneurship and Technology Education Congress, Recep Tayyip Erdogan University, Izmir, 2019 April, p.12-14.

H. S. Ayvaci and S. Er-Nas, "Evaluation of teacher guidebooks based on teacher opinions according to constructivist theory," *Necatibey Education Faculty Electronic Journal of Science and Mathematics Education (EFMED)*, vol. 3(2), pp. 212-225, 2009.

E. Bakar, O. Keles and M. Kocakoglu, "Evaluation of teachers' opinions about MEB 6th grade science and technology course book sets," *Ahi Evran University Journal of Kirsehir Education Faculty (KEFAD)*, vol. 10(1), pp. 41-50, 2009.

H. Dindar and S. Yangin, "Evaluation of teachers' perspectives in the transition process to the primary school science and technology curriculum," *Kastamonu Journal of Education*, vol. 15(1), pp.185-198, 2007.

A. E. Bozdogan and N. Yalcin, "The frequency of experiments in primary school science lessons and the problems encountered in physics experiments," *G.U. Kirsehir Education Faculty Journal*, vol. 5(1), pp. 59-70, 2004.

Y. Sunar, "The use of inquiry teaching method in activities with simple equipment," Master Thesis, Firat University Institute of Educational Sciences, Elazıg, Turkey, 2017.

M. Yucel and S. Karamustafaoglu, Teachers' opinions about secondary school 5th and 6th grade science textbooks," *Amasya University Journal of Education Faculty*, vol. 9(1), pp. 93-120, 2020.

C. Aydogdu and H. I. Akilli, "Examination of secondary school 5th grade science lesson activities in terms of laboratory use techniques and their suitability for learning outcomes," Paper presentation, In International Conference on Education in Mathematics, Science and Technology (pp.), Necmettin Erbakan University, Konya, 2014 May, p. 932-941.

E. B. Klemm and L. A. Plourde, "Examining the multi-sensory characteristics of hands-on science activities*"* (Report No. ED 473 652). St. Louis, MO, 2003.

B. Anilan, A. Berber and N. Suder, "Opinions of pre-service science teachers and secondary school students on experimental applications using simple tools," *Kastamonu Journal of Education*, vol. 28(1), pp. 52-71, 2020.

S. N. Taskoyan, “The effect of inquiry learning strategies in science and technology teaching on students' inquiry learning skills, academic achievement and attitudes” Master thesis, Dokuz Eylul University Institute of Educational Sciences, Izmir, Turkey, 2008.

H. S. Ayvaci and Y. Devecioglu, “Teacher evaluations about the 10th grade physics textbook and the applicability of the activities in the book,” *Journal of Amasya University Faculty of Education* vol. 2(2), pp. 418-450, 2013.

S. Karamustafaoğlu and A. Üstün, “Okul öncesi öğretmen adaylarının fen ve doğa etkinliklerini uygulayabilme düzeylerinin belirlenmesi” *Ondokuz Mayıs Üniversitesi Eğitim Fakültesi Dergisi*, vol. 21, pp. 15-23, 2006.

M. Kallery and D. Psillos, “Pre-school teachers’ content knowledge in science: Their understanding of elementary science concepts and of issues raised by children’s questions,” *International Journal of Early Years Education*, vol. 9(1), pp. 165-179, 2001.

Chapter 9

Cyto-embryological Studies in Male Gametophyte of *Matthiola incana* (L.) R. Br.

Nazlıcan ÇOLAK[1], Nuran EKİCİ[2*]

[1]Trakya University, Institute of Science, Department of Biotechnology and Genetics, Edirne TURKEY
[2]Trakya University, Faculty of Education, Department of Science Education, Edirne/TURKEY
**(nuranekici@yahoo.com) Email of the corresponding author*

Abstract

In this study, anther wall structure, microsporogenesis, microgametogenesis and pollen viability were investigated cytologically and embryologically in *Matthiola incana* (L.) R. Br. from Brassicaceae family which shows limited distribution in Turkey. Preparations made by using the crushing method and paraffin embedding method were examined under a light microscope. The polysaccharide and RNA contents of the anthers at various stages were studied histologically using the PAS method and the toluidine blue staining method. Anthers in *M. incana* are tetrasporangiate. Anther wall consists of epidermis, endothecium, flattened intermediate layer and secretory tapetum, usually with two-nucleated cells. Microsporogenesis and pollen mitosis are generally regular, but abnormalities such as chromosome bridge and micronucleus have also been encountered at some stages. In addition, asynchrony has been observed in microsporogenesis. Pollen sterility rate was determined as 0.2%. The polysaccharide content of the anther is often concentrated in cell walls and microspores. Polysaccharides are denser especially in tapetum cells, in the endothecium layer and epidermis in the mononuclear microspore stage, and in the endothecium layer in the mature pollen stage. It was observed that the RNA content was rich in the anther wall in the early stage of microgametogenesis, in microspores prepared for pollen mitosis, and in the middle layer in the mononuclear microspore stage. The data obtained from this study will contribute to the cyto-embryological, histological and taxonomic studies on *M. incana*.

Keywords: *Matthiola incana, Brassicaceae, microsporogenesis, microgametogenesis, microspore, pollen*

INTRODUCTION

The Brassicaceae family, also known as the Crucifera family, is a monophyletic group consisting of about 321 genera and includes 49 orders, about 3,660 species distributed worldwide. It consists of a wide variety of vegetables and economically important products [1].

The Brassicaceae family spreads on all continents except Antarctica [2]. It is a large family spreads mostly to the North Atlantic Islands, the Mediterranean Basin, the Saharo-Sindian region, Northeast Africa and Asia, and shows taxonomic diversity in Turkey and the Irano-Turan region [3]-[6]. This family is distributed in Marmara Region, West and East Black Sea Region, Coastal Aegean Region and Mediterranean Region in Turkey [7].

Brassicaceae is generally thought to derive from original Brassicaceae tribe Stanleyeae or from the Capparaceae subfamily Cleomoideae that is related to Thelypodieae [8]. Brassicaceae family has been studied phylogenetically. Su et al. [9] used DNA regions of four plastid (matK, ndhF, rbcL, trnL-trnF) and pollen data to determine phylogenetic relationships within Brassicales. Edger et al. [10] analyzed ITS1 and ITS2 (Internal Transcribed Spacer) from 50 species of the Brassicaceae family. Regions of the nuclear ribosomal RNA gene clusters named as ITS1 and ITS2, are the most used nuclear markers for phylogenetic analyzes in many eukaryotic groups, including most plant families [10]. The genus *Matthiola* has about 50 species in the world. It is represented by 12 taxa in Turkey [11]- [14].

Somatic chromosome number (2n) of the species *Matthiola* is determined as 10, 12, 14 and 16 in the karyological studies [6], [14]-[16]. Species; *Matthiola trojana*, *M. odoratissima* (Pall.) R. Br., *M. anchonifolia* Hub.-Mor., *M. montana* Boiss., *M. fruticulosa* (L.) Maire ssp. *fruticulosa* and *M. ovatifolia* (Boiss.) Boiss. 2n=12 chromosomes and *M. incana* (L.) R. Br., *M. longipetala* (Vent.) DC. ssp. *bicornis* (Sibth. & Smith) P. W. Ball, *M. longipetala* (Vent.) DC. ssp. *longipetala*, *M. longipetala* (Vent.) DC. ssp. *pumilio* (Sibth. & Smith) PW Ball, *M. sinuata* (L.) R. Br., and *M. tricuspidata* (L.) R. Br. from Turkey are reported to have 2n=14 chromosomes [5]. Somatic chromosome number (2n = 14) and quantitative karyotypic parameters in root tip cells of *M. incana* cultivars grown in different regions were investigated by [17]. The degree of karyotype asymmetry was examined and evaluated by qualitative and quantitative methods.

Pollen morphology was studied in *Matthiola arabica* Boiss., *M. fruticulosa* (L.) Maire, *M. longipetala* (Vent.) DC. subsp. *longipetala*, *M. parviflora* (Schousb.) R. Br. [18] taxa and *Matthiola longipetala* subsp. *bicornis* species [19].

M. incana is an important product in the flower trade. In recent years, it has noticed with its increasing color range, interesting form and intense scent [20]. There are more biochemical [21]-[23] and genetic [17], [24]-[28] studies with *M. incana.*

Fig. 1 Flowers and buds of *M. incana* in various sizes

In recent years, micropropagation studies have also been carried out using various growth media in the *M. incana* species [29]-[31]. The first record of cytological and embryological studies on *Matthiola incana* was published in 1924. In that study, the number of diploid chromosomes was revealed, and chromosome behaviors during meiosis and pollen formation were investigated in pollen mother cells [15].

In vivo and *in vitro* pollen germination studies have been carried out to explain the single and double flower development [32]. Morphophenological changes in *M. incana* cultivars and chromosome behaviors in the meiosis of pollen mother cells were investigated [33].

Cyto-embryological studies are limited on *M. incana*. And there is no histochemical study on *M. incana* which is frequently used as an ornamental plant, plays an important role in gardening, and contains alpha linolenic acid which is an important fatty acid for human health in its seed oil. In this study, the developmental stages of male gametophyte of *M. incana* were investigated in terms of cyto-embryology and histochemistry. The aim of this study is to contribute to the embryological and cytological data related to the Brassicaceae family.

MATERIALS AND METHOD

In this study, anthers on buds and flowers of various sizes in *Matthiola incana* species were used as material (Fig. 1). The plant was grown in the greenhouse of Trakya University Department of Biology. Buds and flowers of various sizes of *M. incana*, which were fixed in Carnoy (3:1, ethyl alcohol: acetic acid) fixative in March 2017-2019, were stored in 70% ethyl alcohol. Some histological features of the anther wall at different stages of microgametogenesis, microsporogenesis and pollen mitosis were also examined by using paraffin embedding method. In addition, sections of anthers and buds were stained with

PAS (Periodic Acid Schiff) and toluidine blue and examined for polysaccharide and RNA content [34]-[36]. The numbers and shapes of pollen were examined by aceto-orcein crushing method. Pollen viability is studied with lactofenol-anilin and aceto-carmin blue prepared in lactophenol [36]. Photographs were taken with Olympus photomicroscope.

RESULTS

A. Androecium

Androecium consists of 4-6 stamens. Anthers are whitish yellow, basifixed and filaments are green. Mature anthers are usually 4-5 mm, but rarely 6 mm anthers were also seen. The filaments are noticeably shorter than anthers.

B. Anther Wall

The anthers of *Matthiola incana* are tetrasporangiate (Fig. 2a). In early stages of microsporogenesis, the anther wall consists of 3-4 cell lines. At these stages of the anther development, epidermal cells are larger than the other cells. Endothecium thickenings have not started to occur. The middle layer is composed of flattened cells. Tapetum cells are usually binucleated, and mononucleated cells are rarely found. The secretory type of tapetum is seen (Fig. 2b). The tapetum cells are begun to degenerate in the tetrad stage of microsporogenesis (Fig. 2c).

In the early stages of microgametogenesis, it was observed that tapetum cells have not been degenerated in some anthers (Fig. 2d). A line of flat and swollen epidermis cells is seen on the outer part of the mature anther in cross section. These cells remain undegenerated until the end of pollen development. Under the epidermis, 1-2 cell lines of endothecium, usually a single-cell line of middle layer, and residues of fragmented tapetum cells are seen (Fig. 2e).

In the anther wall of *M. incana*, it was observed that the tapetum cells were usually binucleated. Fibrous thickenings were observed in the endothecium layer of the mature anther wall (Fig. 2f).

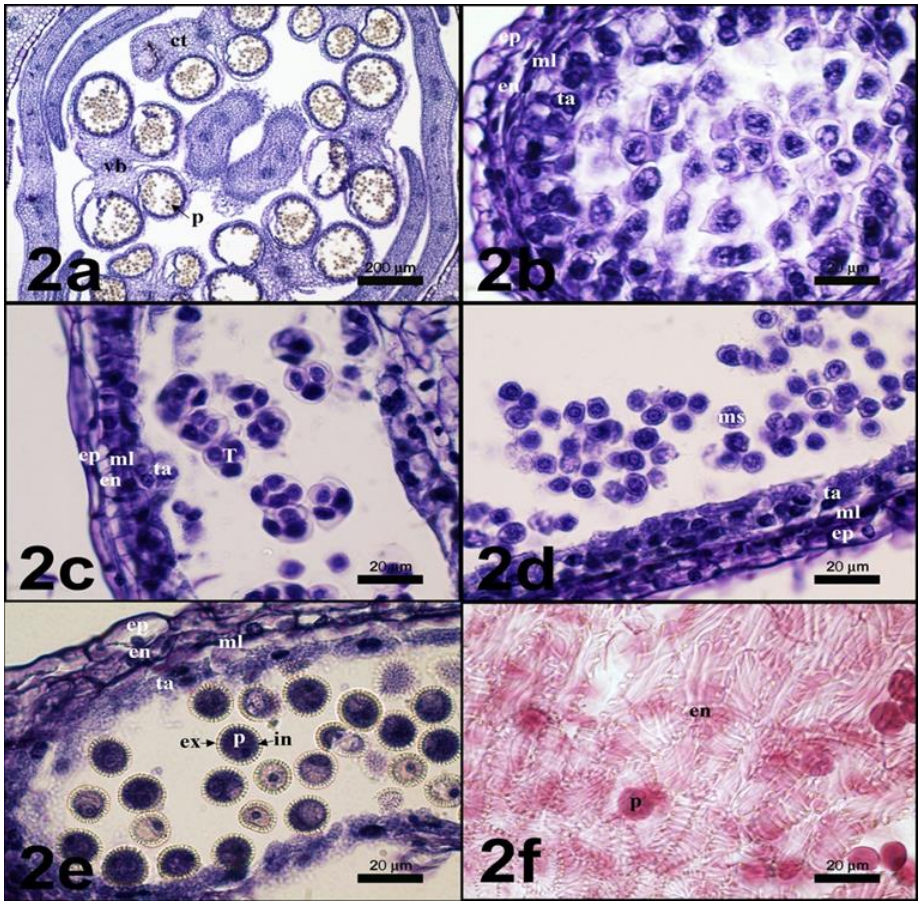

Fig. 2 Anther wall structure of *M. incana.* 2a. Tetrasporangiate anthers 2b. General view of the anther wall in the early phase of microsporogenesis 2c. General view of anther wall in late phase of microsporogenesis; 2d. General view of the anther wall in the early stage of microgametogenesis; 2e. General view of the anther wall in the late stage of microgametogenesis; 2f. Endothecium thickenings on the mature anther wall in *M. incana* (ct, connective tissue; en, endothecium; ep, epidermis; ex, exine; in, intine; ml, middle layer; ms, microspore; p, pollen; T, tetrad; ta, tapetum; vb, vascular bundle)

C. Histochemical characteristics of the anther wall at tetrad stage and at various stages of microgametogenesis

Sections of *Matthiola incana*, generally taken from mature anthers of different sizes, were stained with PAS and toluidine blue and examined in terms of polysaccharide and RNA contents at various stages of gametogenesis. It has been observed that the polysaccharide content in the anther is generally dense in the cell walls, especially in the tapetum cells. Tetrads are also stained densely because of the callose wall. (Fig. 3a). In the wrinkled microspore stage, the degeneration of tapetum cells has increased, so they are stained less dense. It was

observed that the other anther wall layers were stained dense due to their polysaccharide content (Fig. 3b). Accumulation of polysaccharide particles were observed in epidermis and endothecium at the mononucleate microspore phase.

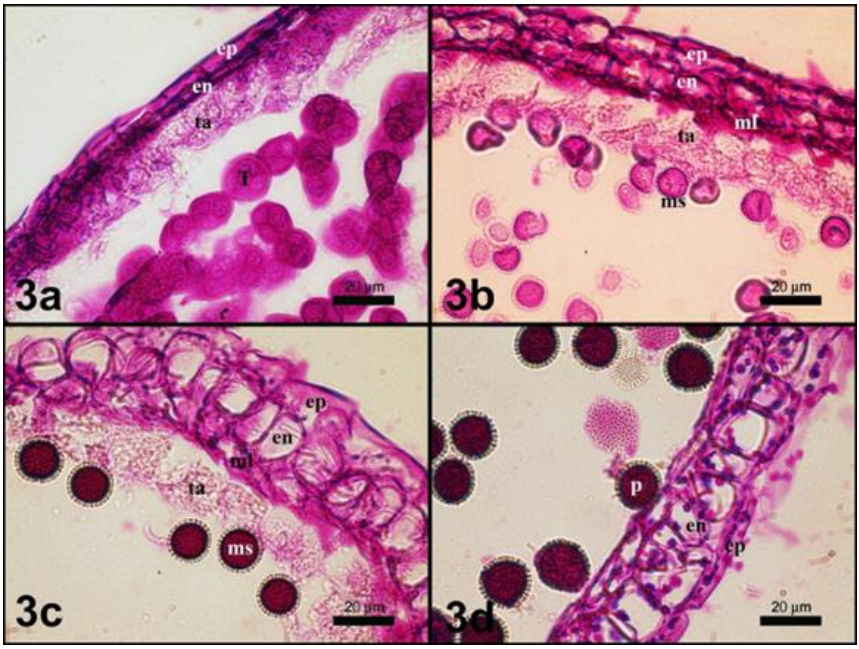

Fig. 3 Cross-section of anthers stained with PAS in tetrad and various stages of microgametogenesis in *M. incana*. 3a. Tetrad phase; 3b. Wrinkled microspore phase; 3c. Mononucleate microspore phase; 3d. Mature pollen phase (en, endothecium; ep, epidermis; ml, middle layer; ms, microspore; p, pollen; T, tetrad; ta, tapetum)

Microspores are stained dense (Fig. 3c). In the mature pollen stage, it was observed that the tapetum cells were completely degenerated, and the polysaccharide content was generally concentrated in the endothecium layer (Fig. 3d).

It has been observed that the anther wall is rich in RNA content at the early stage of microgametogenesis (late tetrad stage). (Fig. 4a). In the wrinkled microspore stage, the RNA content in these cells were decreased due to the degeneration of the tapetum cells. Microspores are rich in RNA content as they are prepared for pollen mitosis (Fig. 4b). In the mononucleate microspore stage, the middle layer was found to be rich in RNA content compared to the other anther wall layers (Fig. 4c). The RNA content of the anther wall in *M. incana* is least dense at mature pollen stage (Fig. 4d).

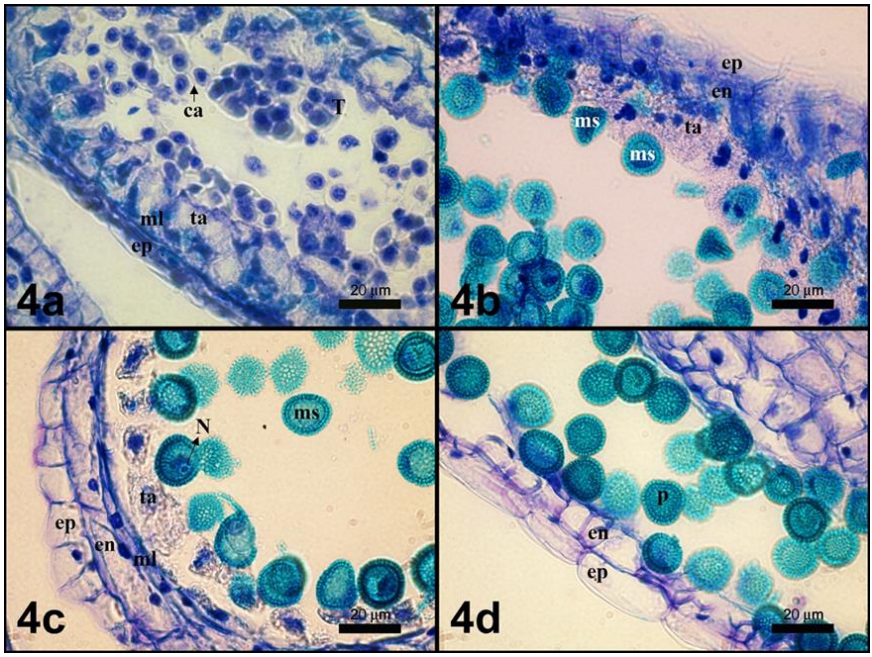

Fig. 4 Cross-section of anthers stained with toluidine blue in late tetrad and various stages of microgametogenesis in *M. incana*. 4a. Late tetrad phase; 4b. Wrinkled microspore phase; 4c. Mononucleate microspore phase; 4d. Mature pollen phase (ca, callose wall; en, endothecium; ep, epidermis; ml, middle layer; ms, microspore; N, nucleus; p, pollen; T, tetrad; ta, tapetum)

D. Microsporogenesis

Microsporogenesis in *Matthiola incana* was examined. Asynchronous meiosis was observed in MMCs (Microspore Mother Cells) at different anther loci in *M. incana*. While prophase I was observed in one locus, telophase I was observed in the other locus (Fig. 5a). In addition, it was observed that meiosis was asynchronous in MMCs in the same anther locus. Different stages of meiosis I were seen in a single anther locus (Fig. 5b).

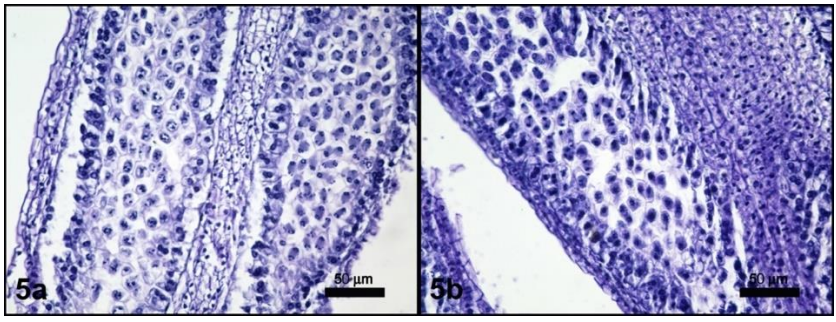

Fig. 5 Phases of asynchronous meiosis in the anther of *M. incana* - longitudinal section. 5a. In an anther 5b. In an anther locus.

Interphase: In the preparations taken from paraffin sections at this stage, the nuclei of the microspore mother cells have similar volume. The callose wall is not visible yet (Fig. 6a, 6b). Micronuclei were observed in some cells (Fig. 8a, arrows).

Leptotene: Chromatin in the nuclei of microspore mother cells is less dense at this stage. Callose wall formation around MMCs has started to be developed (Fig. 6c).

Zygotene: Chromatin material becomes loose at this stage and is spread throughout the cell. Callose wall formation around the MMCs has been completed (Fig. 6d).

Pachytene: Homologous chromosomes gather together (Fig. 6e). Then, the nucleus in the center of the cell was became located at the edge of the cell. Chromatin material is densely located adjacent to the cell membrane. This is called the bouquet configuration of the nucleus in early meiosis (Fig. 6f).

Diplotene: At this stage, the bivalent chromosomes began to shorten in length (Fig. 6g).

Diakinesis: Different bivalent chromosome numbers were observed in different cells due to paraffin sectioning at this stage (Fig. 6h).

Metaphase I: It was observed that the chromosomes were arranged normally in the equatorial plate in the MMCs of *M. incana* (Fig. 6i).

Anaphase I: In the anaphase I stage of meiosis, chromosomes are normally pulled to the poles in most cells (Fig. 6j) but lagging chromosomes (Fig. 8b, thin arrows) and chromosome bridge formation in some cells were also seen (Fig. 8b, thick arrow).

Telophase I: At this stage, the polarization of homologous chromosomes is normally completed (Fig. 6k). At the end of the telophase I, a dyad was formed between the two nuclei without the formation of a middle lamella, so simultaneous type of cytokinesis was observed (Fig. 6l).

Metaphase II: Generally, it was observed that the chromosomes were arranged regularly on the equatorial plate (Fig. 6m, arrowheads).

Anaphase II: The chromatids of chromosomes, which are usually aligned on the equatorial plate, are regularly pulled to the poles in this phase. (Fig. 6n).

Telophase II: It was determined that 3 different types of tetrads were formed at the end of telophase II. Generally rhomboidal (Fig. 7a), tetrahedral and decussate (Fig. 7b) types of tetrads were found. A well-developed callose wall was observed in tetrads (Figs. 6o, 6p).

In the later stages, the callose wall around the microspores was broken down and the microspores were released. Although microsporogenesis was generally regular, some rare irregularities have been observed.

E. Microgametogenesis

In *Matthiola incana*, microspores were released by break down of the callose at tetrad phase (Fig. 9a). In microspores separated from the tetrad, the nucleus is located in the middle. At this phase, the exine has not yet developed around the microspores (Fig. 9b). The next phase was the wrinkled microspore phase. The nucleus moved on one side of the cell. On the other side, a large vacuole was observed. Exine has also begun to form around the microspores at this phase (Fig. 9c). Microspores were swollen by absorbing the liquid from the locus. An evident polarity was observed in the microspores (Fig. 9d). It was observed that the prophase, metaphase, anaphase and telophase were normal in pollen mitosis (Figs. 9e, 9f, 9g, 9h, arrows). At the end of pollen mitosis, it was observed that the nucleus close to the wall formed the generative cell and the other formed the vegetative cell. In mature pollen grains, the generative cell nucleus stained darker, while the vegetative cell nucleus was stained lighter (Fig. 9i).

Pollen mitosis was generally seen to occur normally, but abnormalities were also observed in some phases. It was observed that chromosome bridges were formed in the anaphase of pollen mitosis in some microspores (Fig. 9j, arrow).

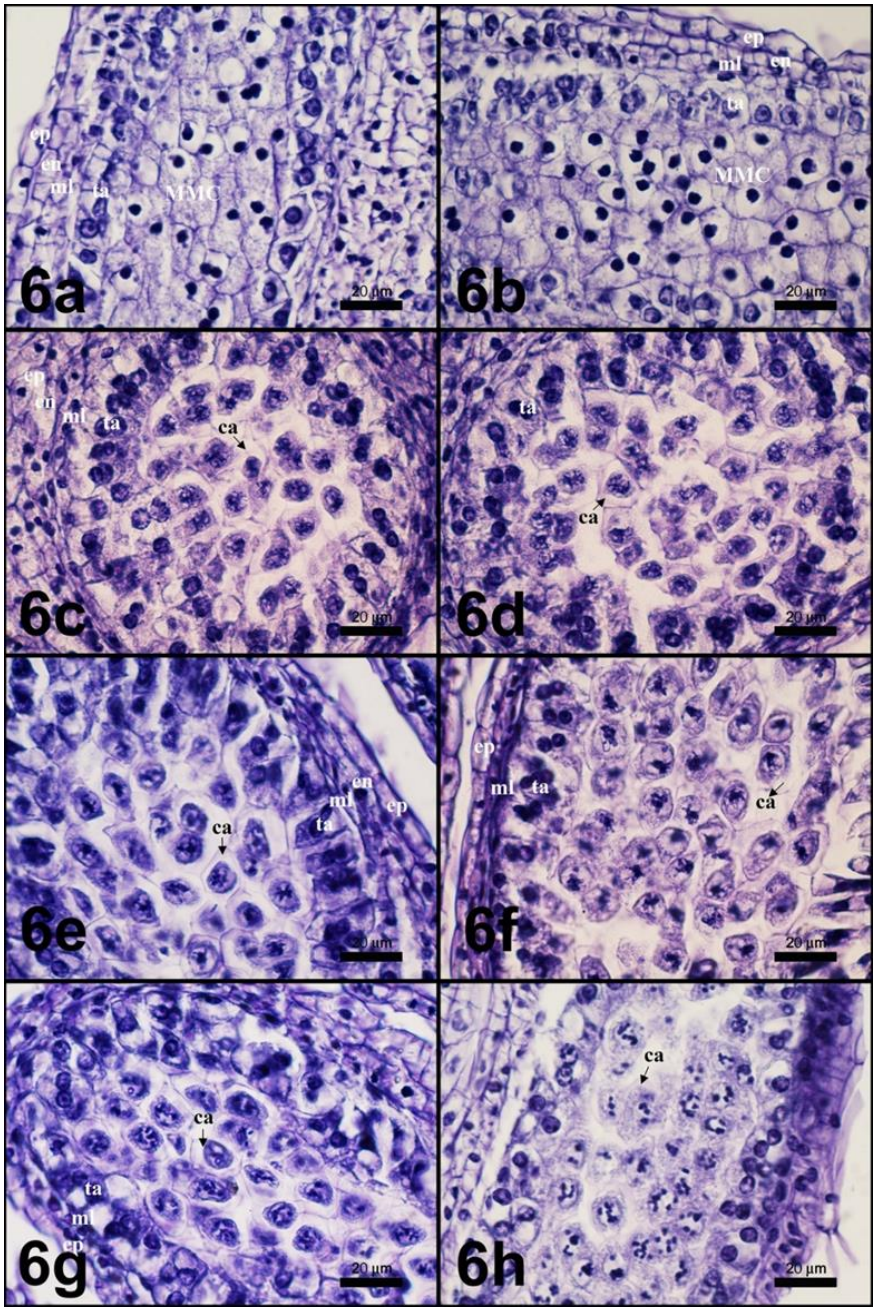
6a
ep
en
ml
ta
MMC
20 µm
6b
ep
ml
en
ta
MMC
20 µm
6c
ep
en
ml
ta
ca
20 µm
6d
ta
ca
20 µm
6e
en
ml
ep
ta
ca
20 µm
6f
ep
ml
ta
ca
20 µm
6g
ca
ta
ml
ep
20 µm
6h
ca
20 µm

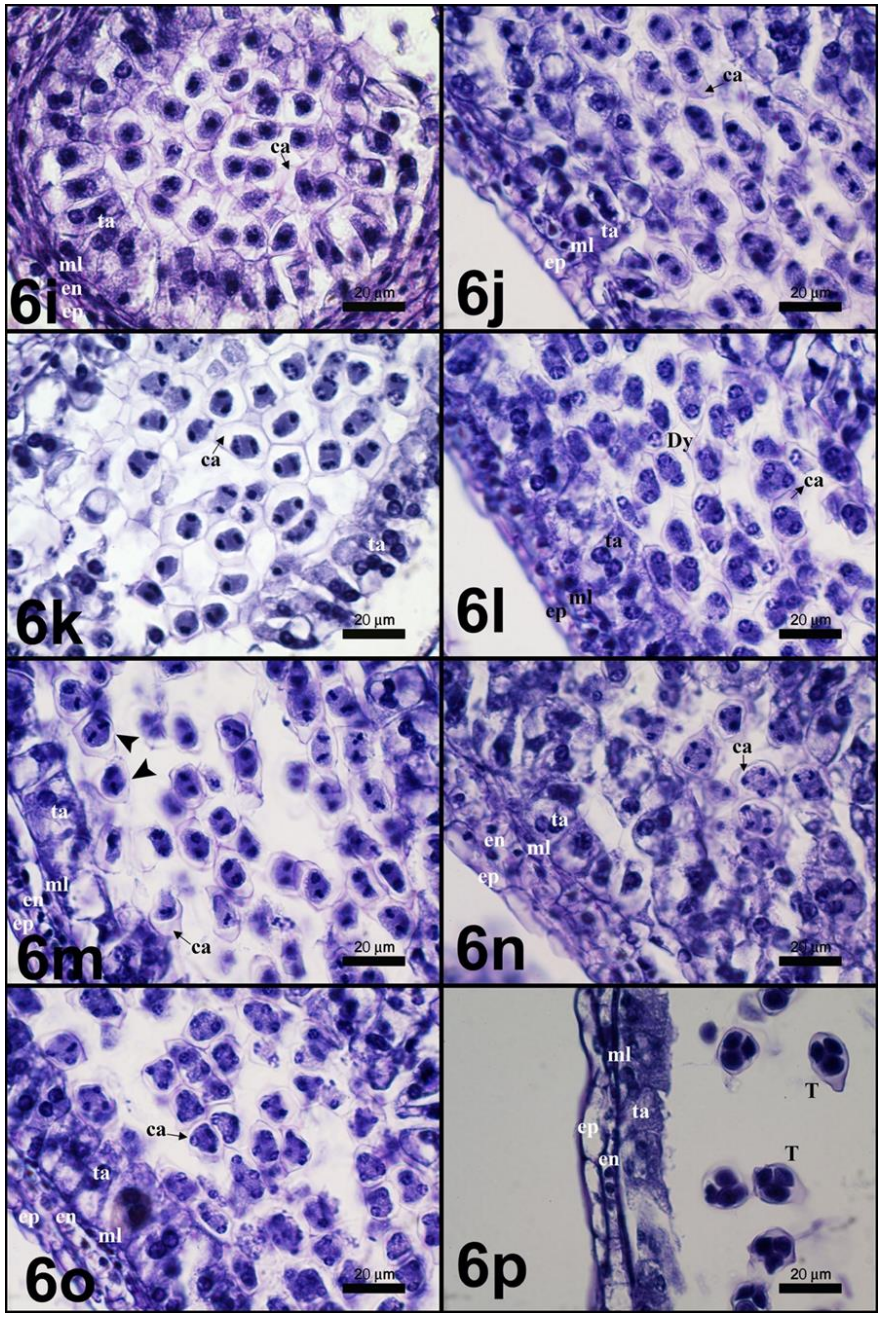

Fig. 6. Simultaneous type of meiosis in the microspore mother cells of *M. incana*. 6a. Interphase; 6b. Early prophase; 6c. Leptotene; 6d. Zygotene; 6e. Pachytene; 6f. Bouquet phase; 6g. Diplotene; 6h. Diakinesis; 6i. Metaphase I; 6j. Anaphase I; 6k. Telophase I; 61. Dyad; 6m. Metaphase II (arrow heads); 6n. Anaphase II; 6o. Telophase II; 6p. Tetrad phase (ca, callose wall; Dy, dyad; en, endothecium; ep, epidermis; ml, middle layer; MMC, microspore mother cell; T, tetrad; ta, tapetum)

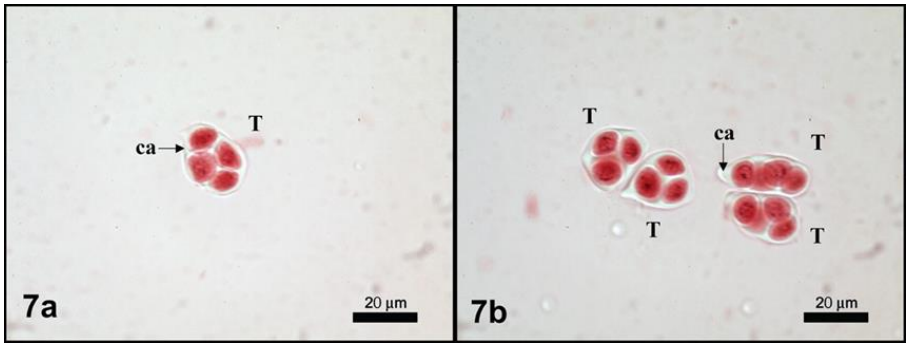

Fig. 7 Tetrad types of *M. incana*. 7a. Rhomboidal; 7b. Decussate, tetrahedral and rhomboidal (ca, callose wall; T, tetrad)

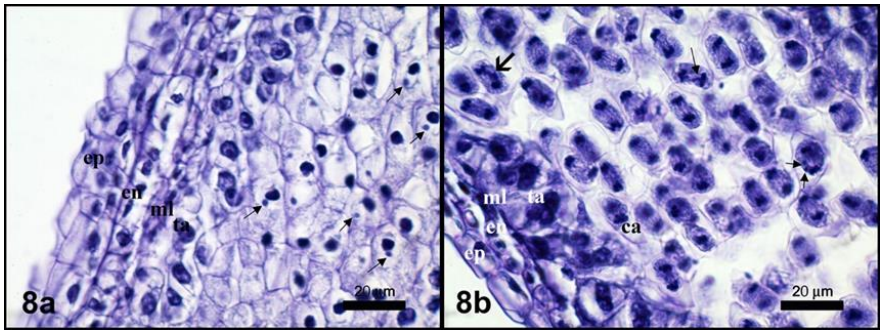

Fig. 8 Abnormalities during microsporogenesis in *M. incana*. 8a. Micronuclei (arrows) in the early prophase I; 8b. Lagging chromosomes (thin arrows) and chromosome bridge (thick arrow) in Anaphase I (ca, callose wall; en, endothecium; ep, epidermis; ml, middle layer; ta, tapetum)

F. Pollen Viability

Pollen viability was examined by using light microscopy method in *Matthiola incana*. Pollens were generally stained well. Pollen grains were stained with aniline blue prepared in lactophenol (Fig. 10a) and aceto-carmin prepared in glycerin (Fig. 10b). Stained pollens were considered as fertile, and unstained ones were considered as sterile. 18044 pollen grains were counted. The pollen sterility rate was found to be 0.2%.

IV. DISCUSSION

In this study, male gametophyte of *Matthiola incana* were examined cytologically and embryologically. The structure and histochemical properties of the anther walls at different developmental stages were investigated. RNA and polysaccharide contents of pollen grains and anther

walls at some different developmental stages were investigated. Sterility rate of pollen grains has been revealed. The data obtained were supported by photographs taken under a photomicroscope.

Various studies have been carried out on *M. incana*, but no cytological or embryological study has been found in Turkey. Since cytological and embryological studies with *M. incana* are limited, our findings on microsporogenesis and microgametogenesis were compared with different species of the genus *Matthiola* and different genera from the Brassicaceae family.

Androecium consists of 4-6 stamens in *M. incana*. Anthers are whitish yellow in color and bazifiks. Mature anther size is usually 4.5 mm and rarely 6 mm. The filaments are green and shorter than the anthers. These features are similar to those previously detected in the Brassicaceae family. Species in Brassicaceae family has mostly six anthers [1].

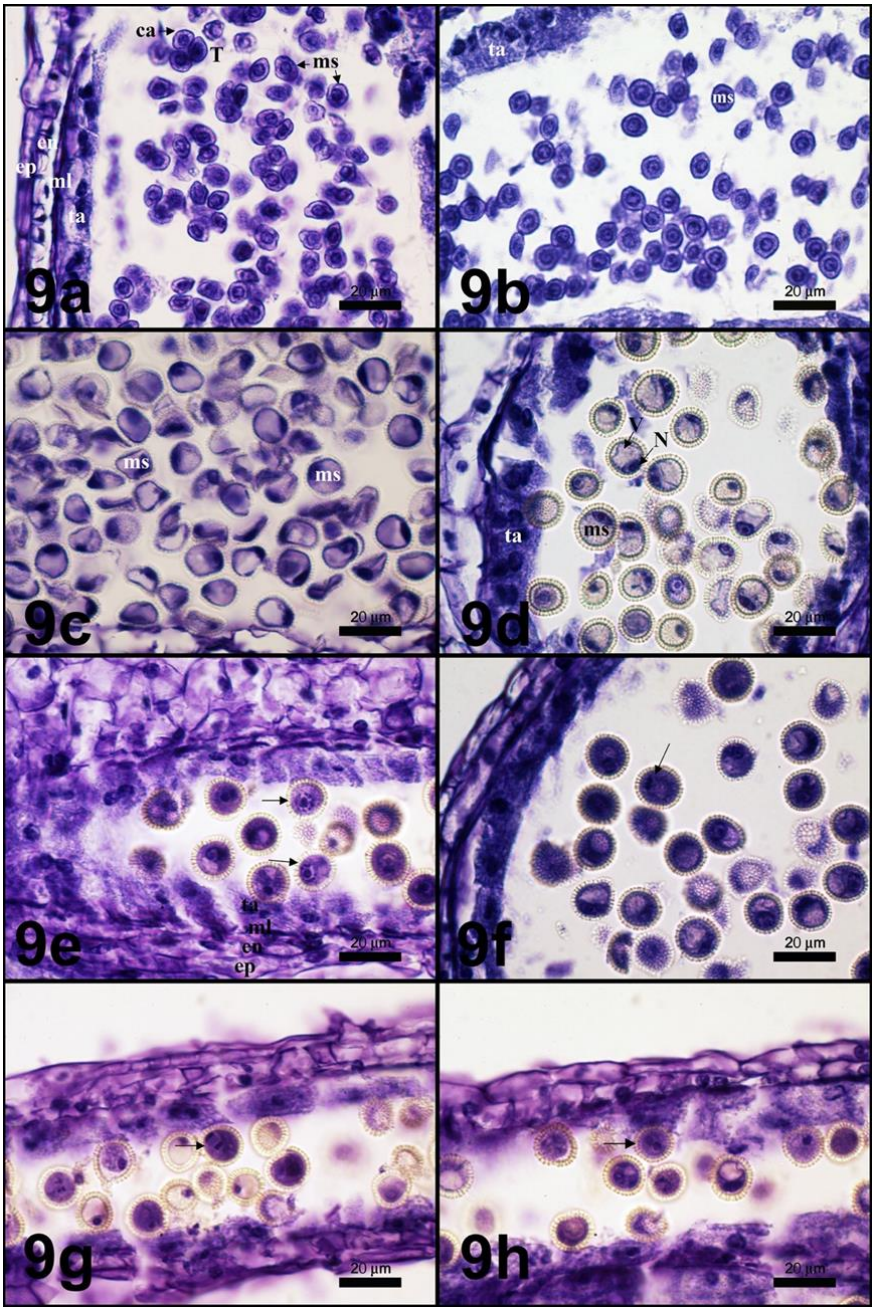
ca
T
ms
ep
ml
ta
9a
20 µm
ta
ms
9b
20 µm
ms
ms
9c
20 µm
V
N
ta
ms
9d
20 µm
ta
ml
en
ep
9e
20 µm
9f
20 µm
9g
20 µm
9h
20 µm

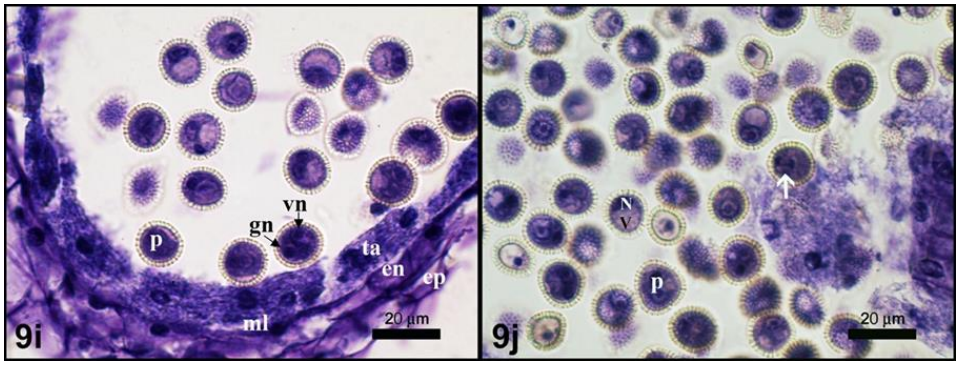

Fig. 9 Microgametogenesis in *M. incana*. 9a-b, Post-tetrad phase; 9c, Wrinkled microspore phase; 9d, Vacuolated microspore phase; 9e, Prophase; 9f, Metaphase; 9g, Anaphase; 9h, Telophase; 9i, binucleated mature pollen phase 9j. Chromosome bridge (arrow) in anaphase of microgametogenesis in *M. incana* (en, endothecium; ep, epidermis; gn, generative nucleus; ml, middle layer; N, nucleus; ms, microspore; p, pollen; ta, tapetum; V, vacuole; vn, vegetative nucleus)

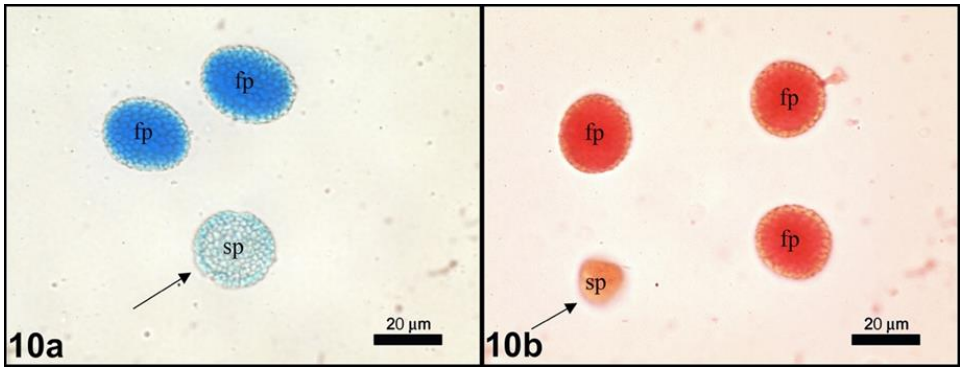

Fig. 10 Pollen viability in *M. incana*. Fertile and sterile (arrows) pollens 10a. Pollens stained with aniline blue 10b. Pollens stained with aceto-carmin (fp; fertile pollen, sp; sterile pollen)

The mature anthers open by the longitudinal dehiscence of each theca. In *M. incana*, anthers are tetrasporangiate. In early stages, the anther wall usually consists of 3-4 cell lines. The young anther wall from outside to inside is composed of epidermis, a single layered endothecium, 1-2 cell lines of middle layer and 1-2 lines of tapetum. In *Lepidium campestre* and *Lepidium ruderale* species from the Brassicaceae family, the anthers are tetrasporangiate, and anther walls are composed of single cell lined epidermis, endothecium, middle layer and secretory tapetum. Anther walls develop in monocotyledonous type [37]. Other Brassicaceae species such as *Biscutella laevigata* L. [38], *Iberis saxatilis* subsp.

saxatilis [39], *Brassica jordanoffii* [40], *Cardamine matthioli*, *Cardamine rivularis* and a triploid hybrid *Cardamine* × *rhodopaea* [41] have tetrasporangiate anthers.

In anther wall of *M. incana*, epidermis cells are larger than other cells. At the outermost part of the mature anther wall, there was a line of flat and swollen epidermis cells. These were not degenerated until the end of the development. Epidermis cells are also remaining intact until the end of pollen development in species such as *L. campestre*, *L. ruderale* [37], *I. saxatilis* [39] and *B. jordanoffii* [40].

In the mature anther wall of *M. incana*, endothecium is well developed under the epidermis. Fibrous thickenings are observed in the endothecium. Fibrous thickenings were also observed in *L. campestre*, *L. ruderale* [37] and *I. saxatilis* [39] from the Brassicaceae family. The fibrous thickenings in the endothecium of *C. x rhodopaea* are less than the thickenings of the endothecium in *C. matthioli* and *C. rivularis* [41].

In *M. incana*, the middle layer consists of 1-2 lines of flattened cells as in *L. campestre*, *L. ruderale* and *I. saxatilis* species. In *C.* × *rhodopaea*, the anther wall usually contains a single cell lined middle layer, while in *C. rivularis* and *C. matthioli*, the formation of 2-cell lined middle layer was observed more frequently. Among these *Cardamine* species, the middle layer is the most transient in *C.* × *rhodopaea* and degenerates by the onset of meiosis II in MAH, and degeneration occurs later in the other two diploid species. In *B. jordanoffii* and *Lepidium vesicarium*, the middle layer is also transient. In *I. saxatilis*, the middle layer remains until the end of microsporogenesis. The middle layer was partially preserved in *L. campestre* and *L. ruderale* [37], [39], [40]- [42]. In *M. incana*, it was seen that the middle layer has been remained until the end of the cell divisions.

In *M. incana*, tapetum is consisted of 1-2 cell lines and of secretory type. Secretory tapetum is also seen in different species from the Brassicaceae family [37], [40]-[42]. In *I. saxatilis*, the tapetum is the secretory type at the beginning of development, but after two-celled pollen formation it transforms into the ameboid pseudo-periplasmodium type. It has almost completely degenerated after differentiation [39]. The tapetum cells of *M. incana* are usually binucleated, but mononucleated cells have also been seen. In *I. saxatalis*, tapetum cells are initially large cells with a single nucleus, and after mitotic divisions they become two or four nuclei [39]. In *B. jordanoffii*, tapetum cells are initially single-nucleated, they become binucleated as a result of mitotic divisions [40]. While the tapetums of *C. matthioli*, *C. rivularis* and *C.* × *rhodopaea* species initially consist of single-nucleated cells, they became two or rarely four nuclei as a result

of mitotic divisions [41]. Tapetum cells were started to degenerate in the tetrad stage of microsporogenesis in *M. incana*. However, in the early stages of microgametogenesis, undegenerated tapetum cells were also detected in some anthers. Remnants of tapetum were observed in the mature pollen stages of *L. campestre* and *L. ruderale* species, their tapetums have degenerated [37]. The tapetums of *C. matthioli*, *C. rivularis* and *C. × rhodopaea* remained to the end of the divisions [41].

In this study, polysaccharide and RNA content of anther wall cells in some developmental stages of *M. incana* were also investigated. In the early developmental stages of the anther wall, the PAS-positive reaction was generally detected in the cell walls, especially in tapetum cells. No PAS-positive reaction was observed in the cytoplasm of the anther wall cells.

Tetrads are also stained in dark color by showing PAS-positive reaction due to the presence of a callose wall. According to [43], insoluble polysaccharides were concentrated in the callose wall of tetrads and in primexin, intin, amyloplasts, and cytoplasmic vesicles in the developing pollen grain. Total polysaccharide content can be reduced by using them in activities such as ATP production, basic metabolic activities, synthesis of other non-PAS-positive molecules and production of soluble sugars by hydrolysis [44]. The polysaccharide content decreased as tapetum cells began to degenerate in the wrinkled microspore stage of *M. incana*. Other anther wall layers are enriched in polysaccharide. In mononuclear microspore stage, the accumulation of polysaccharide particles was observed in endothecium and epidermis. Polysaccharide content is generally concentrated in the endothecium due to the totally degeneration of the tapetum cells in the mature pollen stage. The polysaccharide content, which is concentrated in the late stages, shows that it can be used in the wall differentiation of endothecium cells. The total polysaccharide contents from early microspore stage to mature pollen stage were investigated by Pacini and Viegi [44] using PAS-positive reaction in *Borago officinalis* and *Lycopersicum peruvianum* species. In *B. officinalis* from the Boraginaceae family, the polysaccharide content was increased in the late microspore stage and meiosis II. In *L. peruvianum* from the Solanaceae family, an increase in polysaccharide content was seen only during the late microspore stage. In both species, the total polysaccharide content was significantly reduced in the final stage of pollen development. It was considered that this decrease is caused by the hydrolysis of starch and the transfer of polysaccharide storages of pollen to the cytoplasm [44]. The total polysaccharide content was not analyzed in our plant material, but when we consider the PAS-positive reaction, the stages in which

polysaccharides increase are similar to the stages examined in *B. officinalis* and *L. peruvianum*.

In the early stage of microgametogenesis in *M. incana*, the anther wall is rich in RNA content. The RNA content in the tapetum cells was decreased in wrinkled microspore phase. That was due to increase in degeneration of their cytoplasm. On the other hand, microspores are rich in RNA content as they are prepared for pollen mitosis. In the mononuclear microspore stage, the middle layer has the richest RNA content. It is seen that the RNA content of the anther wall decreases in the mature pollen stage.

Microsporogenesis is generally regular in MMCs of *M. incana*. During meiosis in MMCs, simultaneous type cytokinesis has been seen as in many dicots. Meiosis was not followed by wall formation. The callose formed a tetrad starting from the periphery and moving towards the center. Simultaneous cytokinesis has also occurred in *L. campestre, L. ruderale* [37], *B. laevigata* [38], *C. matthioli*, *C. rivularis* and *C. × rhodopaea* [41], *Cardaminopsis arenosa* (L.) Hayek [45] and *B. jordanoffii* [40] from the Brassicaceae family.

Development of callose wall progresses in the leptotene and its formation is completed in the zygotene. Then it is disappeared towards the end of the tetrad phase of *M. incana*. According to our findings in *M. incana*, asynchrony was frequently observed in both metaphase I and metaphase II. Asynchronization was seen both at different loci within an anther and as multiple phases in the same anther locus. In some anther loci, metaphase I, anaphase I and telophase I were seen together. The most common phases in asynchronization are metaphase-anaphase, anaphase-telophase and dyad-tetrad phases. At the same time, asynchrony was detected in between different anthers of the same bud. While dyad phase is seen in an anther; tetrad phase can be seen in another anther. Asynchrony in nucleus was investigated in the genus *Fibigia* from the Brassicaceae family, and asynchrony was found in most metaphase II populations [46]. In addition, asynchrony was also observed in the anther loci of the triploid population in *I. saxatilis subsp. saxatalis* [39]. Against to these examples, in *L. vesicarium* microspore formation was occurred synchronously and asynchrony was not mentioned [42]. Asynchronization within the same anther locus may result from the gradually delivery of nutrients.

Microsporogenesis was generally regular in *M. incana*, but some chromosomal abnormalities were also observed. In some cells, micronuclei were observed in prophase, and lagging chromosomes and chromosome bridges were also seen in anaphase I. These findings are compatible with the data obtained by Irani and Arab in 2017 for this species. In addition, in many previous studies in the Brassicaceae family, a wide variety of meiotic abnormalities such as

fragmented chromosomes, chromosome bridges, chromosomal nondisjunction, lagging chromosome, asynchronous nuclei, trisomy, and cytomixis were detected in MMCs [33]. Abnormalities such as micronuclei in dyads and triads degenerated microspores in tetrads and rarely empty anthers were observed in *Boechera stricta* [47]. Meiotic division is an important process in eukaryotic life span because it is essential for genetic rearrangement containing the correct haploid set of chromosomes and gamete production. Therefore, its proper execution has great importance for intraspecies continuity, evolution and health of the species, and so it needs to happen fairly regular [48]. Both dyad and tetrad formation were seen in the tetrad phase of *M. incana*. Similar tetrad formation was also seen in *L. campestre*, *L. ruderale* [37], *B. laeviagata* [38], *C. arenosa* [45], *B. stricta* [47] and *B. jordanoffii* [40]. Tetrad formation was generally seen in diploid populations of *I. saxatilis* subsp. *Saxatalis*. Monad, dyad, triad and rarely polyad formation were also seen in triploid populations of the same species [39].

In *M. incana*, tetrads were generally seen as rhomboidal, decussate and tetrahedral. Tetrads in *L. campestre*, *L. ruderale* [37], *B. stricta* [47] and *B. jordanoffii* [40] from Brassicaceae family are tetrahedral. Tedrads of *L. vesicarium* is isobilateral [42]. Tetrads in *B. laeviagata* are mostly linear and T-shaped tetrads have also been seen [38]. In *I. saxatilis* subsp. *saxatalis*, tetrads are usually tetrahedral and isobilateral ones were also seen. Tetrahedral, T-shaped and linear tetrads were also found in the anthers of triploid populations of this species [39]. In diploid *Cardamine* species, tetrads are frequently seen as tetrahedral and rarely isobilateral and T-shaped, while different types of tetrads were seen in the triploid *Cardamine* × *rhodopaea* hybrid. The different tetrad development in triploid species is due to abnormalities in their MMCs and during abnormal phases of meiosis in microsporogenesis [41].

In the tetrad phase of *M. incana*, as the callose begins to break down, separated microspores are released. Microspores newly released from tetrads have an initially irregular shape, as *in L. vesicarium*, with a dense cytoplasm and central nucleus [42]. At this phase, the exine has not yet developed around the microspores. Afterwards, exine formation begins in the cell walls of microspores. The cell walls of microspores have wrinkled shape. As a large vacuole develops on one side of the cell, the nucleus located initially in the central, moves to the other side of the cell. A rather large vacuole was formed in the remaining part of the cell. The microspores separated from the tetrad are swollen by absorbing the liquid in the locus. And at this phase microspores are located close to the tapetum cells. The degeneration of tapetum cells begins at this phase and the tapetum content is transferred to the anther locus. After tapetum degeneration, volume of microspores is increased. An evident polarity in the microspores is seen in pollen mitosis of *M. incana*. At the end of pollen mitosis, it

was detected that the nucleus close to the cell wall formed the generative cell and the other nucleus formed the vegetative cell.

Microgametogenesis in *M. incana* is generally regular, as in previous developmental stages. But chromosome bridges were detected in the anaphase in some microspores. Mature pollen grains of *M. incana* were 2-celled during anther dehiscence like in other members of Brassicaceae such as *L. campestre* in *L. ruderale* [37] and *I. saxatilis* subsp. saxatilis [39]. However, mature pollen grains in *B. laevigata* [38], *B. jordanoffii* [40] and *L. vesicarium* [42] were 3-celled. On the other hand, pollen grains of *Matthiola longipetala* subsp. *bicornis* were monads [19]. *M. incana* pollen grains are also determined as monads. The mature pollen grains of *M. incana* are tricolpate like all other *Matthiola* species. In *M. incana*, the exine sculpture was reticulate and the pollen shape was spheroidal. Pollen morphologies have been characterized earlier in different species of *Matthiola*. The exine ornamentation of *Matthiola longipetala* subsp. *Bicornis* was recorded as reticulate and pollen shape as prolate-spheroidal [19]. Pollen shape of *Matthiola sinuata* (L.) R. Br. is spheroidal and its exine ornamentation is reticulate [49]. The shape of pollen grains is prolate and exine is roughly reticulate in *Matthiola anchoniifolia* Hub.-Mor. Pollen morphology of *Matthiola anchoniifolia* Hub. -Mor. was investigated and compared with other *Matthiola* species by Tekin et al. [50]. Pollen shape is prolate in *M. arabica* Boiss, *M. fruticulosa* (L.) Maire, *M. longipetale* (Vent.) DC subsp. *longipetale* species and subprolate in *M. parviflora* (Schousb.) R. Br. The exine is roughly reticulate in all compared *Matthiola* species in this study. It was determined from this study that the pollen shapes of different species in the genus *Matthiola* were generally similar and the exine surface is generally reticulate [50].

In this study, pollen viability of *M. incana* was determined as 99.8%. In another study, various *M. incana* cultivars were tested and pollen viability averages were found between 82.1% and 98.9% [33]. The fertility rate of *M. incana* was determined quite high. Anthers taken from the genus *Fibigia* belonging to the Brassicaceae family were analyzed in terms of pollen productivity, and pollen viability rates were found to be between 77.29 and 99.70% in the populations compared by Ranjbar et al. [46]. Pollen viability of *Lepidium sativum* L. and *Thlaspi arvense* L. species, which are also from the Brassicaceae family, was investigated and it was determined as 93% - 100% in two cultivars of *L. sativum* and 100% in *T. arvense*, respectively [51]. Pollen viability percentages in two different cultivars of *B. laevigata* were found to be 98% and 87%, respectively [38].

The effect of heavy metals on pollen germination was investigated by Kwiatkowska and Izmailow [45]. While the pollen viability was determined as 98% in *Cardaminopsis arenosa* (L). Hayek from the Brassicaceae family growing in an area without heavy metal pollution. On other side the pollen

viability was recorded as 95% (Boleslow) and 92.5% (Bukowno) in plants grown in two different areas with heavy metal pollution. In *C. arenosa*, it has been determined that male lines are more resistant than female lines and pollen viability was determined at a very high frequency [45]. The findings obtained from pollen viability studies with different species from the Brassicaceae family are similar to the pollen viability findings we obtained in *M. incana*.

A low percentage of sterile pollen grains, few meiotic irregularities and a normal tapetum development were observed in our study material *M. incana*. Few meiotic irregularities were detected in this study. These irregularities can also affect the sterility rate. High pollen viability rates recorded in the Brassicaceae family, especially in the genus *Matthiola*, indicate that many species are resistant to environmental factors, and this is an important feature for plant breeding studies. As a result, in this study, some cytological and embryological features of the male gametophyte development in *M. incana* were tried to be explained. The data obtained from this study will contribute to both the revealing of the reproductive biology of *M. incana* and researches on the taxonomic characteristics of this species.

ACKNOWLEDGEMENT

This study is a part of Nazlıcan Çolak's master thesis.

REFERENCES

I. A. Al-Shehbaz, "A generic and tribal synopsis of the Brassicaceae (Cruciferae)," *Taxon,* vol. 61(5), pp. 931-954, 2012.

M. A. Koch, C. Dobeš, C. Kiefer, R. Schmickl, L. Klimeš and M. A. Lysak, "Supernetwork identifies multiple events of plastid trn F (GAA) pseudogene evolution in the Brassicaceae," *Mol Biol Evol*., vol. 24(1), pp. 63-73, 2006.

I. A. Al-Shehbaz, M. A. Beilstein and E. A. Kellogg, "Systematics and phylogeny of the Brassicaceae (Cruciferae): An overview," *Pl. Syst. Evol*., vol. 259, pp. 89–120, 2006.

Y. H. Heywood, *Flowering Plants of the World*, New York, USA: Oxford Univ. Press, 1993.

E. Martin, M. Ünal, B. Doğan, F. Altınordu, A. Sefalı and A. Kaya, "Karyotype analyses of the genus *Matthiola* (Brassicaceae) in Turkey*" Cytologia*, vol. 81(1), pp. 53-60, 2016.

M. Ranjbar and S. Karami, "Meiotic chromosome number and behavior of *Matthiola shehbazii* sp. nov. (Brassicaceae, Anchonieae) from central Iran," *Nord. J. Bot*., vol. 32(6), pp. 713-716, 2013.

(2020) Bizim Bitkiler® Version 3.1. Published on the Internet [Online]. Available: http://www.bizimbitkiler.org.tr/v3/demo/details.php?id=4173

J. C. Hall, K. K. Sytsma and H. H. Iltis, "Phylogeny of Capparaceae and Brassicaceae based on chloroplast sequence data," *Am. J. Bot*., vol. 89(11), pp. 1826–1842, 2002.

J. Su, W. Wang, L. Zhang and Z. Chen, "Phylogenetic placement of two enigmatic genera, *Borthwickia* and *Stixis*, based on molecular and pollen data, and the description of a new family of *Brassicales*, *Borthwickiaceae*," *Taxon*, vol. 61(3), pp. 601–611, 2012.

P. P. Edger, M. Tang, K. A. Bird, D. R. Mayfield, G. Conant, K. Mummenhoff, M. A. Koch and J. C. Pires, "Secondary structure analyses of the nuclear rRNA internal transcribed spacers and assessment of its phylogenetic utility across the Brassicaceae (Mustards)," *PLoS One*, vol. 9(7), pp. e101341, 2014.

J. Cullen, *Matthiola* W.T. Aiton, *Flora of Turkey and the East Aegean IsIands*, P. H. Davis, Ed.. Edinburgh, Scotland : Edinburgh Univ. Press, 1965.

T. Dirmenci, F. Satıl and G. Tümen, "A new species of *Matthiola* R.Br. (Brassicaceae) from Turkey," *Bot. J. Linn. Soc.*, vol. 151, pp. 431-435, 2006.

A. Güner, S. Aslan, T. Ekim, M. Vural and M. T. Babaç, Eds., *Türkiye Bitkileri Listesi (Damarlı Bitkiler)*. İstanbul, Türkiye: Nezahat Gökyiğit Botanik Bahçesi ve Flora Araştırmaları Derneği Yayını. 2012.

E. Martin, G. Yılmaz and M. Tekin, "Karyology of endemic *Matthiola anchoniifolia* Hub.-Mor. (Brassicaceae) in Turkey," *Caryologia*, vol. 66, pp. 293–295, 2013.

I. M. Allen, "The cytology of *Matthiola incana* with reference to the genetics of certain cultivated varieties," *New Phytol.*, vol. 23(2), pp. 103-112, 1924.

S. M. Ghaffari, "New or rare chromosome counts of some angio- sperm species from Iran," *Iran Journ. Bot*., vol. 11, pp. 185-192, 2006.

S. F. Irani, M. Arab, M. Norouzi and M. Lotfi, "Genetic diversity of stock (*Matthiola incana* L.) cultivars based on cytogenetic characteristics," *Asian J. Adv. Basic Sci.* vol. 4(2), pp. 65-73, 2016.

K. A. Khalik, R. G. Van Den Berg, L. J. G. Van Der Maesen and M.N. El Hadidi, "Pollen morphology of some tribes of Brassicaceae from Egypt and its systematic implications," *Feddes Repert*, vol. 113, pp. 211–223, 2002.

B. Çıtak, H. Dural and B. Gönen, "Selçuk Üniversitesi Alâeddin Keykubat Kampüsü'nde yayılış gösteren bazı bitkilerin polen morfolojileri," *Selçuk Üniv. Fen Fak. Der.,* vol. 42(1), pp. 42-56, 2016.

F. G. Çelikel and M . S. Reid, "Postharvest handling of stock (*Matthiola incana*)," *Hort. Sci*., vol. 37(1), pp. 144-147, 2002.

W. Heller, L. Britsch, G. Forkmann and H. Grisebach, "Leucoanthocyanidins as intermediates in anthocyanidin biosynthesis in flowers of *Matthiola incana* R. Br.," P*lanta*, vol. 163(2), pp. 191-196, 1985.

W. Heller, G. Forkmann, L. Britsch and H. Grisebach, "Enzymatic reduction of (+)-dihydroflavonols to flavan-3, 4-cis-diols with flower extracts from *Matthiola incana* and its role in anthocyanin biosynthesis," *Planta,* vol. 165(2), pp. 284-287, 1985.

N. Saito, F. Tatsuzawa, A. Nishiyama, M. Yokoi, A. Shigihara and T. Honda, "Acylated cyanidin 3-sambubioside-5-glucosides in *Matthiola incana*," *Phytochemistry*, vol. 38(4), pp. 1027-1032, 1995.

R. Ecker, A. Barzilay and E. Osherenko, "Linkage relationships of genes for leaf morphology and double flowering in *Matthiola incana*," *Euphytica*, vol. 74(1-2), pp. 133-136, 1993.

B. Epping, M. Kittel, B. Ruhnau and V. Hemleben, "Isolation and sequence analysis of a chalcone synthase cDNA of *Matthiola incana* R. Br. (Brassicaceae)," *Plant Mol. Biol.*, vol 14(6), pp. 1061-1063, 1990.

V. Hemleben, A. Dressel, B. Epping, R. Lukačin, S. Martens and M. Austin, "Characterization and structural features of a chalcone synthase mutation

in a white-flowering line of *Matthiola incana* R. Br. (Brassicaceae)," *Plant Mol. Biol*., vol. 55(3), pp. 455-465, 2004.

B. L. Johnson, "Evidence for irregularity in crossing over of the S locus in the ever-sporting type of *Matthiola incana* (L.) R. Br.," *Genetics*, vol. 38(3), pp. 229-243, 1953.

R. Spribille and G. Forkmann, "Genetic control of chalcone synthase activity in flowers of *Matthiola incana* R. Br.," *Z. Naturforsch C.* vol. 36(7-8), pp. 619-624, 1981.

A. Ahmadi Hesar, B. Kaviani, D. Hashemabadi, A. R. Tarang, S. Bohlooli Zanjani and M. H. Ansari, "*Matthiola incana* micropropagation using shoot tips and callus induction derived from lamina explants and rooting capacity from callus," *J. O. P*., vol. 1(3), pp. 129-136, 2011.

B. Kaviani, "Micropropagation of ten weeks (*Matthiola incana*) and lisianthus (*Eustoma grandiflorum*) (two ornamental plants) by using kinetin (KIN), naphthalene acetic acid (NAA) and 2,4-dichlorophenoxyacetic acid (2,4-D)," *Acta Sci. Pol. Hortorum Cultus*, vol. 13(1), pp. 141-154, 2014.

B. Kaviani, A. A. Hesar and A. Kharabian-Masouleh, "*In vitro* propagation of *Matthiola incana* (Brassicaceae)-an ornamental plant," *Plant Omics J*., vol. 4(7), pp. 435-440, 2011.

R. Snow, "Germination tests with pollen of stocks," J. Genet., vol. 15(2), pp. 237-243, 1925.

S. F. Irani and M. Arab, "Meiotic behaviour and morpho-phenological variation in cut stock (*Matthiola incana* L.) flower," *Folia Hortic*., vol. 29(1), pp. 51-61, 2017.

M. Gabe, "Détection histochimique des glucides. Techniques histologiques," *Paris; Mason et Cie*, pp. 409-411, 1968.

H. İnce, "Bitki preperasyon teknikleri," *Ege Üniv Fen Fak Yay*., vol. 127, pp. 73-76, 1989.

W. A. Jensen, *Botanical Histochemistry*, San Francisco, USA: W. H. Freeman and Company, 1962.

E. Yankova-Tsvetkova, I. B. Semerdjieva, R. Nikolova and V. D. Zheljazkov, "On the embryology of two species of genus *Lepidium* (Brassicaceae)," *HortScience*, vol. 53(4), pp. 582-588, 2018.

M. Kwiatkowska, K. Kłosowska and E. U. Kurczyńska, "Germline development and seed set of metallophyte *Biscutella laevigata* L. (Brassicaceae)," Flora, vol. 274, pp. 151752, 2021.

P. Yurukova-Grancharova, M. Anchev and V. Goranova, "Embryological study on diploid and triploid populations of *Iberis saxatilis* subsp. *saxatilis*

(Brassicaceae) in the Bulgarian flora," *Phytol. Balc*., vol. 10(1), pp. 69–78, 2004.

E. Yankova-Tsvetkova, P. Yurukova-Grancharova and V. Vladimirov, "On the embryology of *Brassica jordanoffii* (*Brassicaceae*) – an endemic species in the Bulgarian flora," *Phytol. Balc*., vol. 22(2), pp. 149-153, 2016.

M. Ančev, P. Yurukova-Grancharova, P. Ignatova, V. Goranova and S. Stoyanov, "*Cardamine* × *rhodopaea* (Brassicaceae), a triploid hybrid from the West Rhodope Mts: Morphology, distribution, relationships and origin," *Phytol. Balcan.*, vol. 19, pp. 323-338, 2013.

A. Chehregani and M. Sedaghat, "Pollen grain and ovule development in *Lepidium vesicarium* (Brassicaceae)," *Int. J. Agric. Biol*., vol. 11, pp. 601–605, 2009.

E. Pacini and B. J. Juniper, "The ultrastructure of pollen grain development in *Lycopersicum peruvianum*," *Caryologia,* vol. 37, pp. 21-25, 1984.

E. Pacini and L. Viegi, "Total polysaccharide content of developing pollen in two angiosperm species," *Grana*, vol. 34, pp. 237-241, 1995.

M. Kwiatkowska and R. Izmailow, "Ovules, female gametophytes and embryos are more sensitive to heavy metal pollution than anthers and pollen of *Cardaminopsıs arenosa* (L.) Hayek (Brassicaceae), a member of Calamine flora," *Acta Biol. Crac. Ser. Bot.*, vol. 56(1), pp. 128–137, 2014.

M. Ranjbar, S. Karami and M. Rostami, "Cytogenetic study and meiotic behaviour on 13 populations of *Fibigia* (Brassicaceae) in Iran," *Webbia*, pp. 69(2) vol. 269-280, 2014.

. Rojek, M. Kapusta, M. Kozieradzka-Kiszkurno, D. Majcher, M. Górniak, E. Sliwinska, T. F. Sharbel and J. Bohdanowicz, "Establishing the cell biology of apomictic reproduction in diploid *Boechera stricta* (Brassicaceae)," *Ann. Bot.,* vol. 122, pp. 513-539, 2018.

M. Barchi, P. Cohen and S. Keeney, "Special issue on "recent advances in meiotic chromosome structure, recombination and segregation"," *Chromosoma*, vol. 125, pp. 173-175, 2016.

E. Olgaç, "*Matthiola Sinuata* (L.) R. Br. üzerinde morfolojik, palinolojik ve karyolojik araştırmalar," Master's thesis, Marmara Üniversitesi, Fen Bilimleri Enstitüsü, İstanbul, Türkiye, 2014.

M. Tekin, G. Yılmaz and E. Martin, "Morphological, anatomical and palynological studies on endemic *Matthiola anchoniifolia* Hub. -Mor. (Brassicaceae)," Not. Sci. Biol., vol. 5(2), pp. 163-168, 2013.

H. Gupta, R. Kumar, R. C. Gupta and V. K. Singhal, "New chromosome counts and evolutionary tendencies in some dicots analyzed from Parvati Valley, Kullu district, Himachal Pradesh," *Caryologia*, vol. 71(3), pp. 1-25, 2018.

Chapter 10

Some Properties of Face Vertex Incidence Matrix of a Graph[1]

Hasibe Sevgi MORALI[2], Mehmet SEZER[3]

[1] Dr. Öğr. Üyesi; Dokuz Eylül Üniversitesi Buca Eğitim Fakültesi.
sevgi.morali@deu.edu.tr , ORCİD No: 0000-0001-5603-9009
[2] Prof. Dr. Emekli Öğretim Üyesi
mehmetsezer54@gmail.com ORCİD No: 0000-0002-7744-2574

Abstract

Graphs are used to represent relationships and connections and used in many fields in both pure and applied mathematics Mathematicians and scientists are becoming increasingly aware of the significance of graph theory as it is applied to other areas of science and being widely used to solve various real-world problems.

Matrices are a commonly used and are valuable tools in graph theory, and they are used to represent and analyze graph properties and the structures they represent. A somewhat less known matrix is face-vertex incidence matrix. It is connected to areas as coloring, constructing codes. Here, we are going define, give some properties of face-vertex incidence matrix of some special graphs.

Keywords: Graph theory, graph matrices, face-vertex incidence matrix.

1. INTRODUCTION

Graph theory is a branch of mathematics that deals with geometric configurations known as graphs (Tatsuoka, 2014:291). Graphs are used to represent relationships and connections and used in many fields in both pure and applied mathematics as well as computer science. Graph theory is rapidly moving into the mainstream of mathematics mainly because of its applications in diverse fields Mathematicians and scientists are becoming increasingly aware of the significance of graph theory as it is applied to other areas of science and being widely used to solve various real-world problems. (Pirzada, 2007:20070013).

A graph G is an ordered pair (V (G),E(G)) consisting of a set V (G) of vertices and a set E(G), disjoint from V (G), of edges, together with an incidence function ψ_G that associates with each edge of G an unordered pair of (not necessarily distinct) vertices of G. If e is an edge and u and v are vertices such that $\psi_G(e) = \{u,v\}$, then e is said to join u and v, and the vertices u and v are called the ends of e (Bondy and Murty, 2008:2).

Matrices are a commonly used and are valuable tools in graph theory, and they are used to represent and analyze graph properties and the structures they represent. There are several graph matrices that are commonly used. The most commonly known and used matrices are the adjacency matrix and the incidence matrix. A somewhat less known matrix is face-vertex incidence matrix. It is connected to areas as coloring, constructing codes. Here, we are going define, give some properties of face-vertex incidence matrix of some special graphs.

2. SOME DEFINITIONS AND THEOREMS

Let G be a graph without loops, directions. We denote its vertex set by V(G) and the edge set by E(G).

2.1 Definition: A graph G is said to be connected if between any two vertices u, v $\in$V(G) there exists a u-v path.

2.2 Definition: A graph G is regular of degree r if for each vertex v of G, degree of v is r. We denote the degree of v by deg(v).

2.3 Definition: A graph G is called planer if it can be embedded in a plane. In other words G is planer if it can be drawn on a plane so that edges intersect only on the vertices (Harary, 2018:102).

2.4 Definition: (Oral, 1989:11) Let G be a connected, planer graph with vertex set V(G)={1,2,..,n}. We define a face vertex incidence matrix D=[d_{ij}] of G as the matrix with columns indexed by the vertices 1,2,…,n of G, rows indexed by the faces f_1, f_2,…,f_s of G with d defined by,

$$d_{ij} = \begin{cases} 1 & if \ \text{j is incident with } f_i \\ 0 & otherwise \end{cases}$$

2.5 Theorem: (Euler's formula) Let G be a connected, planer graph. |V(G)|=n, |E(G)|=e, |F(G)|=f⇒ n-e+f=2. (Clark and Holton, 1995:163)

2.6 Theorem: Let G be a planer graph and n≥3, then e<3n-6.

2.7 Theorem: Let G be a maximal planer graph with n≥3, then e=3n-6.

2.8 Theorem: Any planer graph G has a vertex of degree at most 5.

3. SOME THEOREMS ABOUT FACE VERTEX INCIDENCE MATRIX

Let G be a planer graph. We denote its face vertex incidence matrix by D.

3.1 Theorem: Let G be a 2-regular graph. The rank of D is 1.

Proof: Since G is two regular, it must be a cycle. A cycle has only two faces, one inner and one outher faces. Both of these faces share the same vertices and the same edges. So, the face vertex incidence matrix has exactly two, nonzero rows which are both the same. The rank of such a matrix must be 1.

3.2 Theorem: Let G be a 3-regular graph, then,

$$rank(D) = \begin{cases} \frac{n}{2} & \text{if and only if G i bipartite,} \\ \frac{n}{2}+1 & \text{if and only if G is not bipartite, and G has a set of nonadjacent faces that covers every vertex exactly once,} \\ \frac{n}{2}+2 & \text{otherwise.} \end{cases}$$

3.3 Theorem: Let G be 4-regular, planer graph such that each of its faces is adjacent to a fixed number, s, of edges. Then s=3.

Proof: From the Euler's fomula we know that n-e+f=2.

Suppose each face has s sides (edges). When we count the faces, we count the edges twice since every edge is in exactly two faces. So, sf=2e

We know that for any graph G,

$$\sum_{v \in V(G)} deg\, v = 2\, e$$

Since G is 4 regular, the sum of all degrees is 4n,

$$4n = 2e \Rightarrow n = \frac{e}{2},\ sf = 2e \Rightarrow f = \frac{2e}{s}$$

$$n\text{-}e+f = \frac{e}{2} - e + \frac{2e}{s} = 2 \Rightarrow e = \frac{4s}{4-s}.$$

4s is always greater than 0, so, 4-s must also be greater than 0.

$4\text{-}s > 0 \Rightarrow s < 4.$

Since any face must have at least 3 edges, s=3.

Result: The only 4 regular planer graph whose faces have fixed number of edges is octahedron.

Proof: Since there are exactly five regular polyhedra, and since octahedron is the only 4 regular one G must be octahedron.

4. SOME SPECIAL GRAPHS

Here we are going to examine the ranks of face vertex incidence matrices of special graphs. The rank of a graph matrix can be used to analyze various properties of a graph, such as its nullity and chromatic number Overall, the rank of a graph matrix is a useful tool in graph theory for analyzing and characterizing graphs, as well as determining their connectivity and other properties.

4.1 Definition: *Fan Graphs*

For n≥2, the Fan graph F_n is the complete bipartite graph $K_{1.n}$. It has n+1 vertices, n edges, and n faces. It is a nonregular, planer graph whose faces are triangles except the outer face. The face vertex incidence matrix of F_n has n rows and n+1 columns.

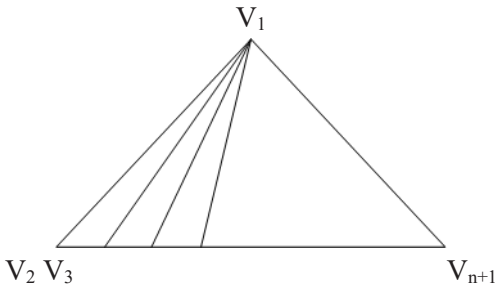

Figure 1: The Fan graph, Fn, with n+1 vertices.

4.2 Theorem: If D is a face vertex incidence matrix of F_n then, rank(D)=n (Moralı, 1999:6)

Proof: When we label the vertices of F_n as in Figure 1, and name the face incident to the vertices V_1, V_i, V_{i+1} by f_{i-1}, the face vertex incidence matrix of such a graph would look like.

$$D = \begin{bmatrix} 1 & 1 & 1 & 0 & 0 & \dots & 0 & 0 \\ 1 & 0 & 1 & 1 & 0 & \dots & 0 & 0 \\ 1 & 0 & 0 & 1 & 1 & \dots & 0 & 0 \\ 1 & 0 & 0 & 0 & 1 & \dots & 0 & 0 \\ \dots & \dots & \dots & \dots & \dots & \dots & \dots & \dots \\ 1 & 0 & 0 & 0 & 0 & \dots & 1 & 1 \\ 1 & 1 & 1 & 1 & 1 & \dots & 1 & 1 \end{bmatrix}$$

Let us call this nxn+1 matrix D, D_n. If we delete the i^{th} column and the $(i-1)^{th}$ row from each D_i for i=3, 4,…,n, we obtain D_{i-1}. So, each D_i contains D_{i-1} as a submatrix.

Now, let us denote the matrix that we obtain by deleting the first column of D_i by B_i. B_i is an nxn squared matrix. By using elementary row operations, we find the following determinants.

$$\left| B_3 \right| = \begin{vmatrix} 1 & 1 & 0 \\ 0 & 1 & 1 \\ 1 & 1 & 1 \end{vmatrix} = 1,$$

$$|B_4| = \begin{vmatrix} 1 & 1 & 0 & 0 \\ 0 & 1 & 1 & 0 \\ 0 & 0 & 1 & 1 \\ 1 & 1 & 1 & 1 \end{vmatrix} = \begin{vmatrix} 1 & 1 & 0 \\ 0 & 1 & 1 \\ 0 & 0 & 1 \end{vmatrix} - \begin{vmatrix} 1 & 1 & 0 \\ 0 & 1 & 1 \\ 1 & 1 & 1 \end{vmatrix} = 1 - |B_3| = 0,$$

$$|B_5| = \begin{vmatrix} 1 & 1 & 0 & 0 & 0 \\ 0 & 1 & 1 & 0 & 0 \\ 0 & 0 & 1 & 1 & 0 \\ 0 & 0 & 0 & 1 & 1 \\ 1 & 1 & 1 & 1 & 1 \end{vmatrix} = \begin{vmatrix} 1 & 1 & 0 & 0 \\ 0 & 1 & 1 & 0 \\ 0 & 0 & 1 & 1 \\ 0 & 0 & 0 & 1 \end{vmatrix} = \begin{vmatrix} 1 & 1 & 0 & 0 \\ 0 & 1 & 1 & 0 \\ 0 & 0 & 1 & 1 \\ 1 & 1 & 1 & 1 \end{vmatrix} = 1 - |B_4|,...,$$

$$|B_n| = \begin{vmatrix} 1 & 1 & 0 & \dots & 0 & 0 \\ 0 & 1 & 1 & \dots & 0 & 0 \\ 0 & 0 & 1 & \dots & 0 & 0 \\ \dots & \dots & \dots & \dots & \dots & \dots \\ 0 & 0 & 0 & \dots & 1 & 1 \\ 1 & 1 & 1 & \dots & 1 & 1 \end{vmatrix} =$$

$$\begin{vmatrix} 1 & 1 & 0 & \dots & 0 & 0 \\ 0 & 1 & 1 & \dots & 0 & 0 \\ \dots & \dots & \dots & \dots & \dots & \dots \\ 0 & 0 & 0 & \dots & 1 & 1 \\ 0 & 0 & 0 & \dots & 0 & 1 \end{vmatrix} + \begin{vmatrix} 1 & 1 & 0 & \dots & 0 & 0 \\ 0 & 1 & 1 & \dots & 0 & 0 \\ \dots & \dots & \dots & \dots & \dots & \dots \\ 0 & 0 & 0 & \dots & 1 & 1 \\ 1 & 1 & 1 & \dots & 1 & 1 \end{vmatrix} = 1 - |B_{n-1}|.$$

So, we get

$$|B_n| = \frac{(-1)^{n+1} + 1}{2}, n \geq 3.$$

Let us denote the matrix that we obtain by deleting the second column of D_i by C_i. C_i is also a nxn squared matrix. Again, by using elementary row operations, we find the following results for C_i's.

$$|C_3| = \begin{vmatrix} 1 & 1 & 0 \\ 1 & 1 & 1 \\ 1 & 1 & 1 \end{vmatrix} = 0,$$

$$|C_4| = \begin{vmatrix} 1 & 1 & 0 & 0 \\ 1 & 1 & 1 & 0 \\ 1 & 0 & 1 & 1 \\ 1 & 1 & 1 & 1 \end{vmatrix} = \begin{vmatrix} 1 & 1 & 0 \\ 0 & 1 & 1 \\ 1 & 1 & 1 \end{vmatrix} - \begin{vmatrix} 1 & 1 & 0 \\ 1 & 1 & 1 \\ 1 & 1 & 1 \end{vmatrix} = |B_3| - |C_3| = 1-0=1,$$

$$|C_5| = \begin{vmatrix} 1 & 1 & 0 & 0 & 0 \\ 1 & 1 & 1 & 0 & 0 \\ 1 & 0 & 1 & 1 & 0 \\ 1 & 0 & 0 & 1 & 1 \\ 1 & 1 & 1 & 1 & 1 \end{vmatrix} = \begin{vmatrix} 1 & 1 & 0 & 0 \\ 0 & 1 & 1 & 0 \\ 0 & 0 & 1 & 1 \\ 1 & 1 & 1 & 1 \end{vmatrix} = \begin{vmatrix} 1 & 1 & 0 & 0 \\ 1 & 1 & 1 & 0 \\ 1 & 0 & 1 & 1 \\ 1 & 1 & 1 & 1 \end{vmatrix} = |B_4| - |C_4| = 0\text{-}1 = -1,$$

$$|C_6| = \begin{vmatrix} 1 & 1 & 0 & 0 & 0 & 0 \\ 1 & 1 & 1 & 0 & 0 & 0 \\ 1 & 0 & 1 & 1 & 0 & 0 \\ 1 & 0 & 0 & 1 & 1 & 0 \\ 1 & 0 & 0 & 0 & 1 & 1 \\ 1 & 1 & 1 & 1 & 1 & 1 \end{vmatrix} = \begin{vmatrix} 1 & 1 & 0 & 0 & 0 \\ 0 & 1 & 1 & 0 & 0 \\ 0 & 0 & 1 & 1 & 0 \\ 0 & 0 & 0 & 1 & 1 \\ 1 & 1 & 1 & 1 & 1 \end{vmatrix} = \begin{vmatrix} 1 & 1 & 0 & 0 & 0 \\ 1 & 1 & 1 & 0 & 0 \\ 1 & 0 & 1 & 1 & 0 \\ 1 & 0 & 0 & 1 & 1 \\ 1 & 1 & 1 & 1 & 1 \end{vmatrix} = |B_5| - |C_5| = 2,\ldots,$$

$$|C_n| = |B_{n-1}| - |C_{n-1}| = \frac{(-1)^{n+1}+1}{2} - |C_{n-1}|, n \geq 3.$$

$$|C_n| \begin{cases} \frac{n-2}{2}, n \text{ is even} \\ \frac{3-n}{2}, n \text{ is odd} \end{cases}, n > 3.$$

We can see that for n>3, $|C_n| \neq 0$.

Since rank $(D_3)=3$, and for all n>3, $|C_n| \neq 0$, we can say that rank $(D_n)=n$.

4.3 Definition: *Wheel Graphs*

For n>3, if we connect all the vertices of the cycle graph C_{n-1} to a vertex which is located inside the cycle and called the central vertex V_1, we call this graph the wheel graph W_n. It has n vertices, 2n edges and n faces. All of its faces are triangles. It is also planer and 3 regular. A face vertex incidence matrix has n rows and n columns.

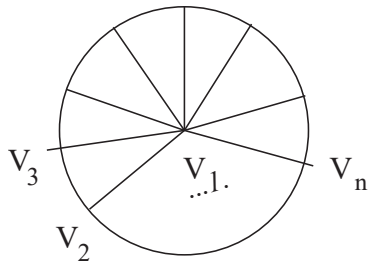

Figure 2: The Wheel graph W_n

4.4 Theorem: If D is a face vertex incidence matrix of W_n then,

$$rank(D) = \begin{cases} n, n \text{ is even} \\ n-1, n \text{ is odd} \end{cases}$$

(Moralı, 1999:9)

Proof: Without loss of generality, if we label the vertices of W_n as we see in Figure 2, the face vertex incidence matrix would look like,

$$D = \begin{bmatrix} 1 & 1 & 1 & 0 & 0 & \dots & 0 \\ 1 & 0 & 1 & 1 & 0 & \dots & 0 \\ 1 & 0 & 0 & 1 & 1 & \dots & 0 \\ 1 & 0 & 0 & 0 & 1 & \dots & 0 \\ \dots & \dots & \dots & \dots & \dots & \dots & \dots \\ 1 & 1 & 0 & 0 & 0 & \dots & 1 \\ 0 & 1 & 1 & 1 & 1 & \dots & 1 \end{bmatrix}$$

Let us call D, D_n, then,

$$|D_4| = \begin{vmatrix} 1 & 1 & 1 & 0 \\ 1 & 0 & 1 & 1 \\ 1 & 1 & 0 & 1 \\ 0 & 1 & 1 & 1 \end{vmatrix} = 3, \qquad |D_5| = \begin{vmatrix} 1 & 1 & 1 & 0 & 0 \\ 1 & 0 & 1 & 1 & 0 \\ 1 & 0 & 0 & 1 & 1 \\ 1 & 1 & 0 & 0 & 1 \\ 0 & 1 & 1 & 1 & 1 \end{vmatrix} = 0,$$

$$|D_6| = \begin{vmatrix} 1 & 1 & 1 & 0 & 0 & 0 \\ 1 & 0 & 1 & 1 & 0 & 0 \\ 1 & 0 & 0 & 1 & 1 & 0 \\ 1 & 0 & 0 & 0 & 1 & 1 \\ 1 & 1 & 0 & 0 & 0 & 1 \\ 0 & 1 & 1 & 1 & 1 & 1 \end{vmatrix} = 5,$$

$$|D_7| = \begin{vmatrix} 1 & 1 & 1 & 0 & 0 & 0 & 0 \\ 1 & 0 & 1 & 1 & 0 & 0 & 0 \\ 1 & 0 & 0 & 1 & 1 & 0 & 0 \\ 1 & 0 & 0 & 0 & 1 & 1 & 0 \\ 1 & 0 & 0 & 0 & 0 & 1 & 1 \\ 1 & 1 & 0 & 0 & 0 & 0 & 1 \\ 0 & 1 & 1 & 1 & 1 & 1 & 1 \end{vmatrix} = 0, \dots,$$

$|D_{2k+1}|=0$,

$|D_{2k}|=2k-1$, for $k\geq 2$.

So, we get,

$$rank(D_n) = \begin{cases} n\,, \text{n is even} \\ n-1\,, n \text{ is odd} \end{cases}.$$

4.5 Definition: *Ladder Graphs*

The ladder graph Ln is defined by Ln = Pn x K2 where Pn is a path with n vertices and x denotes the Cartesian product and K2 is a complete graph with two-vertices (Moussa and Badr, 2016:2).

For n>1, if we take two path graphs P_n with vertex sets $\{v_i\}$ and $\{u_i\}$, i= 1,2,…,n. and connect v_i and u_i with an edge for each i, the graph we obtain is called a Ladder graph L_n . It is a nonregular planer graph whose faces are all C_4's except the outer face. It has 2n vertices, 3n-2 edges and n faces.

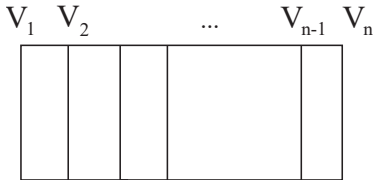

Figure 3: The Ladder graph L_n with 2n vertices

4.6 ***Theorem:*** If D is a face vertex incidence matrix of a Ladder graph L_n, than,

$$rank(D) = \begin{cases} 2k-1 \text{ if } n = 2k \\ 2k+1 \text{ if } n = 2k+1 \end{cases}, k = 1,2,\ldots$$ (Moralı, 1999:11)

Proof: The face vertex incidence matrix of such a graph would look like,

$$D = \begin{bmatrix} 1 & 1 & 0 & 0 & \ldots & 0 & 0 & 0 & 0 & \ldots & 0 & 0 & 1 & 1 \\ 0 & 1 & 1 & 0 & \ldots & 0 & 0 & 0 & 0 & \ldots & 0 & 1 & 1 & 0 \\ 0 & 0 & 1 & 1 & \ldots & 0 & 0 & 0 & 0 & \ldots & 1 & 1 & 0 & 0 \\ \ldots & \ldots & \ldots & \ldots & \ldots & \ldots & \ldots & \ldots & \ldots & \ldots & \ldots & \ldots & \ldots & \ldots \\ 0 & 0 & 0 & 0 & \ldots & 1 & 1 & 1 & 1 & \ldots & 0 & 0 & 0 & 0 \\ 1 & 1 & 1 & 1 & \ldots & 1 & 1 & 1 & 1 & \ldots & 1 & 1 & 1 & 1 \end{bmatrix}$$

It has n rows and 2n columns. Again let us call the matrix with n rows D_n. Let r_i denote the i^{th} row.

$$D_3 = \begin{bmatrix} 1 & 1 & 0 & 0 & 1 & 1 \\ 0 & 1 & 1 & 1 & 1 & 0 \\ 1 & 1 & 1 & 1 & 1 & 1 \end{bmatrix} (-r_2+r_3)\sim \begin{bmatrix} 1 & 1 & 0 & 0 & 1 & 1 \\ 0 & 1 & 1 & 1 & 1 & 0 \\ 1 & 0 & 0 & 0 & 0 & 1 \end{bmatrix} (-r_3+r_1) \sim$$

$$\begin{bmatrix} 0 & 1 & 0 & 0 & 0 & 1 \\ 0 & 1 & 1 & 1 & 1 & 0 \\ 1 & 0 & 0 & 0 & 0 & 1 \end{bmatrix} (-r_1+r_2) \sim \begin{bmatrix} 0 & 1 & 0 & 0 & 0 & 1 \\ 0 & 0 & 1 & 1 & 1 & 0 \\ 1 & 0 & 0 & 0 & 0 & 1 \end{bmatrix}$$

So, the rank of D_3 is 3.

By similar operations, we see that the rank of D_n is n when n is odd.

When n is even the sum of odd number of rows gives us the n^{th} row. So, $r_1+r_2+\ldots+r_{n-1} = r_n$.

This gives us rank $(D_{2k}) < 2k$. And by using elementary row operations we get the rank$(D_{2k}) = 2k-1$. Thus,

$$\text{Rank}(D)= \begin{cases} 2k-1 \; if \; n = 2k \\ 2k+1 \; if \; n = 2k+1 \end{cases} \quad ,k = 1,2,\ldots$$

5. CONCLUSION

Here, we defined and give some theorems and proofs about face-vertex matrix of some special graphs. The face-vertex incidence matrix is a less known graph matrix and the results obtained here may be helpful to researches who work on this subject.

6. REFERENCES

Bondy J. A. Murty U.S.R. (2008). *Graph theory*. Graduate Texts in Mathematics series, Springer

Clark J., Holton D. A. (1995). *A First Look at Graph Theory* Bombay Allied Publishers Ltd.

Harary F. (2018). *Graph Theory.* USA CRC Press Taylor & Francis Group

4.Moralı H. S. (1999). (doktora tezi). *A new way to obtain codes using graphs.* Dokuz Eylül Üniversitesi, Eğitim Bilimleri Enstitüsü, İzmir.

Moussa M. I., Badr E. M. (2016). Ladder and Subdivision of Ladder Graphs with Pendant Edges are Odd Graceful. International Journal on Applications of Graph Theory in Wireless Ad hoc Networks and Sensor Networks(GRAPH-HOC) 8(1), 1-8

Pirzada S. (2007). Applications of graph theory. *Sixth International Congress on Industrial Applied Mathematics (ICIAM07) and GAMM Annual Meeting, Zürich: Vol. 7(1) (pp. 2070013)*

Oral H. (1989). *Self-dual Codes and Graphs.* (Doktora tezi). Simon Frasier University, Canada

8.Tatsuoko M. M. (1986). Graph Theory and Its Applications in Educational Research: A Review and Integration Review of Educational Research, Review of Educational Research, 56(3) 291-329

Chapter 11

Calculation of X-ray Fluorescence Parameters for Zinc and Copper Doped Hydroxyapatite

Oğuz Kağan KÖKSAL[1,2]

[1]Assist. Prof. Dr.; Adiyaman University Faculty of Elecgtrical and Elecronics Engineering Department of Electrical Electronics Engineering,
okoksal@adiyaman.edu.tr, ORCID No: 0000-0003-2671-6683
[2] Assist. Prof. Dr.; Karadeniz Technical University Faculty of Sciences Department of Physics,
okoksal@adiyaman.edu.tr, ORCID No: 0000-0003-2671-6683

ABSTRACT

Through a wet chemical method, stoichiometric hydroxyapatite nanoparticles were created. Pure hydroxyapatite bone powders are given various amounts of zinc and copper to improve their antibacterial properties. The elements in the samples made prior to the X-ray photon interactions were examined using energy-dispersive X-ray spectrometry. Using an Ultra-Low Energy Germanium detector with a resolution of 150 electro volt at 5.9 kilo electro volt, K-shell fluorescence parameters such as cross section, fluorescence yield, intensity ratio, line widths, and transition probabilities have been calculated experimentally for zinc and copper doped hydroxyapatite in various concentrations. Americum-241 radioisotope source photons with a 59.6 kilo electro volt energy level stimulated the samples. In this work, information regarding how it affects the K-shell fluorescence properties of zinc and copper when they are added to the hydroxyapatite structure has been discovered. The results showed that the X-ray interactions were comparable to those of pure zinc and copper. It has been discovered that the X-ray fluorescence parameter values of artificial bone powders with added zinc and copper are comparable to those of actual bone in terms of fluorescence parameters needed to understand the interaction with X-rays.

Keywords : K Shell Fluorescence Parameters; Am-241 Radioactive Source; Metal Doped Hydroxyapatite; X-Ray Interaction, Zinc, Copper

INTRODUCTION

The bulk of an organism's tissues, including bone and the enamel on teeth, have a hierarchical structure. Its hierarchical structure plays a significant role in determining the mechanical properties of bone. Hydroxyapatite (HA), which is nanometric in size, is at the bottom of this hierarchy. Human bone and dental enamel (Dubey & Tomar, 2009) both contain inorganic substance (HA) ($Ca_{10}(PO_4)_6(OH)_2$) [1]. Due to its excellent biocompatibility (Vamze, Pilmane, & Skagers, 2015), HA has been used as metal coating (Sun, Pang, & Zhitomirsky, 2009), scaffolds (Nie et al., 2015), and bone cement cement (Wong et al., 2004). Additionally, due to its capacity to bond with bone, HA is frequently used as a metal coating in biomedical applications (Akazawa & Ueno, 2015; Duraccio, Mussano, & Faga, 2015; Razavi, Fathi, Savabi, Vashaee, & Tayebi, 2015). Because a metallic substrate possesses the requisite mechanical properties, they employ HA to create an osteoconductive surface for the production of new bone. In doing so, the metal implant is immobilized and the load is transferred to the skeleton, assisting in the prevention of bone atrophy (Itokazu, Yang, Aoki, Ohara, & Kato, 1998; Kehoe & Stokes, 2011; Liu, de Groot, & Hunziker, 2005; Minguez, Agra, Luruena, Ramos, & Prieto, 1990). In contrast to metal-free synthetic bone powder, copper and zinc metals are added to pure hydroxyapatite to produce significant antibacterial characteristics (Chen et al., 2010; Ito et al., 2005; Moonga & Dempster, 1995; Yamaguchi, Oishi, & Suketa, 1987).

In earlier research (Ciobanu, Andronescu, & Predoi, 2011; Fujii et al., 2006; Serro, Bastos, Pessoa, & Saramago, 2004; Stipniece, Stepanova, Narkevica, Salma-Ancane, & Boyd, 2018; Wei & Ma, 2004) , the structural analysis, morphological and mechanical properties, adsorption, and corrosion were investigated for a variety of artificial hydroxyapatite bone dust types. The processes of radiation attenuation and radiation protection have attracted a lot of attention from researchers (Agar et al., 2019; F. Akman et al., 2018; Aygün et al., 2019; Erhan Cengiz, Dogan, & Koksal, 2013; Erhan Cengiz & Saritas, 2014; E Cengiz et al., 2015; Ersundu, Büyükyıldız, Çelikbilek Ersundu, Şakar, & Kurudirek, 2018; Gaikwad et al., 2018; Obaid, Gaikwad, & Pawar, 2018; Obaid, Sayyed, Gaikwad, & Pawar, 2018). Also studied were the gamma-ray attenuation properties of solid boronized 304L stainless steel (Araz, Gumus, Bayca, & Aydin, 2021), various NLO materials(Al-Buriahi, Singh, Arslan, Awasarmol, & Tonguc, 2020), cement paste-waste paper composites (Turhan, Akman, Polat, Kaçal, & Demirkol, 2020), barite concrete mixtures containing nanoparticles of thermoplastic polymers (Al-Tersawy, El-Sadany, & Sallam, 2021), and some polymers (Araz et al., 2021).

In addition to performing physical and chemical analyses of materials (Hodoroaba & Rackwitz, 2014; Marinangeli et al., 2015; Rosa et al., 2022), the Energy Dispersive X-ray Fluorescence (EDXRF) method is used to perform photon counts in the computation of fluorescence parameters such as fluorescence cross sections (Gökhan Apaydın & Tıraşoğlu, 2006; V. Aylikci, Apaydin, Tiraşoğlu, Kaya, & Cengiz, 2007; Aylıkcı et al., 2008; Saydam et al., 2012; Tıraşoğlu, Söğüt, Tekbıyık, Apaydın, & Ertuğrul, 2007), fluorescence yield (Hönicke et al., 2023; Madeira et al., 2015; Sampaio et al., 2015), X-ray intensity ratios (G Apaydın et al., 2008; N. K. Aylikci et al., 2011; Erhan Cengiz & Karahan, 2022; Cevik, Değirmencioğlu, Ertuğral, Apaydın, & Baltaş, 2005; B Ertuğral, Apaydın, Çevik, Ertuğrul, & Kobya, 2007; BİROL Ertuğral et al., 2006; Perişanoğlu & Demir, 2015; Perişanoğlu, Kavaz, Urtekin, & Demir, 2020; Uğurlu & Demir, 2020), transition probability (Ertugrul, 2002; Han, Şahin, Demir, & Şahin, 2007; Turhan, Akman, Kaçal, & Durak, 2017), line widths (N. K. Aylikci et al., 2018; Aylıkçı, 2019; Köksal, Apaydın, Cengiz, & Karabulut, 2016; Kündeyi, Aylıkcı, Tıraşoğlu, Kahoul, & Aylıkcı, 2017), and radiation absorption parameters (Ferdi Akman, Durak, & Kaçal, 2015; Damay & Idrissi, 2006; Kirby, Davis, Grant, & Morgan, 2003; Obeid, Balaa, Samad, Awad, & Badawi, 2022). These factors, such as the fluorescence analysis technique, atomic physics study, health physics dosimetry calculation, cancer treatment, radiation transport in matter, etc., create valuable information in the relevant fields.

Studies on the pure and alloyed states of the elements zinc and copper are regularly found in the literature for their X-ray fluorescence properties. It is evident that there is no information available on how to change the X-ray fluorescence qualities when the zinc and copper components are present in a biomaterial compound in different concentrations, such as synthetic bone dust. Then, the observed data will be analyzed in relation to the chemical surroundings and the impact of eliminating electrons. In addition, it is planned to use zinc and copper-doped synthetic hydroxyapatite bone powders to treat bone wounds. Patients may be exposed to X-rays when these materials are used in therapy, according to some experts. In order to enhance atomic level sample identification, the measured results will then be analysed in relation to the chemical surroundings and the results of the electron removal. In addition, it is planned to use zinc and copper-doped synthetic hydroxyapatite bone powders to treat bone wounds. It is thought that using these materials in therapy exposes patients to X-rays. Zinc-doped synthetic hydroxyapatite bone powders and X-ray fluorescence interactions will be researched in order to enhance sample identification at the atomic level.

This study aims to try to explain the interaction between radiation and matter by showing how the K-shell X-ray fluorescence parameters vary in zinc and copper-substituted hydroxyapatite samples with better antibacterial properties, which are used in medicine and whose interaction with radiation has become frequent.

EXPERIMENTAL PROCEDURE

Sampling

The samples were created by wet chemical precipitation. A 0.6 mole solution of phosphate and a 1 mole solution of calcium are combined in the process. The pH of the mixture was then raised by employing NaOH to bind enough OH ions. The two solutions were gradually combined. In the instance of ion addition, a solution is made so that, rather than 1 mole of calcium nitrate, the sample will receive 1 mole of calcium plus the ion. When the phosphate solution is introduced to the metal-containing solution, precipitation happens. Magnetic stirring was used for 30 minutes during the precipitation, followed by ultrasonic mixing for an hour.

The samples were prepared by using wet chemical precipitation process. The process is consisting of A 0.6 mole solution containing phosphate with a 1 mole solution containing calcium. Then, the pH value of the solution was increased by using NaOH to bind sufficient OH ion. These two solutions were slowly mixed together. In the case of ion addition, a solution is prepared in such a way that instead of 1 mole calcium nitrate, the total amount of calcium and the ion to be added to the sample is 1 mole. The precipitate was carried out when the phosphate solution is added to the metal-containing solution. During the precipitation, magnetic stirring was applied for half an hour and then ultrasonic mixing for one hour. After these procedures, hydroxyapatite synthetic bone powders and an insoluble precipitate were produced (Koksal et al., 2019). The objects produced prior to the x-ray interactions were disassembled using energy-dispersive x-ray spectroscopy to determine their elemental composition.

Table 1: EDX concentration values and partial density (ρd) for CuHAp and ZnHAp samples

Samples	O	Na	Ca	P	K	Cl	Cu	Zn	ρd [g/cm^3]
ZnHAP1	70.10±7.9	2.10±0.8	20.39±1.0	4.74±0.3	-	1.12±0.1	-	1.55±0.4	1.568
ZnHAP2	77.64±11.0	15.91±3.7	0.44±0.1	2.98±0.3	0.56±0.1	0.45±0.1	-	2.02±0.7	1.582
ZnHAP3	60.45±7.1	3.11±1.4	21.35±1.1	11.99±0.6	0.43±0.1	0.18±0.1	-	2.49±0.6	1.574
CuHAP1	62.36±6.2	5.27±0.4	19.77±0.9	11.44±0.5	-	0.10±0.0	1.05±0.2	-	1.606
CuHAP2	63.12±7.3	6.41±0.6	14.53±0.7	13.36±0.6	0.32±0.1	0.27±0.1	1.99±0.4		1.603
CuHAP3	66.90±8.8	7.36±0.8	16.99±0.9	4.82±0.3	0.50±0.1	0.83±0.1	2.60±0.6		1.622

Experimental Set-up

The experimental setup geometry for an annular source is depicted in (Aksoy et al., 2012). An annular 50 mCi 241 Am radioactive source was employed in this experimental setup to generate the photons that were released at 59.5 keV. An Ultra-LEGe collimated detector with a 150-eV energy resolution at 5.96 keV was used to find the fluorescence K X-rays from the material. The counting period for each sample in this study was set at 10,000 seconds. Due to the significant peak overlap in the ED-XRF system, spectral deconvolution is one of the major issues that arise while finding these parameters in experimental determinations. A multi-channel analyzer connected to a private computer with appropriate software for data collecting and peak analysis was fed the output preamplifier, which had the ability to reject pulse pile-ups. Using a peak fitting program created by Origin Corporation, the fitting and deconvolution were carried out. The experimental setup for the zinc and copper-doped synthetic hydroxyapatite bone powders is shown in Figure 1 of the current work.

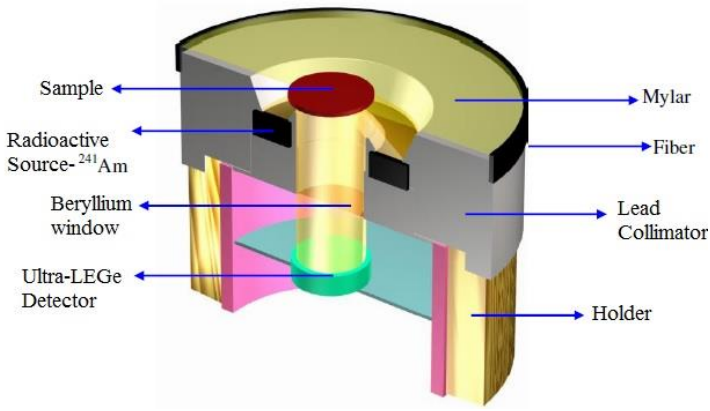

Figure 1: The measurement geometry used in radioactive annular source X-ray fluorescence analysis.

Calculations

A cross section is defined as the probability that the radiation interacting with the sample will interact with the target particle in a particular way. The cross section estimates the likelihood that these interactions will occur. The cross section of a target particle is influenced by the event's nature and energy (Erhan Cengiz, 2011). The following connection allows for the acquisition of the experimental Ki X-ray production cross-sections:

$$\sigma_{X_i} = \frac{N_{Xi}}{I_0 G \varepsilon_{Xi} \beta_{Xi} m_i} [i = \alpha, \beta] \quad (1)$$

where N_{Xi} is the measured intensity for the K_i group of X-rays (the area under the photo peak). The radiation's incidence intensity is denoted by I_0. The geometrical constant is G. The K_i group of X-rays' detection effectiveness is denoted by the symbol Xi. The self-absorption correction factor (β_{Xi}) for the target material takes into consideration both the emission of distinctive X-rays and the incident photons' absorption in the target. m_i is the analyte concentration in grams per cubic centimetre.

The equation is used to determine the self-absorption correction (Hubbell, 1995)

$$\beta = \frac{1 - \exp\left[-\left(\frac{\mu_{inc}}{\cos\theta_1} + \frac{\mu_{emt}}{\cos\theta_2}\right)t\right]}{\left(\frac{\mu_{inc}}{\cos\theta_1} + \frac{\mu_{emt}}{\cos\theta_2}\right)t} \quad (2)$$

where μ_{inc} and μ_{emt} are, respectively, the incident photon's mass attenuation coefficient(Berger, Hubbell, Seltzer, Coursey, & Zucker, 1999) and the typical X-emission ray's coefficient. t represents the target's thickness in grams per square centimeter. In the current experimental setup, the angles of the incident photons and the emitted X-rays with regard to the normal of the surface, were equal to 45^0 and 90^0, respectively.

By gathering the K_α and K_β X-ray spectra of samples of K_2SO_4, Ti, V, Ni, Cu, and As_2SO for Amercium-241 in the same geometry and employing the equation, the product $I_0G\varepsilon$, containing the terms related to the incident photon flux, geometrical factor, and intrinsic absolute efficiency of the X-ray detector, was calculated.

$$I_0 G\varepsilon_{Ki} = \frac{N_{Ki}}{\sigma_{Ki}\beta_{Ki}m}[i = \alpha, \beta] \quad (3)$$

Equation (3) uses the same words and units as Equation (1). The following equation was used to fit the factor $I_0 G\varepsilon_{Ki}$ as a function of energy:

$$I_0 G\varepsilon_{Ki} = A_0 + A_1 E_x + A_2 E_x^2 + A_3 E_x^3$$

A_0, A_1, A_2 and A_3 are constants calculated from a fitting polynomial, and E_x is the K_α and K_β X-ray energy. The mean K X-ray energy determines how the factor $I_0G\varepsilon_{Ki}$ varies. Figure 2 shows the experimental efficiency curve for the germanium ultra-low energy detector as a function of K X-ray energy.

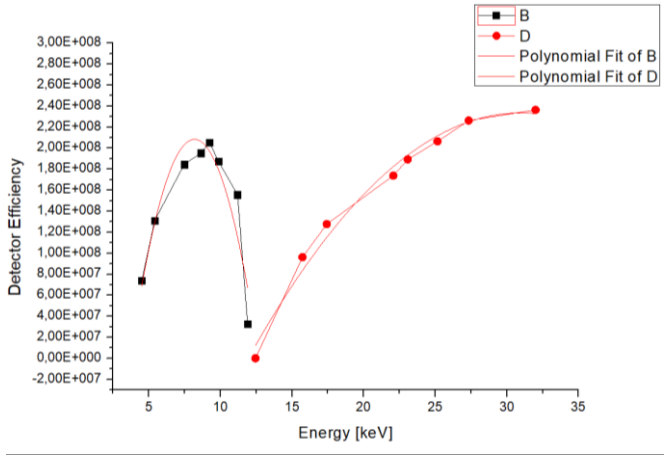

Figure 2: The plot of the experimental efficiency curve for the ultra-low energy germanium detector as a function of K X-ray energy.

The connection is used to analyse the theoretical K X-ray production cross sections;

$$\sigma_{Ki} = \sigma_K(E)\omega_K F_{Ki}$$

Where $\sigma_K(E)$ I s the given element's K-shell photoionization cross-section for excitation energy E (J. Scofield, 1973). F_{Ki} is the emission rate of the fractional X-ray for K_i X-rays, and ω_K is the K-shell X-ray fluorescence yield (Krause, 1979) (Broll, 1986).

The likelihood that an atom will fill a vacancy made in the K layer by any method by producing distinctive X-rays is known as the fluorescence yield of the K layer (Gökhan Apaydın, 2006). The yields of the semi-empirical K shell X-ray fluorescence, or K, are calculated using the following equation:

$$\omega_K = \frac{\sum \sigma_{Ki}}{\sigma_K(E)} (i = \alpha, \beta) \qquad (6)$$

where $\sum \sigma_{Ki}$ is the total K X-ray fluorescence cross-section obtained experimentally, $\sigma_K(E)$ is the theoretical K shell photoionization cross-section of a given element for the excitation energy E (J. Scofield, 1973).

The life of a hole at that level represents the natural level width (M. O. Krause & J. Oliver, 1979). K shell level widths were calculated by dividing the fluorescence yield of the radiative transition rate (Krause, 1979) as using the formula shown below;

$$\Gamma_K = \frac{\Gamma_K(R)}{\omega_K} \tag{7}$$

Where Γ_K is the K shell level width and ω_K is K shell X-ray fluorescence yield.

Any characteristic X-ray intensity of an element is determined by the following expression.

$$I = \frac{N}{\varepsilon\beta} \tag{8}$$

Where N is the net area of the peak of the characteristic X-ray of the desired element, e is the emission from the detector at the characteristic X-ray energy, and b is the absorption correction factor. With helping this expression, intensity ratios of K shell were determined as ratio of cross-sections of K_β and K_α with using the equation illustrated below;

$$\frac{I_{Ki}}{I_{Kj}} = \frac{N_{Ki}}{N_{Kj}}\frac{\varepsilon_{Kj}}{\varepsilon_{Ki}}\frac{\beta_{Kj}}{\beta_{Ki}} \tag{9}$$

The intensity ratio and fluorescence yield values are used to calculate the vacancy transfer probability (Erhan Cengiz, 2011). The vacancy transition from layer K to layer L was calculated using the following equation (Schonfeld & Janssen, 1996).

$$\eta_{KL} = \frac{2-\omega_K}{1+\frac{I_{K\beta}}{I_{K\alpha}}} \tag{10}$$

Where ω_K, K shell X-ray fluorescence yield and is calculated using the equation (6). The K X-ray intensity ratio values were calculated using the $I_{K\beta}$ / $I_{K\alpha}$ equation (9).

RESULTS and DISCUSSION

The K X-ray spectra of zinc for ZnHAP and copper for CuHAP samples were captured by the ultra-low energy germanium detector after being driven by the annular radioactive source Americium-241 in figure 3.

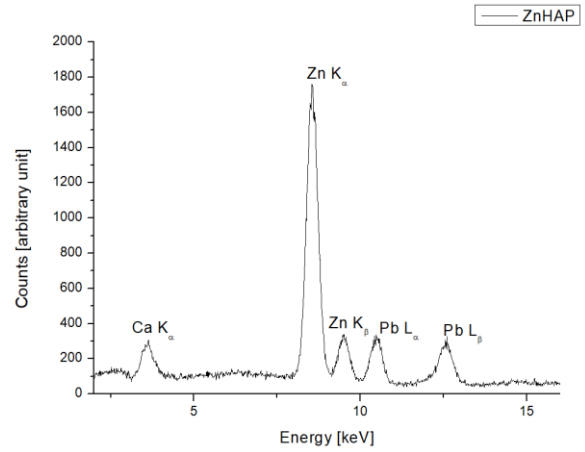

a)

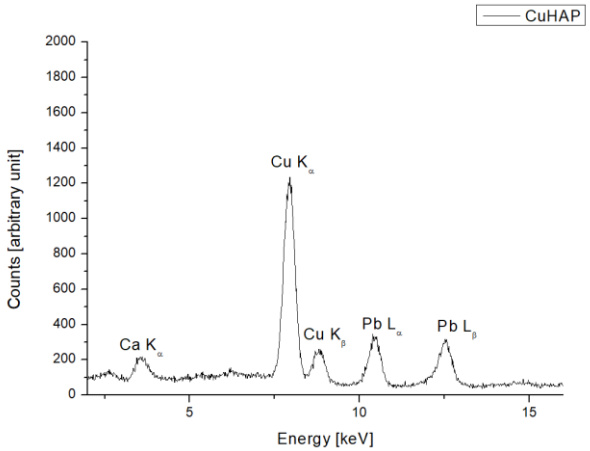

b)

Figure 3: The K X-ray spectra of **a)** zinc for ZnHAP and **b)** copper for CuHAP samples were captured by the ultra-low energy germanium detector after being driven by the annular radioactive source Americium-241.

Examining the peaks reveals that the energy values corresponding to the peaks of zinc and copper have not changed. This suggests that the outcomes are trustworthy.

The calculated σK_α and σK_β cross sections are shown in Table 2.

Table 2: K Shell Fluorescence cross sections in g/cm^2 for ZnHAP and CuHAP

Samples	Zn σK_α [Exp.]	Zn σK_α [Theo.] (J. H. Scofield, 1974)	Zn σK_β [Exp.]	Zn σK_β [Theo.] (J. H. Scofield, 1974)
Zn	-	0.600	-	0.074
ZnHAP1	0.600±0.036	-	0.060±0.004	-
ZnHAP2	0.636±0.038	-	0.094±0.006	-
ZnHAP3	0.623±0.038	-	0.078±0.005	-
Samples	Cu σK_α [Exp.]	Cu σK_α [Theo.] (J. H. Scofield, 1974)	Cu σK_β [Exp.]	Cu σK_β [Theo.] (J. H. Scofield, 1974)
Cu	-	0.814	-	0.099
CuHAP1	0.769±0.046	-	0.090±0.005	-
CuHAP2	0.796±0.048	-	0.126±0.008	-
CuHAP3	0.801±0.048	-	0.120±0.007	-

While the phenomena of σK_α stayed within the error boundaries, the σK_β cross sections of values went above them according to Refs. (J. H. Scofield, 1974). This situation is well seen in the graph in figure 4 and 5.

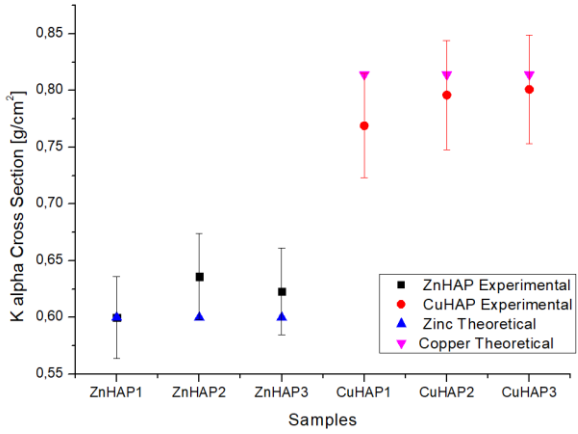

Figure 4: K shell fluorescence K alpha cross sections versus ZnHAP and CuHAP samples.

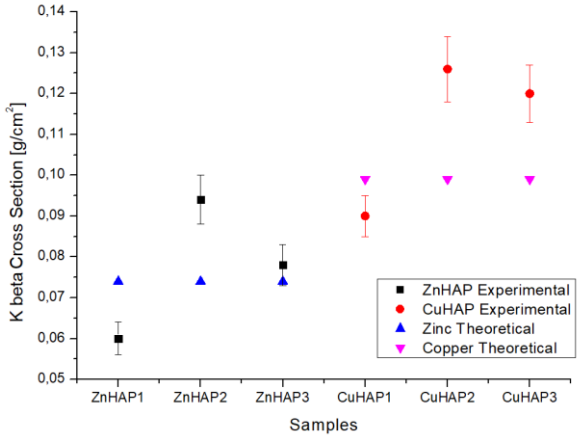

Figure 5: K shell fluorescence K beta cross sections versus ZnHAP and CuHAP samples.

The K_β/K_α intensity ratios are seen in Table 3.

Table 3: K Shell Intensity Ratios for ZnHAP and CuHAP

Samples	Zn $K_\beta\backslash K_\alpha$ [Exp.]	Zn $K_\beta\backslash K_\alpha$ [Theo.] (J. H. Scofield, 1974)
Zn	-	0.1233
ZnHAP1	0.0996±0.0060	
ZnHAP2	0.1484±0.0089	
ZnHAP3	0.1246±0.0075	
Samples	Cu $K_\beta\backslash K_\alpha$ [Exp.]	Cu $K_\beta\backslash K_\alpha$ [Theo.] (J. H. Scofield, 1974)
Cu	-	0.1216
CuHAP1	0.1165±0.0070	-
CuHAP2	0.1582±0.0095	-
CuHAP3	0.1502±0.0090	-

Due to σK_β cross sections, it can be seen that the intensity ratio values are greater than the error thresholds according to Refs. (J. H. Scofield, 1974). Figure 6 shows how things stand in this case. For σK_β cross sections, the causes of this are examined.

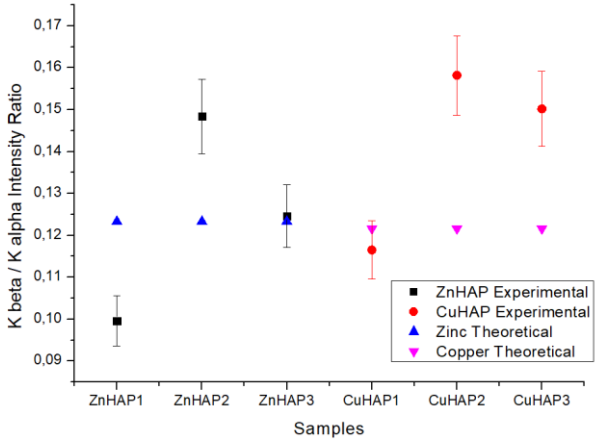

Figure 6: K Shell X-ray intensity ratios for ZnHAP and CuHAP samples

If increase or decrease in K_β and K_α cross-section values are in the same direction, the changes in the K_β/K_α intensity values are small or insignificant within experimental error limits. However, when increase or decrease in K_β and K_α cross-section values are in the opposite direction, deviations between the K_β/K_α intensity values become significant. This situation can be seen obviously from the cross-section values in Table 2.

The influence of removing electrons from K, L, M, N, and other shells could be another factor contributing to differences between practical and theoretical estimates of the production cross-sections. As energetic particles collide with atoms or ions or when the atomic shell is reorganized following the filling of an initial inner-shell vacancy, several ionization processes take place (Zschornack, 2007). the process of an atom's valence energy levels being rearranged (Raj, Padhi, & Polasik, 1999). The ω_K X-ray fluorescence yields values are presented in Table 4.

Table 4: K Shell Fluorescence yields for ZnHAP and CuHAP

Samples	Zn ωK [Exp.]	Zn ωK [Theo.] (Krause, 1979)	Zn ωK [Theo.] (Broll, 1986)
Zn	-	0.486	0.490
ZnHAP1	0.475±0.029	-	-
ZnHAP2	0.526±0.032	-	-
ZnHAP3	0.505±0.030	-	-
Samples	Cu ωK [Exp.]	Cu ωK [Theo.] (Krause, 1979)	Cu ωK[Theo.] (Broll, 1986)
Cu	-	0.454	0.445
CuHAP1	0.427±0.026	-	-
CuHAP2	0.459±0.028	-	-
CuHAP3	0.459±0.028	-	-

The fluorescence yield numbers are seen to remain within the error bounds to match the theoretical value in Refs. (Broll, 1986; Krause, 1979). The variance in fluorescence yield between the samples is depicted in Figure 7.

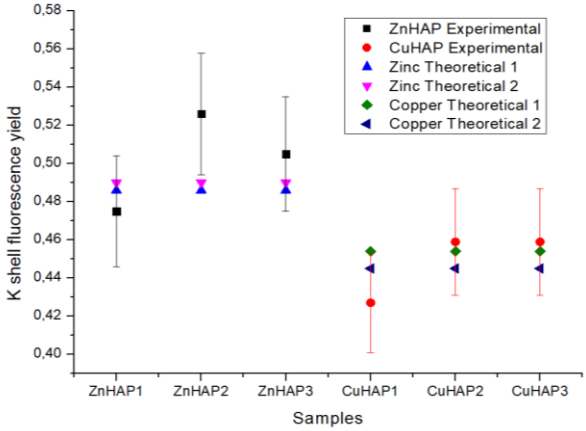

Figure 7: K Shell fluorescence yields for ZnHAP and CuHAP samples

The values of K level widths are tabulated in Table 5 and the measured K_{α}, $K_{\alpha 1}$ and $K_{\alpha 2}$ level widths are in god agreement with the Refs.(M. O. Krause & J. H. Oliver, 1979).

Table 5: K Level Widths for ZnHAP and CuHAP

Samples	Zn K_{α} [Exp.]	Zn K_{α} [Theo.] (M. O. Krause & J. H. Oliver, 1979)	Zn $K_{\alpha 1}$ [Exp.]	Zn $K_{\alpha 1}$ [Theo.] (M. O. Krause & J. H. Oliver, 1979)	Zn $K_{\alpha 2}$ [Exp.]	Zn $K_{\alpha 2}$ [Theo.] (M. O. Krause & J. H. Oliver, 1979)
Zn	-	1.67	-	2.32	-	2.39
ZnHAP1	1.57±0.09	-	2.22±0.13	-	2.29±0.14	-
ZnHAP2	1.42±0.09	-	2.07±0.12	-	2.14±0.13	-
ZnHAP3	1.48±0.09	-	2.13±0.13	-	2.20±0.13	-
Samples	Cu K_{α} [Exp.]	Cu K_{α} [Theo.] (M. O. Krause & J. H. Oliver, 1979)	Cu $K_{\alpha 1}$ [Exp.]	Cu $K_{\alpha 1}$ [Theo.] (M. O. Krause & J. H. Oliver, 1979)	Cu $K_{\alpha 2}$ [Exp.]	Cu $K_{\alpha 2}$ [Theo.] (M. O. Krause & J. H. Oliver, 1979)
Cu	-	1.55	-	2.11	-	2.17
CuHAP1	1.51±0.09	-	2.07±0.12	-	2.13±0.13	-
CuHAP2	1.40±0.08	-	1.96±0.12	-	2.02±0.12	-
CuHAP3	1.40±0.08	-	1.96±0.12	-	2.02±0.12	-

The K level widths variation between the samples is depicted in Figure 8.

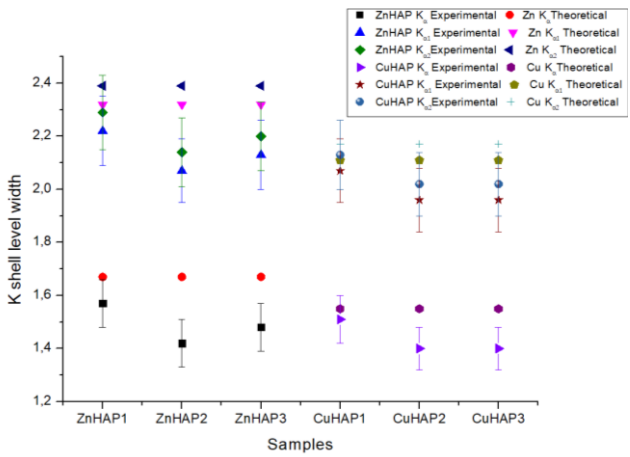

Figure 8: K Shell level width for ZnHAP and CuHAP samples

The transition probabilities are shown in Table 6, and there is good agreement between the measured probabilities and the theoretical values in the references **(Broll, 1986; Krause, 1979)**.

Table 6: Transition Probabilities for ZnHAP and CuHAP

Samples	Zn ηK [Exp.]	Zn ηK [Theo.] (Krause, 1979)	Zn ηK [Theo.] (Broll, 1986)
Zn	-	1.347	1.343
ZnHAP1	1.387±0.083	-	-
ZnHAP2	1.283±0.077	-	-
ZnHAP3	1.329±0.078	-	-
Samples	Cu ηK [Exp.]	Cu ηK [Theo.] (Krause, 1979)	Cu ηK [Theo.] (Broll, 1986)
Cu	-	1.375	1.383
CuHAP1	1.403±0.084	-	-
CuHAP2	1.396±0.084	-	-
CuHAP3	1.393±0.084	-	-

Figure 9 shows the variance in the transition probability between the samples.

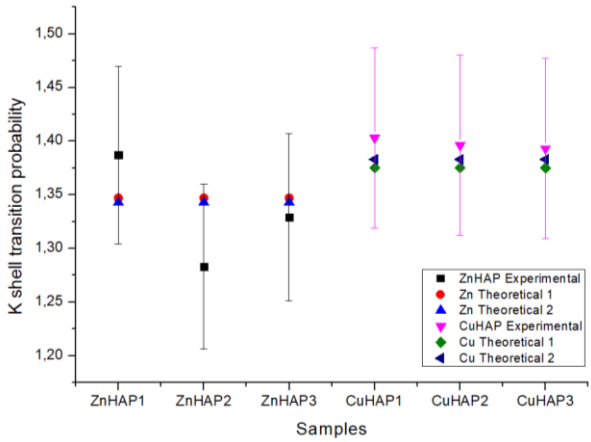

Figure 9: K Shell transition probability for ZnHAP and CuHAP samples

Target thickness (2%), evaluation of the peak area (3%), $I_0G\varepsilon$ product (3%), and absorption correction factor (3%), along with other factors required to assess subshell X-ray fluorescence yield and cross sections, make up the quadrature total of uncertainties in the results. The quadrature sum therefore estimates the overall measurement uncertainties to be less than 6%. Table 7 provides a list of these parameters' uncertainty.

Table 7: Uncertainties in the quantities used to determine the parameters

Quality	Nature of uncertainty	Uncertainty (%)
$N[K_i][i=\alpha, \beta]$	Counting statistic	≤3
$I_0G\varepsilon_{Ki}$	Errors in different parameters used to evaluate factor	≤2
β	Error in the absorption coefficients correction at incident and emitted photon energies	≤3
t	Errors in the weight and thickness of the samples	≤2

CONCLUSION

The fluorescence characteristics of metals in hydroxyapatite bone powders can apparently be determined using the X-ray fluorescence technique. The likelihood of filling a hole created in the K layer by an atom emitting distinctive X-rays in any way (fluorescence yield) and the lifetime (level width) of a hole at this level are both dependent on the likelihood that the radiation interacting with the sample will interact with the target particle in a specific way (fluorescence cross-section). Values are thought to be compatible with pure copper and zinc. This demonstrates that its interaction with X-ray photons is normal. The pure metals zinc and copper are found to be compatible with these conditions. It can be seen that there is no anomaly in the interaction of this structure with X-rays because it does not exhibit a discernible increase in the amount of radiation absorption as a result of its substituted structure. According to theory, the addition of highly doped metals won't result in an anomalous radiation interaction state.

ACKNOWLEDGEMENT

The author would like to thank to Prof. Dr. İsmail Hakkı KARAHAN, Assoc. Prof. Dr. Ali TOZAR from Hatay Mustafa Kemal University and Prof. Dr. Gökhan APAYDIN from Karadeniz Technical University (Türkiye) for laboratory use.

REFERENCES

Agar, O., Tekin, H. O., Sayyed, M. I., Korkmaz, M. E., Culfa, O., & Ertugay, C. (2019). Experimental investigation of photon attenuation behaviors for concretes including natural perlite mineral. *Results in Physics, 12*, 237-243. doi:https://doi.org/10.1016/j.rinp.2018.11.053

Akazawa, H., & Ueno, Y. (2015). Low-temperature crystallization and high-temperature instability of hydroxyapatite thin films deposited on Ru, Ti, and Pt metal substrates. *Surface & Coatings Technology, 266*, 42-48.

Akman, F., Durak, R., & Kaçal, M. R. (2015). Determination of K shell absorption parameters for some lanthanides using the X-ray attenuation method. *Canadian Journal of Physics, 93*(12), 1532-1540.

Akman, F., Geçibesler, I. H., Sayyed, M. I., Tijani, S. A., Tufekci, A. R., & Demirtas, I. (2018). Determination of some useful radiation interaction parameters for waste foods. *Nuclear Engineering and Technology, 50*(6), 944-949. doi:https://doi.org/10.1016/j.net.2018.05.007

Aksoy, C., Tirasoglu, E., Cengiz, E., Apaydin, G., Saydam, M., Aylikci, V., & Aylikci, N. K. (2012). Chemical effects on the L-shell X-ray fluorescence parameters of Ta and W compounds. *Journal of Electron Spectroscopy and Related Phenomena, 184*(11-12), 556-560.

Al-Buriahi, M. S., Singh, V., Arslan, H., Awasarmol, V., & Tonguc, B. T. (2020). Gamma-ray attenuation properties of some NLO materials: potential use in dosimetry. *Radiation and environmental biophysics, 59*(1), 145-150.

Al-Tersawy, S. H., El-Sadany, R. A., & Sallam, H. (2021). Experimental gamma-ray attenuation and theoretical optimization of barite concrete mixtures with nanomaterials against neutrons and gamma rays. *Construction and Building Materials, 289*, 123190.

Apaydın, G. (2006). *65≤ Z≤ 92 bölgesinde bazı elementlerin K ve L X-ışını floresans parametrelerinin ölçülmesi.* Karadeniz Teknik Üniversitesi/Fen Bilimleri Enstitüsü/Fizik Anabilim Dalı,

Apaydın, G., Aylıkcı, V., Cengiz, E., Kaya, N., Kobya, Y., & Tıraşoğlu, E. (2008). Determination of K shell X-ray intensity ratios for some heavy elements. *Radiation Physics and Chemistry, 77*(8), 923-927.

Apaydın, G., & Tıraşoğlu, E. (2006). Measurements of K shell X-ray production cross sections and fluorescence yields of elements in the atomic number range 65⩽ Z⩽ 92 at 123.6 keV. *Nuclear Instruments and Methods in Physics Research Section B: Beam Interactions with Materials and Atoms, 246*(2), 303-308.

Araz, S. O., Gumus, H., Bayca, S. U., & Aydin, A. (2021). Investigation of gamma-ray attenuation coefficients for solid boronized 304L stainless steel. *Applied Radiation and Isotopes, 170*, 109605.

Aygün, B., Şakar, E., Korkut, T., Sayyed, M. I., Karabulut, A., & Zaid, M. H. M. (2019). Fabrication of Ni, Cr, W reinforced new high alloyed stainless steels for radiation shielding applications. *Results in Physics, 12*, 1-6. doi:https://doi.org/10.1016/j.rinp.2018.11.038

Aylikci, N. K., Aylikci, V., Kahoul, A., Tiraşoğlu, E., Karahan, I., & Cengiz, E. (2011). Effect of p H treatment on K-shell x-ray intensity ratios and K-shell x-ray-production cross sections in ZnCo alloys. *Physical Review A, 84*(4), 042509.

Aylikci, N. K., Sancak, K., Aylikci, V., Tirasoglu, E., Unluer, D., & Depci, T. (2018). The semi-empirical determination of KLL Auger, Kα1 and Kα2 X-ray line widths for sulfur atom in new 1, 2, 4-triazol compounds containing thiophene ring. *Chemical Physics Letters, 706*, 40-46.

Aylikci, V., Apaydin, G., Tiraşoğlu, E., Kaya, N., & Cengiz, E. (2007). Chemical effect on the L X-ray cross-sections and average fluorescence yields of Hf compounds. *Chemical Physics, 332*(2-3), 348-352.

Aylıkcı, V., Cengiz, E., Apaydın, G., Ünver, Y., Sancak, K., & Tıraşoğlu, E. (2008). Influence of functional group effect on the K-shell X-ray production cross-sections and average fluorescence yields of sulphur in 1, 2, 4-triazol-5-one compounds containing thiophene. *Chemical Physics Letters, 461*(4-6), 332-337.

Aylıkçı, N. K. (2019). Semi-empirical determination of Kα1, 2, Kβ1, 3, and Kβ2, 4 X-ray natural line widths for various elements between 29≤ Z≤ 74 at 123.6 keV.

Berger, M. J., Hubbell, J. H., Seltzer, S. M., Coursey, J. S., & Zucker, D. S. (1999). XCOM: Photon cross section database (version 1.2). *http://physics. nist. gov/xcom*.

Broll, N. (1986). Quantitative x-ray fluorescence analysis. Theory and practice of the fundamental coefficient method. *X-Ray Spectrometry, 15*(4), 271-285.

Cengiz, E. (2011). *3. sıra geçiş elementi bileşiklerinin K ve L X-ışını floresans parametreleri.* Karadeniz Teknik Üniversitesi/Fen Bilimleri Enstitüsü/Fizik Anabilim Dalı,

Cengiz, E., Dogan, M., & Koksal, O. K. (2013). LIII subshell absorption jump ratio and jump factor of tantalum. *Radiation Physics and Chemistry, 85*, 8-11.

Cengiz, E., & Karahan, İ. H. (2022). Kβ-to-Kα X-ray intensity ratio studies on changes of valance electron structures of nickel in Ni–B/hBN composite coatings. *Radiation Physics and Chemistry, 192*, 109928.

Cengiz, E., & Saritas, N. (2014). Determination of LIII subshell absorption jump ratio and jump factor of wolfram. *Radiation Physics and Chemistry, 97*, 142-146. doi:https://doi.org/10.1016/j.radphyschem.2013.11.010

Cengiz, E., Saritas, N., Dogan, M., OK, K., Karabulut, K., Apaydin, G., & Tirasoglu, E. (2015). Measurement of L III Subshell Absorption Jump Parameters of Hafnium. *光谱学与光谱分析, 35*(12), 3544-3548.

Cevik, U., Değirmencioğlu, İ., Ertuğral, B., Apaydın, G., & Baltaş, H. (2005). Chemical effects on the Kβ/Kα X-ray intensity ratios of Mn, Ni and Cu complexes. *The European Physical Journal D-Atomic, Molecular, Optical and Plasma Physics, 36*(1), 29-32.

Chen, Y. K., Zheng, X. B., Xie, Y. T., Ji, H., Ding, C. X., Li, H. W., & Dai, K. R. (2010). Silver release from silver-containing hydroxyapatite coatings. *Surface & Coatings Technology, 205*(7), 1892-1896. doi:10.1016/j.surfcoat.2010.08.073

Ciobanu, C. S., Andronescu, E., & Predoi, D. (2011). Bet and Xrd Studies on the Hydroxyapatite and Europium Doped Hydroxyapatite. *Digest Journal of Nanomaterials and Biostructures, 6*(3), 1239-1244.

Damay, P., & Idrissi, A. (2006). Evaluation of self-attenuation parameters for neutron and X-ray scattering using a Direct Method. Application to slabs, cylinders and samples of any shape. *Physica B: Condensed Matter, 382*(1-2), 71-75.

Dubey, D. K., & Tomar, V. (2009). Understanding the influence of structural hierarchy and its coupling with chemical environment on the strength of idealized tropocollagen-hydroxyapatite biomaterials. *Journal of the Mechanics and Physics of Solids, 57*(10), 1702-1717.

Duraccio, D., Mussano, F., & Faga, M. G. (2015). Biomaterials for dental implants: current and future trends. *Journal of Materials Science, 50*(14), 4779-4812.

Ersundu, A. E., Büyükyıldız, M., Çelikbilek Ersundu, M., Şakar, E., & Kurudirek, M. (2018). The heavy metal oxide glasses within the WO3-MoO3-TeO2 system to investigate the shielding properties of radiation applications. *Progress in Nuclear Energy, 104*, 280-287. doi:https://doi.org/10.1016/j.pnucene.2017.10.008

Ertugrul, M. (2002). Measurement of K shell radiative transition probabilities and K, L2 and L3 shell/subshell fluorescence yields of some elements in

the atomic number range 30≤ Z≤ 40. *Analytica Chimica Acta, 454*(2), 327-334.

Ertuğral, B., Apaydın, G., Çevik, U., Ertuğrul, M., & Kobya, A. (2007). Kβ/Kα X-ray intensity ratios for elements in the range 16⩽ Z⩽ 92 excited by 5.9, 59.5 and 123.6 keV photons. *Radiation Physics and Chemistry, 76*(1), 15-22.

Ertuğral, B., Apaydın, G., Tekbıyık, A., Tıraşoğlu, E., Çevik, U., Kobya, A., & Ertuğrul, M. (2006). Determination of probabilities of vacancy transfer from K to L shell using K X-ray intensity ratios. *The European Physical Journal D-Atomic, Molecular, Optical and Plasma Physics, 37*(3), 371-375.

Fujii, E., Kawabata, K., Ando, K., Tsuru, K., Hayakawa, S., & Osaka, A. (2006). Synthesis and structural characterization of silica-hybridized hydroxyapatite with gas adsorption capability. *Journal of the Ceramic Society of Japan, 114*(1333), 769-773.

Gaikwad, D. K., Obaid, S. S., Sayyed, M. I., Bhosale, R. R., Awasarmol, V. V., Kumar, A., . . . Pawar, P. P. (2018). Comparative study of gamma ray shielding competence of WO3-TeO2-PbO glass system to different glasses and concretes. *Materials Chemistry and Physics, 213*, 508-517. doi:https://doi.org/10.1016/j.matchemphys.2018.04.019

Han, I., Şahin, M., Demir, L., & Şahin, Y. (2007). Measurement of K X-ray fluorescence cross-sections, fluorescence yields and intensity ratios for some elements in the atomic range 22⩽ Z⩽ 68. *Applied Radiation and Isotopes, 65*(6), 669-675.

Hodoroaba, V.-D., & Rackwitz, V. (2014). Gaining improved chemical composition by exploitation of Compton-to-Rayleigh intensity ratio in XRF analysis. *Analytical chemistry, 86*(14), 6858-6864.

Hönicke, P., Unterumsberger, R., Wauschkuhn, N., Krämer, M., Beckhoff, B., Indelicato, P., . . . Parente, F. (2023). Experimental and theoretical approaches for determining the K-shell fluorescence yield of carbon. *Radiation Physics and Chemistry, 202*, 110501.

Hubbell, J. H. (1995). 1995 and Some Anniversary Reflections. *Radiation Physics and Chemistry, 46*(3), 297-298.

Ito, A., Otsuka, M., Kawamura, H., Ikeuchi, M., Ohgushi, H., Sogo, Y., & Ichinose, N. (2005). Zinc-containing tricalcium phosphate and related materials for promoting bone formation. *Current Applied Physics, 5*(5), 402-406. doi:10.1016/j.cap.2004.10.006

Itokazu, M., Yang, W. Y., Aoki, T., Ohara, A., & Kato, N. (1998). Synthesis of antibiotic-loaded interporous hydroxyapatite blocks by vacuum method and in vitro drug release testing. *Biomaterials, 19*(7-9), 817-819.

Kehoe, S., & Stokes, J. (2011). Box-Behnken Design of Experiments Investigation of Hydroxyapatite Synthesis for Orthopedic Applications. *Journal of Materials Engineering and Performance, 20*(2), 306-316.

Kirby, B., Davis, J. R., Grant, J. A., & Morgan, M. J. (2003). Extracting material parameters from x-ray attenuation: a CT feasibility study using kilovoltage synchrotron x-rays incident upon low atomic number absorbers. *Physics in Medicine & Biology, 48*(20), 3389.

Koksal, O., Wrobel, P., Apaydin, G., Cengiz, E., Lankosz, M., Tozar, A., . . . Özkalayci, F. (2019). Elemental analysis for iron, cobalt, copper and zinc decorated hydroxyapatite synthetic bone dusts by EDXRF and SEM. *Microchemical Journal, 144*, 83-87.

Köksal, O. K., Apaydın, G., Cengiz, E., & Karabulut, K. (2016). *Calculation of K Shell Intensity Ratios and Line Widths of Ti and some of its compounds by means of 5, 96 keV energy.* Paper presented at the Journal of Physics: Conference Series.

Krause, M. O. (1979). Atomic radiative and radiationless yields for K and L shells. *Journal of Physical and Chemical Reference Data, 8*(2), 307-327.

Krause, M. O., & Oliver, J. (1979). Natural widths of atomic K and L levels, K α X-ray lines and several KLL Auger lines. *Journal of physical and chemical reference data, 8*(2), 329-338.

Krause, M. O., & Oliver, J. H. (1979). Natural Widths of Atomic K-Levels and L-Levels,K-Alpha X-Ray-Lines and Several Kll Auger Lines. *Journal of Physical and Chemical Reference Data, 8*(2), 329-338.

Kündeyi, K., Aylıkcı, N. K., Tıraşoğlu, E., Kahoul, A., & Aylıkcı, V. (2017). *Determination of natural line widths of Kα X-ray lines for some elements in the atomic range 50≤ Z≤ 65 at 59.5 keV.* Paper presented at the AIP Conference Proceedings.

Liu, Y., de Groot, K., & Hunziker, E. B. (2005). BMP-2 liberated from biomimetic implant coatings induces and sustains direct ossification in an ectopic rat model. *Bone, 36*(5), 745-757.

Madeira, T., Sampaio, J., Guerra, M., Parente, F., Indelicato, P., Santos, J., & Marques, J. (2015). Relativistic calculation of K-, L-and M-shell x-ray fluorescence yields for Ba. *Physica Scripta, 90*(5), 054009.

Marinangeli, L., Pompilio, L., Baliva, A., Billotta, S., Bonanno, G., Domeneghetti, M. C., . . . Piluso, E. (2015). Development of an ultra-miniaturised XRD/XRF instrument for the in situ mineralogical and

chemical analysis of planetary soils and rocks: implication for archaeometry. *Rendiconti Lincei, 26*(4), 529-537.

Minguez, F., Agra, M., Luruena, S., Ramos, C., & Prieto, J. (1990). Postantibiotic Effect of Isepamicin Compared to That of Other Aminoglycosides. *Drugs under Experimental and Clinical Research, 16*(5), 231-235.

Moonga, B. S., & Dempster, D. W. (1995). Zinc Is a Potent Inhibitor of Osteoclastic Bone-Resorption in-Vitro. *Journal of Bone and Mineral Research, 10*(3), 453-457.

Nie, L., Chen, D., Fu, J., Yang, S., Hou, R., & Suo, J. (2015). Macroporous biphasic calcium phosphate scaffolds reinforced by poly-L-lactic acid/hydroxyapatite nanocomposite coatings for bone regeneration. *Biochemical Engineering Journal, 98*, 29-37.

Obaid, S. S., Gaikwad, D. K., & Pawar, P. P. (2018). Determination of gamma ray shielding parameters of rocks and concrete. *Radiation Physics and Chemistry, 144*, 356-360. doi:https://doi.org/10.1016/j.radphyschem.2017.09.022

Obaid, S. S., Sayyed, M. I., Gaikwad, D. K., & Pawar, P. P. (2018). Attenuation coefficients and exposure buildup factor of some rocks for gamma ray shielding applications. *Radiation Physics and Chemistry, 148*, 86-94. doi:https://doi.org/10.1016/j.radphyschem.2018.02.026

Obeid, A., Balaa, H. E., Samad, O. E., Awad, R., & Badawi, M. S. (2022). Attenuation parameters of HDPE filled with different nano-size and bulk WO3 for X-ray shielding applications. *The European Physical Journal Plus, 137*(11), 1229.

Perişanoğlu, U., & Demir, L. (2015). A study of K shell X-ray intensity ratios of NixCr1− x alloys in external magnetic field and determination of effective atomic numbers of these alloys. *Radiation Physics and Chemistry, 110*, 119-125.

Perişanoğlu, U., Kavaz, E., Urtekin, E., & Demir, L. (2020). Examining alloying effect on KX ray intensity ratios and chemical shifts of the Zn, Mn and mixed spinel ferrites. *Applied Radiation and Isotopes, 156*, 108980.

Raj, S., Padhi, H. C., & Polasik, M. (1999). Influence of alloying effect on K beta/K alpha X-ray intensity ratios of V and Ni in VxNi1-x alloys. *Nuclear Instruments & Methods in Physics Research Section B-Beam Interactions with Materials and Atoms, 155*(1-2), 143-152.

Razavi, M., Fathi, M., Savabi, O., Vashaee, D., & Tayebi, L. (2015). In Vitro Analysis of Electrophoretic Deposited Fluoridated Hydroxyapatite

Coating on Micro-arc Oxidized AZ91 Magnesium Alloy for Biomaterials Applications. *Metallurgical and Materials Transactions a-Physical Metallurgy and Materials Science, 46a*(3), 1394-1404.

Rosa, J., de Carvalho, L. A. B., Ferreira, M. T., Gonçalves, D., Marques, M. P. M., & Gil, F. P. (2022). Chemical trace XRF analysis to detect sharp force trauma in fresh and burned bone. *Science & Justice, 62*(5), 484-493.

Sampaio, J., Madeira, T., Guerra, M., Parente, F., Santos, J., Indelicato, P., & Marques, J. (2015). Dirac-Fock calculations of K−, L−, and M-shell fluorescence and Coster-Kronig yields for Ne, Ar, Kr, Xe, Rn, and Uuo. *Physical Review A, 91*(5), 052507.

Saydam, M., Aksoy, C., Cengiz, E., Alaşalvar, C., Tıraşoğlu, E., & Apaydın, G. (2012). Determination of K shell fluorescence cross-section and Kβ/Kα intensity ratios for Fe, Se, Te, FeSe, FeTe and TeSe. *Radiation Physics and Chemistry, 81*(12), 1837-1841.

Schonfeld, E., & Janssen, H. (1996). Evaluation of atomic shell data. *Nuclear Instruments & Methods in Physics Research Section a-Accelerators Spectrometers Detectors and Associated Equipment, 369*(2-3), 527-533.

Scofield, J. (1973). Lawrence Livermore Laboratory Report No. *UCRL-51326*.

Scofield, J. H. (1974). Relativistic Hartree-Slater values for K and L X-ray emission rates. *Atomic Data and Nuclear Data Tables, 14*(2), 121-137.

Serro, A. P., Bastos, M., Pessoa, J. C., & Saramago, B. (2004). Bovine serum albumin conformational changes upon adsorption on titania and on hydroxyapatite and their relation with biomineralization. *Journal of Biomedical Materials Research Part A, 70a*(3), 420-427.

Stipniece, L., Stepanova, V., Narkevica, I., Salma-Ancane, K., & Boyd, A. R. (2018). Comparative study of surface properties of Mg-substituted hydroxyapatite bioceramic microspheres. *Journal of the European Ceramic Society, 38*(2), 761-768.

Sun, F., Pang, X., & Zhitomirsky, I. (2009). Electrophoretic deposition of composite hydroxyapatite–chitosan–heparin coatings. *Journal of materials processing technology, 209*(3), 1597-1606.

Tıraşoğlu, E., Söğüt, Ö., Tekbıyık, A., Apaydın, G., & Ertuğrul, B. (2007). Measurement of K shell fluorescence cross-section of Ca and K compounds. *Journal of Quantitative Spectroscopy and Radiative Transfer, 103*(2), 275-280.

Turhan, M. F., Akman, F., Kaçal, M. R., & Durak, R. (2017). *Measurements of K X-ray fluorescence cross-sections, fluorescence yields, level widths and radiative vacancy transition probabilities for the elements Zr, Mo, Cd, Er*

at 59.54 keV. Paper presented at the IOP Conference Series: Materials Science and Engineering.

Turhan, M. F., Akman, F., Polat, H., Kaçal, M. R., & Demirkol, İ. (2020). Gamma-ray attenuation behaviors of hematite doped polymer composites. *Progress in Nuclear Energy, 129*, 103504.

Uğurlu, M., & Demir, L. (2020). Relative K X-ray intensity ratios of the first and second transition elements in the magnetic field. *Journal of Molecular Structure, 1203*, 127458.

Vamze, J., Pilmane, M., & Skagers, A. (2015). Biocompatibility of pure and mixed hydroxyapatite and alpha-tricalcium phosphate implanted in rabbit bone. *Journal of Materials Science-Materials in Medicine, 26*(2).

Wei, G. B., & Ma, P. X. (2004). Structure and properties of nano-hydroxyapatite/polymer composite scaffolds for bone tissue engineering. *Biomaterials, 25*(19), 4749-4757.

Wong, C., Lu, W., Chan, W., Cheung, K., Luk, K., Lu, D., . . . Leong, J. (2004). In vivo cancellous bone remodeling on a strontium-containing hydroxyapatite (sr-HA) bioactive cement. *Journal of Biomedical Materials Research Part A: An Official Journal of The Society for Biomaterials, The Japanese Society for Biomaterials, and The Australian Society for Biomaterials and the Korean Society for Biomaterials, 68*(3), 513-521.

Yamaguchi, M., Oishi, H., & Suketa, Y. (1987). Stimulatory Effect of Zinc on Bone-Formation in Tissue-Culture. *Biochemical Pharmacology, 36*(22), 4007-4012. doi:Doi 10.1016/0006-2952(87)90471-0

Zschornack, G. H. (2007). *Handbook of X-ray Data*: Springer Science & Business Media.

Chapter 12

Comparison of Theoretical and Experimental Efficiencies of Plasmonic and Non-plasmonic CZTS/Si Heterojunction Solar Cell

Serap YİĞİT GEZGİN[1], Hamdi Şükür KILIÇ[1,2,3]

[1] Department of Physics, Faculty of Science, University of Selcuk, 42031 Selcuklu, Konya, Turkey
[2] High Technology Research and Application Center, University of Selcuk, 2031, Selcuklu, Konya, Turkey
[3] Directorate of Laser Induced Proton Therapy Application and Research Center, University of Selçuk, 42031, Selcuklu, Konya, Turkey

ABSTRACT

In order to increase the efficiency of solar cells, embedding plasmonic nanoparticles (NPs) into the absorber layers has been used as a light trapping method. NPs having an interesting property as **L**ocalized **S**urface **P**lasmon **R**esonance (LSPR) is not found in their bulk structure. NPs on which the light incidents can absorb photond at wavelengths in UV-Vis and NIR regions and can enhance the absorbance of the absorber layer into which it is embedded. In this way, more photoexcited electron-hole pairs are formed in absorber layer, thus increasing the photovoltaic (PV) electrical parameters and hence, the performance of the solar cell. The number of photons absorbed by very thin absorber layers (ultrathin film) is quite low. By adding NPs to these ultrathin films, the absorbance increases significantly. From this perspective, we have produced ultrathin CZTS films on SLG and n-Si wafers by running **P**ulse **L**aser **D**eposition (PLD) technique. Since films produced are ultra-thin in thickness, Au NPs were embedded into them using PLD technique to increase their absorbance. We studied the optical, electrical, morphological and crystal properties of non-plasmonic and plasmonic CZTS ultrathin films. The produced n-Si/CZTS solar cells showed PV properties. With the doping of Au NPs, a prominent rise in the efficiency of this solar cell was achieved. To verify the efficiency of the solar cell, theoretical calculation is required. Therefore, we have calculated the efficiency of plasmonic and non-plasmonic solar cells using SCAPS-1D program and compared it with experimental data. It has been noticed that the experimental and theoretical results were in well compatible with each other.

Keywords: Solar Cell, plasmonic, nanoparticle, SCAPS-1D, CZTS thin film

Introduction

The thin film solar cells (second generation) are produced based on thin film materials which contain p-type active layers such as $CuInGaSe_2$ (CIGS), CdTe, Cu_2ZnSnS_4 (CZTS) etc [1]. Among these materials, CZTS material has very important advantageous and remarkable properties for the production of solar cells compared to other materials in terms of being environmentally friendly and containing abundant elements in nature. CZTS is a p-type semiconductor consisting of four elements which has $>10^4$ cm^{-1} of high absorption coefficient a in the visible region and 1.5 eV energy band gap [2]. A typical CZTS thin film solar cell consists of Mo back contact, p-type CZTS absorber layer, n-type CdS buffer layer, i-ZnO window layer and AZO-transparent conductive oxide electrode layer. In addition to CZTS thin-film solar cell, studies have also been carried out on p-CZTS/n-Si heterojunction solar cells in recent years. Such solar cells are photovoltaic (PV) devices that are very easy to manufacture and save time and energy, and they have the potential to be used as sub-solar cells in tandem solar cells. However, in these solar cells, the light incomes on CZTS thin film, and the thin film must not be too thick for the some charge carriers to reach the depletion region. Otherwise, this leads the photo-excited minority charge carriers to be limited and lower photocurrent [3]. In order to generate more minority charge carriers in the thin film and increase the charge aggregation in the solar cell, the plasmonic NPs can be used as a light trapping method [4].

Plasmonic metal nanoparticles composed of materials such as Copper (Cu), Silver (Ag) and Gold (Au) that contain an interesting optical property like Localised Surface Plasmon Resonance (LSPR) [4, 5]. When the plasmonic NP is exposed to the light, the plasmons (conduction electrons) in the particle oscillate in harmony with the light oscillating as an electromagnetic field. This event is referred to as LSPR [6, 7]. The position of LSPR occurs at any wavelength in spectrum strongly dependens on particle size, shape, and particle density [4, 6]. LSPR peak wavelength can shift towards longer wavelengths in solar spectrum as the particle size and particle density increase. While most solar cells absorb higher number of photons in visible region, they exhibit low photon absorption in NIR region. At this point, with the embedding of plasmonic NPs inside the solar cell, there are increased that photon absorption in near-infrared region and photo current of the solar cell[8].

The SCAPS-1D (Solar-Cell-Capacitance-Simulator) is a software program that calculates the PV parameters of solar cells such as p-n heterojunction solar cell, dye solar cell and prevoskite solar cell etc [9, 10]. In particular, it calculates and gives information about the possible performance of the solar cell depending on the parameters such as an operating temperature, radiative recombination coefficient, interface defect density, auger electron-hole capture coefficient[11].

In this study, CZTS-ultrathin film was deposited on soda lime glass (SLG) and n-Si wafer substrate with 2400 laser pulse numbers, using Pulse Laser Ablation (PLA). Then, Au NPs were embedded into CZTS-ultrathin film. PV parameters of the produced CZTS/Si and plasmonic CZTS/Si solar cells were determined. In order to prove the accuracy and consistency of the performance of solar cells, there is a need to calculate PV parameters with simulation programs. We have calculated PV parameters of plasmonic solar cells by SCAPS-1D program and we have seen that theoretical and experimental results are compatible with each other. The determined results were discussed in detail in the article.

Experimental

Ag/CZTS/Si/Au solar cells were formed, using PLA technique. For material ablation, the laser beam with a 5 ns width at the first harmonic 1064 nm wavelength, 10 Hz repetition rate which was output from a ns pulsed-Minilite Nd:YAG laser system. Cleaning processes of Si wafer and SLG substrates are given in our other article [2]. Before the experiment, the background pressure in vacuum chamber was reduced to 10^{-6} mbar to ensure a clean medium.

Firstly, CZTS-A ultrathin film was grown on SLG and n-Si wafer substrate with 2400 laser pulse number using a laser beam in 15 mJ energy. Au (back) and Ag (front) contacts were coated on Si wafer back surface and on CZTS-ultrathin film by PLD technique, respectively. CZTS-ultrathin films were heat treated at 375°C sulfurization temperature. Then, Au plasmonic NPs were deposited on SLG substrate with 26 mJ and 36 mJ laser pulse energies. Then, Plasmonic CZTS thin film (CZTS-PA) thin films were produced by doping Au NPs into CZTS thin films with high laser energy. The figure 1 shows a schematic figure of Ag/CZTS-A and CZTS-PA/n-Si/Au solar cells formed.

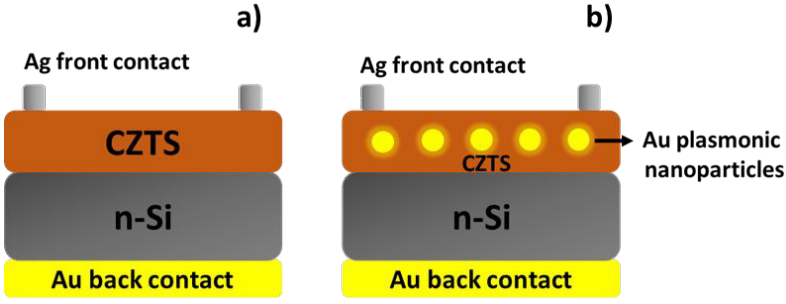

Figure 1. Schematic image of **a)** Ag/(CZTS-A) and **b)**(CZTS-PA)/n-Si/Au solar cells

Structural, crystalline and optical properties of CZTS and plasmonic CZTS-ultrathin films were investigated by AFM, EDX, XRD ve UV-vis analyses. The J-V curve of their solar cells in the illumination environment was obtained and their PV parameters were determined. Then, PV parameters of CZTS and plasmonic CZTS solar cells were calculated using the SCAPS-1D program.

Discussion

1.1. Properties of non-plasmonic and plasmonic CZTS ultrathin films

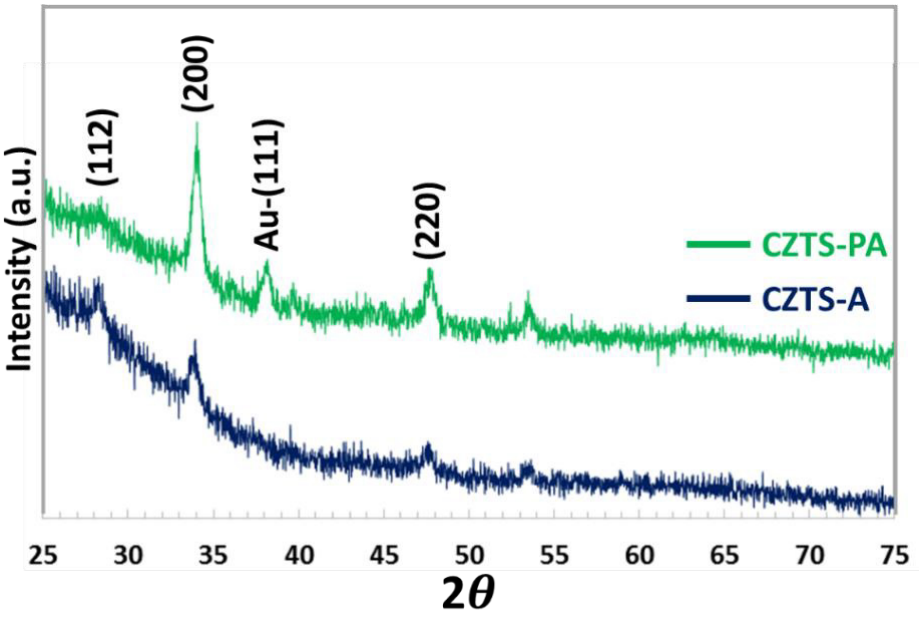

Figure 2. XRD spectra of CZTS-A and CZTS-PA ultrathin films

According to XRD spectrum given by Figure 2, CZTS and plasmonic CZTS thin films were grown in polycrystalline structure. Crystallization occurred in (220), (200) and (112) orientations located on 2θ=47°, 33°, 28°, respectively [2]. In CZTS-PA ultrathin films, Au peak were formed in (111) orientation on 2θ=38° angle. The intensity of the main peak on (112) orientation in CZTS-A thin film decreased while the intensities of peaks on (200) and (220) orientations increased by the embedding of Au NPs. This is due to the fact that Au atoms fill different atomic vacancies in CZTS-ultrathin films depending on the film thickness.

The Scherrer equation expressed in equation (Eq.) 1 that calculates the crystallite size:

$$S = 0.94\lambda/\beta Cos\theta \qquad (1)$$

S is crystallite size, β is the full-width at half-maximum of diffraction main peak, θ is that Bragg diffraction angle, λ is wavelength of X-ray [2]. The crystal sizes of CZTS-A and CZTS-PA ultrathin films that are 7.34 nm and 12.1 nm, respectively. The crystal size of thin films increased significantly with the doping of Au NPs. Au atoms filled the voids in the CZTS thin films, causing the crystal size to expand.

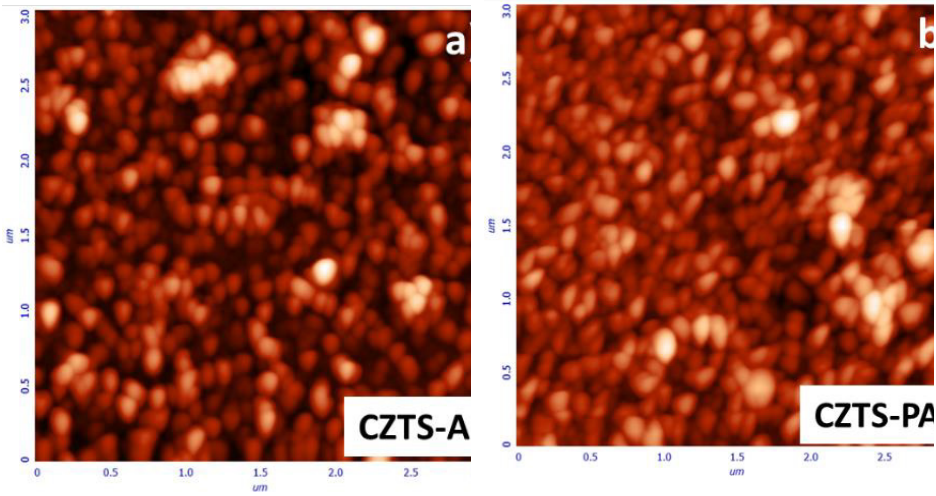

Figure 3. AFM images of **a)** CZTS-A and **b)** CZTS-PA ultrathin films

According to AFM images in figure 3, CZTS-A ultrathin film has non homogeny particle size distribution. As a result of the doping of Au NPs, the size of the particles forming CZTS-PA thin film increased slightly, and partly agglomeration of particles originating from Au NPs occurred in these thin films. This is consistent with the increase in crystal size.

EDX-Spectrum and Table given as an inset of figure 4 show the ratios of atomic weights of Au, Cu, Zn, Sn and S elements formed CZTS-PA ultrathin film. CZTS-PA ultrathin films are Cu- and Sn-rich and Zn poor. Sn_{Zn} donor defects and Cu_{Zn} acceptor defects can occur in CZTS-PA ultrathin films. Also, it can be predicted that Au atoms replace Zn atoms in CZTS thin film with Au atoms embedding into CZTS-A-ultrathin film.

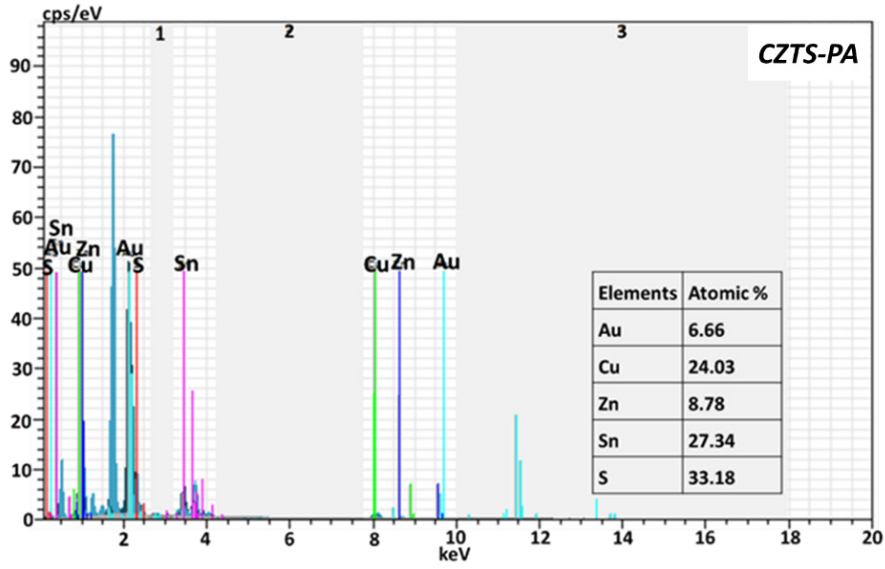

Figure 4. EDX Spectra (the atomic weights of elements in the insert table) of CZTS-PA ultrathin films

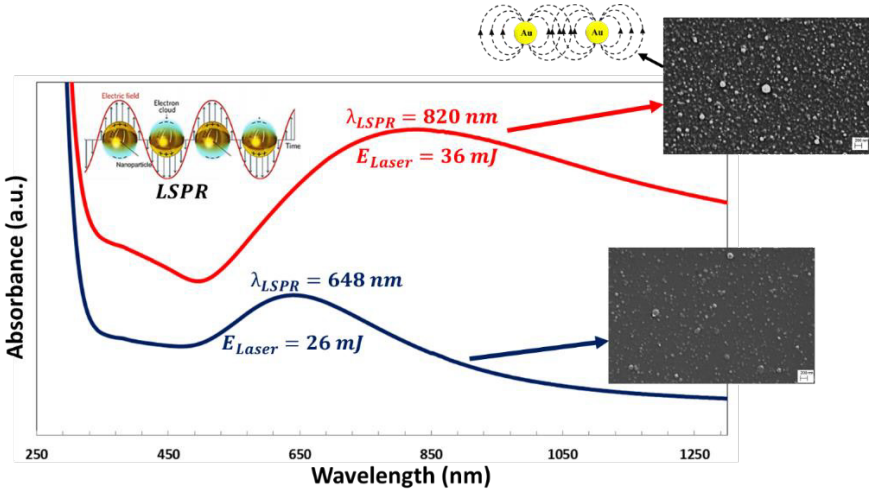

Figure 5. Absorption spectra of Au plasmonic NPs grown based the laser pulse energy of 26 mJ and 36 mJ and SEM images of Au NPs in insert the small square.

Figure 5 represents absorption spectra of Au NPs grown by the laser pulse energy of 26 mJ and 36 mJ. Au plasmonic NPs exhibited LSPR property. So, when light falls on an Au plasmonic NP, electrons in the particle are excited by the light's electric field and accumulate on the other surface of the particle, and

positive charges accumulate on the other surface. Thus, a dipole is formed on the surface of NP[12]. If the electric field created by the particle is opposite to that of the light's electric field, light damping occurs around NP. Thus, light is damped around the plasmonic NPs doped into any thin film, allowing the thin film to absorb more photons and form electron-hole pairs.

The peak wavelength of LSPR of Au NPs shifted towards to longer wavelength with some increase of laser pulse energy. So, according to SEM images in figure 5, as the laser pulse energy risen, the particle size and density enhanced. Close field enhancement occurs between Au NPs located very close to each other, and this field enhancement affects the oscillatory motion of electrons in NPs and causes LSPR wavelength to increase. Also, as the particle size increases, there is a decrease in oscillation and frequency of electrons within particles. This causes the LSPR wavelength to increase and red shift[4, 6, 13, 14].

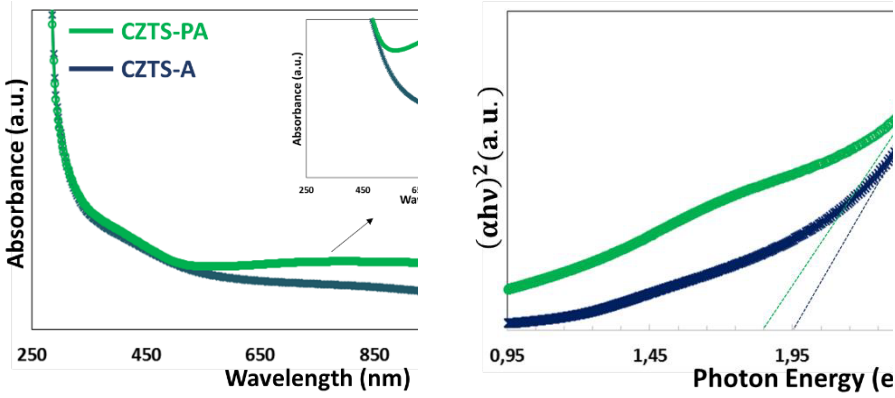

Figure 6. a) The absorption spectrum and **b)** Tauc plots of CZTS-(A&PA)

CZTS-A ultrathin film absorbs very few photons in Vis and UV regions. However, when Au NP is doped into CZTS-A ultrathin film with maximum laser energy, CZTS-PA thin film absorbs a high amount of photons at a wavelength of ~763 nm due to LSPR property of Au NPs.

The band gap of CZTS-ultrathin film that is calculated by Eq (2).

$$\alpha h\nu = A\left(h\nu - E_g\right)^{1/2} \quad \ldots\ldots \quad (2)$$

A, E_g and $h\nu$ are constant, energy band gap and photon energy, respectively. Band gaps of CZTS-(A&PA)-ultrathin films are determined from Tauc graph obtained by using Eq (2). The energy band gap of CZTS-A and CZTS-PA ultrathin films are in 1.95 eV and 1.85 eV, respectively. E_g value of CZTS-PA

thin films decreased, as thin film absorbs a higher photons due to LSPR properties with Au NPs embedded into ultrathin film.

The refractive index (n) of a semiconductor is an important parameter which affects the efficiency of solar cell. The refractive index is calculated based on the band gap, using Moss relation in Eq (3):

$$E_g n^4 = k \tag{3}$$

k is a constant and has a value of 108 eV. n and E_g are stated by Eq (4), using Herve and Vandamme;

$$n = \sqrt{1 + \left(\frac{A}{E_g + B}\right)^2} \tag{4}$$

where A-constant is 13.6 eV and B-constant is 3.4 eV. The refractive indices determined by Moss and Herve and Vanamme methods represent very good agreement with each other as shown in Table 1. Also, the refractive index of CZTS-PA thin film is slightly larger than that of CZTS-A thin film.

Dielectric constant is a coefficient determined by the electric field between charges in a semiconductor, and is a significant parameter that express charge collection in solar cells. In the article, the high frequency dielectric constant (ε_∞) and the static dielectric constant (ε_o) have been obtained by Eq (5) and Eq (6), respectively:

$$\varepsilon_\infty = n^2 \tag{5}$$

$$\varepsilon_o = 18.52 - 3.08E_g \tag{6}$$

CZTS-PA ultrathin film has slightly high dielectric coefficients leading to facilitate charge transitions, increase the lifetime of charges and stabilizes charge mobility in thin films due to LSPR property of Au plasmonic NPs [15, 16].

Table 1. Refractive index (n), high frequency dielectric constant (ε_∞) and static dielectric constant (ε_o) of plasmonic (CZTS-PA) and non plasmonic (CZTS-A) thin films

Samples	E_g (eV)	Moss relation		Herve&Vandemme		Static Dielectric Constant, ε_o
		n	ε_∞	n	ε_∞	
CZTS-A	1.95	2.72	7.44	2.73	7.46	12.51
CZTS-PA (Plas.)	1.90	2.74	7.53	2.75	7.58	12.66

1.2. Determination of theoretical and experimental parameters of CZTS-PA/Si solar cells.

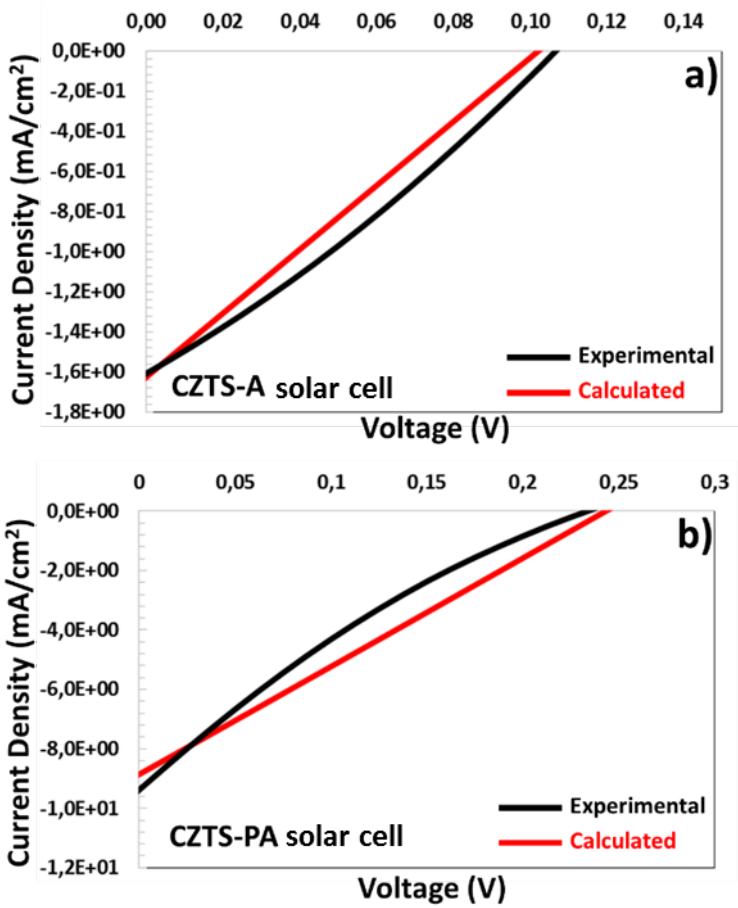

Figure 7. J-V characteristics of experimentally produced and modelled **a)** CZTS-A and **b)** CZTS-PA solar cells

Considering $J-V$ characteristics demonstrated in figure and the data in the Table, the efficiency of CZTS-PA solar cell is higher than the efficiency of

CZTS-A solar cell. CZTS-A thin film contains a high number of defects and traps since it has a very weak crystal structure. Therefore, minority charge carriers easily recombine within these traps, shortening their lifetime and limiting charge aggregation and efficiency in the solar cell. Due to LSPR property of Au NP, plasmonic CZTS-PA solar cell's Jsc value increased 6 times and its η value increased 9 times compared to those of non plasmonic CZTS-A solar cell. This is attributed to the formation of hot electrons [17-21] and the near field enhancement between the Au particles in the solar cell. That is, the light coming into the CZTS-PA thin film excites the electrons in the Au NPs and removes them to the LSP band. Then the electrons are transmitted from the LSP band to the conduction band of the CZTS semiconductor. Thus, it generates a large number of hot electrons in CZTS-PA solar cell. Due to the doped Au NPs, the electrons formed in the area close to the depletion region as shown in figure 8a, easily reach the depletion region quickly [22-25]. Thus, charge accumulation and photocurrent increase in the solar cell, resulting in an augmentation in power conversion efficiency. Also, the electrical fields created by two Au NPs located very close to each other cause overlap and the near field enhancement (in Figure 5). Thus, a large number of electron-hole pairs are occured between NPs by the effect of the electric field, and minority charge carriers easily reach the depletion region (in Figure 8b), increasing charge aggregation and efficiency.

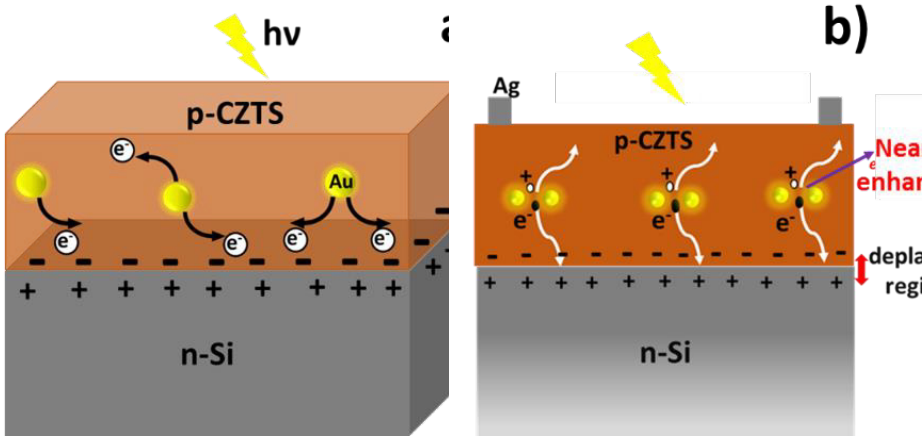

Figure 8. a) Hot electron formation and **b)** the near field enhancement in the solar cell

Tablo 2. The PV parameters of experimentally produced and modelled CZTS-(A&PA) solar cells

Solar Cells	J_{sc}	V_{oc}	*FF*	*η (%)*
CZTS-A (experimental)	1.60 mA/cm^2	100 mV	0.30	0.06
CZTS-A (calculated)	1.62 mA/cm^2	102 mV	0.25	0.04
CZTS-PA (experimental)	9.30 mA/cm^2	250 mV	0.18	0.53
CZTS-PA (calculated)	8.85 mA/cm^2	248 mV	0.24	0.53

Modelling and simulating solar cells is very important to verify PV parameters displayed by solar cells. One of the most commonly used simulation programme for the solar cells is SCAP-1D. In this study, we have used SCAPS-1D program to input the properties of the semiconductors and metal contacts shown in Table 3. Meanwhile, we calculated the absorption coefficient of thin films using $W = 2.303 \times A/T$ (W=Absorption coefficient, A=Absorption, T: Thin film thickness) equation [26] and obtained the wavelength dependent absorption coefficient spectrum presented in Figure 9 and entered the file into the program. In addition, the band gap and thickness of thin films determined experimentally that were introduced to the program.

According to table 2 and $J-V$ graph in Figure 7, PV parameters of experimentally produced CZTS solar cells and the calculated parameters of the modelled solar cells are compatible with each other, by representing slight difference. But, FF values of calculated solar cells are relatively larger than those of experimental CZTS solar cells. Although this difference is not significant, it can be attributed to contact resistance, grain boundary number and dangle bonds in experimentally generated solar cells. As a result, PV performance of all CZTS solar cells has been verified to 300 K operate temperature.

Table 3 Properties of n-Si and CZTS materials.

Parameters of this layers	**n-Si [27]**	**CZTS (61nm) [28-31]**	**Plas. CZTS (61nm)**
Band Gap (eV)	1.12	1.95 (Experimental)	1.85 (Experimental)
Electron affinity (eV)	4.05	3.9	3.7
Dielectric permittivity (relative)	11.9	6.5	9.5
Conduction band effective density of states (cm^{-3})	2.80 E+19	2.20 E+18	2.20 E+18
Valence band effective density of states (cm^{-3})	1.04 E+19	1.80 E+19	1.80 E+19
Electron thermal velocity (cm/s)	1.00 E+7	1.00 E+7	1.00 E+7
Hole thermal velocity (cm/s)	1.00 E+7	1.00 E+7	1.00 E+7
Electron mobility (cm^2/Vs)	1350	26	26
Hole mobility (cm^2/Vs)	500	10	10
Shallow donor density N_D (cm^{-3})	1 E+17	0	0
Shallow acceptor density N_A (cm^{-3})	0	8.00 E+15	1.00 E+16
Absorption coefficient	SCAPS	Calculated absorptions coefficients	Calculated absorptions coefficients
Thickness	500 μm	61 nm (Experimental)	61 nm (Experimental)
Contacts		Back Contact (Au)	Front Contact (Ag)
Metal work function (eV)		5.1	4.6
Surface recombination velocity of electrons (cm/s)		1E+7	1E+5
Surface recombination velocity of holes (cm/s)		1E+5	1E+7
Device parameter			
Cell Temperature (K)			300

CONCLUSIONS

Two Ag/CZTS/n-Si/Au solar cells were fabricated based on CZTS ultrathin film in 61 nm thicknesses, by PLA. Then, Au NPs were produced depending on the laser pulse energy. With some increase in laser pulse energy, LSPR peak shifted from 648 nm to 820 nm wavelength. Au NPs were embedded into CZTS ultrathin film with maximum laser pulse energy. The crystal size, photon absorption of plasmonic CZTS thin films increased, and its band gap decreased. As seen in EDX spectrum, the embedded Au atoms replaced the Zn atoms in CZTS A ultrathin film.

Due to LSPR property of Au plasmonic NPs, the efficiency of plasmonic CZTS-PA solar cells has increased significantly. It is predicted that the increase in efficiency can be due to the hot electron formation and the near field enhancement increase between Au NPs. PV parameters of CZTS-A and CZTS-PA solar cells were calculated using SCAPS-1D simulation program. As a result, the calculated and experimental PV parameters were found to be compatible with each other, by slightly different.

Acknowledgment

Authors kindly would like to thank:

- Selçuk University, High Technology Research and Application Center for supplying with Infrastructure and
- Selçuk University, Scientifc Research Projects Coordination (BAP) Unit for grands via projects with references of 20401018 and 18401178
- Dr. Marc Burgelman's group, University of Gent, Belgium for providing permission for us to use SCAPS-1D simulation program

REFERENCES:

Suryawanshi, M., et al., *CZTS based thin film solar cells: a status review.* Materials Technology, 2013. **28**(1-2): p. 98-109.

Gezgin, S.Y., A. Houimi, and H.Ş. Kılıç, *Production and photovoltaic characterisation of n-Si/p-CZTS heterojunction solar cells based on a CZTS ultrathin active layers.* Optik, 2019. **199**: p. 163370.

Liu, F., et al., *Beyond 8% ultrathin kesterite Cu 2 ZnSnS 4 solar cells by interface reaction route controlling and self-organized nanopattern at the back contact.* NPG Asia Materials, 2017. **9**(7): p. e401-e401.

García, M.A., *Surface plasmons in metallic nanoparticles: fundamentals and applications.* Journal of Physics D: Applied Physics, 2011. **44**(28): p. 283001.

Gezgin, S.Y., A. Kepceoğlu, and H.Ş. Kılıç. *An investigation of localised surface plasmon resonance (LSPR) of Ag nanoparticles produced by pulsed laser deposition (PLD) technique*. in *AIP Conference Proceedings*. 2017. AIP Publishing.

Noguez, C., *Surface plasmons on metal nanoparticles: the influence of shape and physical environment.* The Journal of Physical Chemistry C, 2007. **111**(10): p. 3806-3819.

Gezgin, S.Y., et al. *Plasmonic tuning of gold doped thin films for layers of photovoltaic devices*. in *AIP Conference Proceedings*. 2016. AIP Publishing.

Yiğit Gezgin, S. and H.Ş. Kiliç, *The effect of Ag plasmonic nanoparticles on the efficiency of CZTS solar cell: an experimental investigation and numerical modelling.* Indian Journal of Physics, 2023. **97**(3): p. 779-796.

Piñón Reyes, A.C., et al., *Study of a lead-free perovskite solar cell using CZTS as HTL to achieve a 20% PCE by SCAPS-1D simulation.* Micromachines, 2021. **12**(12): p. 1508.

AlZoubi, T., et al., *Efficiency boost of CZTS solar cells based on double-absorber architecture: Device modeling and analysis.* Solar Energy, 2021. **225**: p. 44-52.

Khaaissa, Y., et al., *Experimental and numerical simulation of deposition time effect on ZnS thin films for CZTS-based solar cells.* Optical and Quantum Electronics, 2021. **53**(9): p. 1-21.

Gezgin, S.Y., et al., *Effect of Ar Gas Pressure on LSPR Property of Au Nanoparticles: Comparison of Experimental and Theoretical Studies.* Nanomaterials, 2020. **10**(6): p. 1071.

Martinsson, E., *Nanoplasmonic sensing using metal nanoparticles*. 2014, Linköping University Electronic Press.

Huang, X. and M.A. El-Sayed, *Gold nanoparticles: Optical properties and implementations in cancer diagnosis and photothermal therapy.* Journal of advanced research, 2010. **1**(1): p. 13-28.

Su, R., et al., *Dielectric screening in perovskite photovoltaics.* Nature communications, 2021. **12**(1): p. 1-11.

Gezgin, S.Y.ğ.t. and H.Ş. Kılıç, *An improvement on the conversion efficiency of Si/CZTS solar cells by LSPR effect of embedded plasmonic Au nanoparticles.* Optical Materials, 2020. **101**: p. 109760.

Meškinis, Š., et al., *Photovoltaic properties and ultrafast plasmon relaxation dynamics of diamond-like carbon nanocomposite films with embedded Ag nanoparticles.* Nanoscale research letters, 2017. **12**(1): p. 1-10.

Mousa, A.M., R.A. Ismail, and M.H. Amin, *Hybrid p-Au@ PbI2/n-Si heterojunction photodetector prepared by pulsed laser ablation in liquid.* Optik, 2019. **183**: p. 933-941.

Wang, L., et al., *Plasmonic silver nanosphere enhanced ZnSe nanoribbon/Si heterojunction optoelectronic devices.* Nanotechnology, 2016. **27**(21): p. 215202.

Boriskina, S.V., H. Ghasemi, and G. Chen, *Plasmonic materials for energy: From physics to applications.* Materials Today, 2013. **16**(10): p. 375-386.

Khan, R., et al., *Localized surface plasmon enhanced photoluminescence of ZnO nanosheets by Au nanoparticles.* Materials Letters, 2016. **163**: p. 8-11.

Saragih, A.D., et al., *Characterization of Ag-doped Cu2ZnSnSe4 bulks material and their application as thin film semiconductor in solar cells.* Materials Science and Engineering: B, 2017. **225**: p. 45-53.

Su, Z., et al. *Cation substitution of CZTS solar cell with> 10% efficiency*. in *2016 IEEE 43rd Photovoltaic Specialists Conference (PVSC)*. 2016. IEEE.

Kaur, K., et al., *Nanoscale charge transport and local surface potential distribution to probe defect passivation in Ag doped Cu2ZnSnS4 absorbing layer.* Nanotechnology, 2018. **30**(6): p. 065706.

Wu, Y., et al., *Substitution of Ag for Cu in Cu2ZnSn (S, Se) 4: Toward wide band gap absorbers with low antisite defects for thin film solar cells.* Nanomaterials, 2020. **10**(1): p. 96.

Bakr, N.A., Z.T. Khodair, and H.I. Mahdi, *Influence of thiourea concentration on some physical properties of chemically sprayed Cu2ZnSnS4 thin films.* International Journal of Materials Science and Applications, 2016. **5**(6): p. 261-270.

Moon, M.M.A., et al., *Design and Simulation of FeSi2-Based Novel Heterojunction Solar Cells for Harnessing Visible and Near-Infrared Light.* physica status solidi (a), 2020. **217**(6): p. 1900921.

Darvishzadeh, P., H. Sohrabpoor, and N.E. Gorji, *Numerical device simulation of carbon nanotube contacted CZTS solar cells.* Optical and Quantum Electronics, 2016. **48**(10): p. 480.

Tousif, M.N., et al., *Investigation of Different Materials as Buffer Layer in CZTS Solar Cells Using SCAPS.* Journal of Clean Energy Technologies, 2018. **6**(4): p. 293-296.

Frisk, C., et al., *Combining strong interface recombination with bandgap narrowing and short diffusion length in Cu2ZnSnS4 device modeling.* Solar Energy Materials and Solar Cells, 2016. **144**: p. 364-370.

Haddout, A., et al., *Influence of composition ratio on the performances of kesterite solar cell with double CZTS layers—A numerical approach.* Solar Energy, 2019. **189**: p. 491-502.

Chapter 13

On Sturm-Liouville Problems Including the Square-Root of the Eigenvalue Parameter in one Boundary Condition

Ayşe KABATAŞ[1]

[1]*Asst. Prof. Dr.; Karadeniz Technical University Science Faculty Department of Mathematics.*
akabatas@ktu.edu.tr ORCID No: 0000-0003-3273-3666

ABSTRACT

Sturm-Liouville theory is based on the works of Sturm and Liouville published in 1836-1837. Until then, analytical solutions for differential equations were sought. Sturm and Liouville were among the first to see the limits of this approach and to interpret the properties of solutions directly from the equation when analytic expressions for the solutions could not be obtained. Their work had such an impact that it extended beyond differential equations to analysis. More than a thousand paper has been written in this field by mathematicians, physicist, engineers and others. This subject is still being actively studied today. Dozens of papers are published on Sturm-Liouville problems every year.

Sturm and Liouville dealt with the regular problem in their 1836-37 papers. Hermann Weyl (1910) started working on singular Sturm-Liouville problems. Neumann and Stone proved the general spectral theorem for unbounded self-adjoint operators in Hilbert space, Titchmarsh (1962) gave essential results and quantum mechanics developed in the 1920's and 1930's. All this has triggered interest into the spectral theory of Sturm-Liouville operators (Zettl, 2010).

Some problems of spectral theory were also studied in (Başkaya, 2020; Başkaya, 2021b; Coşkun et al., 2019; Harris, 1997; Kabataş 2022b). In all these articles, the boundary conditions do not include the spectral parameter. However, the spectral parameters can appear not only in the equation but also in the boundary conditions.

The main goal of this chapter is to show how can be obtained asymptotic formulae of the solutions and Green's functions for a regular Sturm-Liouville problem with the eigenvalue parameter contained in one boundary condition.

Keywords: Sturm-Liouville problem, asymptotic, Green's function, spectral parameter, potential function

INTRODUCTION

We will deal with the second-order ordinary differential equation

$$y'' + [s^2 - q(x)]y = 0 \tag{1}$$

on a finite interval. This equation is called the *Sturm-Liouville equation*, or often the one-dimensional *Schrödinger equation*. The coefficient $q(x)$, frequently called the *potential*, satisfies certain smoothness conditions, depending on the studied problem . The real number s is called the *spectral parameter*.

Consider the equation (1) on the interval $(0, \pi)$. Let q be a real-valued function and its differentiation exists and be integrable. Together with the equation (1), consider the homogeneous boundary conditions

$$y(0) = 0,\ ay'(\pi) + sy(\pi) = 0 \tag{2}$$

where $a \neq 0$ is real. The Sturm-Liouville problem (1)-(2) is treated in (Hochstadt, 1967;1). The asymptotic approximations for the eigenvalues and the corresponding eigenfunctions of the problem are given when the potential $q(x)$ is integrable.

In this chapter, we will show how improve more precise asymptotics for solutions of (1)-(2) by using the similar approach to Harris (1997). In addition, we also gain asymptotic formula for the Green's function of the problem with these new estimates for solutions by Fulton's (1977) method.

Sturm-Liouville problems are typical problems of applied mathematics which are formulated to make clear the real-world applications in physics, engineering and, more recently, in biology and the social sciences. For example, the sounds of a guitar. Plucking a string exposes the sound. Here, the motion of the vibrating string can be described by a wave equation. Seperation of variables in initial boundary value problems and steady-state problems for partial differential equations such as the example lead to Sturm-Liouville eigenvalue and boundary value problems for ordinary differential equations. Usually, the eigenvalue parameter s appears linearly only in the differential equation of the classic problems. However, such problems are encountered in mathematical physics, which contain eigenvalue parameters not only in the differential equation, but also in the boundary conditions linearly or nonlinearly.

In this chapter, the approximate solutions of the Sturm-Liouville problem are focused. Such procedures are essential because explicit evaluation for the

solutions of a differential equation is rarely possible. In 1977, Fulton considered the Sturm-Liouville problem with one boundary condition dependent on the spectral parameter and obtained asymptotic estimates of eigenvalues and eigenfunctions. Since 1977, Sturm-Liouville problems having the spectral parameter in the boundary condition were sought by many authors (Başkaya, 2018a; Başkaya, 2018b; Başkaya, 2018c; Başkaya, 2021a; Benedek and Panzone, 1981; Coşkun and Başkaya, 2010; Coşkun and Başkaya, 2018; Coşkun and Kabataş, 2013).

Boundary value problems can be investigated also through the methods of Green's function. Green's functions are the main device to solve the ordinary and partial differential equations which may be unsolvable by other methods. So those functions are invaluable in the understanding of physical systems because boundary value problems appear frequently in physics.

Burkhardt (1894) firstly used the application of Green's function for ordinary differential equations containing boundary conditions. Today, there are a lot of studies in the literature on this issue (see Coşkun and Kabataş, 2016; Coşkun et al., 2017, Fulton, 1977; Kabataş, 2022a; Kabataş, 2023). Green's function can often be determined explicitly, and this is very useful to solve the problem. Calculation of Green's functions is also possible using the Sturm-Liouville theory. This enables asymptotic representation of Green's function as we will seek in this chapter.

THE METHOD

In this section, the method used by Harris (1997) will be introduced and adapted to the problem under consideration.

Let $y(x,s)$ denote a complex-valued solution of (1). If we apply the following transformation

$$w(x,s)=\frac{y'(x,s)}{y(x,s)}$$

to the equation (1), we find the Riccati equation

$$w'=-s^2+q-w^2. \tag{3}$$

We define

$$M(x,s):=Re\{w(x,s)\}, \tag{4}$$

$$N(x,s) := Im\{w(x,s)\}. \tag{5}$$

It is shown by (Harris, 1997:153) that any nontrivial real-valued solution, z, of (1) can be expressed as

$$z(x,s) = c_1 exp\left(\int_0^x M(t,s)dt\right) cos\left\{c_2 + \int_0^x N(t,s)dt\right\} \tag{6}$$

with

$$z'(x,s) = c_1 M(x,s) exp\left(\int_0^x M(t,s)dt\right) cos\left\{c_2 + \int_0^x N(t,s)dt\right\} - c_1 N(x,s) exp\left(\int_0^x M(t,s)dt\right) sin\left\{c_2 + \int_0^x N(t,s)dt\right\}. \tag{7}$$

We now seek the functions $M(x,s)$ and $N(x,s)$ introduced above in the asymptotical manner. We consider (3) on $[0,\pi]$ and investigate a solution of the form

$$w(x,s) = is + \sum_{n=1}^{\infty} w_n(x,s). \tag{8}$$

Substituation (8) into (3) gives

$$w_1' + 2isw_1 + w_2' + 2isw_2 + \sum_{n=3}^{\infty} (w_n{}' + 2isw_n) = q - w_1^2 - \sum_{n=3}^{\infty} \left(w_{n-1}^2 + 2w_{n-1} \sum_{m=1}^{n-2} w_m \right).$$

We choose

$$w_1' + 2isw_1 = q,$$

$$w_2' + 2isw_2 = -w_1^2,$$

$$w_n{}' + 2isw_n = -\left(w_{n-1}^2 + 2w_{n-1} \sum_{m=1}^{n-2} w_m \right), n \geq 3$$

and we find for the w_n 's that

$$w_1(x,s) = -e^{-2isx}\int_x^\pi e^{2ist}q(t)dt, \tag{9}$$

$$w_2(x,s) = e^{-2isx}\int_x^\pi e^{2ist}w_1^2(t,s)dt, \tag{10}$$

$$w_n(x,s) = e^{-2isx}\int_x^\pi e^{2ist}\left(w_{n-1}^2 + 2w_{n-1}\sum_{m=1}^{n-2} w_m\right)dt\,,\ \ n \geq 3.$$

It is proven by (Harris ,1997:157) that $\sum_{n=1}^{\infty} w_n{}'(x,s)$ is uniformly absolutely convergent and the series $is + \sum_{n=1}^{\infty} w_n(x,s)$ is thus a solution of (3) and

$$M(x,s) = Re\sum_{n=1}^{\infty} w_n(x,s),$$

$$N(x,s) = s + Im\sum_{n=1}^{\infty} w_n(x,s).$$

We suppose that there exist functions $H(x)$ and $\eta(s)$ so that

$$\left|\int_x^\pi e^{2ist}q'(t)dt\right| \leq H(x)\eta(s), \qquad x \in [0,\pi]$$

where

(i) $H(x) := \int_x^\pi |q'(x)|dx$ is a decreasing function of x,
(ii) $H(x) \in L[0,\pi]$,
(iii) $\eta(s) \to 0$ as $s \to \infty$.

For $q' \in L[0,\pi]$ the existence of the H and η functions may be established for s positive as follows. We note that, avoiding the trivial case $\int_x^\pi |q'(x)|dx = 0$, $\left|\int_x^\pi e^{2ist}q'(t)dt\right| \leq \int_x^\pi |q'(x)|dx < \infty$. So, if we define

$$Y(x,s) := \begin{cases} \left|\int_x^\pi e^{2ist}q'(t)dt\right| \leq \int_x^\pi |q'(x)|dx\,, & if\ \int_x^\pi |q'(x)|dx \neq 0\,, \\ 0, & if\ \int_x^\pi |q'(x)|dx = 0, \end{cases} \tag{11}$$

then $0 \leq Y(x,s) \leq 1$ and we set $\eta(s) := sup_{0\leq x\leq \pi} Y(x,s)$. $\eta(s)$ is well-defined by (11) and $s^{-1}\eta(s) \to 0$ as $s \to \infty$ (Başkaya, 2018c:249; Harris, 1997:160).

With the approximation in (Coşkun and Başkaya, 2010:215) that there exist a sequence $\{k_n\}$ of real numbers with

$$|w_n(x,s)| \leq k_n[s^{-1}\eta(s)]^n. \tag{12}$$

Thus, we can write

$$w(x,s) = is^{1/2} + w_1(x,s) + O(s^{-2}\eta^2(s)) \tag{13}$$

where

$$w_1(x,s) = -\frac{1}{2}s^{-1}q(\pi)sin[2s(\pi - x)]$$

$$+\frac{1}{2}s^{-1}cos(2sx)\int_x^\pi q'(t)\sin(2st)\,dt$$

$$-\frac{1}{2}s^{-1}sin(2sx)\int_x^\pi q'(t)cos(2st)dt + O(s^{-2}\eta^2(s)).$$

Let define the following notations:

$$sin\zeta_x := \int_x^\pi q'(t)cos(2st)dt,$$

$$cos\zeta_x := \int_x^\pi q'(t)sin(2st)dt.$$

So, by taking account into (4) and (5) with (13) we find the following asymptotic approximations, respectively

$$M(x,s) = -\frac{1}{2}s^{-1}q(\pi)sin[2s(\pi - x)] + \frac{1}{2}s^{-1}cos(2sx + \zeta_x)$$

$$+O(s^{-2}\eta^2(s)) \tag{14}$$

and

$$N(x,s) = s + \frac{1}{2}s^{-1}q(\pi)cos[2s(\pi - x)] - \frac{1}{2}s^{-1}q(x) - \frac{1}{2}s^{-1}$$

$$\times sin(2sx + \zeta_x) + O(s^{-2}\eta^2(s)). \tag{15}$$

The integrals of these functions are given in the lemma below. We need the results in the next section.

Lemma 1. As $s \to \infty$

(i) $\int_0^x M(t,s)\,dt = \frac{1}{4}s^{-2}\begin{Bmatrix} q(\pi)[\cos(2s\pi) - \cos[2s(\pi - x)]] \\ + \int_0^x q'(t)dt + \sin(2sx + \zeta_x) - sin\zeta_0 \end{Bmatrix}$

$$+O(s^{-3}\eta^2(s)), \tag{16}$$

(ii) $\int_0^x N(t,s)dt = sx - \frac{1}{2}s^{-1}\{xq(x) - \pi q(\pi) + \int_x^\pi tq'(t)dt\} + \frac{1}{4}s^{-2}$

$$\times \{q(\pi)[\sin(2s\pi) - sin[2s(\pi - x)]] + \cos(2sx + \zeta_x) - cos\zeta_0\}$$

$$+O(s^{-3}\eta^2(s)). \tag{17}$$

Proof. (i) We know that the following equality is true:

$$\int_0^x M(t,s)\,dt = \int_0^\pi M(t,s)\,dt - \int_x^\pi M(t,s)\,dt. \tag{18}$$

By using (10), (12), (13), (14) and applying a change of the order of integration and integration by parts to the terms on the right hand side, we obtain the asymptotic approximations such as

$$\int_0^{\pi} M(t,s)\,dt = -\frac{1}{2}s^{-1}\begin{bmatrix} q(\pi)\int_0^{\pi} sin[2s(\pi-t)]dt \\ +\int_0^{\pi} sin(2st)\left(\int_0^{\pi} q'(u)cos(2su)du\right)dt \\ -\int_0^{\pi} cos(2st)\left(\int_0^{\pi} q'(u)sin(2su)du\right)dt \end{bmatrix}$$

$$+O(s^{-3}\eta^2(s))$$

$$= -\frac{1}{2}s^{-1}\begin{Bmatrix} \frac{q(\pi)cos[2s(\pi-x)]}{2s}\Big|_0^{\pi} \\ +\int_0^{\pi} q'(u)cos(2su)\int_0^{u} sin(2st)dt\,du \\ -\int_0^{\pi} q'(u)sin(2su)\int_0^{u} cos(2st)dt\,du \end{Bmatrix} + O(s^{-3}\eta^2(s))$$

$$= -\frac{1}{4}s^{-2}\left\{q(\pi)[1-cos(2s\pi)] - \int_0^{\pi} q'(t)dt + sin\zeta_0\right\} + O(s^{-3}\eta^2(s))$$

and

$$\int_x^{\pi} M(t,s)\,dt = -\frac{1}{2}s^{-1}\begin{bmatrix} q(\pi)\int_x^{\pi} sin[2s(\pi-t)]dt \\ +\int_x^{\pi} sin(2st)\left(\int_t^{\pi} q'(u)cos(2su)du\right)dt \\ -\int_x^{\pi} cos(2st)\left(\int_t^{\pi} q'(u)sin(2su)du\right)dt \end{bmatrix}$$

$$+O(s^{-3}\eta^2(s))$$

$$= -\frac{1}{2}s^{-1}\begin{Bmatrix} \frac{q(\pi)cos[2s(\pi-t)]}{2s}\Big|_x^{\pi} - \left[\frac{cos(2sx)}{2s}\int_x^{\pi} q'(t)cos(2st)dt\right]\Big|_x^{\pi} \\ -\int_x^{\pi}\frac{cos^2(2st)}{2s}q'(t)dt - \left[\frac{sin(2sx)}{2s}\int_x^{\pi} q'(t)sin(2st)dt\right]\Big|_x^{\pi} \\ -\int_x^{\pi}\frac{sin^2(2st)}{2s}q'(t)dt \end{Bmatrix}$$

$$+O(s^{-3}\eta^2(s))$$

$$= -\frac{1}{4}s^{-2}\left\{q(\pi)[1-\cos[2s(\pi-x)]] - \int_x^\pi q'(t)dt + sin(2sx+\zeta_x)\right\}$$

$$+O(s^{-3}\eta^2(s)). \tag{19}$$

The last two equalities are placed in (18). Thus, the proof is completed.

(ii) Similarly we evaluate the terms on the right hand side of the equation

$$\int_0^x N(t,s)\,dt = \int_0^\pi N(t,s)\,dt - \int_x^\pi N(t,s)\,dt \tag{20}$$

as $s \to \infty$. From (10), (12), (13) and (15) we have

$$\int_0^\pi N(t,s)\,dt = \int_0^\pi sdt + \frac{1}{2}s^{-1}\begin{bmatrix} q(\pi)\int_0^\pi cos[2s(\pi-t)]dt \\ +\int_0^\pi cos(2st)\left(\int_t^\pi q'(u)cos(2su)du\right)dt \\ -\int_0^\pi sin(2st)\left(\int_t^\pi q'(u)sin(2su)du\right)dt \end{bmatrix}$$

$$+O(s^{-3}\eta^2(s))$$

$$= s\pi + \frac{1}{2}s^{-1}\begin{Bmatrix} -\frac{q(\pi)sin[2s(\pi-x)]}{2s}\Big|_0^\pi \\ +\int_0^\pi q'(u)cos(2su)\int_0^u cos(2st)dt\,du \\ -\int_0^\pi q'(u)sin(2su)\int_0^u sin(2st)dt\,du \end{Bmatrix} + O(s^{-3}\eta^2(s))$$

$$= s\pi + \frac{1}{4}s^{-2}\{q(\pi)sin(2s\pi) - cos\zeta_0\} + O(s^{-3}\eta^2(s)). \tag{21}$$

and

$$\int_x^\pi N(t,s)\,dt = \int_x^\pi sdt + \frac{1}{2}s^{-1}\begin{bmatrix} q(\pi)\int_x^\pi cos[2s(\pi-t)]dt - \int_x^\pi q(t)dt \\ +\int_x^\pi cos(2st)\left(\int_t^\pi q'(u)cos(2su)du\right)dt \\ -\int_x^\pi sin(2st)\left(\int_t^\pi q'(u)sin(2su)du\right)dt \end{bmatrix}$$

$$+O(s^{-3}\eta^2(s))$$

$$= s(\pi - x) + \frac{1}{2}s^{-1}\left\{xq(x) - \pi q(\pi) + \int_x^\pi tq'(t)dt\right\} + \frac{1}{4}s^{-2}$$

$$\times \{q(\pi)sin[2s(\pi - x)] - cos(2sx + \zeta_x)\} + O(s^{-3}\eta^2(s)). \quad (22)$$

Substituting (21) and (22) into (20) proves the equation (17).

ASYMPTOTIC APPROXIMATIONS FOR THE SOLUTIONS

We define two solutions, $\mathrm{P}(x,s)$ and $\Theta(x,s)$ of the problem (1)-(2) with the initial conditions

$$\mathrm{P}(0,s) = 0,\ \mathrm{P}'(0,s) = 1. \quad (23)$$

and

$$\Theta(\pi,s) = -a,\ \Theta'(\pi,s) = s. \quad (24)$$

Theorem 1. For $\mathrm{P}(x,s)$ and $\Theta(x,s)$, we have

(i) $P(x,s) = \frac{1}{N(0,s)}exp\left(\int_0^x M(t,s)dt\right)sin\left(\int_0^x N(t,s)dt\right)$, (25)

(ii) $\Theta(x,s) = -aexp\left(-\int_x^\pi M(t,s)dt\right)\left\{\begin{matrix}cos\left(\int_x^\pi N(t,s)dt\right) + \\ \frac{1}{a}sin\left(\int_x^\pi N(t,s)dt\right)\end{matrix}\right\}$. (26)

Proof. (i) From (6), (7) and (23) we find that

$$\mathrm{P}(0,s) = c_1 cosc_2 = 0, \quad (27)$$

$$\mathrm{P}'(0,s) = c_1 M(0,s)cosc_2 - c_1 N(0,s)sinc_2 = 1. \quad (28)$$

We use (27) in (28) and obtain

$$c_1 = -\frac{1}{N(0,s)}, c_2 = \frac{\pi}{2}. \quad (29)$$

Substitution the values of c_1 and c_2 into (6) proves the theorem.

(ii) Similarly, by using (6), (7) and (24) it is obtained that

$$\Theta(\pi, s) = c_1 exp\left(\int_0^\pi M(t,s)dt\right) cos\left\{c_2 + \int_0^\pi N(t,s)dt\right\} = -a, \tag{30}$$

$$\Theta'(\pi, s) = c_1 M(\pi, s) exp\left(\int_0^\pi M(t,s)dt\right) cos\left\{c_2 + \int_0^\pi N(t,s)dt\right\}$$

$$-c_1 N(\pi, s) exp\left(\int_0^\pi M(t,s)dt\right) sin\left\{c_2 + \int_0^\pi N(t,s)dt\right\} = s. \tag{31}$$

From (30), we can write

$$c_1 = -\frac{a}{exp\left(\int_0^\pi M(t,s)dt\right) cos\left\{c_2 + \int_0^\pi N(t,s)dt\right\}}. \tag{32}$$

Using this in (31) gives

$$c_2 = tan^{-1}\frac{1}{a} - \int_0^\pi N(t,s)dt. \tag{33}$$

The theorem is proved by replacing the values of c_1 and c_2 into (6).

Theorem 2. Let $P(x, s)$ and $\Theta(x, s)$ be the solutions of (1) satisfying (23) and (24), respectively. Then, we find as $s \to \infty$

(i) $$P(x, s) = s^{-1}\sin(sx) - \frac{1}{2}s^{-2}\left[xq(x) - \pi q(\pi) + \int_x^\pi tq'(t)dt\right]\cos(sx)$$

$$+O(s^{-3}), \tag{34}$$

(ii) $$\Theta(x, s) = -acos[s(\pi - x)] - sin[s(\pi - x)] + \frac{1}{2}s^{-1}[xq(x) - \pi q(\pi)$$

$$+ \int_x^\pi tq'(t)dt]\{asin[s(\pi - x)] - cos[s(\pi - x)]\} + O(s^{-2}). \tag{35}$$

Proof. (i) We evaluate the terms in (25) as $s \to \infty$. Firstly, using (15) together with the series expansion we get

$$\frac{1}{N(0,s)} = \frac{1}{s\left\{1+\frac{1}{2}s^{-2}[q(\pi)\cos(2s\pi) - q(0) - sin\zeta_0] + O\left(s^{-3}\eta^2(s)\right)\right\}}$$

$$= s^{-1} - \tfrac{1}{2}s^{-3}[q(\pi)\cos(2s\pi) - q(0) - sin\zeta_0] + O\left(s^{-4}\eta^2(s)\right). \quad (36)$$

From (16) we find

$$exp\left(\int_0^x M(t,s)dt\right) = 1 + \frac{1}{4}s^{-2}\begin{Bmatrix} q(\pi)[\cos(2s\pi) - \cos[2s(\pi - x)]] \\ + \int_0^x q'(t)dt + \sin(2sx + \zeta_x) - sin\zeta_0 \end{Bmatrix}$$

$$+O(s^{-3}\eta^2(s)) \quad (37)$$

and from (17)

$$sin\left(\int_0^x N(t,s)dt\right) = \sin(sx) - \frac{1}{2}s^{-1}\left[xq(x) - \pi q(\pi) + \int_x^\pi tq'(t)dt\right]$$

$$\times cos(sx) + O(s^{-2}), \quad (38)$$

$$cos\left(\int_0^x N(t,s)dt\right) = \cos(sx) + \frac{1}{2}s^{-1}\left[xq(x) - \pi q(\pi) + \int_x^\pi tq'(t)dt\right]$$

$$\times sin(sx) + O(s^{-2}). \quad (39)$$

Substituting the values of (36), (37) and (38) into (25) and using trigonometric expansions, we obtain $\mathrm{P}(x,s)$ as required.

(ii) We consider (26) as $s \to \infty$. By (19), it is obtained that

$$exp\left(-\int_x^\pi M(t,s)dt\right) = 1 + \frac{1}{4}s^{-2}\{q(\pi)[1 - \cos[2s(\pi - x)]]$$

$$- \textstyle\int_x^\pi q'(t)dt\} + O(s^{-2}\eta(s)) + O(s^{-3}\eta^2(s)) \quad (40)$$

and from (22)

$$cos\left(\int_x^{\pi} N(t,s)dt\right) = cos[s(\pi - x)] - \frac{1}{2}s^{-1}\{xq(x) - \pi q(\pi) + \int_x^{\pi} tq'(t)dt\}sin[s(\pi - x)] + O(s^{-2}), \quad (41)$$

$$sin\left(\int_x^{\pi} N(t,s)dt\right) = sin[s(\pi - x)] + \frac{1}{2}s^{-1}\{xq(x) - \pi q(\pi) + \int_x^{\pi} tq'(t)dt\}cos[s(\pi - x)] + O(s^{-2}). \quad (42)$$

Finally, we replace (40), (41) and (42) in (26). The proof is done.

ASYMPTOTIC APPROXIMATIONS FOR THE GREEN'S FUNCTION

Green's function of the boundary value problem (1)-(2) takes the form

$$G(x,\xi,s) = \begin{cases} \frac{P(\xi,s)\Theta(x,s)}{w(s)}, 0 \le \xi \le x \le \pi \\ \frac{P(x,s)\Theta(\xi,s)}{w(s)}, 0 \le x \le \xi \le \pi \end{cases} \quad (43)$$

where $w(s)$ is the Wronskian determinant of P and Θ which is independent of x, i.e.,

$$w(s) := P(x,s)\,\Theta'(x,s) - P'(x,s)\,\Theta(x,s). \quad (44)$$

Theorem 3. For $0 \le \xi \le x \le \pi$, we find Green's function of the problem (1)-(2) as $s \to \infty$

$$G(x,\xi,s) = -\frac{a}{acos(s\pi) + sin(s\pi)}s^{-1}\{sin(s\xi)cos[s(\pi - x)] - sin(s\xi)sin[s(\pi - x)]\} + \frac{1}{2[acos(s\pi) + sin(s\pi)]}s^{-2}$$

$$\times \{[xq(x) - \pi q(\pi) + \int_x^\pi tq'(t)dt][a\sin[s(\pi - x)]$$

$$-\cos[s(\pi - x)]]sin(s\xi) + [\xi q(\xi) - \pi q(\pi) + \int_\xi^\pi tq'(t)dt]$$

$$\times [a\cos[s(\pi - x)] + sin[s(\pi - x)]]cos(s\xi)\} + O(s^{-3}). \quad (45)$$

Similar result holds for $0 \le x \le \xi \le \pi$ changing the role of x and ξ.

Proof. Firstly, we calculate the Wronskian $w(s)$. So according to (44), we need the derivation of the solutions $\mathrm{P}(x,s)$ and $\Theta(x,s)$. By replacing (29) into (7), we get

$$\mathrm{P}'(\mathrm{x},\mathrm{s}) = \frac{1}{N(0,s)} exp\left(\int_0^x M(t,s)dt\right)\{M(x,s)sin\left(\int_0^x N(t,s)dt\right)$$

$$+N(x,s)cos\left(\int_0^x N(t,s)dt\right)\} \quad (46)$$

and, using (32) and (33) in (7) gives

$$\Theta'(x,s) = -aexp\left(-\int_x^\pi M(t,s)dt\right)\{M(x,s)[cos\left(\int_x^\pi N(t,s)dt\right)$$

$$+\frac{1}{a}sin\left(\int_x^\pi N(t,s)dt\right)] - N(x,s)[\frac{1}{a}cos\left(\int_x^\pi N(t,s)dt\right)$$

$$-sin\left(\int_x^\pi N(t,s)dt\right)]\}. \quad (47)$$

If we evaluate the terms in (46) by (36), (37), (38), (39) it is obtained as

$$\mathrm{P}'(x,s) = cos(sx) + \frac{1}{2}s^{-1}[xq(x) - \pi q(\pi) + \int_x^\pi tq'(t)dt]sin(sx)$$

$$+O(s^{-3}) \quad (48)$$

and applying (40), (41), (42) to the terms in (47) satisfies the following asymptotic approximation for the derivative

$$\Theta'(x,s) = -as\sin[s(\pi - x)] + s\cos[s(\pi - x)] - \frac{1}{2}[xq(x) - \pi q(\pi)$$

$$+ \int_x^\pi tq'(t)dt][a\cos[s(\pi - x)] + \sin[s(\pi - x)] + O(s^{-1}). \quad (49)$$

Hence

$$w(s) = a\cos(s\pi) + \sin(s\pi) + O(s^{-2}). \quad (50)$$

From (50)

$$\frac{1}{w(s)} = \frac{1}{a\cos(s\pi)+\sin(s\pi)} + O(s^{-2}). \quad (51)$$

Finally, the Green's function given by (45) is proved by substituting (34), (35) and (51) into (43).

REFERENCES

Başkaya, E. (2018a). Asymptotics of eigenvalues for Sturm-Liouville problem including eigenparameter-dependent boundary conditions with integrable potential. New Trends in Mathematical Sciences, 6(3), 39-47.

Başkaya, E. (2018b). Asymptotics of eigenvalues for Sturm-Liouville problem including quadratic eigenvalue in the boundary condition. New Trends in Mathematical Sciences, 6(3), 76-82.

Başkaya, E. (2018c). Asymptotics of eigenvalues for Sturm-Liouville problem with eigenparameter dependent-boundary conditions. New Trends in Mathematical Sciences, 6(2), 247-257.

Baskaya, E. (2020). Periodic and semi-periodic eigenvalues of Hill's equation with symmetric double well potential. TWMS Journal of Applied and Engineering Mathematics, 10(2), 346-352.

Başkaya, E. (2021a). Asymptotic eigenvalues of regular Sturm-Liouville problems with spectral parameter-dependent boundary conditions and symmetric single well potential. Turkish Journal of Mathematics and Computer Science, 13(1), 44-50.

Başkaya, E. (2021b). On the gaps of Neumann eigenvalues for Hill's equation with symmetric double well potential. Tbilisi Mathematical Journal, 8, 139-145.

Benedek A. I., and Panzone R. (1981). On Sturm-Liouville Problems With the Square-Root of the Eigenvalue Parameter Contained in the Boundary Conditions. Notas De Algebra Y Analisis, 10, 1-59.

Burkhardt, H. (1894). Sur Les Fonction de Green Relatives â un Domain D'une Dimension. Bulletin de la Société Mathématique de France, 22, 71-75.

Coşkun, H., and Başkaya, E. (2010). Asymptotics of eigenvalues of regular Sturm-Liouville problems with eigenvalue parameter in the boundary condition for integrable potential. Mathematica Scandinavica, 107(2), 209-223.

Coşkun, H., and Başkaya, E. (2018). Asymptotics of eigenvalues for Sturm-Liouville problem with eigenvalue in the boundary condition for differentiable potential. Annals of Pure and Applied Mathematics, 16(1), 7-19.

Coşkun, H., Başkaya E., and Kabataş, A. (2019). Instability intervals for Hill's equation with symmetric single well potential. Ukrainian Mathematical Journal, 71(6), 977-983.

Coşkun, H., and Kabataş, A. (2013). Asymptotic approximations of eigenfunctions for regular Sturm-Liouville problems with eigenvalue

parameter in the boundary condition for integrable potential, Mathematica Scandinavica, 113(1), 143-160.

Coşkun, H., and Kabataş, A. (2016). Green's function of regular Sturm-Liouville problem having eigenparameter in one boundary condition. Turkish Journal of Mathematics and Computer Sciences, 4, 1-9.

Coşkun, H., Kabataş, A., and Başkaya. E. (2017). On Green's function for boundary value problem with eigenvalue dependent quadratic boundary condition. Boundary Value Problems. Article number:71.

Fulton, C. T. (1977). Two-Point Boundary Value problems With Eigenvalue Parameter Contained in the Boundary Conditions. Proceedings of the Royal Society of Edinburgh Section A:Mathematics, 77(3-4), 293-308.

Harris, B. (1997). The form of the spectral functions associated with Sturm-Liouville problems with continuous spectrum. Mathematika, 44(1), 149-161.

Hochstadt, H. (1967). On Inverse Problems Associated With Second-Order Differential Operators. Acta Mathematica, 119, 173-192.

Kabataş, A. (2022a). Eigenfunction and Green's function asymptotics for Hill's equation with symmetric single well potential. Ukrainian Mathematical Journal, 74(2), 218-231.

Kabataş, A. (2022b). On eigenfunctions of Hill's equation with symmetric double well potential. Communications Faculty of Sciences University of Ankara Series A1 Mathematics and Statistics, 71(3), 634-649.

Kabataş, A. (2023). One boundary value problem including a spectral parameter in all boundary conditions. Opuscula Mathematica, 43(5), 651-661.

Li, Y.-S. (1965). On an eigenvalue Problem for a Second-Order Differential Equation with Boundary Dependence on the Parameter. Acta Mathematika Sinica, 15, 375-381.

Titchmarsh, E. C. (1962). Eigenfunction Expansions Associated with Second Order Differential Equations, Part I-II. Oxford: Clarendon Press.

Weyl, H. (1910). Ueber gewoehnliche Differentialgleichungen mit Singularitaeten und die Zugehoerigen Entwicklungen Willkuerlicher Funktionen. Mathematische Annalen, 68, 220-269.

Zettl, A. (2010). Sturm-Liouville Theory. United States of America: American Mathematical Society.

Chapter 14

Benzimidazoles in Therapy: Recent Advances

Sümeyya SERİN[1]

[1] *Dr..; Inonu University, Scientific and Technological Research Center.*
sumeyya.alatas@inonu.edu.tr ORCID No: 0000-0002-4637-1734

ABSTRACT

Heterocyclic compounds are indispensable parts of drug design studies due to their superior properties. In particular, since heterocycles containing nitrogen atoms provide advantages in many aspects, these compounds are preferred by the pharmaceutical industry for the discovery of new therapeutic agents. There are many studies on the synthesis and applications of new bioactive compounds. Although many classes of effective compounds have been discovered, it is noteworthy that the benzimidazole scaffold remains popular. On the other hand, hybridization studies also have an important place in the literature in order to diversify and support pharmacological activity. At the end of the study, examining the structure-activity relationships (SAR) of newly synthesized compounds sheds light on further studies. Based on this information, in the current chapter, the recent developments regarding the synthesis and pharmacological activities of benzimidazole derivatives are discussed. Synthesis methods, structure elucidation studies, remarkable findings in pharmacological activities, and SAR analyses of newly synthesized benzimidazole derivatives are presented in a comparative manner. Therefore, it is thought that it will have an important place in the literature as a resource where researchers can easily access current data on this topic.

Keywords: Benzimidazole, Synthesis, Bioactivity, Anticancer, Antimicrobial

INTRODUCTION

Heterocyclic compounds occupy a wide place in the literature, especially due to their pharmaceutical activities. Literature survey reveals that heterocyclic compounds containing nitrogen atom are becoming more prominent in drug discovery and development studies (Tandon et al., 2019:362; Hossain and Nanda, 2018:83; Alam et al., 2020:390). In this context, benzimidazole (BZ) (Figure 1) appears as a frequently used starting material for the synthesis of biologically active compounds due to its heterocyclic nature (Bansal and Silakari, 2012:6208). BZ is an aromatic conjugated acid compound with tautomeric structure and molecular weight of 118.14 g/mol. The structural similarity of BZs to naturally occurring purine nucleotides enables them to easily interact with biopolymers in the living system. Interactions such as hydrogen bonds, pi bonds, aromatic ring interactions, and lipophilic interactions formed with targets support pharmaceutical activity (Kamanna, 2019). In this way, it has been stated in many studies that BZ derivatives show a wide range of pharmaceutical activities. Anticancer, anti-tuberculosis, antiviral, antiulcer, anti-inflammatory, antidiabetic, anticonvulsant, and antihypertensive activities can be given as examples (Kumar et al., 2011:374; Tonelli et al., 2010:2937; Noor et al., 2017:85; Sharma et al., 2017:3007; Shingalapur et al., 2010:1753; Zhang et al., 2015:541). Figure 1 presents the chemical structures and names of some commercially available BZ-based compounds used as drugs in relevant fields. Due to the promising properties of BZ derivatives in medicinal chemistry, numerous studies have been conducted to synthesize new derivatives and determine their bioactivity behaviors. Some of the compounds obtained from these studies have been patented and their potential to be transformed into clinical drugs has been discussed (Law and Yeong, 2021:1861). Keeping these considerations in mind, this study presents a comparative review on the structural characterizations and pharmacological activities of BZ-based compounds synthesized in recent years.

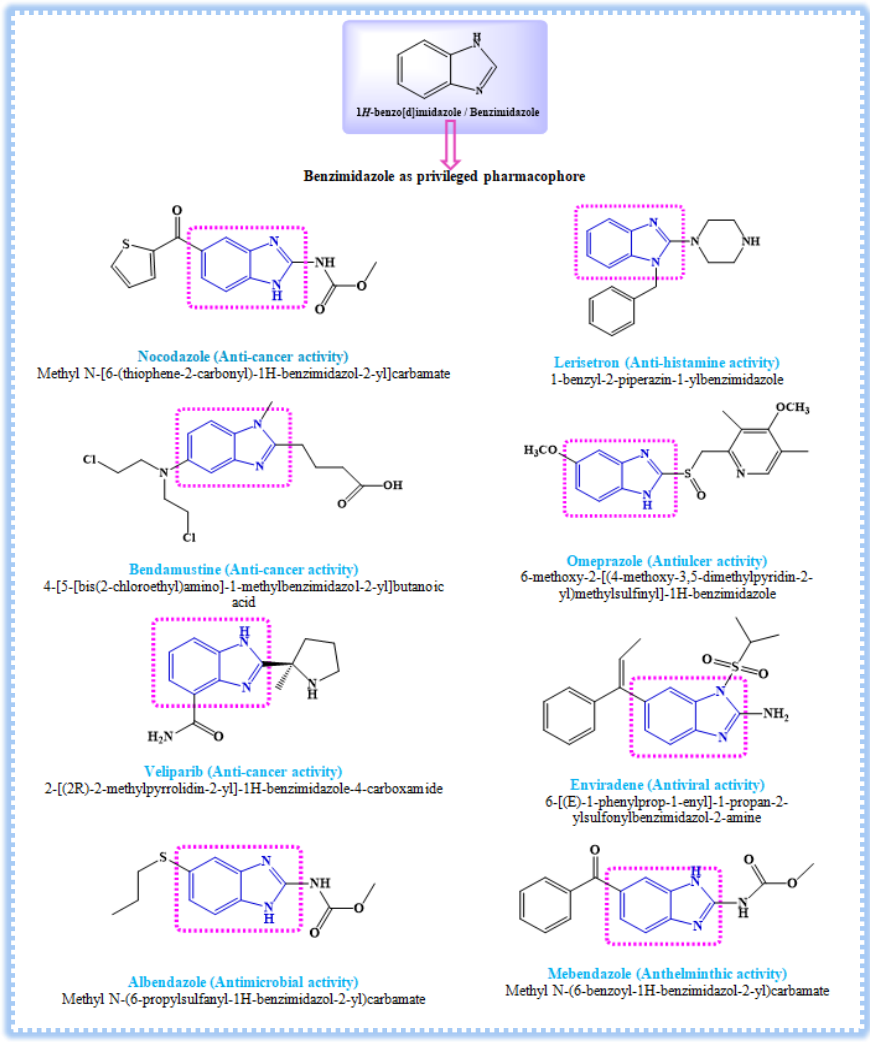

Figure 1. Commercially available BZ-based drugs

PHARMACOLOGICAL ACTIVITIES

As mentioned above, derivatives containing the benzimidazole core have achieved many different medical applications. In this section, current studies in which newly synthesized BZ derivatives were evaluated in terms of many different pharmacological activities were selected and outlined. Details of the selected studies are represented under the headings of purpose, model, and findings. In the purpose section, the pharmacological activity that stands out in the relevant study is emphasized. In the model section, details of the methods, analyses, and tests utilized in the study are given. The findings section focuses on the structural properties, activity behaviors and SAR analyzes of the synthesized

BZ derivatives. In this context, it is thought that the studies presented below will guide researchers interested in the topic.

Purpose	Model
*To synthesize novel thymol-based BZ derivatives *To examine their **antimalarial**, **antioxidant**, **and antimicrobial activities** *To study SAR (Bhoi et al., 2023: 101112)	*In vitro *In silico ADMET analysis *Molecular Docking

Findings: Within the scope of the study, a novel series of BZ-thymol hybrids with mixed substituents were synthesized. The molecular structures of the hybrids were elucidated by ^{1}H NMR, ^{13}C NMR, Mass and FT-IR spectroscopic analyses. Very important results were obtained in the in vitro antimalarial, antimicrobial and antioxidant activity determination studies of the synthesized hybrids. In particular, it was determined that three compounds with -H (IC_{50}= 0.49 μg/mL), -CF_3 (IC_{50}= 0.44 μg/mL), and -Cl (IC_{50}= 0.32 μg/mL) as substituents on the BZ ring exhibited excellent antimalarial activity. Furthermore, the SAR study revealed how the activities of the compounds were affected depending on the kinds and positions of substituents on the BZ ring. Moreover, in silico predictions have highlighted the potential of the synthesized BZ hybrids as oral chemotherapeutic agents.

Purpose	Model
*To synthesize new BZ derivatives having Schiff base, carbothioamide, thiadiazol, and triazole moiety *To investigate their **antioxidant and elastase inhibitory activities** (Albay, and Tekbaş, 2023:1374)	*Spectrophotometric methods *DPPH free radical scavenging activity * Iron reducing power capacities.

Findings: Eight new 5,6-dichloro-2-phenyl-1H-benzimidazole derivatives were synthesized in the study. The structures of the derivatives were elucidated by NMR spectroscopy, mass, and elemental analyses. It can be concluded that the synthesized new derivatives exhibited good antioxidant and elastase inhibitory activities. Namely, the DPPH radical scavenging activity values (SC50) of the synthesized derivatives were assigned between 407.2 and 895.76 μM. Considering reducing power activity absorbance values, it was indicated that acetohydrazide derivative exhibited more remarkable activity than BHT at the same concentrations BHT (butylated hydroxy toluene) is a well-known compound used as a standard antioxidant. It has been determined that the number of NH in the structure of molecules positively affects both antioxidant activity and elastase inhibition.

Purpose	Model
*To synthesize new substituted benzimidazole derivatives *To examine their **antimicrobial**, **anticancer**, **antioxidant, anti-diabetic and cytotoxic properties** *To perform statistical analysis of the results (Champa et al., 2023:101018)	*Determination of relative percentage inhibition *DPPH free radical scavenging assay *Ferrous-ion chelating assay *Cell culture technique * DFT study *Molecular Docking

Findings: In the relevant study, six BZ-substituted derivatives were synthesized. The structures of the derivatives were elucidated using FT-IR, ^{1}H NMR, ^{13}C NMR, and mass spectrometry techniques. The antioxidant, antidiabetic and cytotoxic potentials of the examined derivatives were determined. One of the prominent findings is that (E)-2-(4-((6-**nitro**-1H-benzo[d]imidazol-2-yl)thio)benzylidene)hydrazinecarbothioamide and (E)-2-(4-((5-**chloro**-1H-benzo[d]imidazol-2-yl)thio)benzylidene)hydrazinecarbothioamide derivatives show the best activity. Therefore, it can be concluded that the nitro and chloro groups attached to benzimidazole support the activity. Also, it has been reported that the antibacterial behavior of the nitro-substituted derivative is more effective than other derivatives. Besides, in silico analysis results support the effectiveness of the nitro-derivative. Namely, in molecular docking studies, the binding energy of the nitro derivative was determined as -5.9 Kcal/mol, and it was stated that its three hydrogen bonds affected the binding affinity.

Purpose	Model
*To synthesize novel 5-Methoxy-6-substituted-1H-BZ derivatives *To evaluate of **anti-proliferative activities** *To perform statistical analysis of the results *To study SAR (Wu et al., 2023:129469)	*MTT (methyl thiazolyl tetrazolium) assay * Cell Cycle Analysis * Western blot * Molecular Docking

Findings: In this very comprehensive study, 24 new BZ derivatives were synthesized. The structures of all synthesized derivatives were confirmed by ^{1}H NMR, ^{13}C NMR, and HRMS. At the same time, the following cell lines were selected to evaluate the antitumor activities of the compounds: lung adenocarcinoma (A549), cervical cancer (Siha), breast cancer (MCF-7), hepatocellular carcinoma (HepG2), prostate cancer (PC3), and colorectal carcinoma (HCT-116). Among the synthesized compounds, it was determined that the 2-fluorophenyl)ethynyl substituted benzimidazole derivative exhibited

the best antitumor activity against A549 cells ($IC_{50} = 1.55 \pm 0.18$ μM). Therefore, most of the study focused on compound

6-((2-fluorophenyl)ethynyl)-5-methoxy-2-(2,4,5-trimethoxyphenyl)-1H-benzo[d]imidazole. Moreover, based on the results of the molecular docking study, it was concluded that the mentioned derivative has potential as a pan-PI3K inhibitor and is promising for further research.

Purpose	Model
*To synthesize new pyrimido[1,2-*a*]benzimidazole derivatives *To evaluate their in vitro **anti-tumor activities** *To study SAR (Shaldam et al., 2023: 115610)	*Screening on NCI cancer cells *Preliminary one dose screening *In vitro five dose assay *Cell cycle effects *Levels of regulatory proteins *Kinase assay

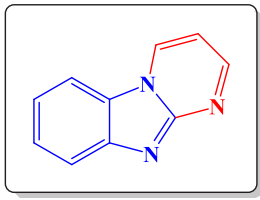

Chemical structure of pyrimido[1,2-*a*]benzimidazole

Findings: As shown in the figure above, pyrimido[1,2-*a*]benzimidazole is the fusion of benzimidazole and pyrimidine to form a tricyclic structure. In this study, sixteen new pyrimido[1,2-*a*]benzimidazole derivatives were synthesized and the structures of the compounds were elucidated using ^{1}H NMR, ^{13}C NMR, ESI-MS and elemental analysis techniques. The anti-cancer activities of the synthesized derivatives against a panel of 5 human acute leukemia cell lines were investigated and their IC_{50} values were assigned. Based on the SAR analysis results, it was emphasized that the addition of 1-naphthyl moiety as a substituent to the tricyclic structure revealed the strongest anti-proliferative effect within the scope of the study. GI values (average percentage inhibition of growth) of 4 derivatives containing 1-naphthyl were determined as 42, 41, 55, and 65%.

Purpose	Model
*To synthesize novel benzimidazole-containing sulfonamide derivatives *To test new derivatives against the **enzymes α-glucosidase and α-amylase** *To study SAR (Ullah et al., 2023: 101070)	*In vitro *Molecular docking

Findings: In this study, fourteen BZ-bearing sulfonamide derivatives were synthesized. The structures of the derivatives were elucidated using IR, ^{1}H NMR, ^{13}C NMR, HREI-MS, and mass spectrometry techniques. Among the synthesized derivatives, the strongest α-glucosidase activity was observed for compounds with 4-chloro (IC_{50} = 13.20 ± 0.30 μM), 3, 4-dichloro (IC_{50} = 9.20 ± 0.10 μM), and 2-methoxy (IC_{50} = 10.20 ± 0.30 μM) groups attached to the phenyl ring. On the other hand, in the case of α-amylase, the highest activity was observed in the derivatives to which 4-nitro (IC_{50} = 5.20 ± 0.30 μM), 4-chloro and 2-methoxy groups were attached.

Purpose	Model
*To synthesize a new series of bis-benzimidazole derivatives *To evaluate their **inhibitory activity of α-amylase and α-glucosidase** *To study SAR (Khan et al., 2023: 104847)	*In vitro *Molecular docking *In silico ADME analysis

Findings: Within the scope of the study, eighteen thiadiazole derivatives containing bis-BZ motif were synthesized. The synthetic route is described in detail. The structures of the synthesized derivatives were confirmed using ^{1}H NMR, ^{13}C NMR, and HREI-MS techniques. The bioactivity behaviors of the synthesized derivatives were tested and compared with each other and the standard drug acarbose. SAR analysis revealed that differences in bioactivity may depend on attributes such as location, number, and kind of substituents. Among the mentioned derivatives, it was determined that 5-nitrophenol, 3-chloro-5-(trifluoromethyl)phenyl, 3-nitro-5-(trifluoromethyl)phenyl, and benzene-1,3-diol substituted derivatives displayed the most potent activity. While the α-amylase inhibition IC_{50} values of the 4 mentioned derivatives were determined as 1.10 ± 0.10 μM, 1.20 ± 0.20 μM, 0.10 ± 0.50 μM, and 0.70 ± 0.50 μM, respectively, the α-glucosidase inhibition IC_{50} values were determined as 1.80 ± 0.10 μM, 2.0 ± 0.20 μM, 0.20 ± 0.50 μM, and 1.20 ± 0.10 μM.

Purpose	Model
*To synthesize new pyrido[1,2-*a*]benzimidazole derivative *To evaluate **anti-tumor activities** (Begunov et al., 2023:237)	* MTT assay * TBA ((thiobartituric acid) test

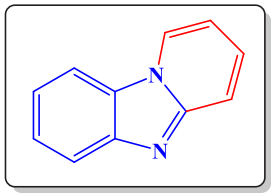

Chemical structure of pyrido[1,2-*a*]benzimidazole

Findings: As with pyrimido[1,2-*a*]benzimidazole, the combination of benzimidazole and pyridine forms a tricyclic structure: pyrido[1,2-a]benzimidazole, shown above. In this study, 8-bromo-7-chloropyrido[1,2-*a*]benzimidazole-6,9-dione and its 1,2,3,4-tetrahydro analogue have been successfully synthesized. Structure elucidation studies of the obtained compounds were completed through ^{1}H NMR, ^{13}C NMR, and ESI-HRMS techniques. The antitumour activity determination studies against cancer cell lines were performed. It was determined that both derivatives could trigger lipid peroxidation in rat brain homogenate. The efficient synthetic route developed in this study has the potential to enable the preparation of many new tricyclic benzimidazole derivatives.

Purpose	Model
*To synthesize benzimidazole Schiff base complexes	* MTT assay
*To evaluate their **anti-cancer activities**	* Cell migration
(Hou et al., 2023: 105144)	* Exploration of apoptosis

Findings: In the study, three new benzimidazole Schiff base metal complexes were synthesized via the solvothermal method. The structures of the synthesized Cu, Ni, and Co complexes were elucidated by FT-IR spectrometry, elemental analysis, thermogravimetric analysis and X-ray single crystal diffraction. The MTT method was utilized to determine the antitumor activity of the complexes on human cancer cells. Studies have shown that the anti-proliferative activity of the Ni complex, six-coordinated tetranuclear molecule, against CNE-2Z cells is better than that of standard cis-platinum.

Purpose	Model
*To synthesize new 5-fluoro-substituted benzimidazole based sulfonyl derivatives *To evaluate their **antibacterial activities** (Roy et al., 2023:336)	* Disk diffusion test *Minimum inhibitory concentration (MIC) *Bacterial growth and inhibition * Molecular docking * In silico ADME predictions

Findings: In this study, six new BZ derivatives were synthesized and characterized by ^{1}H-NMR, ^{13}C-NMR, ^{19}F-NMR and mass spectroscopy. Phenyl, methyl and tosyl groups were chosen as substituents. The antibacterial properties of the synthesized derivatives against gram-negative and gram-positive bacteria were examined. It was determined that the tosyl substituted derivative showed the best activity against both E. coli and S. aureus. Moreover, the results of the molecular docking study performed against monoamine oxidase B (MAO-B), responsible for Parkinson's disease, revealed that the synthesized compounds exhibited effective affinity against MAO-B protein strain 2C65. According to the results obtained from in silico ADME analysis, it is predicted that the mentioned derivatives will show sufficient drug-like properties. Therefore, it is thought that the data obtained from the study will provide motivation for further studies.

Purpose	Model
*To describe the synthesis of new bis-BZ derivatives * To evaluate their **antimicrobial activities** (Rajagopal et al., 2023: 135253)	*Minimum inhibitory concentration (MIC) * Hemolysis assay *Microscopic observation of red blood cells * Molecular docking

Findings: Inspired by the success of bis-benzimidazoles in pharmacological activities, eight new bis-benzimidazole derivatives were synthesized in this study. Structures of derivatives were elucidated by ^{1}H NMR, ^{13}C NMR and mass spectroscopic techniques. Among them, 2-(chloromethyl)-3,4-dimethoxypyridine substituted derivative possess crystal nature and confirmed by single crystal X-ray study. In order to examine their antimicrobial activities, the synthesized derivatives were tested against Gram-positive (Bacillus subtilis, Staphylococcus aureus), Gram-negative (Escherichia coli, Serratia sp.), and fungal (Candida albicans) pathogens. It was determined that the 1-(2-chloroethyl)piperidine substituted derivative showed the best activity with a MIC value of 16 μg/mL (for C. albicans).

Purpose	Model
*To design and synthesis of new morpholine-benzimidazole hybrids *To evaluate their **antimicrobial and cytotoxic properties** *To study SAR (Aaghaz et al., 2023: 106538)	*Minimum inhibitory concentration (MIC) *Flow cytometric analysis *Time kill kinetics assay *Cell morphology analysis *Ultra-structure analysis by HRTEM

Findings: Within the scope of the study, fifteen 4-(1,3-thiazol-2-yl)morpholine-BZ hybrid molecules containing mixed substituents were synthesized. Structures of hybrids were elucidated by FT-IR, ^{1}H NMR, ^{13}C NMR and mass spectroscopic techniques. In antimicrobial activity determination studies, the derivative containing *m*-OCH_3 and CH_3 substituents showed the strongest activity against Cryptococcus neoformans. IC_{50}, MIC and MFC (minimum fungicidal concentration) values were determined as 1.3 μM, 2.4 μM, and 2.4 μM, respectively. In vitro mammalian cell cytotoxicity of the same derivative was examined against HEK293 and HeLa cells. Based on the MIC values, it was determined that the relevant derivative was non-cytotoxic. One of the important results of the study is that the synthesized BZ hybrids are characterized as a new and effective class of antifungal agents.

Purpose	Model
*To synthesize a new series of benzimidazole-isoxazole derivatives containing amide moiety *To evaluate their **anti-cancer activities** (Bandaru et al., 2023: 100994)	*MTT assay

Findings: Ten new structurally diverse BZ derivatives were synthesized in this study. ^{1}H NMR, ^{13}C NMR, and mass spectral techniques were used in structure elucidation studies. Also, the following cell lines were selected to evaluate the anticancer activities of the synthesized derivatives: lung adenocarcinoma (A549), breast cancer (MCF-7), prostate cancer (PC3), and prostate cancer (DU-145). For the relevant derivatives, IC_{50} values have been reported to vary between 0.022 ± 0.0051 and 18.6 ± 6.22 μM. It was determined that the derivatives containing 3,4,5-trimethoxy, 3,5-dimethoxy, 4-methoxy, 4-nitro, 3,5-dinitro and 4-cyano substituents on the phenyl ring showed the strongest activity.

Purpose	Model
*To synthesize new benzotriazole-BZ metal complexes *To evaluate their **antidiabetic activities** * To study SAR (Wang et al., 2023: 136141)	*Cell cultures and cytotoxicity assay *Glucose consumption assay

Findings: In this study, four BZ-derived Cu and Zn complexes were synthesized. The structures of the complexes were confirmed with the help of elemental analysis, IR and X-ray crystallography. In the light of the obtained experimental data and SAR analysis, it was concluded that the Cu (II) ion plays

a crucial role in the complexes to inhibit the enzymes. It has been reported that $[Cu_2(ebmb)_2Cl_4]$ and $[Cu(mbmb)SO_4]_n$ complexes may be efficient candidates for the improvement of antidiabetic drugs.

CONCLUSIONS

When the chemical structures of active agents in a wide variety of fields such as antimicrobial, antiviral, anticancer, antidiabetic, anti-inflammatory, antioxidant, proton pump inhibitor, antihypertensive, and anticoagulant are examined, BZ scaffolds are found in many of them. This explains the intense interest in BZ derivatives. By changing the groups around BZ core, new compounds exhibiting different activities have been obtained. Even in 2023, hundreds of BZ derivatives have been synthesized and their activities have been studied. Therefore, it is necessary to follow the recent developments closely in order to learn the point that the BZ core has reached in medicinal applications. In this context, the current study gains importance. It is noteworthy that in the studies examined, computational methods were utilized as well as experimental tests. Many studies were supported by in silico ADME(T) analyses and molecular docking studies. Similarly, in many studies, SAR analyses were carried out by examining the changes reflected in the activity depending on the position, nature, type, and number of substituents. Considering these circumstances, this study will contribute to the development of new bioactive BZ derivatives.

REFERENCES

Aaghaz, S., Digwal, C.S., Neshat, N., Maurya, I.K., Kumar, V., Tikoo, K., Jain, R., Kamal, A. (2023). Synthesis, biological evaluation and mechanistic studies of 4-(1,3-thiazol-2-yl)morpholine-benzimidazole hybrids as a new structural class of antimicrobials. *Bioorganic Chemistry*, 136, 106538.

Alam, M.M., Almalki, A.S.A., Neamatallah, T., Ali, N.M., Malebari, A.M., Nazreen, S. (2020). Synthesis of new 1, 3, 4-oxadiazoleincorporated 1, 2,3-triazole moieties as potential anticancer agents targeting thymidylate synthase and their docking studies. *Pharmaceuticals (Basel),* 13(11), 390-404.

Albay, C., Tekbaş, G. (2023). Desing, synthesis, and characterization of some 5,6-dichloro benzimidazole derivatives with investigation of their antioxidant and elastase inhibitory activities. *Journal of Heterocyclic Chemistry*. 60, 1374–1382.

Bandaru, P.K., Rao, N.S., Radhika, G., Rao, B.V. (2023).Synthesis of amide derivatives of benzimidazole-isoxazoles as anticancer agents. *Chemical Data Collections*, 44, 100994.

Bansal, Y., Silakari, O. (2012). The therapeutic journey of benzimidazoles: A review. *Bioorganic & Medicinal Chemistry*, 20, 6208–6236.

Begunov, R.S., Aleksandrova, Y.R., Yandulova, E.Y., Nikolaeva, N.S., Neganova, M.E. (2023). Synthesis and cytotoxicity of 7,8-dihalopyrido[1,2-a]benzimidazole-6,9-dione and its 1,2,3,4-tetrahydro analogue. *Mendeleev Communications*, 33, 237–239.

Bhoi, R.T., Bhoi, C.N., Nikume, S.R., Bendre, R.S. (2023). Design, synthesis, and in silico studies of benzimidazoles of thymol as potent antiplasmodial and antimicrobial agents. *Results in Chemistry*, 6, 101112.

Champa, R., Vishnumurthy, K.A., Bodke, Y.D., Naik, H.S.B., Pushpavathi, I., Meghana, P., Kadam, P.R. (2023). Synthesis, characterization, and biological investigations of potentially bioactive heterocyclic compounds containing benzimidazole nucleus. *Results in Chemistry*, 6,101018.

Hossain, M., Nanda, A.K. (2018). A review on heterocyclic: synthesis and their application in medicinal chemistry of imidazole moiety. *Science Journal of Chemistry*, 6(5), 83–94.

Hou, M., Li, H.C., An, N., Li, W.G., Tong, J. (2023). Synthesis, structure and anticancer studies of Cu (II), Ni (II) and Co (II) complexes based on 2,3-dihydroxybenzaldehyde-2-(2-aminophenyl) benzimidazole Schiff base. *Arabian Journal of Chemistry*, 16, 105144.

Kamanna, K. (2019). Synthesis and pharmacological profile of benzimidazoles. In: Marinescu M, editor. Chemistry and applications of benzimidazole and its derivatives. London: IntchOpen.

Khan, S., Iqbal, S., Rehman, W., Hussain, N., Hussain, R., Shah, M., Ali, F., Fouda, A.M., Khan, Y., Dera, A.A., Alahmdi, M.I., Bahadur, A., Al-ghulikah, H.A., Elkaeed, E.B. (2023). Synthesis, molecular docking and ADMET studies of bis-benzimidazole-based thiadiazole derivatives as potent inhibitors, in vitro α-amylase and α-glucosidase. *Arabian Journal of Chemistry*, 16, 104847.

Kumar, K., Awasthi, D., Lee, S.Y., Zanardi, I., Ruzsicska, B., Knudson, S. et al. (2011). Novel trisubstituted benzimidazoles, targeting Mtb FtsZ, as a new class of antitubercular agents. *Journal of Medicinal Chemistry*, 54, 374-381.

Law, C.S.W., Yeong, K.Y. (2021). Benzimidazoles in Drug Discovery: A Patent Review, *ChemMedChem*, 16, 1861–1877.

Noor, A., Qazi, N.G., Nadeem, H., Khan, A.U., Paracha, R.Z., Ali, F. et al. (2017). Synthesis, characterization, anti-ulcer action and molecular docking evaluation of novel benzimidazole–pyrazole hybrids. *Chemistry Central Journal*, 11, 85.

Rajagopal, K., Dhandayutham, S., Nandhagopal, M., Narayanasamy, M. (2023). Study on new series of bis-benzimidazole derivatives synthesis, characterization, single crystal XRD, biological activity and molecular docking. *Journal of Molecular Structure*, 1283, 135253.

Roy, S., Sen, S., Saha, S., Deb, S.K., Singh, B., Biswas, G. (2023) Design, synthesis and molecular docking studies of 5-fluoro 1-aryl/alkyl sulfonyl benzimidazole derivatives for treatment of Parkinson's disease, *Phosphorus, Sulfur, and Silicon and the Related Elements*, 198:4, 336–344.

Shaldam, M.A., Hendrychova, D., El-Haggar, R., Vojackova, V., Majrashi, T.A., Elkaeed, E.B., Masurier, N., Krystof, V., Tawfik, H.O., Eldehna, W.M. (2023). 2,4-Diaryl-pyrimido[1,2-a]benzimidazole derivatives as novel anticancer agents endowed with potent anti-leukemia activity: Synthesis, biological evaluation and kinase profiling. *European Journal of Medicinal Chemistry*, 258, 115610.

Sharma, R., Bali, A., Chaudhari, B.B. (2017). Synthesis of methane sulphonamido-benzimidazole derivatives as gastro-sparing antiinflammatory agents with antioxidant effect. *Bioorganic & Medicinal Chemistry Letters,* 27, 3007-3013.

Shingalapur, R.V., Hosamani, K.M., Keri, R.S., Hugar, M.H. (2010). Derivatives of benzimidazole pharmacophore: synthesis, anticonvulsant, antidiabetic and DNA cleavage studies. *European Journal of Medicinal Chemistry*, 45, 1753-1759

Tandon, R., Singh, I., Luxami, V., Tandon, N., Paul, K. (2019). Recent advances and developments of in vitro evaluation of heterocyclic moieties on cancer cell lines. *Chemical Record*, 19, 362–393.

Tonelli, M., Simone, M., Tasso, B., Novelli, F., Boido, V., Sparatore, F. et al. (2010). Antiviral activity of benzimidazole derivatives. II. Antiviral activity of 2-phenylbenzimidazole derivatives. *Bioorganic & Medicinal Chemistry*, 18, 2937-2953.

Ullah, H., Batool, T., Nawaz, A., Rahim, F., Khan, F., Hussain, A.(2023). Synthesis, in vitro α-glucosidase, α-amylase inhibitory potentials and molecular docking study of benzimidazole bearing sulfonamide analogues. *Chemical Data Collections*, 47, 101070.

Wang, X., Du, J., Zhou, T., Fang, X., Yang, H. (2023). Novel benzotriazole-benzimidazole metal complexes: structure-activity relationship, synthesis, characterization, and antidiabetic activity. *Journal of Molecular Structure*, 1292, 136141.

Wu, W., Li, S., Chen, J., Duo, T., Ma, C. (2023). Design, synthesis and antitumor effects of novel benzimidazole derivatives as PI3K inhibitors. *Bioorganic & Medicinal Chemistry Letters*, 95, 129469.

Zhang, Y., Xu, J,. Li, Y., Yao, H., Wu, X. (2015). Design, synthesis and pharmacological evaluation of novel no-releasing benzimidazole hybrids as potential antihypertensive candidate. *Chemical Biology & Drug Design*, 85, 541-548.

Chapter 15

Evaluation of the Cytotoxic and Genotoxic Effects of Fluquinconazole Using *Allium cepa* L. as a Bioindicator

Şifa TÜRKOĞLU[1]

[1] *Sivas Cumhuriyet University, Faculty of Science, Department of Biology, Sivas, TURKEY*
e-mail: turkoglu@cumhuriyet.edu.tr

Abstract: Fluquinconazole is the active substance of a synthetic fungicide which is used extensively in agricultural areas in the world and Turkey. In this study, 30, 60, 90 and 100 mg/l doses of the substance were applied to *Allium cepa* root tips for 12, 24 and 48 hours. Distilled water was used as a negative control while methyl methane sulfonate (MMS, 10 ppm) was used as a positive control. As a result of the application, it was observed that the substance caused mitotic inhibition by decreasing the mitotic index, leading to changes in mitotic stage ratios. It was also observed that this substance caused chromosomal (anaphase bridges, stickiness, c-mitosis, laggards, and breakages) and nuclear abnormalities (binucleus and micronucleus). At the end of the statistical analysis and examinations, it was detected that the substance caused cytotoxic and genotoxic effects.

Key words: Cytotoxicity, genotoxicity, Mitotic index, Allium assay, Micronuclei, Fluquinconazole

INTRODUCTION

Substances such as chemicals, some organic compounds, and disinfectants that are used to destroy the harmful effects of bacteria, viruses, and pests, to increase the quality of life of plants and to help them grow, develop and produce are called "Pesticides". There are many genotoxic, cytotoxic, or mutagenic studies on pesticides, which are categorized into different groups according to their area of use and purpose. As a result of these studies, which focused especially on insecticides and herbicides, it was found that the pesticides used caused many adverse conditions, the most common ones of which were an increase or decrease in the mitotic index and structural and/or numerical abnormalities in chromosomes (de Sousa et al. 2019; de Morais et al. 2019; Ilyushina et al. 2020; Gallego and Olivero-Verbel 2021). Another group of pesticides are fungicides. Fungicide, also called antimycotic, is an antimycotic agent, a toxic substance used to kill or inhibit the growth of fungi, fungal spores, and fungal infections. Fungicides, which can be either in natural or in synthetic form, are often used to control parasitic fungi that cause economic damage to crop or ornamental plants. Usually found in synthetic form, commercial fungicides are widely used in agricultural activities to kill fungal pathogens infecting plants.

Fungal pathogens are the number one cause of crop loss worldwide. They can cause serious damage and loss of both quality and profit in agricultural production. Applied in powder or in liquid form, fungicides can be applied at different time periods, ranging from seed to storage. Currently in world agriculture, approximately 140 different fungicidal active substances are sold under different trade names that are several times as the number of substances themselves. One of these, Fluquinconazole, is preferred as a wheat seed treatment. Preferred especially in the applications in seed stage, this substance is used to kill pathogens on the seed or to protect the young plant from pathogens in the soil. Whether fungicides have direct or indirect toxic effects on organisms other than the target organisms is still a widely researched topic (Shishatskaya et al. 2018; Wua et al. 2018; Maurya et al. 2019; Marinho et al. 2020; Pitombeira de Figueirêdo et al. 2020). Since fungicides are used regularly every year, they have a different usage pattern from other herbicides and insecticides, which are used intermittently or as needed. Therefore, the genotoxic effects of these substances need further examination.

A flowable concentrate (FS) formulation for seed dressing, Fluquinconazole is available in the market under different trade names and is regularly used to control the root rot pathogen induced by *Gaeumannomyces graminis* especially in wheat and to help control seed-borne diseases caused by various fungal species

(BKU 2023). The fungicide Fluquinconazole has a molecular formula of C16H8Cl2FN5O, a molecular weight of 376.2 g/mol, a CAS number 136426-54-5, and an open formula 3-(2,4-dichlorophenyl)-6-fluoro-2-(1H-1,2,4-triazol-1-yl)-4(3H)-quinazolinone, belonging to the triazole class (PUBCHEM 2023). In studies conducted with this fungicide, it has been shown to have protective properties against diseases caused by fungi at varying rates and that it helps increase the productivity by significantly reducing disease occurrence (Bateman et al. 2004; Gutteridge et al. 2007; Scherm et al. 2009). In literature review on toxicology studies with Fluquinconazole, studies on residue contamination in water, soil, and products caused by the substance were generally found (EFSA 2011; Szpyrka and Walorczyk 2013; Ramanauskienė et al. 2018).

Allium test is an excellent genetic model and biomarker for the investigation of genotoxic, mutagenic, and cytotoxic effects caused by environmental pollutants. Factors such as lower cost, obtaining similar results to animal studies, the possibility of conducting studies with less use of experimental animals, chromosome size and easy examination under light microscope have led researchers to use *Allium cepa* and plants with similar characteristics in this field. Introduced to the science world in 1938 by Levan, this test method was developed with some modifications by Fiskesjö in 1985 and Rank in 2003 and has been used for many years. The genotoxic effects of a lot of chemicals (pesticides, food additives, environmental pollutants, etc.) have been investigated with this test, which is also accepted by the United Nations Environment Program (UNEP), the International Program on Plant Testing (IPPB), the U.S. Environmental Protection Agency Genetic Toxicology Program (EPA Gen-Tox Program), and the World Health Organization (WHO) (Stapulionytė et al. 2019; Bellani et al. 2020; Khan et al. 2020; Souza et al. 2020; Lovinskaya et al. 2021; Thesai et al. 2021). Although a great number of articles on the subject can be found in the literature review, articles from recent years were mentioned in this study.

Although there are genotoxic studies with various fungicides in the literature, there are no studies showing the effect of this substance on mitotic index and chromosomes. For this reason, it was aimed to investigate the positive and/or negative effects of the active substance Fluquinconazole on mitotic index, mitotic stages, and chromosomes with the Allium test method, which serves as a marker in genotoxic and cytogenotoxic studies. While changes in mitotic index and mitotic stages indicate the cytogenetic effect of the substance used, chromosomal abnormalities will give us information about the genotoxic effect of the same substance. In addition, results regarding the mutagenic effect of the substance will be obtained by looking at whether it causes micronucleus formation in the cell.

MATERIAL AND METHODS

Onion tubers (*A. cepa* L., 2n = 16) with a diameter of 25-30 mm were purchased from a local market in Sivas. The seed treatment Galmano FS 167, which has been marketed by Bayer Company and whose active substance is Fluquinconazole (167 g/L Fluquinconazole), was used in the study. A growth inhibition test was performed to determine the EC50 concentration (effective concentration=EC50 value) of the substance purchased from an agrochemical company. Determination of the EC50 value has been shown to be a useful parameter for selecting test concentrations in genotoxicity tests (Chauhan et al. 1999; Seth et al. 2007). For this purpose, onions were treated with 10 different concentrations of Fluquinconazole for 4 days. These selected concentrations were prepared considering the amount of active substance 10, 20, 30, 40, 50, 60, 70, 80, 90 and 100 mg/L. For each concentration, 5 different onion tubers were used and the length of 10 roots was measured in each tuber. The control group was treated with distilled water. As a result of the evaluations, it was found that the dose that caused a 50% shortening in root length compared to the control group, i.e., the EC50 value, was 60 mg/L. After identifying this value, 4 concentrations (120, 90, 60 and 30 mg/L) were determined as EC50x2, EC50x3/2, EC50x1 and EC50x1/2 respectively. Kihlman (1971) reported that the cell cycle of root tip meristem cells of *Allium cepa* is 20-24 hours. Considering this, the application periods of the fungicide for mitotic index and chromosomal aberrations were chosen as 12, 24 and 48 hours. Since the highest mitotic frequency in onion was obtained between 6.00 and 9.00 in the morning (Sharma 1983), sampling of root tip materials was completed between 7.00 and 8.00 in the morning.

Germinated for 24 hours in distilled water at room temperature, the onions were treated with 4 different doses of Fluquinconazole for 12, 24, and 48 hours. Onions in the negative control were treated with distilled water for indicated periods while those in the positive control were treated with Methyl methanesulfonate (MMS, Sigma–Aldrich, CAS No 66-27-3) (10 mg/L). 10 onions were used for each concentration in all application groups. At the end of the application periods, the lengths of the root tips were measured and recorded. Then, the roots were cut with sterile scissors, washed in distilled water, and fixated in carnoy solution for 24 hours. After fixation, the roots were stored in 70% alcohol in the refrigerator until use. In order to separate the meristem tissue cells from each other and to ensure better observation of the cells in microscopic examinations, the roots were placed in 1N HCl and hydrolyzed in a water bath at 60ºC for 7 minutes after they were removed from 70% alcohol. After hydrolysis, the roots were placed in distilled water to stop the effect of HCl and kept for 15 minutes, replenishing the water every 5 minutes. The roots were then stained with

aceto orcein and well-dispersed preparates were made into permanent for microscopic examination. Microscopic analyses were performed on an Olympus microscope at 100X magnification and mitotic index, chromosomal aberrations in anaphase and telophase, and micronuclei in interphase cells were observed. In identifying the mitotic index of root tip meristem cells, cells divided were counted in a total of approximately 5000-6000 cells, over 1000 cells in each of the 5 preparates prepared for each application, and the formula of General Mitotic Index (GMI) = (number of mitotic cells/total number of cells) X 100 was used. To determine the ratio of mitotic phases, cells in prophase, metaphase, anaphase, and telophase were counted separately and the ratios of Prophase Mitotic Index (PMI), Metaphase Mitotic Index (MMI), Anaphase Mitotic Index (AMI), and Telophase Mitotic Index (TMI) were calculated according to the formula below (Causil Vargas et al. 2017; Mercado and Caleño 2020).

PMI = (Number of cells in prophase/number of dividing cells) X 100

MMI = (Number of cells in metaphase/ number of dividing cells) X 100

AMI = (Number of cells in anaphase/number of dividing cells) X 100

TMI = Number of cells in telophase/number of dividing cells) X 100

After mitotic index calculations, in order to identify the ratio of chromosomal aberrations, 5 preparates were selected for each application group and 500 cells, 100 of which were anaphase or telophase cells, were examined in each preparate and the number of chromosomal abnormalities (CA), nuclear abnormalities (NA) and micronucleus ratios were determined. Chromosomal abnormalities such as stickiness, C-mitosis, anaphase bridges, breakages, and laggards were analyzed. In the investigation of nuclear abnormalities, abnormalities in interphase nuclei were taken into consideration.

Analysis of variance (ANOVA) was applied to the data obtained and statistical analyses were performed using SPSS v.23 package program. Significant differences between data means were determined by Tukey Test.

RESULTS AND DISCUSSION

In this study where the cytotoxic, genotoxic, and mutagenic effects of Fluquinconazole were investigated, root growth inhibition, which is both a macroscopic observation and an indicator of toxic effect, was first investigated. Table 1 shows the root inhibition ratios of *Allium cepa* treated with 10 different doses of Fluquinconazole. Among the doses applied to the test material, the 60 mg/L one was determined as the EC50 value and the doses to be used in the study were selected accordingly. In general, root growth retardation has been identified at doses above this dose. Color and structure changes in the roots, growth retardation, and little or no development of lateral roots are macroscopic

indicators of the symptoms caused by the toxic effect (Fusconi et al. 2006; Wójicik and Tukendorf 1999). It is believed that the elongation inhibition in root growth may be due to a decline in root apical meristematic activity, which may be the result of a cytotoxic effect (Webster and MacLeod 1996; Yıldız et al. 2009). Moreover, it is stated that an inhibition in protein synthesis may also be effective in root growth (Seth et al. 2007). In the light of these opinions and results that we obtained, we think that Fluquinconazole fungicide inhibited protein synthesis in *Allium cepa* root cells and slowed or prevented cell division by causing a cytotoxic effect, resulting in a decrease in mitotic index, which in turn caused root growth inhibition.

Table 1. *A. cepa* root growth subjected to different concentrations of fluquinconazole.

Concentrations (mg/L)	**Root length of *A. cepa* (cm)**	**Growth (%)**
Control	3.46 a	100
10	3.05 ab	88
20	2.65 ac	77
30	2.49 abc	72
40	2.06 bd	60
50	1.97 bd	57
60	1.72 cd	50
70	1.58 cd	46
80	1.63 cd	47
90	1.24 d	36
100	1.08 d	31

The means ± SD values with different letter (a, b, c, d) indicate statistically significant differences, according to Tukey ($P \leq 0.05$). SD: Standard deviation.

Table 2. Mitotic indexes of the cells from *A. cepa* roots, submitted to different concentrations of fluquinconazole.

Time of treatment (h)	Doses (mg/L)	Total cells observed	Dividing cells	GMI± SD *	MI % to control	PMI (%)±S.D	MMI (%)±S.D	AMI (%)±S.D	TMI (%)±S.D
	Control	5054	3296	65.21± 0.62 a	100	33.54± 0.19 a	12.85± 0.84 a	9.63±1.64 a	9.19±0.55 a
	MMS	5048	2046	40.54± 0.24 b	62	17.19± 0.11 b	11.93± 0.73 b	5.49±0.87 b	5.93±0.45 bg
	30	5107	2476	48.48± 0.15 c	74	31.27± 0.23 c	10.24± 0.89 c	3.51±0.12 c	3.46±0.58 c
12 h	60	5066	2285	45.10± 0.20 d	69	32.78± 0.16 a	9.12±1.51 d	1.09±0.17 d	2.11±1.02 df
	90	5041	2193	43.50± 0.19 e	67	31.28± 0.14 c	8.17±0.70 ej	3.07±0.49 c	0.98±0.56 ef

	120	5123	1925	37.57± 1.64 f	58	29.62± 1.43 d	6.11±1. 39 f	1.30±0. 84 d	0.54±0 .91 e
	Cont rol	5049	3461	68.54± 1.25 g	100	36.91± 1.49 e	17.67± 1.67 g	7.51±1. 73 e	6.45±0 .97 b
	MM S	5061	2084	41.17± 1.35 b	60	18.35± 0.75 f	10.89± 1.92 h	6.64±1. 54 f	5.29±1 .25 g
	30	5072	1772	34.93± 0.76 h	51	21.18± 0.28 g	8.21±1. 34 ej	3.0±0.6 5 c	2.54±0 .46 d
24 h	60	5165	1619	31.34± 1.11 i	46	18.57± 0.47 f	9.45±0. 45 d	1.87±1. 14 g	1.45±0 .95 dfk
	90	5082	1411	27.76± 0.94 j	40	11.83± 0.59 h	9.36±0. 89 d	4.12±0. 37 hk	2.45±1 .76 dhj
	120	5097	1245	24.42± 1.79 k	36	9.35±1. 94 i	8.29±1. 25 ej	4.31±0. 96 hjk	2.47±1 .14 d
	Cont rol	5034	3247	64.50± 1.54 a	100	35.84± 0.98 j	13.47± 1.32 i	10.51± 1.24 i	4.68±0 .76 g
	MM S	5097	1859	36.47± 0.39 l	57	21.18± 0.73 g	8.51±0. 28 e	4.81±0. 78 j	1.97±1 .81 df
	30	5059	1172	23.16± 0.38 m	36	9.15±0. 33 ikm	7.82±0. 18 j	4.16±0. 41 k	2.03±0 .97 dhi
48 h	60	5124	955	18.63± 0.72 n	29	9.76±1. 10 im	5.17±0. 23 k	2.11±1. 28 g	1.59±0 .25 hfj
	90	5098	845	16.57± 0.47 o	26	8.42±0. 93 ik	4.92±0. 35 k	2.14±0. 64 g	1.09±0 .96 ef
	120	5024	528	10.50± 1.36 p	16	5.13±1. 29 n	3.68±1. 56 l	1.05±0. 87 d	0.64±1 .25 ek

The means ± SD values with different letter indicate statistically significant differences, according to Tukey ($P \leq 0.05$). SD: Standard deviation. GMI: General mitotic index. PMI: Prophase mitotic index. MMI: Metaphase mitotic index. AMI: Anaphase mitotic index. TMI: Telephase mitotic index.

The proportional changes in mitotic index as a result of the application of different doses of Fluquinconazole to *A. cepa* roots with 12, 24, and 48 hours of application periods are given in Table 2. Changes in mitotic phase are also shown in the same table. At the end of the evaluations, it was identified that the mitotic index declined at all application doses and times compared to the negative and positive control groups, which was statistically significant. Statistical analysis for mitotic phases showed a decrease in all phases compared to the control group. Increases or decreases in mitotic index and mitotic phases are important indicators that are used to show the cytotoxic effect of the substances tested (Marcano et al. 2004; Fernandes et al. 2007; Leme and Marin-Morales 2009). Although there are many studies showing the changes in mitotic index and mitotic stage ratios caused by pesticides, there is no study on this effect of

Fluquinconazole (Bernardes et al. 2015; Verma and Srivastava 2018; Salazar-Mercado et al. 2020; Sheikh et al. 2020; Kalefetoğlu Macar 2020; Aragão et al. 2021; Gallego and Olivero-Verbel 2021; Khan et al. 2021). Mitotic index is an acceptable cytotoxic criterion for all living organisms. The cytotoxic level can be determined by a decrease in the mitotic index ratio. Reductions of less than 50% usually indicate a sublethal effect. If the reduction in mitotic index ratio exceeds 50%, it may have a lethal effect on the test organism. Inhibition of the mitotic index may be caused by the suppression of any of the G1, S, or G2 phases of DNA or by the impairment of RNA and/or protein synthesis (Grossmann et al. 2001; Sudhakar et al. 2001; Saxena et al. 2005; Kaymak 2005; Barriuso et al. 2010; Siddiqui et al. 2012; Singh and Roy 2017; Fioresi et al. 2020). In addition, mutations in cyclin and kinase proteins involved in the control of cell division also cause inhibition of mitotic index and mitotic stages (Marc et al. 2002, 2004; Aragão et al. 2021; Altman 2017). We believe that Fluquinconazole used in this study effectively decreased the mitotic index in *A. cepa* root tip cells compared to the control. The inhibition in root growth rates also supports this conclusion.

Table 3. Frequency of Chromosomal Anomalies (CA) at *A. cepa* tip of the root treated with different concentrations of fluquinconazole.

Time of treatment (h)	Concentrations (mg/L)	Total studied cells	Anaphase bridges (%)	Stickiness (%)	C-mitosis (%)	Laggards (%)	Breaks (%)	Chromosomal aberration (%)
12 h	Control	500	0.74	1.01	0.38	0.28	-	2.41±1.27 a
	MMS	500	4.56	6.14	3.54	0.31	0.95	15.50±2.14 b
	30	500	3.21	5.24	3.16	0.70	1.57	13.88±2.49 b
	60	500	4.87	7.61	6.25	0.98	1.78	21.49±1.04 c
	90	500	4.96	8.23	5.38	2.45	2.76	23.78±0.57 cd
	120	500	5.19	7.86	6.31	3.95	2.17	25.48±2.04 d
24 h	Control	500	0.12	0.89	0.51	0.60	0.23	2.35±0.23 a
	MMS	500	7.21	8.17	6.87	1.72	1.09	25.06±0.18 b
	30	500	5.23	10.45	4.39	2.43	2.64	25.14±0.15 b
	60	500	8.47	15.28	9.51	5.71	3.28	42.25±0.21 c
	90	500	9.34	19.79	13.47	7.36	2.69	52.65±1.14 d
	120	500	11.63	20.87	15.41	3.00	2.36	53.27±0.22 d

	Control	500	0.24	1.05	0.87	0.39	0.16	2.71±0.28 a
	MMS	500	12.02	11.35	11.16	3.05	1.51	39.09±0.11 b
	30	500	13.21	15.69	15.48	10.27	1.75	56.40±1.25 c
48 h	60	500	17.24	24.03	19.94	10.78	3.05	59.04±1.97 c
	90	500	16.17	19.36	14.26	10.65	2.09	62.53±2.48 d
	120	500	12.64	21.67	15.97	11.28	3,41	64.97±1.76 d

The means ± SD values with different letter indicate statistically significant differences, according to Tukey ($P \leq 0.05$). SD: Standard deviation.

Table 3 shows the types and ratios of chromosomal abnormalities caused by Fluquinconazole in *A. cepa* root tip cells and the total abnormality ratio. As can be also seen in the table, all doses we used in the study at 12, 24 and 48 hours of application caused more abnormalities than the control. In the statistical evaluations, it was identified that this situation was significant compared to the negative control group. There was no statistical difference between the 120 mg/L dose in the 12-hours application and the 30 mg/L dose in the 24-hours application. It was also detected that these groups showed similar ratios with the positive control group. In addition, 90 and 120 mg/L doses in the 24-hours application were found to be statistically insignificant. When the types of fungicide-induced chromosomal abnormalities were analyzed, stickiness was observed to occur at the highest rate. This was followed by C-mitosis, anaphase bridges, laggards, and chromosome breakages. At 48 hours of application, the number of these abnormalities increased. Used as a biological indicator of chromosomal damage and genome instability, the chromosomal abnormality test is one of the most widely applied and rapid tests in populations exposed to genotoxic agents (El-Zein et al. 2011; Suspiro and Prista 2011; Yüzbaşıoğlu et al. 2003, 2014). Chromosomal abnormalities are changes in normal chromosome structure (structural abnormality) or number (numerical abnormality) that occur spontaneously or as a result of exposure to chemicals/radiation (Russel 2002). The assessment of chromosomal abnormalities takes into account the disturbances in the four phases of the cell cycle (prophase, metaphase, anaphase, and telophase). Chromosomal abnormality analysis not only allows the prediction of genotoxic effects, but also helps in the evaluation of clastogenic and aneugenic formations. Chromosomal abnormalities include changes in chromosomal structure or chromosomal number. Changes in chromosomal structure can result from DNA breakdown, inhibition of DNA synthesis, and

modification of DNA replication. The clastogenic effect causes various chromosomal abnormalities, including chromosomal breakages and bridges. Aneuploidy and polyploidy are numerical abnormalities caused by abnormal chromosome segregation (stickiness, C-metaphases, laggards, chromosome losses and multipolarity) either under the influence of aneugenic agents or spontaneously.

Studies have shown that chromosome stickiness is induced by most of the pesticides (Pulate and Tarar 2014a; Kutluer et al. 2019; Verma and Srivastava 2018). Chromosome stickiness can also be observed at high frequency due to the disruption of the nucleic acid metabolism of the cell. The sticky chromosomes caused abnormal unwinding of chromosomes during the transition from anaphase to telophase. Chromosome stickiness may be due to the delay in chromosome movement caused by fungicide application. Thus, the chromosome could not reach the poles and remained dispersed in the cytoplasm, resulting in a dense and sticky appearance. Chromosome stickiness is caused by the misfolding of chromosome fibers into single chromatids and chromosomes. As a result, the fibers become tangled, and the chromosomes are connected to each other via subchromatid bridges. The stickiness may occur due to the effect of the fungicide on the polymerization process or may result in the fragmentation of chromosomes (Chidambaram et al. 2009; Yüzbaşıoglu et al. 2003; Pulate and Tarar 2014b). It is stated that the stickiness of chromosomes is the result of a cytotoxic effect, which is irreversible and ultimately leads to cell death (Dizdari and Kopliku 2013; Goujon et al. 2014, Basu and Tripura 2021; Kundu and Ray 2016).

Another chromosome abnormality caused by Fluquinconazole is C-mitosis (Table 3). The term C-mitosis was coined by Levan (1938) and refers to a type of abnormality in which colchicine inhibits the formation of spindle apparatus, causing chromosomes to disperse within the cell. C-mitosis formation has been found in many studies investigating the genotoxic effects of pesticides (Türkoğlu 2007; Dizdari and Kopliku 2013; Fatma et al. 2018; Datta et al. 2018; Zeyad et al. 2019; Gallego and Olivero-Verbe 2021). Hsu et al. (1986) suggested that c-mitosis induced by mutagens is due to the blockage of tubulin polymerization or aggregation of microtubules and tubulin into crystalline forms. Fluquinconazole might have a colchicine-like effect, causing a change in the protein structure of spindle apparatus.

Another chromosome abnormality that occurred as a result of the study was recorded as anaphase bridge (Table 3). It has been reported that bridges are formed by the breakage and reassembly of chromosomes. The adhesion of chromosomes prevents the chromatids from separating from each other, leading them to remain attached to each other by bridges (Kabarity et al. 1974, Badr et

al. 1992). It has been reported that adherent bridges may be the result of incomplete replication of chromosomes due to defective or underactivated replication enzymes (Sinha 1979) or late replication of telomeric heterochromatin DNA sequences (Bennet 1977). If heterochromatin blocks have not completed DNA replication when the nucleus is ready to divide, bridge formation might occur (Kaltsikes et al. 1984). In our study, the bridges observed in ana-telophase were usually single whereas double and triple bridges were also observed. Double and triple bridges are also noted to occur as a result of unequal polarization or dyscentric chromosomes, or due to chromosome breakages or fragmentation and failure of terminalisation (El-Ghamery et al. 2000, Luo et al. 2004).

Another abnormality caused by the chemical under investigation is laggard (Table 3). These chromosomes may have resulted from chromosomes that could not be attached to the spindle apparatus and moved towards each other from the two poles, or from acentric fragments. C-mitosis formations, which are among the abnormalities we obtained as a result of our study, are also due to disruption of the spindle apparatus structure. In this case, it can be thought that the substance we used disrupted the spindle apparatus structure and interfered with chromosome attachment in the metaphase phase of mitosis, resulting in laggards (Patil and Bhat 1992; Pulate and Tarar 2014 a, b; El-Ghamery and Mousa 2017). Laggards can lead to micronuclei formation and sometimes contribute to chromosomal evolution by causing aneuploid gametes.

Chromosome breakages occur when chromosomes are exposed to physical or chemical agents outside of normal conditions (Table 3). Different chemicals have been found to cause breakage by many researchers (Inceer et al. 2000; Kumar and Pannverselvan 2007; Khan et al. 2020, 2021; Hobs et al. 2017). Rieger et al. (1973) reported that heterochromatic regions of chromosomes are primarily broken. Fluquinconazole showed a clastogenic effect and caused breakages and fragments in the chromosomes of *A. cepa* root tip meristem cells. In this case, it can be said that this substance is also effective especially on heterochromatic regions.

Table 4. Frequency of Nucleer Anomalies (NA) at *A. cepa* tip of the root treated with different concentrations of fluquinconazole.

Time of treatment (h)	Concentrations (mg/L)	Total studied cells	Micronuclei (%)	Binucleate cell (%)	Total Nuclear aberration (%)
	Control	500	0.00	0.00	0.00 a
	MMS	500	2.18	1.61	3.79 b
	30	500	5.34	4.29	9.63 c
12 h	60	500	8.21	8.35	16.56 d
	90	500	7.36	9.21	16.57 d
	120	500	9.17	10.87	20.04 e
	Control	500	0.00	0.00	0.00 a
	MMS	500	4.35	1.42	5.77 b
	30	500	1.24	4.54	5.78 b
24 h	60	500	6.38	7.63	14.01 c
	90	500	9.46	8.97	18.43 d
	120	500	13.41	11.13	24.54 e
	Control	500	0.00	0.00	0.00 a
	MMS	500	7.56	1.87	9.43 b
	30	500	13.43	6.51	19.94 c
48 h	60	500	17.51	9.28	26.79 d
	90	500	24.02	13.49	37.51 e
	120	500	25.98	12.98	38.96 e

The means ± SD values with different letter indicate statistically significant differences, according to Tukey ($P \leq 0.05$). SD: Standard deviation.

The effects of the substance used in this study on the nucleus were also investigated and the nuclear abnormalities observed are given in Table 4. The observation of NA in *A. cepa* root tip cells is an indicator of cytotoxic and genotoxic effect. Nuclear abnormalities in addition to chromosomal abnormalities have been examined in recent studies, paving the way for a better understanding of the effects of the test material used on the DNA of the organism to which it is applied and a more sensitive analysis of the results (Leme et al. 2008; Fernandes et al. 2009; Abdel Migid et al. 2007; Caritá and Marin-Morales 2008; Leme and Marin-Morales 2009; Nefic et al. 2013; Kassa 2021; Bonciu et al. 2018; Adrovic et al. 2021). NAs are categorized into five main groups: binuclei, notched nuclei, blebbed nuclei, MN, and lobed nuclei. In addition, cellular abnormalities with vacuoles, which is a sign of cytotoxic effect, can also be included in this group. These formations are observed in the interphase phase of the cell cycle. In our study, binucleated cells and vacuolated cells were

observed. Binuclear cells are the result of a faulty cell division process in which karyokinesis is complete while cytokinesis is incomplete. According to Leme et al. (2008), the presence of these abnormal nucleated cells indicates a process of cell death. In addition, the presence of NAs can also occur as a result of clastogenic and aneugenic effects, which supports the toxic effect of the substance we used. Disruptions in the structure of the spindle apparatus and microtubules involved in the formation of the middle lamellae with the effect of the substance used cause errors in the anaphase phase, resulting in the formation of multinucleated cells as a result of karyokinesis followed by unsuccessful cytokinesis (Verma and Srivastava 2018; Fernandes et al. 2007; Fenech 2000, 2005; Fernandes et al. 2009, Nefic et al. 2013). Another nuclear abnormality we detected in the study was micronucleus (Table 4). Micronuclei (MN) are formations consisting of whole chromosomes or chromosome fragments without centromere, independent of the main nucleus, and located in the cytoplasm during mitosis. They are caused by deficiencies in genes involved in the control of the cell cycle, by defects in spindle apparatus, kinetochore or other parts of the mitotic apparatus, or by defects that cause chromosomal damage. Aneuploidy-inducing agents cause MN formation by preventing the centromeres from dividing properly and the spindle apparatus from functioning properly while clastogens cause chromosome breakages (Fenech et al. 2010, Kisurina-Evgenieva et al. 2016; Fernandes et al. 2007). Micronucleated cells (MNs) represent permanent DNA damage due to the gradual loss of genetic material induced by the first mitotic cycle after chemical treatment (Kopliko and Mesi 2012). This DNA damage can also be observed as chromosomal abnormalities (CAs) when cells divide. Table 4 shows that the fungicide used in the study triggered micronucleus formation in Allium and micronucleus rates increased significantly compared to the control, which was statistically significant. According to these results, Fluquinconazole triggered micronucleus formation in *Allium cepa* stem cells by causing disruptions in the structure of DNA and/or spindle apparatus or by causing breakages in chromosomes. In addition to micronucleus formation, the presence of binucleated cells and the observation of laggards in chromosome abnormalities also support this theory.

CONCLUSION

The results of this study have shown that the fungicide with Fluquinconazole active substance, which is widely used in Turkish agriculture especially in wheat production and sold in the market under different trade names, causes cytotoxic and genotoxic effects in *Allium cepa* root tip meristem cells. Reduction in root growth, inhibition of mitotic index, and chromosomal and nuclear abnormalities

were identified, indicating that this substance should be considered an environmental hazard. The EC50 value is a useful parameter for selecting test concentrations in genotoxicity assays. The root inhibition observed in this process is detected as a decrease in meristematic activity, which is associated with inhibition of DNA and/or protein synthesis. In this case, it can be said that the fungicide used negatively affected root elongation by inhibiting protein synthesis and apical meristematic activity in *A. cepa* root tip meristem cells. The cytotoxicity levels of different chemicals can be identified by the variation in MI. A mitotic index lower than the negative control may indicate that the growth and development of the test organisms were affected by the test chemicals. The fungicide used was found to effectively reduce the mitotic index. This effect of the fungicide may occur at different stages of the cell cycle as well as at later stages. Based on the data we obtained, this substance is thought to be cytotoxic due to its mitodepressive effect. In addition, chromosomal (anaphase bridges, stickiness, c-mitosis, breakages, and laggards) and nuclear abnormalities (binucleus, micronucleus) observed at the end of the study indicate that the fungicide used is aneugenic and clastogenic. Furthermore, the *A. cepa* test proved once again to be a rapid and sensitive test in detecting environmental genotoxics and mutagens.

Fungi have evolved over one billion years and can be found in many habitats worldwide thanks to their adaptability and flexibility. Among a lot of species of fungi, some are pathogenic. People use fungicides to reduce production losses. However, while fungicides have contributed to a significant increase in agricultural productivity, their overuse has led to both health and environmental impacts. The first cytotoxic and genotoxic data related with Fluquinconazole have been obtained in this study. This fungicide and others containing Fluquinconazole will continue to be a cornerstone of the agricultural industry. However, in order to advocate for sustainable and environmentally friendly agriculture, it is recommended to develop safer formulations and to conduct research on lower concentrations and shorter exposure times. Since the data obtained in this study indicate that the fungicide has a cytogenotoxic effect, caution should also be exercised against unintended damage to both the applicators and the crops applied.

Authors and Affiliations

Sivas Cumhuriyet University, Faculty of Science, Department of Biology, 58070, Sivas, Turkey.

Şifa Türkoğlu

Data availability

The data that supports the findings of this study is available for sharing from the corresponding author upon reasonable request.

Contributions

All of the scientific studies in this article were carried out by the author, Şifa Türkoğlu, and he critically revised the manuscript, commented on the drafts of the manuscript, and approved the final manuscript.

Corresponding author

Correspondence to Şifa Türkoğlu.

Ethics approval and consent to participate.

Not applicable.

Consent for publication

Not applicable.

Competing interests

The author declares no competing interests.

Funding

No funding was obtained for this study

REFERENCES

Abdel Migid HM, Azab YA, & Ibrahim WM (2007) Use of plant genotoxicity bioassay for the evaluation of efficiency of algal biofilters in bioremediation of toxic industrial effluent. Ecotoxicology and Environmental Safety 66(1): 57–64. DOI: 10.1016/j.ecoenv.2005.10.011

Adrovic J, Eminovic I, Stojko Vidovic S, and Feriz Adrovic F (2021) Chromosomal aberrations and nuclear anomalies in root tip cells of *Allium cepa* L. caused by radon in water. IJMBR (Int. J. Mod. Biol. Res.) 9: 25-36. doi.org/10.33500/ijmbr.2020.9.003

Altman J (2017) Pesticide interactions in crop production: Beneficial and deleterious effects. CRC Press. ISBN 9781315896359, 591 Pages.

Aragão FB, Duarte ID, Fantinato DE, Galter IN, Silveira GL, dos Reis GB, Andrade-Vieira LF, & Matsumoto ST (2021) Toxicogenetic of tebuconazole based fungicide through *Lactuca sativa* bioassays. Ecotoxicology and Environmental Safety 213, 111985. https://doi.org/10.1016/j.ecoenv.2021.111985

Badr A, Ghareeb A and El-Din HM (1992). Cytotoxicity of some pesticides in mitotic cells of *V. faba* roots. Egyptian Journal of Applied Sciences 7: 457–468.

Barriuso J, Marín S, & Mellado RP (2010) Effect of the herbicide glyphosate on glyphosate-tolerant maize rhizobacterial communities: A comparison with pre-emergency applied herbicide consisting of a combination of acetochlor and terbuthylazine. Environmental Microbiology 12(4): 1021–1030. DOI: 10.1111/j.1462-2920.2009.02146.x

Basu S and Tripura K (2021). Differential sensitivity of *Allium cepa* L. and *Vicia faba* L. to aqueous extracts of *Cascabela thevetia* (L.) lippold. South African Journal of Botany 139: 67–78. https://doi.org/10.1016/j.sajb.2021.01.033

Bateman GL, Gutterıdge RJ and Jenkyn JF (2004). Take-all and grain yields in sequences of winter wheat crops testing fluquinconazole seed treatment applied in different combinations of years. Ann. Appl. Biol. 145: 317-330. **https://doi.org/10.1111/j.1744-7348.2004.tb00389.x**

Bellani L, Muccifora S, Barbieri F, Tassi E, Ruffini Castiglione M, & Giorgetti L (2020). Genotoxicity of the food additive E171, titanium dioxide, in the plants *Lens culinaris* L. and *Allium cepa* L. Mutation Research/Genetic Toxicology and Environmental Mutagenesis 849, 503142. https://doi.org/10.1016/j.mrgentox.2020.503142

Bennet MD (1977) Heterochromatin, aberrant endosperm nuclei and grain shriveling in wheat-rye genotypes. Heredity 39: 411-419.

Bernardes PM, Andrade-Vieira LF, Aragão FB, Ferreira A, & da Silva Ferreira MF (2015) Toxicity of Difenoconazole and tebuconazole in *Allium cepa*. Water, Air, & Soil Pollution 226(7). DOI: 10.1007/s11270-015-2462-y

Bonciu E, Roșculete E, Olaru AL, & Roșculete CA (2018) Evaluation of the mitodepressive effect, chromosomal aberrations and nuclear abnormalities induced by urea fertilization in the meristematic tissues of *Allium cepa* L. Caryologia 71(4): 350–356. https://doi.org/10.1080/00087114.2018.1473918

BKU (2023) https://bku.tarimorman.gov.tr/AktifMaddeGrup/Details/159?csrt=10387680295507611051&undefined=undefined (Last Access Date: 01/24/2023)

Caritá R and Marin-Morales MA (2008) Induction of chromosome aberrations in the *Allium cepa* test system caused by the exposure of seeds to industrial effluents contaminated with azo dyes. Chemosphere 72(5): 722–725. DOI: 10.1016/j.chemosphere.2008.03.056

Causil Vargas LA, Coronado JL, Verbel LF, Vega J, MF, Donado E, KA, & Pacheco GC (2017). Efecto Citotóxico del Hipoclorito de Sodio (naclo), en células ápicales de raíces de cebolla (*Allium cepa* L.). Revista Colombiana De Ciencias Hortícolas 11(1): 97–104. https://doi.org/10.17584/rcch.2017v11i1.5662.

Chauhan LKS, Saxena PN & Gupta SK (1999) Cytogenetic effects of cypermethrin and fenvalerate on the root meristem cells of *Allium cepa*. Environmental and Experimental Botany 42(3): 181–189. https://doi.org/10.1016/S0098-8472(99)00033-7

Chidambaram A, Sundaramoorthy P, Murugan A, Ganesh SK, Baskaran L (2009) Chromium induced cytotoxicity in Black gram (*Vigna mungo* L.). Ind. J. Environ. Health. Sci. Eng. 6 (1): 17-22.

Datta S, Singh J, Singh J, Singh S & Singh S (2018) Assessment of genotoxic effects of pesticide and vermicompost treated soil with *Allium cepa* test. Sustainable Environment Research 28(4): 171–178. https://doi.org/10.1016/j.serj.2018.01.005

de Morais CR, Pereira BB, Almeida Sousa PC, Vieira Santos VS, Campos CF, Carvalho SM, Spanó MA, de Rezende AAA, Bonetti AM (2019) Evaluation of the genotoxicity of neurotoxic insecticides using the micronucleus test in *Tradescantia pallida*. Chemosphere 227: 371-380. DOI: 10.1016/j.chemosphere.2019.04.073

de Sousa FA, de Morais CR, Vieira JS, Maranho LS, Machado FL, Pereira S, Barbosa LC, Coelho HE, Campos CF, Bonetti AM (2019) Genotoxicity

and carcinogenicity of ivermectin and amoxicillin in vivo systems. Environ Toxicol Pharmacol. 70, 103196. DOI: 10.1016/j.etap.2019.103196

Dizdari AM and Kopliku D (2013) Cytotoxic and genotoxic potency screening of two pesticides on *Allium cepa* L. Procedia Technology 8: 19–26. https://doi.org/10.1016/j.protcy.2013.11.005

EFSA (2011) Conclusion on the peer review of the pesticide risk assessment of the active substance fluquinconazole, EFSA Journal 9(5): 2096

El-Ghamery AA and Mousa MA (2017) Investigation on the effect of benzyladenine on the germination, radicle growth and meristematic cells of *Nigella sativa* L. and *Allium cepa* L. Annals of Agricultural Sciences 62(1): 11–21. https://doi.org/10.1016/j.aoas.2016.11.002

El-Ghamery AA, El Nahas AI and Mansour MM (2000) The action of atrazine herbicide as an inhibitor of cell division on chromosomes and nucleic acids content in root meristems of *Allium cepa* and *Vicia faba*. Cytologia 55: 209–215. https://doi.org/10.1508/cytologia.65.277

El-Zein R, Vral A, & Etzel CJ (2011) Cytokinesis-blocked micronucleus assay and cancer risk assessment. Mutagenesis 26(1): 101–106. DOI: 10.1093/mutage/geq071

Fatma F, Verma S, Kamal A & Srivastava A (2018). Monitoring of morphotoxic, cytotoxic and genotoxic potential of Mancozeb using Allium assay. Chemosphere 195: 864–870. DOI: 10.1016/j.chemosphere.2017.12.052

Fenech M (2005) In vitro micronucleus technique to predict chemosensitivity. Methods Mol Med. 111:3-32. DOI: 10.1385/1-59259-889-7:003

Fenech M (2000). The in vitro micronucleus technique. Mutat Res. 455(1-2):81-95. https://doi.org/10.1016/S0027-5107(00)00065-8

Fenech M, Kirsch-Volders M, Natarajan AT, Surralles J, Crott JW, Parry J, Norppa H, Eastmond DA, Tucker JD & Thomas P (2010) Molecular mechanisms of micronucleus, nucleoplasmic bridge and nuclear bud formation in mammalian and human cells. Mutagenesis 26(1): 125–132. DOI: 10.1093/mutage/geq052

Fernandes TC, Mazzeo DE & Marin-Morales MA (2009) Origin of nuclear and chromosomal alterations derived from the action of an aneugenic agent—Trifluralin herbicide. Ecotoxicology and Environmental Safety 72(6): 1680–1686. DOI: 10.1016/j.ecoenv.2009.03.014

Fernandes, T.C.C., Mazzeo, D.E., & Marin-Morales, M.A., 2007. Mechanism of micronuclei formation in polyploidizated cells of *Allium cepa* exposed to trifluralin herbicide. Pesticide Biochemistry and Physiology, *88*(3), 252–259. https://doi.org/10.1016/j.pestbp.2006.12.003

Fioresi VS, de Cássia Ribeiro Vieira B, de Campos JM & da Silva Souza T (2020) Cytogenotoxic activity of the pesticides imidacloprid and iprodione on *Allium cepa* root meristem. Environmental Science and Pollution Research 27(22): 28066–28076. DOI: 10.1007/s11356-020-09201-5

Fiskesjö G (1985) The *Allium cepa* test as a standard in environmental monitoring. Hereditas 102: 99-112.

Fusconi A, Repetto O, Bona E, Massa N, Gallo C, Dumas-Gaudot E & Berta G (2006) Effects of cadmium on meristem activity and nucleus ploidy in roots of *Pisum sativum* L. cv. frisson seedlings. Environmental and Experimental Botany 58(1-3): 253–260. https://doi.org/10.1016/j.envexpbot.2005.09.008

Gallego JL and Olivero-Verbel J (2021) Cytogenetic toxicity from pesticide and trace element mixtures in soils used for conventional and organic crops of *Allium cepa* L. Environmental Pollution 276, 116558. DOI: 10.1016/j.envpol.2021.116558

Goujon E, Sta C, Trivella A, Goupil P, Richard C & Ledoigt G (2014) Genotoxicity of Sulcotrione pesticide and photoproducts on *Allium cepa* root meristem. Pesticide Biochemistry and Physiology 113: 47–54. https://doi.org/10.1016/j.pestbp.2014.06.002

Grossmann K, Tresch S and Plath P (2001) Triaziflam and diaminotriazine derivatives affect enantioselectively multiple herbicide target sites. Zeitschrift Für Naturforschung C 56(7-8): 559–569. DOI: 10.1515/znc-2001-7-814

Gutteridge RJ, Jenkyn JF, Bateman GL (2007) The potential of non-pathogenic Gaeumannomyces spp., occurring naturally or introduced into wheat crops or preceding crops, for controlling take-all in wheat. Ann Appl Biol., 150: 53–64. https://doi.org/10.1111/j.1744-7348.2006.00107.x

Hobs CA, Saigo K, Koyanagi M & Hayashi S (2017) Magnesium stearate, a widely-used food additive, exhibits a lack of in vitro and in vivo genotoxic potential. Toxicology Reports, 4: 554–559. DOI: 10.1016/j.toxrep.2017.10.003

Hsu TC, Liang JC and Sataya-Prakash KL (1986) Cytogeneticassays for mitotic poisons using somatic animal cells. In: Serres FJ [ed.], Chemical mutagens, principles and methods for their detection, 10: 155–182. ISBN: 978-1-4613-3694-5, Plenum Press.

Ilyushina NA, Egorova OV, Masaltsev GV, Averianova NS, Revazova YA, Rakitskii VN, Goumenou M, Vardavas A, Stivaktakis P, Tsatsakis A (2020) Genotoxicity of mixture of imidacloprid, imazalil and tebuconazole. Toxicology Reports 7: 1090-1094. DOI: 10.1016/j.toxrep.2020.08.021

Inceer H, Beyazoglu O and Ergul HA (2000) Cytogenetic Effects of Wastes of Copper Mine on Root Tip Cells of *Allium cepa* L. Pakistan Journal of Biological Sciences 3: 376-377. DOI: 10.3923/pjbs.2000.376.377

Kabarity A, El-Bayoumi AS and Habib AA (1974) Effect of morphine sulphate on mitosis of *Allium cepa* root tips. Biologia Plantarum 16: 275–282.

Kalefetoğlu Macar T (2020) Investigation of cytotoxicity and genotoxicity of abamectin pesticide in *Allium cepa* L. Environmental Science and Pollution Research 28(2): 2391–2399. DOI: 10.1007/s11356-020-10708-0

Kaltsikes PJ (1984) Breeding vegetable varieties resistant to diseases. Proc. 3rd Meeting on Protected Vegetables and Flowers, May 911, Heraklion, Crete, p. 60. Abstract.

Kassa BA (2021) Cytotoxicity and genotoxicity evaluation of municipal wastewater discharged into the head of Blue Nile River using the *Allium cepa* test. Scientific African 13, e00911. https://doi.org/10.1016/j.sciaf.2021.e00911

Kaymak F (2005) Cytogenetic effects of maleic hydrazide on *Helianthus annuus* L. Pakistan Journal of Biological Sciences 8(1): 104–108. DOI: 10.3923/pjbs.2005.104.108

Khan A, Kumar V, Srivastava A, Saxena G & Verma PC (2021) Biomarker-based evaluation of cytogenotoxic potential of glyphosate in *Vigna Mungo* (L.) Hepper genotypes. Environmental Monitoring and Assessment 193(2): 73. DOI: 10.1007/s10661-021-08865-x

Khan IS, Ali MN, Hamid R & Ganie SA (2020) Genotoxic effect of two commonly used food dyes metanil yellow and Carmoisine using *Allium cepa* L. as indicator. Toxicology Reports 7: 370–375. DOI: 10.1016/j.toxrep.2020.02.009

Kihlman BA (1971) Root tips for studying the effects of chemicals on chromosomes. In: Hollaender, A., (Ed.), Chemical Mutagens, Plenum Press, New York, pp.489-514.

Kisurina-Evgenieva OP, Sutiagina, OI & Onishchenko GE (2016) Biogenesis of micronuclei. Biochemistry (Moscow) 81(5): 453–464. DOI: 10.1134/S0006297916050035

Kumar LP and Pannverselvan N (2007) Cytogenetic studies of food preservative in *Allium cepa* root meristematic cells. Facta Universitatis 14: 60-63.

Kundu LM & Ray S (2016) Mitotic abnormalities and micronuclei inducing potentials of colchicine and leaf aqueous extracts of *Clerodendrum viscosum* vent. in *Allium cepa* root apical meristem cells. Caryologia 70(1): 7–14. https://doi.org/10.1080/00087114.2016.1254452

Kutluer F, Çavuşoğlu K, Yalçın E (2019) The investigation of the physiological, anatomical and genotoxic effects in *Allium cepa* L. of Deltamethrin. Duzce University Journal of Science and Technology 7: 961-972. https://doi.org/10.29130/dubited.457074

Leme DM, Angelis D de & Marin-Morales MA (2008) Action mechanisms of petroleum hydrocarbons present in waters impacted by an oil spill on the genetic material of *Allium cepa* root cells. Aquatic Toxicology 88(4): 214–219. DOI: 10.1016/j.aquatox.2008.04.012

Leme DM and Marin-Morales MA (2009) *Allium cepa* test in environmental monitoring: A review on its Application. Mutation Research/Reviews in Mutation Research 682(1): 71–81. https://doi.org/10.1016/j.mrrev.2009.06.002

Levan A (1938) The effect of colchicine on root mitoses in Allium. Hereditas 24: 471-486.

Lovinskaya A, Kolumbayeva S, Begimbetova D, Suvorova M, Bekmagambetova N & Abilev S (2021). Toxic and genotoxic activity of river waters of the Kazakhstan. Acta Ecologica Sinica 41(6): 499–511. https://doi.org/10.1016/j.chnaes.2021.01.011

Luo LZ, Werner KM, Gollin SM & Saunders WS (2004) Cigarette smoke induces anaphase bridges and genomic imbalances in normal cells. Mutation Research/Fundamental and Molecular Mechanisms of Mutagenesis 554(1-2): 375–385. https://doi.org/10.1016/j.mrfmmm.2004.06.031

Marc J, Mulner-Lorillon O, Boulben S, Hureau D, Durand G & Bellé R (2002) Pesticide roundup provokes cell division dysfunction at the level of Cdk1/cyclin B activation. Chemical Research in Toxicology 15(3): 326–331. https://doi.org/10.1021/tx015543g

Marc J, Mulner-Lorillon O & Bellé R (2004) Glyphosate-based pesticides affect cell cycle regulation. Biology of the Cell 96(3): 245–249. DOI: 10.1016/j.biolcel.2003.11.010

Marcano L, Carruyo I, Del Campo A & Montiel X (2004) Cytotoxicity and mode of action of maleic hydrazide in root tips of *Allium cepa* L. Environmental Research 94(2): 221–226. DOI: 10.1016/s0013-9351(03)00121-x

Marinho MDC, Diogo BS, Lage OM, Antunes SC (2020) Ecotoxicological evaluation of fungicides used in viticulture in non-target organisms. Environ Sci Pollut Res Int. 27(35): 43958-43969. DOI: 10.1007/s11356-020-10245-w

Maurya R, Dubey K, Singh D, Jain AK, Pandey AK (2019) Effect of difenoconazole fungicide on physiological responses and ultrastructural

modifications in model organism Tetrahymena pyriformis. Ecotoxicol Environ Saf. 182, 109375. DOI: 10.1016/j.ecoenv.2019.109375

Mercado SAS and Caleño JD (2020) Cytotoxic evaluation of glyphosate, using *Allium cepa* L. as bioindicator. Science of The Total Environment 700, 134452. DOI: 10.1016/j.scitotenv.2019.134452

Nefic H, Musanovic J, Metovic A & Kurteshi K (2013) Chromosomal and nuclear alterations in root tip cells of *Allium cepa* L. induced by Alprazolam. Medical Archives 67(6), 388. doi: 10.5455/medarh.2013.67.388-392

Pitombeira de Figueirêdo, L, Athayde DB, Daam MA, van Gestel CAM, Guerra GDS, Duarte-Neto PJ, Espíndola ELG (2020) Impact of temperature on the toxicity of Kraft 36 EC® (a.s. abamectin) and Score 250 EC® (a.s. difenoconazole) to soil organisms under realistic environmental exposure scenarios. Ecotoxicol Environ Saf., 194, 110446. DOI: 10.1016/j.ecoenv.2020.110446

PUBCHEM (2023) https://pubchem.ncbi.nlm.nih.gov/compound/Fluquinconazole (Last Access Date: 01/24/2023)

Pulate PV and Tarar JL (2014a) Cytogenetic effects of tilt on root tip meristem of onion *Allium cepa* L. International Journal of Plant, Animal and Environmental Sciences (IJPAES) 4(2): 53-57.

Pulate PV and Tarar JL (2014b) Cytogenetic effect of systemic fungicide calixin on root meristem cells of *Allium cepa* L. International Journal of Life-Sciences Scientific Research 2: 341-345

Patil BC and Bhat GI (1992) A comparative study of MH and EMS in the induction of chromosomal aberrations on lateral root meristem in *Clitoria ternatea* L.. Cytologia 57(2): 259–264.

Ramanauskienė J, Semaškienė R, Jonavičienė A & Ronis A (2018) The effect of crop rotation and fungicide seed treatment on take-all in winter cereals in Lithuania. Crop Protection 110: 14–20. DOI: 10.1016/j.cropro.2018.03.011

Rank J (2003) The method of allium anaphase-telophase chromosome aberration assay. Ekologija Vilnius 1: 38- 42.

Rieger R, Nicolof H, Michaelis A (1973) Intro chromosomal clustering of chromatic aberrations induced by N-Methyl-N-NitrosoUrethan in *Vicia faba* and Barley. Biol. Zent. 92: 681-189.

Russel PJ (2002) Chromosomal mutation B. Cummings (Ed.), Genetics, Pearson Education Inc., San Francisco, pp. 595-621

Salazar-Mercado AA, Caleño JDQ, Jhan Piero Rojas Suárez JPR (2020) Cytogenotoxic effect of propanil using the *Lens culinaris* Med and *Allium cepa* L test. Chemosphere 249, 126193. DOI: 10.1016/j.chemosphere.2020.126193

Saxena PN, Chauhan LKS & Gupta SK (2005) Cytogenetic effects of commercial formulation of cypermethrin in root meristem cells of *Allium sativum*: Spectroscopic basis of chromosome damage. Toxicology 216(2-3): 244–252. DOI: 10.1016/j.tox.2005.08.008

Scherm H, Christiano RSC, Esker PD, Del Ponte EM, Godoy CV (2009) Quantitative review of fungicide efficacy trials for managing soybean rust in Brazil. Crop Protection 28, (9): 774-782. DOI: 10.1016/j.cropro.2009.05.006

Seth CS, Chaturvedi PK & Misra V (2007). Toxic effect of arsenate and cadmium alone and in combination on giant duckweed (*Spirodela Polyrrhiza* L.) in response to its accumulation. Environmental Toxicology 22(6): 539–549. DOI: 10.1002/tox.20292

Sharma CBSR (1983) Plant meristems as Monitors of genetic toxicity of environmental chemicals. Current Science 52(21): 1000–1002.

Sheikh N, Patowary H & Laskar RA (2020) Screening of cytotoxic and genotoxic potency of two pesticides (malathion and cypermethrin) on Allium cepa L. Molecular & Cellular Toxicology 16(3): 291–299. DOI:10.1007/s13273-020-00077-7

Shishatskaya E, Menzyanova N, Zhila N, Prudnikova S, Volova T, Thomas S (2018) Toxic effects of the fungicide tebuconazole on the root system of fusarium-infected wheat plants. Plant Physiology and Biochemistry 132: 400-407. DOI: 10.1016/j.plaphy.2018.09.025

Siddiqui S, Meghvansi MK & Khan SS (2012) Glyphosate, alachor and maleic hydrazide have genotoxic effect on *Trigonella foenum-Graecum* L. Bulletin of Environmental Contamination and Toxicology 88(5): 659–665. DOI: 10.1007/s00128-012-0570-6

Singh D and Roy BK (2017) Evaluation of malathion-induced cytogenetical effects and oxidative stress in plants using Allium test. Acta Physiologiae Plantarum 39(4), 92. DOI : 10.1007/s11738-017-2391-z

Sinha U (1979) Cytomorphological and macromolecular changes induced by p-flurophenylalanine in *Allium cepa* and Triticale. Journal of Cytologia and Genetics 14: 198

Souza IR, Silva LR, Fernandes LSP, Salgado LD, Silva de Assis HC, Firak DS, Bach L, Santos-Filho R, Voigt CL, Barros AC, Peralta-Zamora P, Mattoso N, Franco CR, Soares Medeiros LC, Marcon BH, Cestari MM, Sant'Anna-

Santos BF & Leme DM (2020) Visible-light reduced silver nanoparticles' toxicity in *Allium cepa* test system. Environmental Pollution 257, 113551. https://doi.org/10.1016/j.envpol.2019.113551

Stapulionytė A, Kleizaitė V, Šiukšta R, Žvingila D, Taraškevičius R & Čėsnienė T (2019) Cyto/genotoxicological evaluation of hot spots of soil pollution using allium bioassays in relation to geochemistry. Mutation Research - Genetic Toxicology and Environmental Mutagenesis 842: 102-110. DOI: 10.1016/j.mrgentox.2019.01.001

Sudhakar R, Gowda KN & Venu G (2001) Mitotic abnormalities induced by silk dyeing industry effluents in the cells of Allium cepa. Cytologia 66(3): 235–239.

Suspiro A and Prista J (2011) Biomarkers of occupational exposure do anticancer agents: A minireview. Toxicology Letters 207(1): 42–52. DOI: 10.1016/j.toxlet.2011.08.022

Szpyrka E and Walorczyk S (2013). Dissipation kinetics of fluquinconazole and pyrimethanil residues in apples intended for Baby Food Production. Food Chemistry 141(4): 3525–3530. DOI: 10.1016/j.foodchem.2013.06.055

Thesai AS, Nagarajan G, Rajakumar S, Pugazhendhi A & Ayyasamy PM (2021) Bioaccumulation of fluoride from aqueous system and genotoxicity study on Allium cepa using Bacillus licheniformis. Journal of Hazardous Materials 407, 124367. https://doi.org/10.1016/j.jhazmat.2020.124367

Türkoğlu Ş (2007) Genotoxicity of five food preservatives tested on root tips of *Allium cepa* L. Mutation Research/Genetic Toxicology and Environmental Mutagenesis 626(1-2): 4–14. DOI: 10.1016/j.mrgentox.2006.07.006

Verma S and Srivastava A (2018) Morphotoxicity and cytogenotoxicity of Pendimethalin in the test plant *Allium cepa* L. - a biomarker based study. Chemosphere 206: 248–254. DOI: 10.1016/j.chemosphere.2018.04.177

Webster PL and MacLeod RD (1996) The root apical meristem and its margin. Plant Roots. The Hidden Half (second ed.), Y. Waishel, A. Eshel, U. Kafkafi (Eds.), Marcel Dekker, New York, ISBN 0-8247-9685-3 pp. 51-76

Wójicik M and Tukendorf A (1999) CD - tolerance of maize, rye and wheat seedlings. Acta Physiologiae Plantarum 21(2): 99–107. DOI: 10.1007/s11738-999-0063-3

Wu S, Lei L, Liu M, Song Y, Lu S, Li D, Shi H, Raley-Susman KM, He D (2018) Single and mixture toxicity of strobilurin and SDHI fungicides to *Xenopus tropicalis* embryos. Ecotoxicol Environ Saf.,153: 8-15. DOI: 10.1016/j.ecoenv.2018.01.045

Yıldız M, Ciğerci İH, Konuk M, Fatih Fidan A & Terzi H (2009) Determination of genotoxic effects of copper sulphate and cobalt chloride in *Allium cepa* root cells by chromosome aberration and comet assays. Chemosphere 75(7): 934–938. DOI: 10.1016/j.chemosphere.2009.01.023

Yüzbaşıoğlu D, Ünal F, Sancak C & Kasap R (2003) Cytological effects of the herbicide racer "flurochloridone" on *Allium cepa*. Caryologia 56(1): 97–105.

Yüzbaşıoğlu D, Zengin N, Ünal F (2014) Gıda koruyucuları ve genotoksisite testleri. Gıda, 39 (3), 179-186. doi: 10.5505/gida.24861

Zeyad MT, Kumar M & Malik A (2019) Mutagenicity, genotoxicity and oxidative stress induced by pesticide industry wastewater using bacterial and plant bioassays. Biotechnology Reports, 24, e00389. Doi: 10.1016/j.btre.2019.e00389

Chapter 16

The Effect of the Autocorrelation Coefficient on the Performance Metrics of a Regression Model with AR(1) Structure

Tuğba SÖKÜT AÇAR[1]

[1] *Doç. Dr.; Çanakkale Onsekiz Mart University, Faculty of Science, Department of Statistics, Çanakkale-Türkiye*
t.sokut@comu.edu.tr ORCID No: 0000-0002-4444-1671

INTRODUCTION

Regression analysis is a multivariate approach commonly applied in various fields such as natural sciences, social sciences, and healthcare. The purpose of regression analysis is to model functional relationships between one or more independent variables and a dependent variable. Regression analysis in statistics serves as a fundamental topic for both theoretical investigations and practical applications across various fields, involving the development of new linear or nonlinear models and predictors. These theoretical advancements provide opportunities for application in numerous areas. The aim of these applications is to predict or forecast the dependent variable, which is relatively more challenging compared to the observed independent variables. The types of variables that will undergo regression analysis hold significance in this context. Modelling will vary depending on whether the dependent variable is quantitative or qualitative, as well as whether the functional relationship is linear or nonlinear. Within the scope of this study, it is assumed that the dependent and independent variables are measured at least on an equal interval level, and a linear functional relationship is presumed. The assumed regression model to include p independent variables, is presented in Equation 1:

$$y = \beta_0 + \beta_1 x_1 + \cdots \beta_p x_p + \varepsilon. \tag{1}$$

In this model, y represents the observed vector of the dependent variable consisting of n observations, $x_1, x_2, \ldots, x_p$ represent the observed vectors of each independent variable consisting of n observations, $\beta_1, \beta_2, \ldots, \beta_p$ represent the unobserved regression coefficients. Additionally, β_0 represents the constant term parameter in the model. ε represents the unobserved error vector resembling the probability distribution of the dependent variable. The matrix form of Eq.1 is as follows (Toutenburg, 1982)

$$y = X\beta + \varepsilon. \tag{2}$$

X is referred to as the design matrix or regressor matrix. The mathematical representation of the model given in Eqs. 1 and 2 relies on modelling the functional relationship, aiming to estimate the unknown regression parameters. Due to its simplicity in parameter estimation of unknown regression parameters, the ordinary least squares (OLS) method is often preferred. In the OLS method, the aim is to minimize the sum of squared errors of the model while estimating

the unknown regression parameters. If we differentiate the model's error from Eq. 2

$$\varepsilon = y - X\beta \tag{3}$$

Thus, the sum of squared errors becomes as

$$\sum_{i=1}^{n} \varepsilon_i^2 = \varepsilon'\varepsilon = (y - X\beta)'(y - X\beta) \tag{4}$$

The vector β that minimizes Eq. 4 can be found using the normal equations as

$$\hat{\beta}_{OLS} = (X'X)^{-1}X'y. \tag{5}$$

The estimator given in Eq. 5 is referred to as the OLS estimator. The *i*th observed value of the dependent variable fitted with OLS is obtained as

$$\hat{y}_i = \hat{\beta}_{OLS}X_i \tag{6}$$

where y represents the observed values of the dependent variable and $\hat{y}$ represents the predicted values based on the parameter estimate, the OLS residual vector is defined as

$$e = y - \hat{y} \tag{7}$$

Although it may not always be a primary consideration in practice, the least squares method relies on certain assumptions to produce valid and reliable results. These assumptions include (Groß, 2003):

- X is a non-stochastic $n \times (p+1)$ matrix with $(p+1) < n$
- X matrix has rank (p+1), that is, X is off full column rank
- The elements of the y vector are observable random
- ε are non-observable random variables such as $E(\varepsilon) = 0, Cov(\varepsilon) = \sigma^2 I_n$ with $\sigma^2 > 0$.

If these assumptions are met, then according to the Gauss-Markov theorem, the OLS estimator is the Best Linear Unbiased Estimator, BLUE, (Vinod and Ullah, 1981). If the regressor matrix is not full column rank, multicollinearity problem arises. In this case, if the assumption is violated and OLS is applied,

the model variance increases. To overcome this, statistical literature suggests biased estimators. If there are violations of the assumptions regarding the error term, there can be two problems: The first one is the problem of heteroscedasticity which can be addressed by applying weighted least squares (WLS). The second one is if the assumption of independence of errors is violated, in which case autocorrelation problem arises. This study is based on the problem of autocorrelation. However, as previously emphasized, practitioners often do not conduct these assumption checks. This study is designed to demonstrate how model performance is affected if the issue of autocorrelation is overlooked. A well-structured regression model is equivalent to high model performance.

There are many metrics available to measure the performance of a fitted regression model. Among these, the performance metrics commonly discussed in interdisciplinary applications are listed below.

Root Mean Square Error, RMSE: The calculation of RMSE which is a popular measure in applied statistics for assessing the accuracy of a predictive model or the quality of predictions, is given in the following formula

$$RMSE = \sqrt{\frac{1}{n}\sum_{i=1}^{n} \tilde{e}_i^{\,2}}. \tag{8}$$

Mean Absolute Error, MAE: The calculation of MAE, which measures how far, on average, your predictions are from the actual values, is obtained as follows

$$MAE = \frac{1}{n}\sum_{i=1}^{n} |\tilde{e}_i|. \tag{9}$$

Mean Absolute Percentage Error, MAPE: MAPE is very useful for determining the relative error between forecasts and actual results, especially when working with data of varying sizes or magnitudes. Because of its simple interpretation in terms of relative error, the MAPE is frequently utilized in practice (De Myttenaere, et al., 2016). The MAPE formula is as follows

$$MAPE = \frac{100}{n}\sum_{i=1}^{n} \left|\frac{\tilde{e}_i}{y_i}\right|. \tag{10}$$

Akaike Information Criterion, AIC: AIC is the most common tool used in statistics when there is more than one candidate model and it is desired to

determine the best one (Cavanaugh and Neath, 2019). This measure criterion emerged as an extension of the maximum likelihood principle. Its calculation is as follows

$$AIC = 2(p+1) + nlog(\tilde{\sigma}^2). \tag{11}$$

Coefficient of Determination, R^2***:*** R^2 is a statistical measure used in regression analysis to assess the goodness of fit of a regression model to the data. It provides information about the proportion of the variance in the dependent variable that is explained by the independent variables in the model. In other words, it quantifies how well the regression model predicts the variation in the dependent variable. The calculation is as follows

$$R^2 = 1 - \frac{\sum_{i=1}^{n} \tilde{e}_i^2}{\sum_{i=1}^{n} (y_i - \bar{y})^2}. \tag{12}$$

F-test score: F which is used for testing the hypothesis that the regression coefficients of all predictor variables, excluding the constant), are zero as follows (Chatterjee et al., 2000)

$$F = \frac{\sum_{i=1}^{n} (\hat{y}_i - \bar{y})^2 / p}{\sum_{i=1}^{n} \tilde{e}_i^2 / (n-p-1)}. \tag{13}$$

Here, $\tilde{e}$ represents the error vector of the model fitted with any estimation procedure, $\tilde{\sigma}^2$ represents the maximum value of the model's likelihood function, and n represents the number of observations. An R^2 of 0 means that the dependent variable cannot be explained by the independent variables, and the model provides no meaningful information. An R^2 of 1 means that the dependent variable is perfectly explained by the independent variables, and the model fits the data perfectly. A model is considered best when its error criteria such as RMSE, MAE, MAPE, AIC values are minimized, or when the R^2 value is maximized.

The remainder of the study is organized as follows: In the second section, the multiple regression model with autocorrelation problems and the best unbiased estimator under that model are discussed. In the third section, two example based on simulated data sets are presented to observe the behaviour of model performance metrics with respect to the autocorrelation coefficient. The final section includes the study's conclusions and recommendations.

AUTOCORRELATION PROBLEM AND COPING WITH THIS

In Eqs.1 and 2, the variance-covariance matrix of errors should, by assumption, be $E(\varepsilon\varepsilon') = \sigma^2 I_n$. If $E(\varepsilon\varepsilon') = \sigma^2\Omega$, where $\Omega \neq I_n$, it indicates that this assumption is not satisfied, and there is an problem of autocorrelation. So, it means that the errors are no longer uncorrelated. Since Ω is symmetric and positive definite of $n \times n$ type, there always exists a unique $n \times n$ type V matrix such that $\Omega^{-1} = P'P$, or $P\Omega P' = I_n$ (Judge et al., 1988). If the equations are multiplied from the left by the P matrix, the transformed model is obtained as follows

$$Py = PX\beta + P\varepsilon. \tag{14}$$

When examining the newly formed error term in Eq. 14 $E(P\varepsilon) = PE(\varepsilon) = 0$ and $E(P\varepsilon\varepsilon'P') = PE(\varepsilon\varepsilon')P' = \sigma^2 P\Omega P' = \sigma^2 I_n$.

It is clearly seen that the assumption $E(\varepsilon\varepsilon') = \sigma^2 I_n$ is satisfied. So, when the generalized least squares method is applied to the final model, the newly formed estimator is referred to as the Generalized Least Squares (GLS) estimator and it is as follows

$$\hat{\beta}_{GLS} = (X'\Omega^{-1}X)^{-1}X'^{\Omega^{-1}}y. \tag{15}$$

The fitted values with GLS are $\hat{y}_{GLS} = PX\hat{\beta}_{GLS}$.

The residuals of the model fitted with GLS are defined as: $e_{GLS} = Py - \hat{y}_{GLS} = Py - PX\hat{\beta}_{GLS} = Py - PX(X'P'PX)^{-1}X'P'Py =$

$[I_n - PX(X'P'PX)^{-1}X'P']Py$. The structure of the Ω matrix varies depending on the structure of autocorrelation. Autocorrelation problem arises in autoregressive, moving average, and autoregressive moving average processes. The modelling of processes in its most general form is provided below (Judge et al., 1988):

pth-order autoregressive process (AR(p)):

$$\varepsilon_t = \rho_1\varepsilon_{t-1} + \rho_2\varepsilon_{t-2} + \cdots + \rho_p\varepsilon_{t-p} + u_t \tag{16}$$

qth-order moving average process (MA(q)):

$$\varepsilon_t = u_t + \theta_1 u_{t-1} + \cdots + \theta_q u_{t-q} \tag{17}$$

pq-th order autoregressive moving average pro-cess(ARMA(p,q)):

$$\varepsilon_t = \rho_1\varepsilon_{t-1} + \rho_2\varepsilon_{t-2} + \cdots + \rho_p\varepsilon_{t-p} + u_t + \theta_1 u_{t-1} + \cdots + \theta_q u_{t-q} \quad (18)$$

where $u_t$is white noise, that is, $E(u_t) = 0$ for all t and $E(u_t u_s) = 0$ for s≠t.

This study focuses only on the first-order autoregressive (AR(1)) error model. In other words, the assumed relationship between errors will be considered as follows

$$\varepsilon_t = \rho\varepsilon_{t-1} + u_t,\ |\rho| < 1\,. \quad (19)$$

Graphical representations or systematic tests are used to detect an autocorrelation problem in data from an AR(1) process. In visualization, autocorrelation function (ACF) and partial autocorrelation functions (PACF) graphs are used. This plots illustrate how the error is related to its own past values. While an exponential or sinusoidal decrease is observed in the ACF graph for the AR(1) process, it is observed that only first autocorrelation coefficient goes out of the confidence limits in the PACF graph (Eğrioğlu and Baş, 2020).

The most common and powerful approach for detecting AR(1) errors in a linear model was developed by Durbin and Watson (1950). This test is based on the DW statistic with values between 0 and 4. DW a statistical procedure used to detect auto correlation among the error terms in regression analysis. DW evaluates the relationship between consecutive observations of the error terms in a regression model.

It is important to correctly evaluate error structures in regression analyses. Neglecting autocorrelation can lead to inaccurate pre-dictions and unreliable results. Therefore, the Durbin-Watson test is used to enhance the reliability of regression analyses by detecting and addressing autocorrelation issues. The DW test statistic is based on the following formula

$$d = \frac{\sum_{t=2}^{n}(\hat{\varepsilon}_t - \hat{\varepsilon}_{t-1})^2}{\sum_{t=1}^{n}\hat{\varepsilon}_t^2} \quad (20)$$

where $\hat{\varepsilon}_t$ is the OLS residuals. Griffiths et al., (1933) gave the approximate DW is $d = 2(1-\hat{\rho})$. A DW value of approximately 2 is considered an indicator that errors in the model are independent, and there is no autocorrelation problem. However, if DW is less than 2, it indicates positive autocorrelation, and if DW is greater than 2, it indicates negative

autocorrelation. In other words, if the DW value is either greater or less than 2, it provides information about the presence or type of autocorrelation (Griffiths, et al., 1993).

In Eq. 19, it is important for applications to know or estimate the ρ coefficient. Approaches suggested for the estimation of ρ in the AR(1) model are provided below.

The most commonly used estimation procedure is based on solving Eq. 19 with the least squares procedure

$$\hat{\rho}_1 = \frac{\sum_{t=2}^{n} \hat{\varepsilon}_t \hat{\varepsilon}_{t-1}}{\sum_{t=1}^{n} \hat{\varepsilon}_t^{\,2}}. \tag{21}$$

The estimation method proposed by Theil (1971) is as follows

$$\hat{\rho}_2 = \frac{(n-p)\sum_{t=2}^{n} \hat{\varepsilon}_t \hat{\varepsilon}_{t-1}}{(n-1)\sum_{t=1}^{n} \hat{\varepsilon}_t^{\,2}}. \tag{22}$$

As a result of calculating the Durbin-Watson (1950) statistic, the approximate autocorrelation estimate is suggested as follows

$$\hat{\rho}_3 = 1 - \frac{1}{2} dw. \tag{23}$$

Theil and Nagar (1961) have extended the approximate coefficient of DW as follows

$$\hat{\rho}_4 = \frac{n^2 \hat{\rho}_3 + p^2}{n^2 - p^2}. \tag{24}$$

Bhandary et al. (2022) proposed a Bayesian estimation technique to estimate autocorrelation coefficients in statistical modelling. It is crucial to assess multiple performance metrics together by checking model assumptions as much as possible.

If the autocorrelation coefficient is unknown, which is often estimated in practice, one of the estimation procedures listed above is chosen, and a $\boldsymbol{P}$ matrix is constructed to proceed with modelling. The matrix $\boldsymbol{P}$ for AR(1) structure is generally represented as follows

$$P = \begin{bmatrix} \sqrt{1-\rho^2} & 0 & 0 & \dots & 0 & 0 \\ -\rho & 1 & 0 & \dots & 0 & 0 \\ 0 & -\rho & 1 & \dots & 0 & 0 \\ \vdots & \vdots & \vdots & \ddots & \vdots & \vdots \\ 0 & 0 & 0 & \dots & 1 & 0 \\ 0 & 0 & 0 & \dots & -\rho & 1 \end{bmatrix}. \quad (25)$$

The different autocorrelation coefficients clearly lead to different P matrices. Therefore, modelling will differ, and model performance criteria will also change.

The first error term of the transformed model is given by $\sqrt{1-\rho^2}\varepsilon_1$, whereas for the others are given by $\varepsilon_t - \rho\varepsilon_{t-1}$, $t = 2,3,\dots,n$. That is, the first error term ε_1 is adjusted by the innovation factor $\sqrt{1-\rho^2}$, and subsequent error terms ε_t depend on the previous error term ε_{t-1} with a scaling factor of ρ.

The performance metrics of a model are based on the errors. From this point onward, two separate implementations have been introduced to determine how different autocorrelation coefficients affect these metrics. The data to be used in the implementations has been simulated to be both positively and negatively autocorrelated in its original form.

APPLICATION OF SIMULATED DATASETS

In this section, two separate data sets have been considered to understand and evaluate the impact of autocorrelation on the predictive abilities of regression models. These two data sets represent two different scenarios: one with positive autocorrelation and the other with negative autocorrelation. These two scenarios can have different effects on the success and accuracy metrics of the regression model. The steps involved in obtaining the simulation data to assess these effects are listed below.

- In both applications, the sample size was set to $n = 20$, and the number of independent variables was determined as $p = 2$.
- The independent variables were generated as follows:
-

$$x_{ij} = \begin{cases} 1 & j = 1, \quad i = 1,\dots,n \\ z_{ij}, & j = 2,3, \quad i = 1,\dots,n \end{cases}$$

Here, $z_{ij}{}'s$ are the independent standard normal pseudo-random numbers with linear independence.

• The β vector, referred to as regression parameters, was generated parallel to Holgersson (2015) as $\beta = \left(\frac{1}{\sqrt{p+1}}\right)1_{(p+1)\times 1}$.

• Autocorrelated errors were generated based on Eq. 19. However, initially, the terms u_i were generated as white noise, where $u_i \sim N(0,1)$.

First Application

This dataset was originally simulated with a value of $\rho = 0.75$. The other steps are as mentioned above.

The correlation matrix of the independent variables has been plotted in Figure 1.

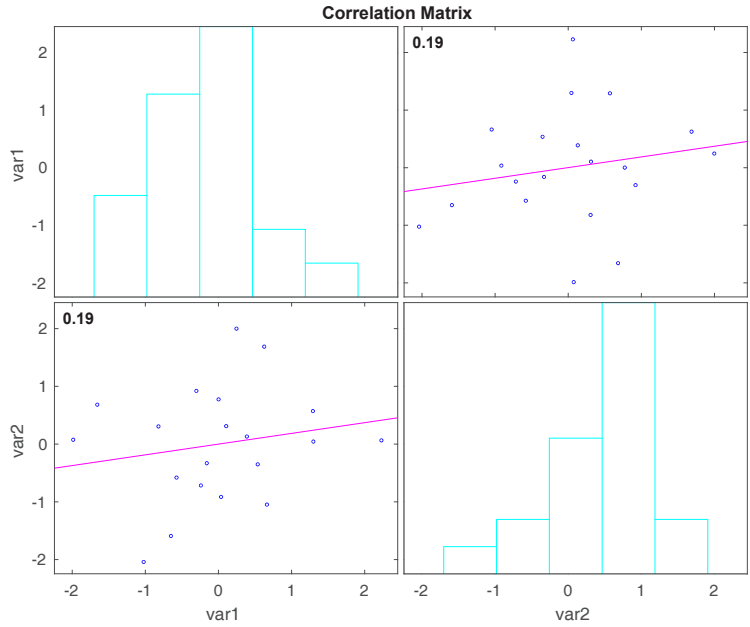

Figure 1: Correlation plot for the first dataset

Fig.1 illustrates the following: The correlation coefficient between the first independent variable and the second independent variable has been calculated as $r = 0.19, (p = 0.43 > \alpha = 0.05)$, indicating statistical insignificance. Therefore, there is no multicollinearity problem in the model.

The parameter value for autocorrelation was initially assumed to be 0.75. However, the autocorrelation problem was also examined through the DW test, and for the first data set, $DW = 0.39$ was calculated. This value falls in the range of 0-2 and is close to zero, indicating a strong positive autocorrelation.

At this stage, performance criteria have been calculated for two separate models. The first one represents performance evaluations of modelling using OLS without testing of autocorrelation (assuming $\rho = 0$), while the second one reflects performance evaluations of modeling using GLS while taking autocorrelation into account (Table 1).

Table 1: Comparing performance metrics when positive autocorrelation is ignored for the first dataset

	ρ= 0	**ρ**=0.75
RMSE	1.5713	**0.8831**
MAE	1.3681	**0.7658**
MAPE	90.7171	**53.1564**
AIC	82.8341	**59.7852**
R^2	0.6026	**0.9109**
F	12.8903	86.8728
p-value	0.00392	<0.00001

$F_{2;17,0.05}$ =3.5915

Table 1 illustrates that if a dataset originally exhibiting autocorrelation is subjected to regression modelling using the OLS procedure without addressing the issue, the model may be statistically significant (p=0.00392<0.05); but, the performance metrics have yielded worse results. Additionally, when autocorrelation is detected and a model is constructed, it is evident that the R-squared value increases by 55.16%.

However, it should be noted that in practice, the parameter value of the autocorrelation coefficient is often unknown and needs to be estimated. Approaches for estimation were presented through four different coefficient estimations (Eqs. 21-24). Now, graphical representations of performance metrics for the widest range of ρ (-1 to +1) are provided (Fig.2).

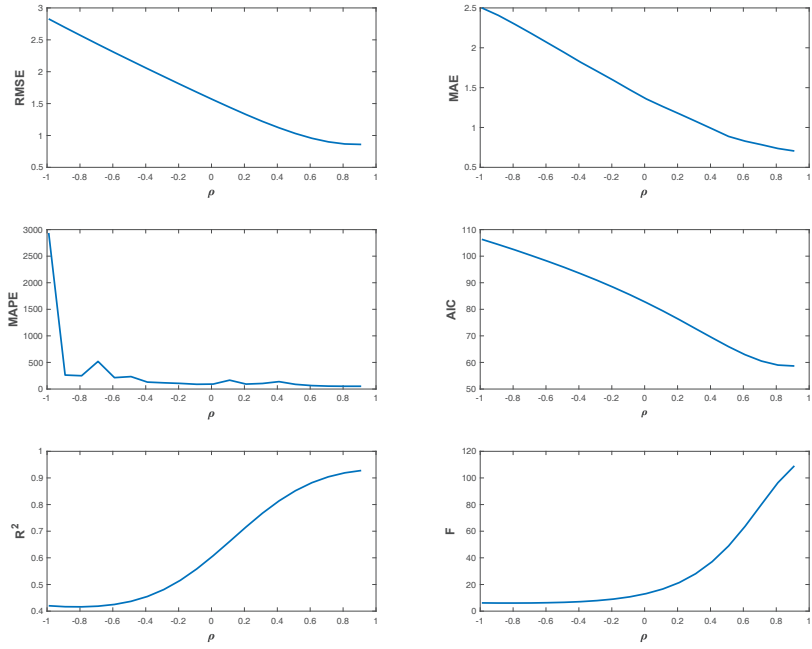

Figure 2: Performance criteria against different autocorrelation coefficients for the first dataset

It is observed that at the true autocorrelation value of 0.75, RMSE, MAE, MAPE, and AIC values are minimized, and at the same time, $R^2$and F-values are higher. Additionally, it is clear that correctly determining the direction of autocorrelation is crucial for model performance (Fig.2).

Second Application

In this application, the parameter value of the autocorrelation coefficient has been assigned as 0.75, as in the first example, but its direction has been determined as negative, that is, $\rho = -0.75$. The correlation matrix of the independent variables fort his data set has been plotted in Figure 3.

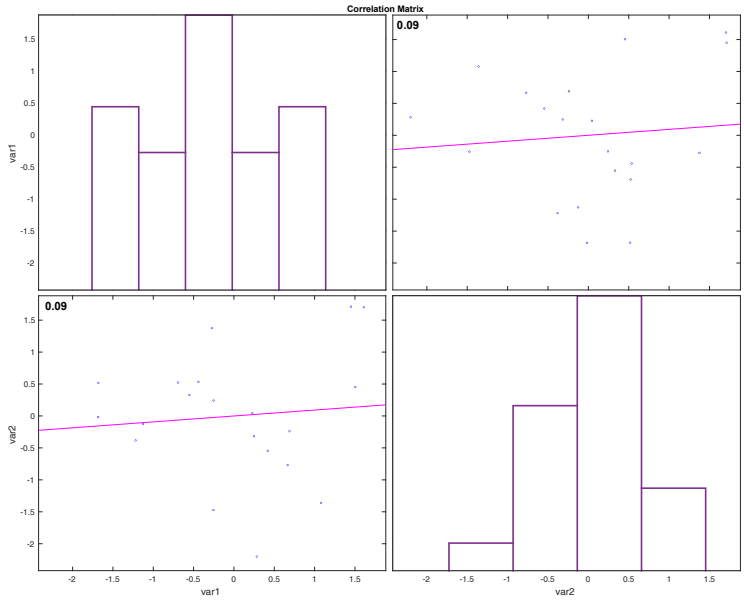

Figure 3: Correlation plot for the second dataset

Figure 3 depicts that the correlation coefficient between the independent variables was determined as r=0.09, (p=0.69>0.05) and its showing statistical insignificance. As a result, there is no multicollinearity in the model. The DW test statistic value for the second dataset has been calculated as 3.49, which is close to its upper limit 4, indicating negative autocorrelation.

As in the first example, the performance of the true negative autocorrelation model has been compared with the performance metrics of the model where autocorrelation is ignored, i.e., where the autocorrelation coefficient is assumed to be zero (Table 2).

Table 2: Comparing performance metrics when negative autocorrelation is ignored for the second dataset

	$\rho = 0$	$\rho = 0.75$
RMSE	1.6404	**0.9097**
MAE	1.3637	**0.7949**
MAPE	242.3661	**70.4100**
AIC	84.5554	**60.9735**
R^2	0.5555	**0.9044**
F	10.6205	80.4440
p-value	0.001017	<0.00001

$F_{2;17,0.05} = 3.5915$

In Table 2, it can be observed that both the models fitted with OLS and GLS are statistically significant (p=0.001017<0.05). However, there are significant differences in model performances. In fact, when autocorrelation, which actually exists as negative, is ignored, RMSE, MAE, MAPE, and AIC values increase, indicating poor model performance. Additionally, if autocorrelation had not been ignored and had been tested, it is clear that in this case, the R^2 value would have increased by 62.86%.

The comparison of model performances for different autocorrelation coefficients is presented in Figure 4.

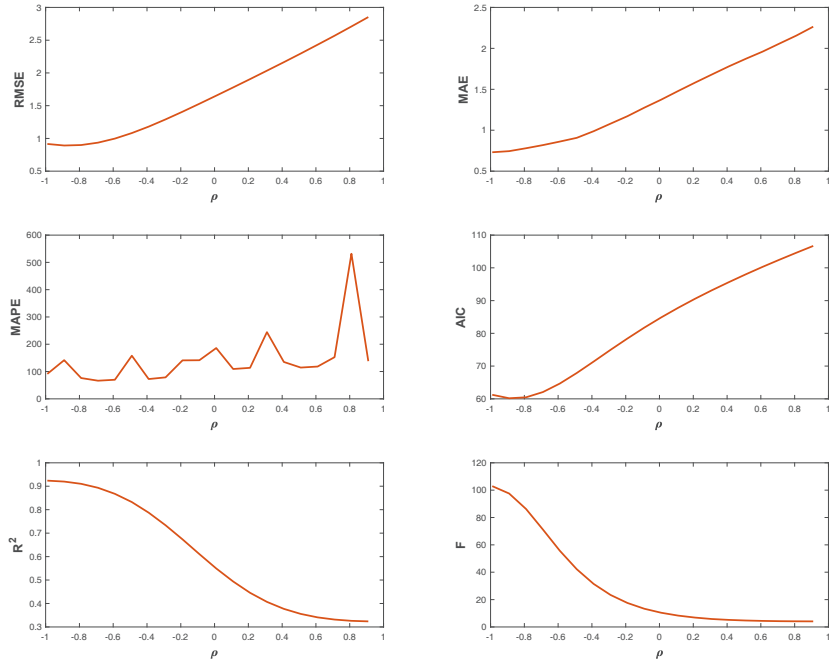

Figure 4: Performance criteria against different autocorrelation coefficients for the second dataset

Noticeable improvement in model performances is observed at the true autocorrelation value of -0.75. It is evident that at the point ρ=0, all metrics do not exhibit better performance. Furthermore, when the direction of the coefficient is incorrectly determined, performances have deteriorated even further (Fig. 4).

CONCLUSION

This section belongs to a study that investigates the impact of autocorrelation coefficients on the performance metrics of a regression model. It addresses the problem of autocorrelation, which is one of the fundamental issues in regression analysis. Autocorrelation is a common problem in regression analysis when trying to model functional relations-hips between independent variables and the dependent variable. However, it is often ignored in some applied studies. This study is designed to demonstrate how autocorrelation can affect the performance of a regression model. Various metrics such as Root Mean Square Error, Mean Absolute Error, Mean Absolute Percentage Error, Akaike

Information Criterion, Coefficient of Determination and F-score were used to measure the performance of the regression model. The study was applied to data sets with positive and negative autocorrelation, and the impact of autocorrelation coefficients on performance metrics was examined. The results indicate that ignoring autocorrelation can negatively affect model performance. Furthermore, it was observed that correctly identifying and addressing autocorrelation can significantly improve model performance. The findings of the study emphasize that autocorrelation should not be overlooked in regression analysis and that mishandling it can adversely affect model performance.

REFERENCES

Bhandary, M., Dai, H., Bansal, N.K., and Shin, H. (2022). Bayes estimation of autocorrelation coefficient. Journal of Statistics and Management Systems, 25(4), 771-779.

Cavanaugh, J.E., and Neath, A.A. (2019). The Akaike information criterion: Background, derivation, properties, application, interpretation, and refinements. Wiley Interdisciplinary Reviews: Computational Statistics, 11(3), e1460.

Chatterjee, S., Hadi, A.S., and Price, B. (2000). *Regression analysis by example*. John Wiley & Sons.

De Myttenaere, A., Golden, B., Le Grand, B., and Rossi, F. (2016). Mean absolute percentage error for regression models. Neurocomputing, 192, 38-48.

Durbin, J., and Watson, G. S. (1950). Testing for serial correlation in least squares regression: I. Biometrika, 37(3/4), 409-428.

Eğrioğlu, E., and Baş, E. (2020). *Zaman serileri ve öngörü yöntemleri - R uygulamalı*. Nobel Akademik Yayıncılık Eğitim Danışmanlık Tic. Ltd. Şti.

Griffiths, W.E., Hill, R.C., and Judge, G.G. (1993). *Learning and practicing econometrics*. Jon Wiley & Sons, Inc.

Groß, J. (2003). *Linear regression* (Vol. 175). Springer Science & Business Media.

Holgersson, H.E.T. (2015). A note on a commonly used ridge regression Monte Carlo design. Communications in Statistics-Theory and Methods, 44(10), 2176-2179.

Judge, G.G., Hill, R.C., Griffiths, W., and Lütkepohl, H.T. Lee, (1988). *Introduction to the Theory and Practice of Econometrics*. Wiley, 2, 189-198.

Theil, H. (1971). *Principles of econometrics*. John Wiley & Sons, New York and North-Holland Publishing Company, Amsterdam.

Theil, H., and Nagar, A.L. (1961). Testing the independence of regression disturbances. Journal of the American Statistical Association, 56(296), 793-806.

Toutenburg, H. (1982). *Prior information in linear models*. John Wiley & Sons.

Vinod, H.D., and Ullah, A. (1981). *Recent advances in regression methods.* Marcel Dkker, Inc.